TÉCNICO LISBOA

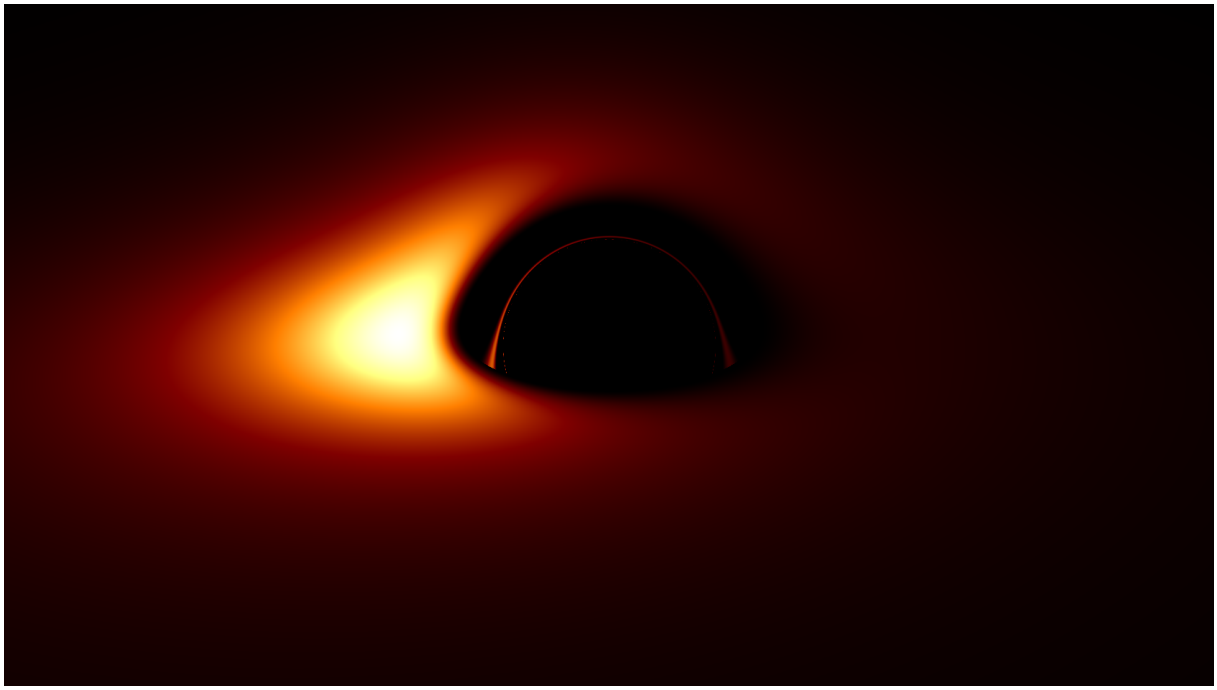

Electrically Charged Hyperboloidal Evolution

João Dinis Ribeiro Machado de Carvalho Álvares

Thesis to obtain the Master of Science Degree in

Engineering Physics

Supervisor: Prof. Dr. Alex Vañó-Viñuales
Prof. Dr. Edgar Gasperín García

Examination Committee

Chairperson: Prof. Dr. David Matthew Hilditch
Supervisor: Prof. Dr. Alex Vañó-Viñuales
Member of the Committee: Prof. Dr. Miguel Rodrigues Zilhão Nogueira

May 2025

I declare that this document is an original work of my own authorship and that it fulfills all the requirements of the Code of Conduct and Good Practices of the Universidadae de Lisboa.

To the ones that gave me the strength to continue on and to the ones who did me wrong and taught me, without wanting, what not to be.

Acknowledgements

Nothing in this world is done by one person alone. I want to thank Alex, my supervisor, for constantly motivating me to do this work. It was a continuous struggle, with many setbacks, but he never stopped believing. The following pages would not have been finished if not for this. I would also like to thank Edgar, my co-supervisor, who guided me through my first steps in hyperboloidal slices, back when I was awarded one of the first ten Gulbenkian "New Talents in Physics" scholarships. I must also thank David Hilditch for sharing his knowledge during our meetings and for the simultaneous professionalism and good humor he brought. These acknowledgments naturally extend to Jorge Expósito Patiño, who read the entire thesis and provided with very important comments, that further made this thesis clearer. I also have to thank Valentin Boyanov, Tiago Fernandes, and Hannes Rüter for the discussions around charged scalar fields and late-time behavior of the scalar field. A big acknowledgement goes to Miguel Zilhão, who helped me understand how to model correctly the Reissner-Nördstrom spacetime in GBSSN, without whom the setup for the simulations would have taken much longer. Lastly, I would also like to thank Nicolas Aimar for having helped me understand how to use Gyoto [1, 2], a relativistic ray-tracing code which provided with the cover image of this thesis.

Outside of the work done for the thesis, I would also like to thank some important people who made me go on each day at a time.

To my mother and my sisters, who, although far away from me, always gave me much love when I had the time to go back home, even if only for a few days.

To Francisco Toldy, Raquel Moreira, Bruno Castiço, Ivo Gonçalves, Rita Matos, and Patrícia Fernandes, my friends from home, although we did not see so frequently, everything was always as it was before I left Braga to study in Lisbon.

To António Onofre, the man who, since I was 14 years old, has given me guidance in the academic world and served as an example. I would not be writing these same words if it weren't for him.

To Ângela Rodrigues, for the long hours discussing problems which shall never end and for the constant support. And also for making me believe that there is still something worth fighting for.

To Francisco Raposo, António Luciano, and Miguel Gaspar, a group that naturally formed through the years, with whom many dinners were passed during the thesis.

To the Executive Director of Ciência Viva, Dr. Ana Noronha, for having invited me to the Portuguese Science Congress back in 2019, where I had the pleasure of meeting the then Science, Technology and Higher Education Minister Manuel Heitor and the then president of Instituto Superior Técnico, Dr. Arlindo

Oliveira, which together allowed me to overcome my financial barriers and study in Lisbon. For this, I will also have to thank Dr. Rita Wahl, for she was the person who always accompanied me during these years at Técnico.

To the heroes of the Portuguese Revolution of 25th April 1974, which celebrated its 50th anniversary this year. To them, I also dedicate this thesis, for they allowed Portugal to be what it is today and for me to reach the place where I am.

I would also like to thank the following people, for I have shared with them many great memories and stories which shall be lost in time, but which I will hold dearly in my mind until the days have ceased: Ana Sofia Sousa, Dr. Ana Mourão, Andrei Kolesnikov, Anita Ribeiro, António Alves Redol, Beatriz Dinis, Beatriz Mestre, Bernardo Jordão, Bruna Lima, Bruna Raquel, Bruno Semião, Dr. Carla Mouro, Carolina Serranito, Catarina Caramalho, Catarina Curado, Diogo Faustino, Diogo Ribeiro, Diogo Simões, Diogo Soares, Dinis Felgueiras, Dragan, Duarte Mihuta, Edoardo Contente, Filipa Paz, Filipa Rio, Filipe Malveiro, Filipe Paiva, Francisco Alves, Francisco Simões, Francisca Branco, Francisca Sousa, Gabriel Rouxinol, Gonçalo Nunes, Gonçalo Ribeiro, Guilherme Lourinho, Gustavo Neves, Haidar Anbar, Inês Martins, Inês Moreira, Isabel Alexandre, Íris Brée, Jafar Mortada, João Carranca, Dr. João Paulo Silva, João Rebelo, João Santos, João Teixeira, Jordan Grujić, Jörge, Dr. Jorge Drumond, Julia Cheng, Julia Mestre, Marc Schroeder, Madalena Nunes, Manuel Ratola, Márcia Flores, Mariana Campos, Mariana Lameiro, Marta Ianni, Matilde Sardinha, Miguel Graça, Miguel Rodrigues, Mónica Santos, Patrícia Marques, Dr. Pedro Abreu, Pedro Azóia, Pedro Baptista, Pedro Cosme, Rafael Dias, Rafael Russo, Dr. Raquel Seruca, Renato Mântua, Serhiy Kolyada, Sofia Calado, Stefan Katić, Susana Chaves, Talha Kaan Ünlü, Tânia Machado, Tiago Jorge, Tiago Vieira, Tomás Cabrito, Tomás Vieira, Dr. Vasco Guerra, Vasco Lourenço and Vítor Sá.

I run the risk of forgetting some names, and if I did, I would like to apologize for that. Many of the people that I have listed were members of the newspaper Diferencial, of which I was one of the directors while doing this thesis. As a director of the newspaper of Técnico, I had to talk to many different people, but I would like to above all thank the following people for having collaborated with me and made Técnico a more transparent place because of that: the President of Instituto Superior Técnico, Dr. Rogério Colaço; the President of the Student's Association (AEIST), Pedro Monteiro, and its' Treasurer, Rita Mendes; the Administrator of the Social Services of the University of Lisbon (SASUL), Dr. Pedro Simão; the Rector of the University of Lisbon, Dr. Luis Ferreira; the President of the Municipal Council of Oeiras, Dr. Isaltino Morais; and the Social History Archive, from the Social Sciences Institute of the University of Lisbon, in the names of João Pedro Santos and Inês Ponte. I will still leave a kind thanks to the now-retired Administrator of SASUL, Carlos Dá Mesquita, who is an unknown hero of the University of Lisbon, but with whom I had many meetings to solve some problems in the University's housing, where I stayed these past years.

Besides having been the director of Diferencial, during my stay at Técnico, I was also the director of the Astronomy Section of NFIST (*Núcleo de Física do IST*), where I worked with some of the incredible people who fight to keep astronomy alive. Thus, I would like to thank the Director of the Astronomical Observatory, Bruno Ribeiro, who revived one of the most important treasures of Astronomy in Portugal; the Director of the Constância Ciência Viva Center, Dr. Máximo Ferreira, also the founder of Astrofesta,

the first event in Portugal to celebrate astronomy; Dr. Nelson Nunes and Lionel Godinho, the founders and directors of the Alqueva Astronomical Observatory; Dr. Nuno Peixinho, together with Dr. João Fernandes, which together keep Coimbra's Geophysical and Astronomical Observatory of the University of Coimbra up and running, together with a bigger team which unfortunately I could not meet; Dr. Carlos Herdeiro, which came to Lisbon directly to give a Cosmology and Gravitational Waves lecture to the Astronomy Summer School which I had the pleasure of organizing, back in 2022; in that same School, Dr. Robert Wald was present as well, to whom I am thankful; the Technical Director of the Navy Planetarium, Dr. Vasco Teixeira, which took me in and showed me how to work with the million-budget exhibition machinery that sits nowadays at the Planetarium - it was a pleasure to comemorate the Day of the Navy with him and the Vice Admiral Edgar Bastos Ribeiro, the director of the Cultural Comission of the Navy.

The story of these years at Técnico is somewhere in between all of these people and many more. To all, my most sincere gratitude.

Resumo

Apresentamos aqui o sistema Einstein-Maxwell-Klein-Gordon em foliações hiperboloidais, uma formulação mais recente para a extração de radiação, no infinito futuro nulo. Tanto quanto sabemos, é a primeira vez que este sistema é evoluído usando uma formulação comum como BSSN/Z4. Usando as foliações hiperboloidais, conseguimos chegar ao infinito futuro nulo continuamente, ao contrário de outros métodos recentes como a Correspondência de Características de Cauchy. Com este sistema, conseguimos simular como um campo escalar carregado se comporta num espaço-tempo plano e perto de um buraco negro carregado. Conseguimos para além disso ver os modos quasi-normais e as leis de decaimento de potência, para tempos tardios. Ambos os fenómenos foram testados para perceber como são influenciados pelo acoplamento eletromagnético entre o buraco negro e o campo escalar carregado. Uma comparação dos resultados analíticos previamente estudados com as nossas simulações é apresentada. Também mostramos o colapso do campo escalar carregado num buraco negro de Reissner-Nördstrom.

Palavras-Chave: Reissner-Nördstrom, BSSN, Campo Escalar Complexo, Foliações Hiperboloidais, Z4

Abstract

We present the Einstein-Maxwell-Klein-Gordon system in hyperboloidal slices, a recent formulation for extracting signals at future null infinity. As far as we know, this is the first time this setup is evolved with a common formulation like BSSN/Z4. Using hyperboloidal slices, contrary to other recent methods like Cauchy-Characteristic Matching, we can continuously reach future null infinity. With this system, we simulate how a charged scalar field behaves in flat spacetime and near a charged black hole. We are further able to see the scalar field's quasi-normal modes and analyze the late-time power-law tail decays. Both phenomena were tested to see how they change with the electromagnetic coupling between the black hole and the charged scalar field. A comparison of previously studied analytical results to our simulations is shown. We also showcase the collapse of the charged scalar field into a Reissner-Nördstrom black hole.

Keywords: Reissner-Nördstrom, BSSN, Complex Scalar Field, Hyperboloidal Slices, Z4

Contents

List of Figures

List of Tables

List of Acronyms

GR	General Relativity
BH	Black Hole
ODE	Ordinary Differential Equation
PDE	Partial Differential Equation
CCM	Cauchy Characteristic Matching
EFE	Einstein's Field Equations
BSSN	Baumgarte-Shapiro-Shibata-Nakamura (formalism)
GBSSN	Generalized BSSN (formalism)
RN	Reissner-Nördstrom
CMC	Constant Mean Curvature
KG	Klein-Gordon
NR	Numerical Relativity
ADM	Arnowitt-Deser-Misner (formalism)
RHS	Right-Hand-Side
LHS	Left-Hand-Side
MoL	Method of Lines
RK4	Runge-Kutta 4
CFL	Courant-Friedrichs-Lewy
QNM	Quasi-Normal Modes

List of Symbols

$\tilde{g}_{\mu\nu}$ 4-dimensional physical metric

$\bar{g}_{\mu\nu}$ 4-dimensional conformally compactified metric ($\bar{g}_{\mu\nu} = \Omega^2 \tilde{g}_{\mu\nu}$)

$\bar{\gamma}_{ab}$ 3-dimensional spatial projection of $\bar{g}_{\mu\nu}$

γ_{ab} 3-dimensional conformal rescaling of $\bar{\gamma}_{ab}$ ($\gamma_{ab} = \chi \bar{\gamma}_{ab}$)

$T_{\mu\nu}$ Stress-energy Tensor

$G_{\mu\nu}$ Einstein Tensor

Ω Conformal Factor

χ Rescaling Factor of Spatial Part (GBSSN)

$F_{\mu\nu}$ Faraday Tensor

E_i (Compactified) Electric Field

B_i (Compactified) Magnetic Field

A_μ 4-potential

A_{3r} Vector potential (spatial projection of A_μ)

Φ Scalar potential

c_ϕ Real Part of Complex Scalar Field

d_ϕ Imaginary Part of Complex Scalar Field

c_Π Time Derivative of Real Part of Complex Scalar Field

d_Π Time Derivative of Imaginary Part of Complex Scalar Field

Part I

What to Know and Why

Chapter 1

Motivation and Structure of the Thesis

The first question to answer is why this work is relevant or, at least, what its aim is and how it extends our current knowledge of General Relativity (GR).

GR is a four-dimensional gravitational theory, and its remarkable success comes from tying time and space together. To slice it as a continuum of 3D instants, we have to decompose spacetime into its corresponding components, space and time. Traditionally, this was done by slicing spacetime along (Cauchy) slices of the usual constant time t. One then gives initial data on a slice and applies the decomposed Einstein's Field Equations (EFEs) to see how the initial geometry evolves according to GR. This procedure is called the Cauchy evolution. One of its defects is its inability to reach a very specific infinity, which only light rays (or null rays) extend to: future null infinity. There is also the correspondent past null infinity, where "light rays are born", as Edgar, my co-supervisor, usually says. Future null infinity would then be where photons meet their end.

Foremost, we must understand why we should care about future null infinity. As discussed in previous works [3, 4, 5], we know that our position on Earth, concerning a source of gravitational radiation at a given distance, can be approximated as being at future null infinity. This means that the radiation we detect here on planet Earth is a very good approximation to the radiation we can extract, theoretically, at the source's future null infinity. This is valid within some limitations, depending on the radiation frequency.

The problem of reaching future null infinity has already been dealt with with some degree of success, through Cauchy Characteristic Matching (CCM) [6, 7]. This method evolves initial data along Cauchy slices in a tube and then matches (hence the name) the data on the tube to null cones which go to future null infinity. The matching may be a source of systematic errors that can affect the accuracy of the extracted radiation at future null infinity [6].

Fortunately, we have some freedom in how we slice spacetime. Hyperboloidal slices [8] have the advantage that they reach future null infinity continuously. Although the idea of using these slices has been around for more than a decade [9, 10], a lot of work is still to be done. It is still unclear which numerical method, CCM or hyperboloidal slices, will perform better at radiation extraction at future null infinity. The main goal of this work is to expand on the current applications of the latter method.

We will hence focus on the Einstein-Maxwell-Klein-Gordon system, which has been extensively

investigated in Cauchy slices [11], but never in the hyperboloidal formulation. The question one should be asking now is why this system is interesting. First, it allows us to model a charged complex scalar field, a concept closely related to boson stars [12]. I left some further considerations on scalar fields in D.2, that might help motivate this part. Second, it is possible to model a charged black hole, called the Reissner-Nordström (RN) black hole or Reissner-Nordström solution. One can argue that there are still no conclusive observations pointing to the presence of charge in black holes [13, 14]. Furthermore, it has been stated that since RN black holes behave like a point charge, it is "not likely to be important astrophysically" [15]. However, it preserves spherical symmetry, which is significantly easier to simulate. Also, in the extreme charge-to-mass ratio, i.e., in the limit where the charge equals the mass, RN black holes can give us some insight into the behavior of extremal Kerr black holes (i.e., rotating black holes). Lastly, the whole system will allow one to see exactly how a charged scalar field decays at late-times in charged background, for several papers point to very different behaviours [16, 17].

In the end, by working out the evolution equations of this system in hyperboloidal slices, we provide a continuous formulation of how to evolve initial data for a charged black hole and lay the groundwork for the extraction of gravitational waves in the following years. It will also broaden the understanding of the dynamics between a charged complex scalar field and a charged black hole. Alas, we will see how the electromagnetic interaction between these two charged objects masks the gravitational effects of the curvature, at future null infinity and at timelike infinity [18].

Let us then start this journey.

Chapter 2

Introduction

In this section, we shall start with Einstein's field equations, see how they change under a conformal transformation, and adapt them to the formulation of hyperboloidal slices.

2.1 Einstein's Field Equations

The EFEs are given by:

$$G_{\mu\nu} = 8\pi T_{\mu\nu}, \tag{2.1}$$

where $G_{\mu\nu}$ is the Einstein tensor and $T_{\mu\nu}$ the stress-energy tensor. $G_{\mu\nu}$ is a symmetric divergence-free quantity that describes the geometry of spacetime, and $T_{\mu\nu}$ is the energy and matter content present in it. Energy and matter change the geometry of spacetime, and spacetime tells energy and matter how to behave. I left some phenomenological remarks about this in Sec. D.1. The Einstein tensor is defined as

$$G_{\mu\nu} = R_{\mu\nu} - \frac{1}{2} g_{\mu\nu} R, \tag{2.2}$$

where $R_{\mu\nu}$ is the Ricci tensor, $g_{\mu\nu}$ the metric tensor, and R the Ricci scalar, themselves defined as

$$R = g^{\mu\nu} R_{\mu\nu}, \quad R_{\mu\nu} = R^{\alpha}_{\mu\alpha\nu}, \tag{2.3}$$

where $R^{\alpha}_{\mu\beta\nu}$ is the Riemann tensor, given by

$$R^{\alpha}_{\mu\beta\nu} = \partial_\beta \Gamma^{\alpha}_{\mu\nu} - \partial_\nu \Gamma^{\alpha}_{\mu\beta} + \Gamma^{\alpha}_{\sigma\beta} \Gamma^{\sigma}_{\mu\nu} - \Gamma^{\alpha}_{\sigma\nu} \Gamma^{\sigma}_{\mu\beta}, \tag{2.4}$$

where $\Gamma^{\alpha}_{\mu\nu}$ are called the Christoffel symbols of the second kind. We are only missing out on the definition of the Christoffel symbols in terms of the derivatives of the metric:

$$\Gamma^{\alpha}_{\mu\nu} = \frac{1}{2} g^{\alpha\sigma} (\partial_\mu g_{\nu\sigma} + \partial_\nu g_{\mu\sigma} - \partial_\sigma g_{\mu\nu}). \tag{2.5}$$

Let us now reverse-engineer these definitions to give them some physical meaning. The metric tensor encodes the geometric information of our spacetime. In flat spacetime (called Minkowski spacetime), the metric tensor looks like the following (Diag means diagonal matrix):

$$g_{\mu\nu} = \mathrm{Diag}(-1, 1, 1, 1) \tag{2.6}$$

It treats all the spatial components equivalently and the time component in the opposite fashion. The sign of each component is a matter of convention: the first entry could be positive, and the spatial entries would have to be negative. A concise way of expressing the convention is $(+,-,-,-)$ or $(-,+,+,+)$ and **here the latter one will be used**. The metric is also used to measure distances between points: suppose we had two points separated by a given (very) small distance in space and time, depicted by this displacement vector: $dx^\mu = (dt, dx, dy, dz)$. We could calculate the total distance ds between the two points by using the metric as the inner product matrix, i.e.,

$$ds^2 = dx^\mu dx^\nu g_{\mu\nu} = -dt^2 + dx^2 + dy^2 + dz^2. \tag{2.7}$$

ds^2 is called the line element and is a popular way of writing the solutions to the EFEs. The metric just used has constant coefficients equal to 1, and it corresponds to Minkowski spacetime. For example, for a Schwarzschild black hole [19], we would have

$$ds^2 = -\left(1 - \frac{2M}{r}\right) dt^2 + \left(1 - \frac{2M}{r}\right)^{-1} dr^2 + r^2(d\theta^2 + \sin^2\theta d\phi^2), \tag{2.8}$$

which represents a static black hole, without charge or angular momentum. It is the simplest black hole solution. If the black hole has charge Q [20], it is called the Reissner-Nördstrom black hole. It preserves spherical symmetry, and its line element is written as,

$$ds^2 = -\left(1 - \frac{2M}{r} + \frac{Q^2}{r^2}\right) dt^2 + \left(1 - \frac{2M}{r} + \frac{Q^2}{r^2}\right)^{-1} dr^2 + r^2(d\theta^2 + \sin^2\theta d\phi^2), \tag{2.9}$$

On the other side of (2.1), we have the stress-energy tensor, $T_{\mu\nu}$. Its composition will change according to what we want to model in our system [19]. The equations of motion of this model can be written through the vanishing covariant derivative of $T_{\mu\nu}$,

$$\nabla_\nu T^{\mu\nu} = 0. \tag{2.10}$$

These equations state the conservation of energy and momentum. For the case of the massless scalar field, they translate to:

$$T_{\mu\nu} = \nabla_\mu\phi\nabla_\nu\phi - \frac{1}{2} g_{\mu\nu}\nabla^\alpha\phi\nabla_\alpha\phi, \tag{2.11}$$

where ϕ is the scalar field. If we apply (2.10), we get the Klein-Gordon equation,

$$\nabla^\mu\nabla_\mu\phi = 0. \tag{2.12}$$

Another example is the electromagnetic component, whose stress-energy tensor is given by

$$T_{\mu\nu} = F_{\mu\alpha}F_\nu^\alpha - \frac{1}{4} g_{\mu\nu}F_{\alpha\beta}F^{\alpha\beta}, \tag{2.13}$$

where $F_{\mu\nu}$ is the electromagnetic tensor. Applying (2.10), we get Maxwell's equations,

$$g^{\beta\mu}\nabla_\beta F_{\mu\nu} = 4\pi J_\nu \tag{2.14}$$

$$\nabla_{[\mu} F_{\nu\sigma]} = 0. \tag{2.15}$$

Sometimes, instead of 4π, a -4π will appear. The sign change has to do with the signature of the metric used. In our case, given that we are using $(-,+,+,+)$, the sign should be positive. The last equation can be rewritten in terms of the dual Faraday tensor, defined as,

$$F^*_{\alpha\beta} = \frac{1}{2}\epsilon_{\alpha\beta\mu\nu}F^{\mu\nu} \rightarrow \nabla_{[\mu}F_{\nu\sigma]} = \nabla^{\mu}F^*_{\mu\nu} = 0\,.$$

An alternative way of deriving these equations would be to look at the action that describes the system [11, 21]:

$$S = \int \left(R - 8\pi\left[(\mathcal{D}_\mu\phi)^*(\mathcal{D}^\mu\phi)\right] - F^{\mu\nu}F_{\mu\nu}\right)\sqrt{-g}\,d^4x\,, \tag{2.16}$$

with $\mathcal{D}_\mu = \nabla_\mu + iqA_\mu$ and q being the charge of the complex scalar field. A_μ is the four potential, and we will return to it later. By the usual definition of the stress-energy tensor from the action [19], we recover (2.11) and (2.13). Varying (2.16) with respect to the fields ϕ and $F^{\mu\nu}$, we would get (2.12) and (2.14).

2.2 On Nomenclature, Conventions and the Structure of the Thesis

Throughout this work, we will need to distinguish between different manifolds. We shall: start with the physical metric; compactify it through a conformal transformation; decompose it into the time and spatial parts (ADM equations); and change them into a well-posed formulation (GBSSN+Z4). Thus, we have three different stages, and we must give the appropriate names to each. Parallel to this, we will have some time-independent quantities.

For: **physical quantities**, we will have them with a **tilde on top** : $\tilde{g}_{ab}, \tilde{K}_{ab}, \tilde{\Gamma}^c_{ab}, \tilde{\nabla}_a, \tilde{n}_a$, etc.; **conformally compactified quantities**, with a **bar on top**: $\bar{g}_{ab}, \bar{K}_{ab}, \bar{\Gamma}^c_{ab}, \bar{\nabla}_a, \bar{n}_a$, etc.; **3+1 decomposed and spatially conformally rescaled quantities**, **without anything on top**: $\gamma_{ab}, K_{ab}, \Gamma^c_{ab}, \nabla_a, n_a$, etc.; the **time independent quantities**, with a **hat on top**: $\hat{g}_{ab}, \hat{K}_{ab}, \hat{\Gamma}^c_{ab}, \hat{\nabla}_a, \hat{n}_a$, etc.

2.3 Conformal Transformations

To put infinity in a finite place, we will follow [22], where the benefits of using conformal transformations are explored more indepth. Under this type of transformation, the metric changes as,

$$\bar{g}_{\mu\nu} = \Omega^2\tilde{g}_{\mu\nu}, \tag{2.17}$$

where Ω is called the conformal factor. This factor will be important to take away the divergent terms from the metric, when we put infinity at a finite place.

2.3.1 Cauchy Slices and A Brief Example of a Conformal Transformation

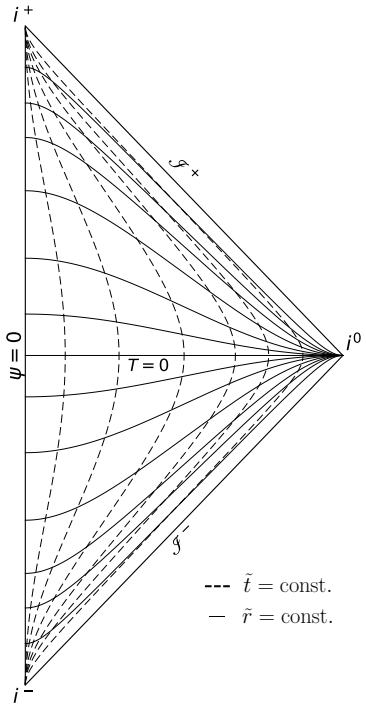

Figure 2.1: Penrose Diagram with lines of constant $\tilde{t}$ (Cauchy slices) and constant $\tilde{r}$.

Let us look at a classic example of a conformal transformation. Consider the flat metric in Minkowski spacetime, given by,

$$d\tilde{s}^2 = -d\tilde{t}^2 + d\tilde{r}^2 + \tilde{r}^2 d\tilde{\sigma}^2.$$

where $d\tilde{\sigma}^2 = d\tilde{\theta}^2 + \sin^2\tilde{\theta} d\tilde{\phi}^2$ is the usual angular part of the line element. Here, $(\tilde{r}, \tilde{t}) \in [0, +\infty[\times]-\infty, +\infty[$. Doing the following change of coordinates,

$$\tilde{t} = \frac{\tan V + \tan U}{2}\,, \qquad \tilde{r} = \frac{\tan V - \tan U}{2}\,,$$

the line element becomes

$$d\tilde{s}^2 = (2\cos U \cos V)^{-2}\left[-4dUdV + \sin^2(V-U)d\tilde{\sigma}^2\right]\,.$$

If we define the conformal factor as $\Omega = 2\cos U \cos V$, the compactified line element reads,

$$d\bar{s}^2 = \Omega^2 d\tilde{s}^2 = -4dUdV + \sin^2(V-U)d\tilde{\sigma}^2\,.$$

We perform a last change of coordinates,

$$T = V + U\,, \qquad \psi = V - U\,, \qquad ds^2 = -dT^2 + d\psi^2 + \sin^2\psi d\tilde{\sigma}^2\,,$$

to reach the coordinates in which the Penrose Diagram is usually written. You can see the diagram in Fig. 2.1. Note the lines of constant $\tilde{t}$, which are called Cauchy Slices. The overall coordinate change can

be expressed as,

$$T = \arctan(\tilde{t}+\tilde{r}) + \arctan(\tilde{t}+\tilde{r}), \quad \psi = \arctan(\tilde{t}+\tilde{r}) - \arctan(\tilde{t}+\tilde{r})\,. \tag{2.18}$$

We are now capable of defining some regions of spacetime, already named in Fig. 2.1: **spatial infinity**, i^0, the place where all slices of constant $\tilde{t}$ will meet, as $\tilde{r} \to +\infty$; **future and past timelike infinities**, $i^{\pm}$, the endpoints of any slice of constant $\tilde{r}$, as $\tilde{t} \to \pm\infty$; and **future and past null infinities**, $\mathscr{I}^{\pm}$, that can only be reached when $\tilde{t} \to \pm\infty$ and $\tilde{r} \to \pm\infty$, but $\tilde{t} - \tilde{r} < \pm\infty$. This latter condition is satisfied solely by null geodesics, i.e., the paths taken by massless particles (photons) or gravitational waves. $\mathscr{I}^{\pm}$ will also be addressed as scri+ and scri-, respectively. Similar (albeit more complicated) compactifications can be made for Kerr black holes, in general. For Schwarzschild and Reissner-Nördstrom Penrose diagrams, check Fig. 2.2. These diagrams were done using Kruskal-Szekeres type coordinates, and we provide the rest of the details of their construction in Appendix C.

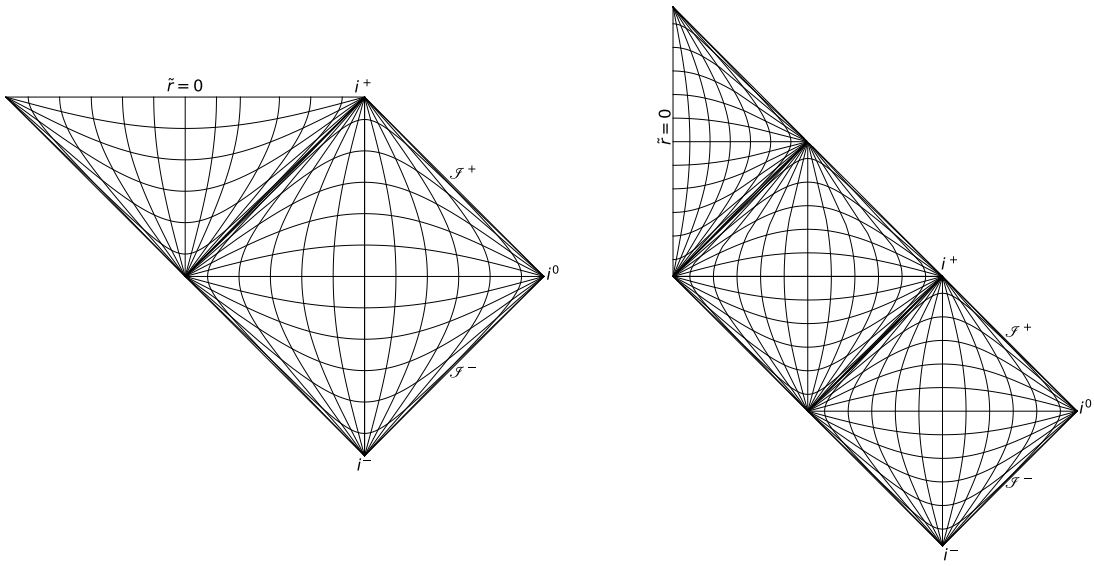

Figure 2.2: Penrose diagrams for Schwarzschild and (non-extremal) Reissner-Nördstrom black hole spacetimes, respectively.

2.3.2 Hyperboloidal Slices

We already saw Cauchy slices in a Penrose Diagram, and now it is time to focus on hyperboloidal slices. The starting point of using this formulation is making a change of time coordinate,

$$\tau = \tilde{t} - h(\tilde{r}), \tag{2.19}$$

where $h(\tilde{r})$ is called the height function [8], that depends only on the spatial components. The behavior that these height functions must follow is that they have to "go up" as $\tilde{r} \to +\infty$, to mimic the behavior of null slices, asymptotically. The derivation of such height functions is varied, and there are several options. An example coming from [10] uses,

$$h(\tilde{r}) = \sqrt{\tilde{r}^2 + \left(\frac{3}{K_{CMC}}\right)^2}, \tag{2.20}$$

where K_{CMC} is the trace of the extrinsic curvature of a Constant Mean Curvature slice (CMC). It means that the positions of static observers in space are expanding, contracting, or unchanging at the same rate. We will define the extrinsic curvature afterward. The idea to retain for now is that K_{CMC} = constant. When we make slices of constant τ (2.19), these are called hyperboloidal slices, depicted in Fig. 2.3. These slices are spacelike (similar to $\tilde{t}$ = ct. slices) but as they approach $\mathscr{I}^+$, they become tangent to null rays (45-degree lines). We will be dealing with this type of slicing condition from now on.

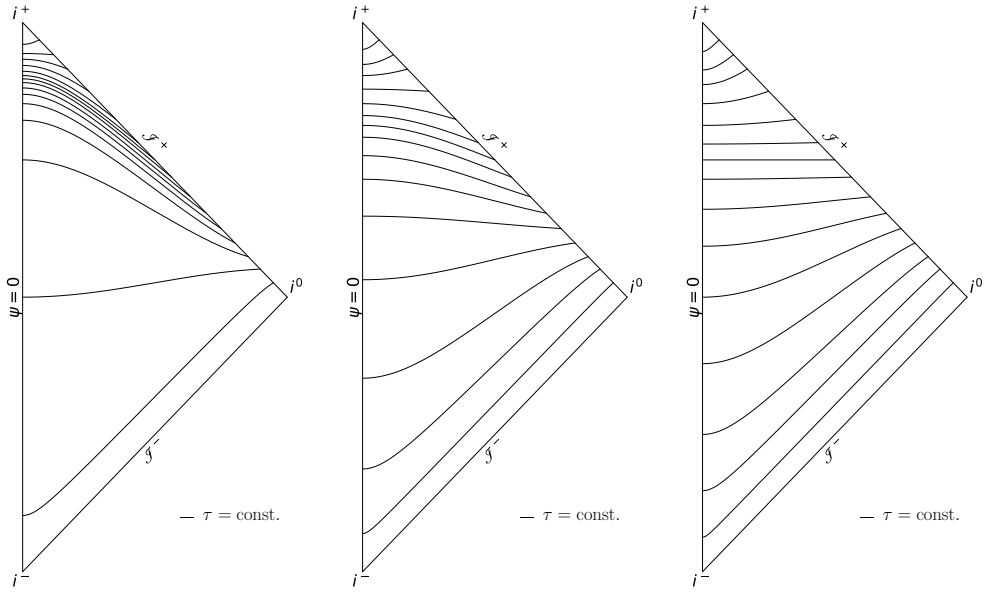

(a) $K_{CMC} = \pm 1$ **(b)** $K_{CMC} = \pm 2$ **(c)** $K_{CMC} = \pm 3$

Figure 2.3: Penrose Diagram with lines of constant τ (Hyperboloidal slices). The slices correspond to the same values of τ but with different values of K_{CMC}.

Regions of Spacetime and Hyperboloidal Slices

In Fig. 2.2, we have two regions, I and II, that correspond to the regions outside and inside the event horizon, respectively. The event horizon corresponds to the coordinate singularity appearing in the line element of Schwarzschild spacetime (2.8), i.e., $\tilde{r} = 2M$. In the diagram, it is the straight line, 45 45-degree inclination, that separates both regions. As we will see after, the hyperboloidal slices in this spacetime continue to reach future null infinity, $\mathscr{I}^+$, although in a slightly different way compared to Fig. 2.3. The specific type of slices we will choose will also be horizon-penetrating, but never touching the singularity, for this would be numerically complicated to evolve. We can now go back to the EFEs (2.1) and see how they change under conformal transformations.

2.4 Einstein's Field Equations Under Conformal Transformations

Here we will follow [10, 23]. Applying a conformal transformation to the metric (2.17), the Christoffel symbols (2.5) change as

$$\tilde{\Gamma}^{\beta}_{\mu\nu} = \bar{\Gamma}^{\beta}_{\mu\nu} - \frac{1}{\Omega}\left(\delta^{\beta}_{\mu}\bar{\nabla}_{\nu}\Omega + \delta^{\beta}_{\nu}\bar{\nabla}_{\mu}\Omega - \bar{g}_{\mu\nu}\bar{g}^{\beta\alpha}\bar{\nabla}_{\alpha}\Omega\right). \tag{2.21}$$

This means that the Riemann tensor transforms as,

$$\tilde{R}_{\alpha\beta\mu\nu} = \bar{R}_{\alpha\beta\mu\nu} + \frac{\bar{g}_{\beta\nu}\bar{\nabla}_\mu\bar{\nabla}_\nu\Omega}{\Omega} - \frac{\bar{g}_{\alpha\mu}\bar{\nabla}_\nu\bar{\nabla}_\beta\Omega}{\Omega} - \frac{\bar{g}_{\beta\mu}\bar{\nabla}_\nu\bar{\nabla}_\alpha\Omega}{\Omega} + \frac{\bar{g}_{\alpha\nu}\bar{\nabla}_\mu\bar{\nabla}_\beta\Omega}{\Omega} + \frac{\bar{g}_{\alpha\mu}\bar{g}_{\beta\mu}\bar{g}_{\iota\xi}\bar{\nabla}^\iota\bar{\nabla}^\xi\Omega}{\Omega^2} - \frac{\bar{g}_{\alpha\mu}\bar{g}_{\beta\nu}\bar{g}_{\iota\xi}\bar{\nabla}^\iota\bar{\nabla}^\xi\Omega}{\Omega^2}. \tag{2.22}$$

From the definitions of the Ricci tensor and scalar (2.3), we get that they must change as,

$$\tilde{R}_{\mu\nu} = \bar{R}_{\mu\nu} + \frac{2\bar{\nabla}_\mu\bar{\nabla}_\nu\Omega}{\Omega} + \frac{\bar{g}_{\mu\nu}\bar{g}^{\alpha\beta}\bar{\nabla}_\alpha\bar{\nabla}_\beta\Omega}{\Omega} - \frac{3\bar{g}_{\mu\nu}\bar{g}^{\alpha\beta}\bar{\nabla}_\alpha\Omega\bar{\nabla}_\beta\Omega}{\Omega^2}, \tag{2.23}$$

$$\tilde{R} = \Omega^2\bar{R} + 6\bar{g}_{\mu\nu}\Omega\bar{\nabla}_\mu\bar{\nabla}_\nu\Omega - 12\bar{g}_{\mu\nu}\bar{\nabla}^\mu\Omega\bar{\nabla}^\nu\Omega. \tag{2.24}$$

Going from (2.2) and adding all the previous results, we see that the EFEs are now given by,

$$\tilde{G}_{\mu\nu} = \bar{G}_{\mu\nu} + \frac{2}{\Omega}(\bar{\nabla}_\mu\bar{\nabla}_\nu\Omega - \bar{g}_{\mu\nu}\bar{\nabla}^\mu\bar{\nabla}_\nu\Omega) + \frac{3}{\Omega^2}\bar{g}_{\mu\nu}\bar{\nabla}^\alpha\Omega\bar{\nabla}_\alpha\Omega = 8\pi\tilde{T}_{\mu\nu}. \tag{2.25}$$

Here $\bar{G}_{\mu\nu}$ is constructed as a function of $\bar{g}_{\mu\nu}$. The other two factors on the LHS of the equation become divergent due to the compactification. The stress-energy tensor should also be written in terms of the rescaled metric and fall off fast enough asymptotically for the whole system to work.

2.5 Z4 Formalism

To have better numerical properties when simulating the system, we introduce here the Z4 formalism [24, 25], which consists of adding a variable $\tilde{Z}_\mu$ to the EFEs. This new formulation reads

$$\tilde{G}_{\mu\nu} + 2\tilde{\nabla}_\mu\tilde{Z}_\nu - \tilde{g}_{\mu\nu}\tilde{\nabla}^\alpha\tilde{Z}_\alpha - \kappa_1(2\tilde{n}_{(\mu}\tilde{Z}_{\nu)} + \kappa_2\tilde{g}_{\mu\nu}\tilde{n}^\alpha\tilde{Z}_\alpha) = 8\pi\tilde{T}_{\mu\nu}, \tag{2.26}$$

where κ_1 and κ_2 being parameters to choose empirically [10]. $\tilde{n}_\mu$ is a unitary timelike normal vector (we will introduce it formally in 3.1). Note that we regain the EFEs (2.1) by setting $\tilde{Z}_\mu = 0$. Equation (2.25), in the Z4 formalism, becomes

$$\tilde{G}_{\mu\nu} + 2\bar{\nabla}_{(\mu}\bar{Z}_{\nu)} - \bar{g}_{\mu\nu}\bar{\nabla}^\alpha\bar{Z}_\alpha + \frac{4}{\Omega}\bar{Z}_{(\mu}\bar{\nabla}_{\nu)}\Omega - \frac{\kappa_1}{\Omega}(2\bar{n}_{(\mu}\bar{Z}_{\nu)} + \kappa_2\bar{g}_{\mu\nu}\bar{n}^\alpha\bar{Z}_\alpha) = 8\pi\tilde{T}_{\mu\nu}. \tag{2.27}$$

If we introduce the Z4 formalism after the conformal transformation, i.e., defining it as a function of the conformally compactified variables, (2.27) would simply look like (pay attention to the tildes and the bars),

$$\tilde{G}_{\mu\nu} + 2\bar{\nabla}_{(\mu}\bar{Z}_{\nu)} - \bar{g}_{\mu\nu}\bar{\nabla}^\alpha\bar{Z}_\alpha - \kappa_1(2\bar{n}_{(\mu}\bar{Z}_{\nu)} + \kappa_2\bar{g}_{\mu\nu}\bar{n}^\alpha\bar{Z}_\alpha) = 8\pi\tilde{T}_{\mu\nu}. \tag{2.28}$$

It was shown that the (2.27) formulation has better stability properties [10], and we will work with that one.

2.6 Maxwell's Equations Under Conformal Transformations

Recalling (2.14), Maxwell's equations [23] are defined as a function of the electromagnetic tensor $\tilde{F}_{\mu\nu}$ and the four-current $\tilde{J}_\nu$. The former is defined in terms of the four-potential $\tilde{A}_\mu$:

$$\tilde{F}_{\mu\nu} = \tilde{\nabla}_\mu\tilde{A}_\nu - \tilde{\nabla}_\nu\tilde{A}_\mu = \partial_\mu\tilde{A}_\nu - \partial_\nu\tilde{A}_\mu. \tag{2.29}$$

To check that these equations can be made conformally invariant, we propose that the (compactified) electromagnetic tensor be defined according to:

$$\bar{F}_{\mu\nu} = \Omega^s \tilde{F}_{\mu\nu}, \tag{2.30}$$

where s is a constant to be determined. Looking at the covariant derivative of the electromagnetic tensor, as done in [23], in n dimensions,

$$\bar{g}^{\beta\mu}\bar{\nabla}_\beta \bar{F}_{\mu\nu} = \Omega^{s+2}\tilde{g}^{\beta\mu}\tilde{\nabla}_\beta \tilde{F}_{\mu\nu} + (n-4+s)\Omega^{s+1}\tilde{g}^{\beta\mu}\tilde{F}_{\mu\nu}\tilde{\nabla}_\beta\Omega\,. \tag{2.31}$$

In the physically relevant case, $n = 4$, imposing $s = 0$ will make the most right-hand-side term vanish. This, in turn, gives,

$$\bar{g}^{\beta\mu}\bar{\nabla}_\beta \bar{F}_{\mu\nu} = \Omega^2\tilde{g}^{\beta\mu}\tilde{\nabla}_\beta \tilde{F}_{\mu\nu}. \tag{2.32}$$

With this, it would already be enough to demonstrate the conformal invariance of Maxwell's equations in vacuum. However, if we consider a non-zero four-current [26, 27], this means that the current must also scale properly under conformal transformations:

$$\bar{J}_\mu = \Omega^2 \tilde{J}_\mu, \tag{2.33}$$

to preserve the invariance of the equations, as was already observed in [27]. This will be checked later with the conserved current coming from the Klein-Gordon field. As a side note, the value of $s-2$ is related to the mass of the photon. In [26], it is proposed that the conformal factor Ω can be considered as a background field related to electromagnetism. Our choice, $s = 0$, indicates we are assuming that the photon is massless. Proca dynamics would require a different value. That is beyond the scope of this work. Note also that (2.29) implies that the electromagnetic potential A_μ does not change under conformal transformations.

2.7 Klein-Gordon Equation Under Conformal Transformations

Similar to before, we propose that the scalar field changes, under a conformal transformation, as

$$\bar{\phi} = \Omega^s\tilde{\phi} \tag{2.34}$$

Thus, (2.12) becomes,

$$\begin{aligned}\bar{g}^{\mu\nu}\bar{\nabla}_\mu\bar{\nabla}_\nu\bar{\phi} = \Omega^{s-2}\tilde{g}^{\mu\nu}\tilde{\nabla}_\mu\tilde{\nabla}_\nu\tilde{\phi} + (2s+n-2)\Omega^{s-3}\tilde{g}^{\mu\nu}\tilde{\nabla}_\mu\Omega\tilde{\nabla}_\nu\tilde{\phi} \\ + s\Omega^{s-3}\tilde{\phi}\tilde{g}^{\mu\nu}\tilde{\nabla}_\mu\tilde{\nabla}_\nu\Omega + s(n+s-3)\Omega^{s-4}\tilde{\nabla}_\mu\Omega\tilde{\nabla}_\nu\Omega\end{aligned}$$

Only when $n = 2$ and $s = 0$ is the Klein-Gordon (KG) equation conformally invariant. In our case, where $n = 4$, we get,

$$\bar{g}^{\mu\nu}\bar{\nabla}_\mu\bar{\nabla}_\nu\bar{\phi} = \Omega^{s-2}\tilde{g}^{\mu\nu}\tilde{\nabla}_\mu\tilde{\nabla}_\nu\tilde{\phi} + (2s+2)\Omega^{s-3}\tilde{g}^{\mu\nu}\tilde{\nabla}_\mu\Omega\tilde{\nabla}_\nu\tilde{\phi}+$$

$$+s\Omega^{s-3}\tilde{\phi}\tilde{g}^{\mu\nu}\tilde{\nabla}_\mu\tilde{\nabla}_\nu\Omega + s(1+s)\Omega^{s-4}\tilde{\nabla}_\mu\Omega\tilde{\nabla}_\nu\Omega,$$

and the simplest transformation happens when $s = -1$ (this can be generalized [23] for n dimensions, where $s = 1 - n/2$)):

$$\bar{g}^{\mu\nu}\bar{\nabla}_\mu\bar{\nabla}_\nu\bar{\phi} = \Omega^{-3}\tilde{g}^{\mu\nu}\tilde{\nabla}_\mu\tilde{\nabla}_\nu\tilde{\phi} - \Omega^{-4}\tilde{\phi}\tilde{g}^{\mu\nu}\tilde{\nabla}_\mu\tilde{\nabla}_\nu\Omega. \tag{2.35}$$

In the case we are considering, the massless KG equation, this would give us that the conformal KG equation is,

$$\bar{g}^{\mu\nu}\bar{\nabla}_\mu\bar{\nabla}_\nu\bar{\phi} = -\Omega^{-4}\tilde{\phi}\tilde{g}^{\mu\nu}\tilde{\nabla}_\mu\tilde{\nabla}_\nu\Omega, \tag{2.36}$$

where the conformal factor would appear as a new potential for the KG conformally compactified field (we used (2.12) to conclude this). There is an alternative way of writing the KG equation so that it is conformally invariant, involving the use of the Ricci scalar, but we shall not go into this. This choice makes the presence of formally singular terms unavoidable. However, if the simulation can handle them, then the conformally invariant formulation should not present a problem. To get the charged Klein-Gordon equation one has to change the covariant derivative in (2.12) for the covariant derivative concerning the electromagnetic field, $\mathcal{D}_\mu = \nabla_\mu + iqA_\mu$, where q is the charge of the scalar field:

$$\tilde{g}^{\mu\nu}\tilde{\mathcal{D}}_\mu\tilde{\mathcal{D}}_\nu\tilde{\phi} = 0 \iff \tilde{g}^{\mu\nu}(\tilde{\nabla}_\mu + iq\tilde{A}_\mu)(\tilde{\nabla}_\nu + iq\tilde{A}_\nu)\tilde{\phi} = 0\,. \tag{2.37}$$

In the conformal compactified world, it reads

$$\begin{aligned} &- q^2\bar{A}_\mu\bar{A}^\mu\Omega^3\bar{\phi} + iq\Omega^3\bar{\phi}\bar{\nabla}_\mu\bar{A}^\mu + 2iq\bar{A}^\mu\Omega^3\bar{\nabla}_\mu\bar{\phi} + \bar{g}^{\mu\nu}\Omega^2\bar{\phi}\bar{\nabla}_\nu\bar{\nabla}_\mu\Omega \\ &+ \bar{g}^{\mu\nu}\Omega^3\bar{\nabla}_\nu\bar{\nabla}_\mu\bar{\phi} - 2\bar{g}_{\mu\nu}\Omega\bar{\phi}\bar{\nabla}^\mu\Omega\bar{\nabla}^\nu\Omega = 0\,. \end{aligned} \tag{2.38}$$

If we are to impose the physical Lorenz gauge, $\tilde{\nabla}_\mu\tilde{A}^\mu = 0$, (2.38) becomes,

$$-q^2\bar{A}_\mu\bar{A}^\mu\Omega^3\bar{\phi} + 2iq\bar{A}^\mu\Omega^2\bar{\phi}\bar{\nabla}_\mu\Omega + 2iq\bar{A}^\mu\Omega^3\bar{\nabla}_\mu\bar{\phi} - 2\Omega\bar{\phi}\bar{\nabla}_\mu\Omega\bar{\nabla}^\mu\Omega + \bar{g}^{\mu\nu}\Omega^2\bar{\phi}\bar{\nabla}_\nu\bar{\nabla}_\mu\Omega + \bar{g}^{\mu\nu}\Omega^3\bar{\nabla}_\nu\bar{\nabla}_\mu\bar{\phi} = 0\,,$$

while if we use the conformal Lorenz gauge, $\bar{\nabla}_\mu\bar{A}^\mu = 0$, we get

$$-q^2\bar{A}_\mu\bar{A}^\mu\Omega^3\bar{\phi} + 2iq\bar{A}^\mu\Omega^3\bar{\nabla}_\mu\bar{\phi} - 2\Omega\bar{\phi}\bar{\nabla}_\mu\Omega\bar{\nabla}^\mu\Omega + \bar{g}^{\mu\nu}\Omega^2\bar{\phi}\bar{\nabla}_\nu\bar{\nabla}_\mu\Omega + \bar{g}^{\mu\nu}\Omega^3\bar{\nabla}_\nu\bar{\nabla}_\mu\bar{\phi} = 0\,.$$

We will discuss the Lorenz gauge in more detail afterward.

Conserved Current

The stress-energy component of the complex scalar field is invariant under local $U(1)$ transformations [28],

$$\tilde{\phi} \to e^{iq\theta(x^\alpha)}\tilde{\phi}, \quad \tilde{A}_\mu \to \tilde{A}_\mu - \partial_\mu\theta(x^\alpha) \tag{2.39}$$

and, by Noether's theorem, if there is some degree of symmetry to our system, this implies a conserved current. Perturbing our field $\tilde{\phi} \to e^{iq\theta(x^\alpha)}\tilde{\phi}$, this means that

$$\delta\tilde{\phi} = iq\theta(x^\alpha)\tilde{\phi}, \quad \delta\tilde{\phi}^* = -iq\theta(x^\alpha)\tilde{\phi}^*. \tag{2.40}$$

Noether's theorem then states that our conserved current is given by,

$$\tilde{J}_\nu = \frac{\partial\mathcal{L}}{\partial(\partial^\mu\tilde{\phi})}\delta\tilde{\phi} + \frac{\partial\mathcal{L}}{\partial(\partial^\mu\tilde{\phi}^*)}\delta\tilde{\phi}^*, \tag{2.41}$$

where $\mathcal{L}$ is the lagrangian density, corresponding to the integrand in (2.16). This gives us [29, 12, 11, 30],

$$\tilde{J}_\nu = i\left(\left(\tilde{\mathcal{D}}_\nu\tilde{\phi}\right)^*\tilde{\phi} - \left(\tilde{\mathcal{D}}_\nu\tilde{\phi}\right)\tilde{\phi}^*\right). \tag{2.42}$$

Writing the conserved current explicitly as a function of the rescaled variables, we get,

$$\tilde{J}_\mu = \Omega^2(-q^2\bar{A}_\mu\bar{\phi}^*\bar{\phi} - \tfrac{1}{2}iq\bar{\phi}\bar{\nabla}_\mu\bar{\phi}^* + \tfrac{1}{2}iq\bar{\phi}^*\bar{\nabla}_\mu\bar{\phi}). \tag{2.43}$$

If we define the compactified four current $\bar{J}_\mu$ as

$$\bar{J}_\mu = -q^2\bar{A}_\mu\bar{\phi}^*\bar{\phi} - \tfrac{1}{2}iq\bar{\phi}\bar{\nabla}_\mu\bar{\phi}^* + \tfrac{1}{2}iq\bar{\phi}^*\bar{\nabla}_\mu\bar{\phi}\,, \tag{2.44}$$

we have made sure that $\tilde{J}_\nu$ does in fact change as,

$$\tilde{J}_\nu = \Omega^2\bar{J}_\nu\,. \tag{2.45}$$

We have ensured that Maxwell's equations are conformally invariant. The set of rules that describes how the electromagnetic fields change is shown in Sec. 3.4.1. It will be with the conformally compactified current that we shall work with. Let us now move on to the last thing affected by the conformal transformations, the stress-energy tensor.

2.8 Stress-energy Tensor Under Conformal Transformations

The stress-energy tensor, when one takes into account several fields (recall (2.11), (2.13)), can be divided into the corresponding components. The resulting stress-energy tensor will be the sum of these components. Thus, to take into account the charged scalar field $\tilde{\phi}$ and Maxwell's equations, we have [11],

$$\begin{aligned}
(\tilde{T}_{\text{em.}})_{\mu\nu} &= \frac{1}{4\pi}\left[\tilde{F}_{\mu\lambda}\tilde{F}^\lambda_\nu - \frac{1}{4}\tilde{g}_{\mu\nu}\tilde{F}_{\lambda\sigma}\tilde{F}^{\lambda\sigma}\right], \\
(\tilde{T}_\phi)_{\mu\nu} &= \frac{1}{2}\left[(\tilde{\mathcal{D}}_\mu\tilde{\phi})^*(\tilde{\mathcal{D}}_\nu\tilde{\phi}) + (\tilde{\mathcal{D}}_\nu\tilde{\phi})(\tilde{\mathcal{D}}_\mu\tilde{\phi})^* - \tilde{g}_{\mu\nu}\left((\tilde{\mathcal{D}}_\lambda\tilde{\phi})(\tilde{\mathcal{D}}^\lambda\tilde{\phi})^*\right)\right], \\
\tilde{T}_{\mu\nu} &= (\tilde{T}_{\text{em.}})_{\mu\nu} + (\tilde{T}_\phi)_{\mu\nu}.
\end{aligned} \tag{2.46}$$

Under conformal transformations, recall that we have $\bar{F}_{\mu\nu} = \tilde{F}_{\mu\nu}$. This means that [27],

$$\tilde{F}_{\mu\nu} = F_{\mu\nu}, \quad \tilde{F}^{\mu}_{\nu} = \Omega^2 \bar{F}^{\mu}_{\nu}, \quad \tilde{F}^{\mu\nu} = \Omega^4 \bar{F}^{\mu\nu}.$$

Therefore we conclude that $\tilde{T}_{\text{em.}} = \Omega^2 \bar{T}_{\text{em.}}$. The complex charged scalar field, on the other hand, does not have such a simple transformation. Inserting (2.34) into the stress-energy tensor component of the KG field, we get,

$$\begin{aligned}
(\tilde{T}_{\phi})_{\mu\nu} = {} & q^2 \bar{A}_{\mu}\bar{A}_{\nu}\bar{\phi}^{*}\Omega^6\bar{\phi} - \tfrac{1}{2}q^2\bar{A}_{\sigma}\bar{A}^{\sigma}\bar{\phi} * \bar{g}_{\mu\nu}\Omega^6\bar{\phi} + \tfrac{1}{2}iq\bar{A}_{\nu}\Omega^4\bar{\phi}\bar{\nabla}_{\mu}\bar{\phi}^{*} - \tfrac{1}{2}iq\bar{A}_{\nu}\bar{\phi} * \Omega^4\bar{\nabla}_{\mu}\bar{\phi} \\
& + \tfrac{1}{2}iq\bar{A}_{\mu}\Omega^4\bar{\phi}\bar{\nabla}_{\nu}\bar{\phi}^{*} + \tfrac{1}{2}\Omega\bar{\phi}\bar{\nabla}_{\mu}\Omega\bar{\nabla}_{\nu}\bar{\phi} * + \tfrac{1}{2}\Omega^2\bar{\nabla}_{\mu}\bar{\phi}\bar{\nabla}_{\nu}\bar{\phi}^{*} + \tfrac{1}{2}\Omega\bar{\phi}\bar{\nabla}_{\mu}\bar{\phi}^{*}\bar{\nabla}_{\nu}\Omega + \bar{\phi}^{*}\bar{\phi}\bar{\nabla}_{\mu}\Omega\bar{\nabla}_{\nu}\Omega \\
& + \tfrac{1}{2}\bar{\phi}^{*}\Omega\bar{\nabla}_{\mu}\bar{\phi}\bar{\nabla}_{\nu}\Omega - \tfrac{1}{2}iq\bar{A}_{\mu}\bar{\phi}^{*}\Omega^4\bar{\nabla}_{\nu}\bar{\phi} + \tfrac{1}{2}\Omega^2\bar{\nabla}_{\mu}\bar{\phi}^{*}\bar{\nabla}_{\nu}\bar{\phi} + \tfrac{1}{2}\bar{\phi}^{*}\Omega\bar{\nabla}_{\mu}\Omega\bar{\nabla}_{\nu}\bar{\phi} \\
& - \tfrac{1}{2}iq\bar{A}^{\sigma}\bar{g}_{\mu\nu}\Omega^4\bar{\phi}\bar{\nabla}_{\sigma}\bar{\phi}^{*} + \tfrac{1}{2}iq\bar{A}^{\sigma}\bar{\phi}^{*}\bar{g}_{\mu\nu}\Omega^4\bar{\nabla}_{\sigma}\bar{\phi} - \tfrac{1}{2}\bar{g}_{\mu\nu}\Omega\bar{\phi}\bar{\nabla}_{\sigma}\Omega\bar{\nabla}^{\sigma}\bar{\phi}^{*} - \tfrac{1}{2}\bar{g}_{\mu\nu}\Omega^2\bar{\nabla}_{\sigma}\bar{\phi}\bar{\nabla}^{\sigma}\bar{\phi} * \\
& - \tfrac{1}{2}\bar{\phi}^{*}\bar{g}_{\mu\nu}\bar{\phi}\bar{\nabla}_{\sigma}\Omega\bar{\nabla}^{\sigma}\Omega - \tfrac{1}{2}\bar{\phi} * \bar{g}_{\mu\nu}\Omega\bar{\nabla}_{\sigma}\bar{\phi}\bar{\nabla}^{\sigma}\Omega
\end{aligned}$$

It is clear from this that the whole stress-energy tensor is not conformally invariant.

Having derived the conformal Z4 formulation of the EFEs, it is now time for the 3+1 decomposition.

Chapter 3

3+1 Decomposition

3+1 decomposition, a standard procedure in Numerical Relativity (NR), is the act of defining a spacetime foliation, Σ, that slices the 4 dimensions into a continuous family of non-intersecting 3D hypersurfaces, with a normal vector orthogonal to them (hence the +1). At the end of this section, we will have the partial differential equations (PDEs) that describe the evolution and constraints of the Einstein-Maxwell-Klein-Gordon system.

3.1 Lapse and Shift

The foliations can be thought of as the level curves of a scalar function ϕ, called the time function [19]. Other authors call it t [10]. We shall stick to the latter convention to not create confusion with the complex scalar field ϕ. The normal vector to the hypersurfaces, $\bar{n}^\mu$, must then be proportional to the gradient of the time function (we call this factor of proportionality N for now). We shall require that the normal is unitary and future-pointing:

$$\bar{n}_\mu = -N\nabla_\mu t \ , \qquad N^2 = -\frac{1}{g^{\mu\nu}\nabla_\mu t \nabla_\nu t} \ . \tag{3.1}$$

Following [19], consider an arbitrary congruence of curves that are nowhere tangent to the slices of the foliation Σ_t (a fibration). The vector that identifies the points of a given slice to the points in the next slice is called a rigging vector and we shall call it T^μ. This vector will have a component parallel to $\bar{n}^\mu$ and another one tangent to the hypersurfaces, β^μ, being defined as

$$T^\mu = \alpha \bar{n}^\mu + \beta^\mu \tag{3.2}$$

The mapping from Σ_t to $\Sigma_{t+\delta t}$ is, very loosely, $\delta t T^\mu$. Given (3.1), then, in order to restore the physical significance of T^μ, we must have,

$$\alpha^2 = N^2 = -\frac{1}{g^{\mu\nu}\nabla_\mu t \nabla_\nu t} \ . \tag{3.3}$$

α is called the lapse because of this. β, on the other hand, is intuitively the "spatial shift" in the hypersurface that occurs when passing on from Σ_t to $\Sigma_{t+\delta t}$. Thus, it is called the shift. All of these definitions can be reverted to get a new way of writing the normal vector,

$$\bar{n}^\mu = \frac{1}{\alpha}\left(T^\mu - \beta^\mu\right) \tag{3.4}$$

To maintain the unitary characteristic of the normal vector (recall 2.5), when passing from the physical to the conformally compactified worlds, we impose that $\tilde{n}_\mu \tilde{n}^\mu = \bar{n}_\mu \bar{n}^\mu = -1$. This also implies that the normal vector changes as,

$$\tilde{n}^\mu = \Omega \bar{n}^\mu, \quad \tilde{n}_\mu = \Omega^{-1} \bar{n}_\mu. \tag{3.5}$$

3.2 Induced Metric and Extrinsic Curvature

Let us define the induced metric $\bar{\gamma}_{\mu\nu}$ as,

$$\bar{\gamma}_{\mu\nu} = \bar{g}_{\mu\nu} + \bar{n}_\mu \bar{n}_\nu \quad . \tag{3.6}$$

This metric describes the 3D foliations and is defined as such to take away any contributions along the normal vector when applied to any tensor. Another way of looking at it is that the metric projects quantities along spacelike hypersurfaces. If we pick (3.4), we can get an equation that describes the metric $\bar{g}_{\mu\nu}$ as a function of the induced metric, the lapse, and the shift. Using the fact that β^μ is tangent to the foliations, if we are to define $T = \partial_t$, this imposes β as only having spatial components $\beta^\mu = (0, \beta^i)$. From now on, Latin indices shall always be used together with spatial quantities only, while Greek ones will be used for 4-dimensional tensors. In adapted coordinates, the metric then takes the form,

$$\bar{g}_{\mu\nu} = \begin{pmatrix} -\bar{\alpha}^2 + \beta_m \beta^m & \beta_j \\ \beta_i & \bar{\gamma}_{ij} \end{pmatrix}, \qquad \bar{g}^{\mu\nu} = \frac{1}{\bar{\alpha}^2} \begin{pmatrix} -1 & \beta^j \\ \beta^i & \bar{\alpha}^2 \bar{\gamma}^{ij} - \beta^i \beta^j \end{pmatrix}, \tag{3.7}$$

where $\bar{\gamma}^{ij}$ is the strictly spatial part of $\bar{\gamma}^{\mu\nu}$ ($\bar{\gamma}^{\mu\nu} = (0, \bar{\gamma}^{ij})$). The line element $d\bar{s}^2$ becomes,

$$d\bar{s}^2 = \bar{g}_{\mu\nu} d\bar{x}^\mu d\bar{x}^\nu = -(\bar{\alpha}^2 - \beta_m \beta^m) d\bar{t}^2 + 2\beta_j d\bar{t} d\bar{x}^j + \bar{\gamma}_{ij} d\bar{x}^i d\bar{x}^j \tag{3.8}$$

From this, we can also define a projecting operator [19, 10]. It is usually called B^ν_μ, but this letter will be for the magnetic field. We will call it $\bar{\perp}^\nu_\mu$:

$$\bar{\perp}^\nu_\mu = \delta^\nu_\mu + \bar{n}^\mu \bar{n}_\nu \,, \tag{3.9}$$

that is equivalent to (3.6) by raising one index. This allows us to define the extrinsic curvature,

$$\bar{K}_{ij} = -\bar{\perp}^\mu_i \bar{\nabla}_\mu \bar{n}_j \,. \tag{3.10}$$

If one checks the expression of $\mathcal{L}_n \bar{\gamma}_{ij}$, one immediately reaches the following equation,

$$\mathcal{L}_{\bar{n}} \bar{\gamma}_{ij} = -2\bar{K}_{ij} \tag{3.11}$$

where $\mathcal{L}_{\bar{n}}$ is the Lie derivative along the normal vector. These equations are not only a definition of $\bar{K}_{ij}$ but also the evolution equations for the induced metric components. We can then interpret the extrinsic curvature as how much a surface is "moving" perpendicular to it at a specific point. The next steps of the 3+1 decomposition of the EFEs require some algebraic manipulation. We will sketch them briefly, but redirect the reader to more informative references if needed [28, 19].

3.3 3+1 Decomposition of Einstein's Equations

3.3.1 Projections of Riemann tensor

Let $\bar{D}_a$ be the induced covariant derivative and $\bar{R}^3_{abcd}$ the Riemann tensor defined from the induced Christoffel symbols. Start with the projections of the Riemann tensor [19],

$$\bar{\perp}^e_a \bar{\perp}^f_b \bar{\perp}^g_c \bar{\perp}^h_d \bar{R}_{efgh} = \bar{R}^3_{abcd} + \bar{K}_{ad}\bar{K}_{bc} - \bar{K}_{ac}K_{bd} \tag{3.12}$$

$$\bar{\perp}^e_a \bar{\perp}^f_b \bar{\perp}^g_c \bar{n}^h \bar{R}_{efgh} = \bar{D}_b \bar{K}_{ac} - \bar{D}_a \bar{K}_{bc} \tag{3.13}$$

$$\bar{\perp}^e_a \bar{\perp}^f_c \bar{n}^b \bar{n}^d \bar{R}_{ebfd} = \mathcal{L}_{\bar{n}} \bar{K}_{ab} + \frac{1}{\bar{\alpha}} \bar{D}_a \bar{D}_c \bar{\alpha} + \bar{K}_{ac}\bar{K}^d_c \tag{3.14}$$

Each of these equations has a name: the Gauss equation (3.12), the Codazzi equation (3.13), and the Ricci equation (3.14). When we contract the Gauss equation with $\bar{\gamma}^{ac} = \bar{g}^{ac} + \bar{n}^a \bar{n}^c$, we get,

$$\bar{\perp}^f_b \bar{\perp}^h_d \bar{R}_{fh} - \bar{n}^e \bar{n}^b \bar{\perp}^f_b \bar{\perp}^h_d \bar{R}_{efgh} = \bar{R}^3_{bd} + \bar{K}^a_a \bar{K}_{bd} - \bar{K}^a_d \bar{K}_{ba} \tag{3.15}$$

And if we again contract in order to take out the projection operators,

$$\bar{R}^3 - 2\bar{n}^b \bar{n}^d \bar{R}_{bd} = \bar{R}^3 + \bar{K}^a_a \bar{K}^b_b - \bar{K}^{ab}\bar{K}_{ab} = 2\bar{n}^a \bar{n}^b \bar{G}_{ab} \tag{3.16}$$

We just then have to insert (2.27) to reach

$$\begin{aligned} \bar{R} + \bar{K}^2 - \bar{K}_{ab}\bar{K}^{ab} + \frac{4\left(\bar{\gamma}^{ab}\bar{D}_a\bar{D}_b\Omega + \bar{K}\mathcal{L}_{\bar{n}}\Omega\right)}{\Omega} + \frac{6\left[(\mathcal{L}_{\bar{n}}\Omega)^2 - \bar{\gamma}^{ab}(\bar{D}_a\Omega)(\bar{D}_b\Omega)\right]}{\Omega^2} \\ - 2\bar{K}\Theta + 2\bar{D}_a Z^a - \frac{2Z^a\bar{D}_a\bar{\alpha}}{\bar{\alpha}} - \frac{2\kappa_1(2+\kappa_2)\Theta}{\Omega} - 2\mathcal{L}_n\Theta - \frac{8\Theta\mathcal{L}_n\Omega}{\Omega} = 16\pi\rho, \end{aligned} \tag{3.17}$$

where $\Theta = -\bar{n}^a \bar{Z}_a$ and $Z^a = \bar{\perp}^a_b \bar{Z}^b$ correspond to the 3+1 decomposition of Z^a. The ρ on the RHS of the equation is one of the contractions of the stress-energy tensor, $\rho = \bar{n}^\mu \bar{n}^\nu \bar{T}_{\mu\nu}$. It can be interpreted as the total energy of the system [31]. There are other projections of the stress-energy tensor that will be useful afterward,

$$\bar{J}^\mu = -\bar{\perp}^{\mu\nu}\bar{n}^\alpha \bar{T}_{\nu\alpha}, \quad \bar{S}_{\mu\nu} = \bar{\perp}^\alpha_\mu \bar{\perp}^\beta_\nu \bar{T}_{\alpha\beta}, \quad \bar{S} = \bar{\gamma}^{\mu\nu}\bar{S}_{\mu\nu}, \tag{3.18}$$

According to [31], $\bar{J}^a$ is called the momentum density, S_{ab} is called the spatial stress tensor and S its trace. Note that equation (3.17) will become the evolution equation for the Θ variable. It is also the Hamiltonian constraint, when setting $\Theta = Z^a = 0$.

3.3.2 ADM equations

Contracting the Codazzi equation (3.13) we get,

$$\bar{\perp}^c_b \bar{n}^d \bar{R}_{cd} = \bar{D}_b \bar{K}^a_a - \bar{D}_a \bar{K}^a_b, \tag{3.19}$$

but also note that

$$\bar{\perp}^c_b \bar{n}^d \bar{G}_{cd} = \bar{D}_b \bar{K}^a_a - \bar{D}_a \bar{K}^a_b. \tag{3.20}$$

From the EFEs, we get $\perp^c_b \bar{n}^d \bar{G}_{cd} = \perp^c_b \bar{n}^d \bar{T}_{cd} = -\bar{J}_b$. Thus, we get:

$$\begin{aligned} \bar{D}_b \bar{K}^{ab} - \bar{D}^a \bar{K} - \frac{2\left[\bar{K}^{ab}\bar{D}_b\Omega + \bar{\gamma}^{ab}\bar{D}_b\mathcal{L}_{\bar{n}}\Omega\right]}{\Omega} - 2\bar{K}^{ab}Z_b - \frac{\kappa_1 Z^a}{\Omega} + \gamma^{ab}\bar{D}_b\Theta \\ -\frac{\bar{\gamma}^{ab}\Theta\bar{D}_b\alpha}{\alpha} + \frac{2\bar{\gamma}^{ab}\Theta\bar{D}_b\Omega}{\Omega} - \bar{\gamma}^{ab}\mathcal{L}_{\bar{n}}Z_b - \frac{2Z^a\mathcal{L}_{\bar{n}}\Omega}{\Omega} = 8\pi\bar{J}^a \end{aligned}, \tag{3.21}$$

which will serve as an evolution equation for the Z^a variable. This equation is also called the momentum constraint, when $Z^a = \Theta = 0$. Together with the Hamiltonian constraint, it becomes clearer that the Z4 variables serve to control the behaviour of the constraints and propagate away constraint violations. Going back to (3.15), the second term of the LHS is the same as the LHS of the Ricci equation (3.14). Putting everything together,

$$\begin{aligned} \perp^c_a \perp^d_b \bar{R}_{cd} = \perp^c_a \perp^d_b \Bigg[8\pi\left(\bar{T}_{cd} - \frac{1}{2}\bar{g}_{cd}\bar{g}^{ef}\bar{T}_{ef}\right) - \left(\frac{2\bar{\nabla}_a\bar{\nabla}_b\Omega + \bar{g}_{ab}\bar{\Box}\Omega}{\Omega} - \frac{3\bar{g}_{ab}(\bar{\nabla}_c\Omega)(\bar{\nabla}^c\Omega)}{\Omega^2}\right) \\ -\left(2\bar{\nabla}_{(a}\bar{Z}_{b)} + \frac{4\bar{Z}_{(a}\bar{\nabla}_{b)}\Omega}{\Omega} - \frac{2\bar{g}_{ab}\bar{Z}^c\bar{\nabla}_c\Omega}{\Omega} - \frac{\kappa_1(2\bar{n}_{(a}\bar{Z}_{b)} - (1+\kappa_2)\bar{g}_{ab}\bar{n}^c\bar{Z}_c)}{\Omega}\right)\Bigg], \end{aligned} \tag{3.22}$$

where $\bar{\Box} = \bar{g}^{ab}\bar{\nabla}_a\bar{\nabla}_b$ is the D'Alembertian. The equation rewritten is an evolution equation for the extrinsic curvature,

$$\begin{aligned} \mathcal{L}_{\bar{n}}\bar{K}_{ab} = -\frac{1}{\bar{\alpha}}\bar{D}_a\bar{D}_b\bar{\alpha} + \bar{R} - 2\bar{K}_{ac}\bar{K}^c_{\ b} + \bar{K}_{ab}(\bar{K} - 2\Theta) + 2\bar{D}_{(a}Z_{b)} - \frac{\kappa_1(1+\kappa_2)\bar{\gamma}_{ab}\Theta}{\Omega} \\ + 3\bar{\gamma}_{ab}\left[\frac{(\partial_\perp\Omega)^2 - \bar{\alpha}^2\bar{D}_c\Omega\bar{D}^c\Omega}{\bar{\alpha}^2\Omega^2}\right] + \frac{4Z_{(a}\bar{D}_{b)}\Omega}{\Omega} + \frac{2\bar{D}_b\bar{D}_a\Omega}{\Omega} - \frac{2\gamma_{ab}Z^c\bar{D}_c\Omega}{\Omega} + \frac{\bar{\gamma}_{ab}\bar{D}^c\bar{\alpha}\bar{D}_c\Omega}{\bar{\alpha}\Omega}, \\ + \frac{\bar{\gamma}_{ab}\Delta\Omega}{\Omega} + \frac{2\bar{K}_{ab}\mathcal{L}_{\bar{n}}\Omega}{\Omega} + \frac{\bar{\gamma}_{ab}(\bar{K} - 2\Theta)\mathcal{L}_{\bar{n}}\Omega}{\Omega} - \frac{\bar{\gamma}_{ab}\mathcal{L}_{\bar{n}}\mathcal{L}_{\bar{n}}\Omega}{\Omega} + 4\pi[\bar{\gamma}_{ab}(S-\rho) - 2S_{ab}] \end{aligned} \tag{3.23}$$

where we define $\partial_\perp = \partial_t - \mathcal{L}_\beta$ to be the partial derivative along the normal vector. Having finished all the decompositions of the Riemann tensor and extracted all the information we needed, we can now add a coordinate system to these equations. We will define $\mathcal{L}_n = \frac{\partial_\perp}{\bar{\alpha}}$, which means that $\mathcal{L}_n = \frac{\partial_t - \mathcal{L}_\beta}{\bar{\alpha}}$. Writing all of the equations as evolution equations, we get,

$$\begin{aligned} \partial_\perp\bar{\gamma}_{ab} &= \mathcal{L}_\beta\bar{\gamma}_{ab} - 2\bar{\alpha}\bar{K}_{ab}, \\ \partial_\perp\bar{K}_{ab} &= \mathcal{L}_\beta\bar{K}_{ab} + \bar{\alpha}\left[\bar{R}_{ab} - 2\bar{K}^c_a\bar{K}_{bc} + \bar{K}_{ab}(\bar{K} - 2C_{Z_4c}\Theta) + 2\bar{D}_{(a}\bar{Z}_{b)} - \frac{\kappa_1(1+\kappa_2)\bar{\gamma}_{ab}\Theta}{\Omega}\right] - \bar{D}_b\bar{D}_a\bar{\alpha} \\ &\quad + 3\bar{\gamma}_{ab}\left[\frac{(\partial_\perp\Omega)^2 - \bar{\alpha}^2\bar{D}_c\Omega\bar{D}^c\Omega}{\bar{\alpha}^2\Omega^2}\right] + \frac{4\bar{\alpha}\bar{Z}_{(a}\bar{D}_{b)}\Omega}{\Omega} + \frac{2\bar{\alpha}\bar{D}_b\bar{D}_a\Omega}{\Omega} - \frac{2\bar{\alpha}\bar{\gamma}_{ab}\bar{Z}^c\bar{D}_c\Omega}{\Omega} \\ &\quad + \frac{\bar{\gamma}_{ab}\partial_\perp\Omega\partial_\perp\Omega}{\bar{\alpha}^2\Omega} + \frac{\bar{\gamma}_{ab}\Delta\Omega}{\Omega} + \frac{2\bar{K}_{ab}\partial_\perp\Omega}{\Omega} + \frac{\bar{\gamma}_{ab}(\bar{K} - 2C_{Z_4c}\Theta)\partial_\perp\Omega}{\Omega} - \frac{\bar{\gamma}_{ab}\partial_\perp\partial_\perp\Omega}{\Omega} \\ &\quad + 4\pi\bar{\alpha}[\bar{\gamma}_{ab}(\bar{S} - \bar{\rho}) - 2\bar{S}_{ab}] \\ \partial_\perp\Theta &= \mathcal{L}_\beta\Theta + \frac{\bar{\alpha}}{2}\left[\bar{R} - \bar{K}_{ab}\bar{K}^{ab} + \bar{K}(\bar{K} - 2C_{Z_4c}\Theta) + 2\bar{D}_a\bar{Z}^a - \frac{2\kappa_1(2+\kappa_2)\Theta}{\Omega}\right] - C_{Z_4c}\bar{Z}^a\bar{D}_a\bar{\alpha} \\ &\quad + 3\frac{[(\partial_\perp\Omega)^2 - \bar{\alpha}^2\bar{D}^a\Omega\bar{D}_a\Omega]}{\bar{\alpha}\Omega^2} + \frac{2\bar{\alpha}\bar{\Delta}\Omega}{\Omega} + \frac{2(\bar{K} - 2C_{Z_4c}\Theta)\partial_\perp\Omega}{\Omega} - 8\pi\bar{\alpha}\bar{\rho}, \\ \partial_\perp\bar{Z}_a &= \mathcal{L}_\beta\bar{Z}_a + \bar{\alpha}\left[\bar{D}_b\bar{K}^b_a - \bar{D}_a\bar{K} - \bar{D}_a\Theta - 2\bar{K}_{ab}\bar{Z}^b - \frac{\kappa_1\bar{Z}_a}{\Omega}\right] - C_{Z_4c}\Theta\bar{D}_a\bar{\alpha} + \frac{2\bar{\alpha}\Theta\bar{D}_a\Omega}{\Omega} \end{aligned}$$

$$-\frac{2\bar{D}_a\partial_\perp\Omega}{\Omega}-\frac{2\bar{\alpha}\bar{K}^b_a\bar{D}_b\Omega}{\Omega}-\frac{2\bar{Z}_a\partial_\perp\Omega}{\Omega}+\frac{2\bar{D}_a\bar{\alpha}\partial_\perp\Omega}{\bar{\alpha}\Omega}-8\pi\bar{\alpha}\bar{J}_a,$$

where $\bar{\Delta}=\bar{\gamma}^{ab}\bar{D}_a\bar{D}_b$. The equations for the Hamiltonian (3.17) and momentum (3.21) constraints are given by,

$$\mathcal{H}=\bar{R}-\bar{K}_{ab}\bar{K}^{ab}+\bar{K}^2+\frac{6\left[(\partial_\perp\Omega)^2-\bar{\alpha}^2\bar{D}_a\Omega\bar{D}^a\Omega\right]}{\bar{\alpha}^2\Omega^2}+\frac{4\bar{\Delta}\Omega}{\Omega}+\frac{4\bar{K}\partial_\perp\Omega}{\bar{\alpha}\Omega}-16\pi\bar{\rho},$$
$$\mathcal{M}^a=\bar{D}_b\bar{K}^{ab}-\bar{\gamma}^{ab}\bar{D}_b\bar{K}-\frac{2\bar{K}^{ab}\bar{D}_b\Omega}{\Omega}-\frac{2\bar{\gamma}^{ab}\bar{D}_b\partial_\perp\Omega}{\bar{\alpha}\Omega}+\frac{2\bar{\gamma}^{ab}\bar{D}_b\bar{\alpha}\partial_\perp\Omega}{\bar{\alpha}^2\Omega}-8\pi\bar{J}^a.$$

These equations describe the Arnowitt-Deser-Misner formalism (ADM), the most common EFEs (Hamiltonian-like) formulation [32]. The coefficient $C_{Z_{4c}}$ signals the components coming from Z4. The set of rules for how most of the variables change under the conformal transformation is the following:

$$\bar{g}_{ab}=\Omega^2\tilde{g}_{ab},\quad \bar{\gamma}_{ab}=\Omega^2\tilde{\gamma}_{ab}\quad \bar{\alpha}=\Omega\tilde{\alpha},\quad \Theta=\frac{\tilde{\Theta}}{\Omega},\quad \bar{\beta}^a=\tilde{\beta}^a$$
$$\bar{K}_{ab}=\Omega\tilde{K}_{ab}-\frac{\tilde{\gamma}_{ab}\partial_\perp\Omega}{\tilde{\alpha}},\quad \bar{K}=\frac{\tilde{K}}{\Omega}-\frac{3\partial_\perp\Omega}{\tilde{\alpha}\Omega^2}$$

3.3.3 Generalized BSSN and Z4 formalism

One of the disadvantages of the ADM formalism is the fact that the system of equations is not strongly hyperbolic [33]. To fix this, we can use the Baumgarte-Shapiro-Shibata-Nakamura (BSSN) formalism [34, 35], introducing a conformal rescaling of the ADM equations. The new conformal factor χ will be defined as [10]

$$\chi=\left(\frac{\gamma}{\bar{\gamma}}\right)^{1/3},\tag{3.24}$$

where γ is the determinant of the conformally rescaled spatial metric and $\bar{\gamma}$ the determinant of the spatial metric. BSSN also requires the determinant of the conformally rescaled metric (γ) to be unitary. However, this is not suitable for spherical coordinates and thus we will choose the Generalized BSSN (GBSSN) [36], which discards this assumption. (3.24) also implies that,

$$\gamma_{ab}=\chi\bar{\gamma}_{ab},\quad \gamma^{ab}=\chi^{-1}\bar{\gamma}^{ab}.\tag{3.25}$$

This means that the extrinsic curvature has to change as $K_{ab}=\chi\bar{K}_{ab}$, $K^{ab}=\bar{K}^{ab}\chi^{-1}$, leaving the trace of the extrinsic curvature unchanged, $K^i_i=\bar{K}^i_i$. The extrinsic curvature tensor should also be separated into trace and trace-free components. The trace-free part is defined as

$$A_{ab}=K_{ab}-\frac{1}{3}\gamma_{ab}\bar{K}=\chi\bar{A}_{ab}.\tag{3.26}$$

Following the original BSSN, we will define the new variable K, which is not the "pure" extrinsic curvature trace, since it has a mixed part of the $Z4$ formalism:

$$K=\bar{K}-2\Theta\tag{3.27}$$

We also define a new variable $\Delta\Gamma^a$:

$$\Delta\Gamma^a = \Gamma^a - \hat{\Gamma}^a, \tag{3.28}$$

where Γ^a allows for good hyperbolicity properties of the EFEs [10]. These new Γ^a are a contraction of the Christoffel symbols,

$$\Gamma^a = \gamma^{bc}\Gamma^a_{bc} = -\frac{1}{\sqrt{\gamma}}\partial_b(\sqrt{\gamma}\gamma^{ab}), \tag{3.29}$$

while $\hat{\Gamma} = \gamma^{bc}\hat{\Gamma}^a_{bc}$ is defined along with $\hat{\Gamma}^a_{bc}$, a connection derived from a time-independent background metric $\hat{\gamma}_{ab}$. This metric can be arbitrary, so it is simpler to define it as having the components that a stationary solution of the EFEs would have. To finish off, we define a new variable which will be useful later on,

$$\Lambda^a = \Delta\Gamma^a + 2\gamma^{ab}Z_b. \tag{3.30}$$

We show the rewriting of the evolution equations [10] in Appendix A. We will pass on to the 3+1 decomposition of Maxwell's and Klein-Gordon equations.

3.4 3+1 Decomposition of Maxwell's and Klein-Gordon equations

3.4.1 Maxwell's Equations

We will now assume spherical symmetry, which implies the vanishing of the magnetic field [28, 30]. Following [37], we shall add a scalar field, $\tilde{\psi}$, whose purpose is to provide numerical stabilization for the Gauss constraint:

$$\tilde{\nabla}^\mu\left(\tilde{F}_{\mu\nu} + \tilde{g}_{\mu\nu}\tilde{\psi}\right) = 4\pi(\tilde{J}_\nu - \tilde{n}_\nu k\tilde{\psi}) \ , \tag{3.31}$$

where k is an empirical constant to control the evolution of $\tilde{\psi}$. This method could also be applied to the conformally compactified variables,

$$\bar{\nabla}^\mu\left(\bar{F}_{\mu\nu} + \bar{g}_{\mu\nu}\psi\right) = 4\pi(\bar{J}_\nu - \bar{n}_\nu k\bar{\psi}) \ ,$$

but we will work with (3.31). An important aspect of the Maxwell tensor is that we can write it as [37],

$$\tilde{F}_{\mu\nu} = \tilde{n}_\mu\tilde{E}_\nu - \tilde{n}_\nu\tilde{E}_\mu + \tilde{\epsilon}_{\mu\nu\alpha\beta}\tilde{B}^\alpha\tilde{n}^\beta, \tag{3.32}$$

where $\tilde{E}_\nu$ and $\tilde{B}_\alpha$ are the electric and magnetic fields respectively. The quantity $\tilde{\epsilon}^{\mu\nu\alpha\beta}$ is the Levi-Civita tensor, defined with respect to the Levi-Civita symbol $\eta^{\mu\nu\alpha\beta}$ by:

$$\tilde{\epsilon}_{\mu\nu\alpha\beta} = \frac{1}{\sqrt{\tilde{g}}}\eta_{\mu\nu\alpha\beta}. \tag{3.33}$$

We saw that the electromagnetic tensor is invariant under conformal transformations. If we were to rewrite this equation in terms of the conformally compactified variables, we would get (using (3.5)),

$$\tilde{F}_{\mu\nu} = \bar{F}_{\mu\nu} = \tilde{n}_\mu\tilde{E}_\nu - \tilde{n}_\nu\tilde{E}_\mu + \tilde{\epsilon}_{\mu\nu\alpha\beta}\tilde{B}^\alpha\tilde{n}^\beta = \Omega^{-1}\bar{n}_\mu\tilde{E}_\nu - \Omega^{-1}\bar{n}_\nu\tilde{E}_\mu + \Omega^4\bar{\epsilon}_{\mu\nu\alpha\beta}\tilde{B}^\alpha\Omega\bar{n}^\beta, \tag{3.34}$$

where we recall (3.33) to get the transformation law $\tilde{\epsilon}_{\mu\nu\alpha\beta} = \Omega^4 \bar{\epsilon}_{\mu\nu\alpha\beta}$ and $\tilde{\epsilon}^{\mu\nu\alpha\beta} = \Omega^{-4} \bar{\epsilon}^{\mu\nu\alpha\beta}$. Although the electric and magnetic fields do not transform in the same way as tensors, one can propose that their rescaled counterparts are

$$\bar{E}_\mu = \frac{\tilde{E}_\mu}{\Omega}, \quad \tilde{E}_\mu = \Omega \bar{E}_\mu, \quad \bar{B}^\mu = \Omega^5 \tilde{B}^\mu, \quad \tilde{B}^\mu = \frac{\bar{B}^\mu}{\Omega^5}. \tag{3.35}$$

Using the fact $\tilde{F}^{\mu\nu} = \Omega^4 \bar{F}^{\mu\nu}$, we also have the "transformation" rules for the contravariant fields,

$$\bar{E}^\mu = \frac{\tilde{E}^\mu}{\Omega^3}, \quad \tilde{E}^\mu = \Omega^3 \bar{E}^\mu, \quad \bar{B}_\mu = \frac{\tilde{B}_\mu}{\Omega^9}, \quad \tilde{B}_\mu = \Omega^9 \bar{B}_\mu. \tag{3.36}$$

Note that the electric and magnetic fields "transform" in opposite ways under conformal transformations. This agrees with the fact that (in flat spacetime) the electric field is a vector and the magnetic field is a pseudovector. From electrodynamics [31], we know that there are two invariants arising from the Faraday tensor,

$$\tilde{F}_{\mu\nu}\tilde{F}^{\mu\nu} = 2(\tilde{B}_\mu \tilde{B}^\mu - \tilde{E}_\mu \tilde{E}^\mu), \quad \tilde{F}_{\mu\nu}\tilde{F}^{*\mu\nu} = 4\tilde{E}^\mu \tilde{B}_\mu, \tag{3.37}$$

where the dual Faraday tensor $F^{*\mu\nu}$ is given by,

$$\tilde{F}^{*\mu\nu} = -\frac{1}{2}\tilde{\epsilon}^{\mu\nu\alpha\beta}\tilde{F}_{\alpha\beta}. \tag{3.38}$$

Under a conformal transformation, both of these invariants change as,

$$\begin{aligned} \tilde{F}_{\mu\nu}\tilde{F}^{\mu\nu} &= 2(\tilde{B}_\mu \tilde{B}^\mu - \tilde{E}_\mu \tilde{E}^\mu) = 2(\bar{B}_\mu \bar{B}^\mu - \bar{E}_\mu \bar{E}^\mu)\Omega^4 = \Omega^4 \bar{F}_{\mu\nu}\bar{F}^{\mu\nu} \\ \tilde{F}_{\mu\nu}\tilde{F}^{*\mu\nu} &= 4\tilde{E}^\mu \tilde{B}_\mu = 4\bar{E}^\mu \bar{B}_\mu \Omega^4 = \Omega^4 \bar{F}_{\mu\nu}\bar{F}^{*\mu\nu}, \end{aligned} \tag{3.39}$$

agreeing with the transformations of the Faraday tensor that we had gotten before. For the 3+1 decomposition, we will stick to the conformally compactified electromagnetic fields. Projecting (3.32) along the normal vector we get,

$$\bar{E}_\nu = -\bar{n}^\mu \bar{F}_{\mu\nu} = -\bar{n}^\mu (\bar{\nabla}_\mu \bar{A}_\nu - \bar{\nabla}_\nu \bar{A}_\mu), \tag{3.40}$$

and it is also useful to decompose the four potential $\bar{A}^\mu$:

$$\bar{\Phi} = -\bar{n}_\mu \bar{A}^\mu \quad , \qquad \bar{A}^i_3 = \bar{\gamma}^i_\mu \bar{A}^\mu \quad , \tag{3.41}$$

where $\bar{A}_{3i}$ is the vector potential and $\bar{\Phi}$ is a scalar potential related to the electric potential. We will see how these last two quantities are related later.

Evolution Equations

Projecting (3.40), it becomes an evolution equation for the vector potential $\bar{A}_3$,

$$\partial_t \bar{A}^i_3 = \mathcal{L}_\beta \bar{A}^i_3 + \bar{\alpha}\bar{E}^i + \bar{D}^i(\bar{\alpha}\bar{\Phi}), \tag{3.42}$$

Going back to (3.31), as discussed in [37], and inserting (3.40), we just apply the covariant derivative and we retrieve the evolution equations for the electric field and for the $\bar{\psi}$ scalar,

$$\partial_t \bar{E}_i = \mathcal{L}_\beta \bar{E}_i + \bar{\alpha}\bar{E}_i\bar{K} + 4\pi\bar{\alpha}\bar{j}_i - \frac{\bar{\alpha}\bar{D}_i\bar{\psi}}{\Omega^2} \tag{3.43}$$

$$\partial_t \bar{\psi} = \mathcal{L}_\beta \bar{\psi} - \Omega^2\bar{\alpha}\bar{D}_i\bar{E}^i - 4\pi\Omega^2\bar{\alpha}\bar{q}_{\text{dens.}} + 4\pi\Omega^2\bar{\alpha}k\bar{\psi} \ , \tag{3.44}$$

where $\bar{j}^i$ is the current density and $\bar{q}_{\text{dens.}}$ is the charge density. These are the result of the 3+1 decomposition of the conformally compactified 4-current,

$$\bar{j}_i = \bar{\gamma}^\mu_i \bar{J}_\mu \ , \qquad \bar{q}_{\text{dens.}} = -\bar{n}^\mu \bar{J}_\mu \ . \tag{3.45}$$

If we were to define the scalar $\bar{\psi}$ directly in the conformally compactified version of Maxwell's equations, the evolution equation for the scalar field would become simply,

$$\partial_t \bar{E}_i = \mathcal{L}_\beta \bar{E}_i - \bar{\alpha}\bar{E}_i\bar{K} + 4\pi\bar{\alpha}\bar{j}_i - \bar{\alpha}\bar{D}_i\bar{\psi} \tag{3.46}$$

$$\partial_t \bar{\psi} = \mathcal{L}_\beta \bar{\psi} - \bar{\alpha}\bar{D}_i\bar{E}^i - 4\pi\bar{\alpha}\bar{q}_{\text{dens.}} + 4\pi\bar{\alpha}k\bar{\psi} \ . \tag{3.47}$$

Both formulations worked fine in the simulation, so we stuck with (3.43) and (3.44). We can also test four-current conservation by applying the covariant derivative to $\bar{J}_\mu$, which gives the following evolution equation,

$$\tilde{\nabla}^\mu \tilde{J}_\mu = 0 \iff \partial_\perp \tilde{q}_{\text{dens.}} = \mathcal{L}_\beta \tilde{q}_{\text{dens.}} + \bar{\alpha}\bar{K}\tilde{q}_{\text{dens.}} - \bar{\alpha}\bar{D}^i\tilde{j}_i - \tilde{j}^i\bar{D}_i\bar{\alpha} + \frac{2\tilde{j}^i\bar{\alpha}\bar{D}_i\Omega}{\Omega} + \frac{2\tilde{q}_{\text{dens.}}\mathcal{L}_n\Omega}{\Omega} , \tag{3.48}$$

In terms of nomenclature, $\bar{q}_{\text{dens.}}$, the charge density is what sometimes is referred to as ρ [30], but here we make the distinction because ρ is already in use as the energy-momentum tensor trace.

Gauss Constraint

If we impose in (3.44) (or in (3.47)) that $\psi = 0$ in (3.44), we recover the Gauss constraint in [28]:

$$\mathcal{G} = \bar{D}_i\bar{E}^i + 4\pi\bar{q}_{\text{dens.}} \ . \tag{3.49}$$

This is the usual Gauss equation in a standard book on electromagnetism [38], with some extra terms coming from the conformal transformation.

3.4.2 Complex Klein-Gordon Equation

Regarding the complex scalar field, to implement the evolution system we divide the scalar field into the real and complex parts, $\tilde{c}_\phi$ and $\tilde{d}_\phi$,

$$\tilde{\phi} = \tilde{c}_\phi + i\tilde{d}_\phi \ , \quad \tilde{c}_\phi, \tilde{d}_\phi \in \mathbb{R} \ . \tag{3.50}$$

We also define the corresponding conformally rescaled real and complex parts of the scalar field,

$$\bar{c}_\phi = \Omega^{-1}\tilde{c}_\phi \ , \quad \bar{d}_\phi = \Omega^{-1}\tilde{d}_\phi \ .$$

To break down the KG equation in a first-order system of PDEs, we add an extra variable $\bar{\Pi}$, such that

$$\bar{\Pi} = \partial_t\bar{\phi} \rightarrow \bar{c}_\Pi = \partial_t\bar{c}_\phi, \quad \bar{d}_\Pi = \partial_t\bar{d}_\phi \, . \tag{3.51}$$

If we go back into the Klein-Gordon equation (2.12), recall that it expands into,

$$\tilde{\nabla}^\mu\tilde{\nabla}_\mu\phi + iq\tilde{A}^\mu\tilde{\nabla}_\mu\tilde{\phi} + iq\tilde{\nabla}^\mu(\tilde{A}_\mu\tilde{\phi}) - q^2\tilde{A}^\mu\tilde{A}_\mu\tilde{\phi} = 0 \ , \tag{3.52}$$

Writing the equation after the conformal transformation and the 3+1 decomposition in its real and imaginary parts,

$$\begin{aligned}
\partial_t\bar{c}_\Pi &= \bar{c}_\Pi\bar{K} - q^2\bar{A}_{3i}\bar{A}_3{}^i\bar{c}_\phi\bar{\alpha} - 2q\bar{c}_\Pi\bar{\Phi} + q\bar{d}_\phi\bar{K}\bar{\alpha}\bar{\Phi} + q^2\bar{c}_\phi\bar{\alpha}\bar{\Phi}^2 - q\bar{d}_\phi\bar{\gamma}^{ji}\bar{\alpha}\bar{D}_j\bar{A}_{3i} - q\bar{A}_3{}^j\bar{\alpha}\bar{D}_j\bar{d}_\phi \\
&- q\bar{A}_3{}^j\bar{d}_\phi\bar{D}_j\bar{\alpha} + \frac{2q\bar{A}_3{}^j\bar{d}_\phi\bar{\alpha}\bar{D}_j\Omega}{\Omega} + \bar{\gamma}^{ij}\bar{D}_j\bar{\alpha}\bar{D}_i\bar{c}_\phi + \frac{2\bar{\gamma}^{ji}\bar{\alpha}\bar{D}_j\Omega\bar{D}_i\bar{c}_\phi}{\Omega} - q\bar{A}_3{}^i\bar{\alpha}\bar{D}_i\bar{d}_\phi \\
&- \frac{2q\bar{A}_3{}^i\bar{d}_\phi\bar{\alpha}\bar{D}_i\Omega}{\Omega} - \frac{2\bar{\gamma}^{ji}\bar{\alpha}\bar{D}_j\bar{c}_\phi\bar{D}_i\Omega}{\Omega} + \frac{\bar{c}_\phi\bar{\gamma}^{ij}\bar{D}_j\bar{\alpha}\bar{D}_i\Omega}{\Omega} - \frac{2\bar{c}_\phi\bar{\gamma}^{ji}\bar{\alpha}\bar{D}_j\Omega\bar{D}_i\Omega}{\Omega^2} + \bar{\gamma}^{ji}\bar{\alpha}\bar{D}_i\bar{D}_j\bar{c}_\phi \\
&+ \frac{\bar{c}_\phi\bar{\gamma}^{ji}\bar{\alpha}\bar{D}_i\bar{D}_j\Omega}{\Omega} + \frac{\bar{c}_\Pi\mathcal{L}_n\bar{\alpha}}{\bar{\alpha}} + \frac{\bar{c}_\phi\bar{K}\bar{\alpha}\mathcal{L}_n\Omega}{\Omega} + \frac{2\bar{c}_\phi\bar{\alpha}(\mathcal{L}_n\Omega)^2}{\Omega^2} - q\bar{d}_\phi\bar{\alpha}\mathcal{L}_n\bar{\Phi} - \frac{\bar{c}_\phi\bar{\alpha}\mathcal{L}_n\mathcal{L}_n\Omega}{\Omega} + \mathcal{L}_\beta\bar{c}_\Pi \\
&+ \frac{\mathcal{L}_\beta\bar{c}_\Pi}{\bar{\alpha}} - \bar{K}\mathcal{L}_\beta\bar{c}_\phi - \frac{\mathcal{L}_n\bar{\alpha}\mathcal{L}_\beta\bar{c}_\phi}{\bar{\alpha}} + 2q\bar{\Phi}\mathcal{L}_\beta\bar{d}_\phi - \frac{\mathcal{L}_\beta\mathcal{L}_\beta\bar{c}_\phi}{\bar{\alpha}}
\end{aligned} \tag{3.53}$$

$$\begin{aligned}
\partial_t\bar{d}_\Pi &= \bar{d}_\Pi\bar{K} - q^2\bar{A}_{3i}\bar{A}_3{}^i\bar{d}_\phi\bar{\alpha} + 2q\bar{c}_\Pi\bar{\Phi} - q\bar{c}_\phi\bar{K}\bar{\alpha}\bar{\Phi} + q^2\bar{d}_\phi\bar{\alpha}\bar{\Phi}^2 + q\bar{c}_\phi\bar{\gamma}^{ji}\bar{\alpha}\bar{D}_j\bar{A}_{3i} + q\bar{A}_3{}^j\bar{\alpha}\bar{D}_j\bar{c}_\phi \\
&+ q\bar{A}_3{}^j\bar{c}_\phi\bar{D}_j\bar{\alpha} - \frac{2q\bar{A}_3{}^j\bar{c}_\phi\bar{\alpha}\bar{D}_j\Omega}{\Omega} + q\bar{A}_3{}^i\bar{\alpha}\bar{D}_i\bar{c}_\phi + \bar{\gamma}^{ij}\bar{D}_j\bar{\alpha}\bar{D}_i\bar{d}_\phi + \frac{2\bar{\gamma}^{ji}\bar{\alpha}\bar{D}_j\Omega\bar{D}_i\bar{d}_\phi}{\Omega} \\
&+ \frac{2q\bar{A}_3{}^i\bar{c}_\phi\bar{\alpha}\bar{D}_i\Omega}{\Omega} - \frac{2\bar{\gamma}^{ji}\bar{\alpha}\bar{D}_j\bar{d}_\phi\bar{D}_i\Omega}{\Omega} + \frac{\bar{d}_\phi\bar{\gamma}^{ij}\bar{D}_j\bar{\alpha}\bar{D}_i\Omega}{\Omega} - \frac{2\bar{d}_\phi\bar{\gamma}^{ji}\bar{\alpha}\bar{D}_j\Omega\bar{D}_i\Omega}{\Omega^2} + \bar{\gamma}^{ji}\bar{\alpha}\bar{D}_i\bar{D}_j\bar{d}_\phi \\
&+ \frac{\bar{d}_\phi\bar{\gamma}^{ji}\bar{\alpha}\bar{D}_i\bar{D}_j\Omega}{\Omega} + \frac{\bar{d}_\Pi\mathcal{L}_n\bar{\alpha}}{\bar{\alpha}} + \frac{\bar{d}_\phi\bar{K}\bar{\alpha}\mathcal{L}_n\Omega}{\Omega} + \frac{2\bar{d}_\phi\bar{\alpha}(\mathcal{L}_n\Omega)^2}{\Omega^2} + q\bar{c}_\phi\bar{\alpha}\mathcal{L}_n\bar{\Phi} - \frac{\bar{d}_\phi\bar{\alpha}\mathcal{L}_n\mathcal{L}_n\Omega}{\Omega} + \mathcal{L}_\beta\bar{d}_\Pi \\
&+ \frac{\mathcal{L}_\beta\bar{d}_\Pi}{\bar{\alpha}} - \bar{K}\mathcal{L}_\beta\bar{d}_\phi - \frac{\mathcal{L}_n\bar{\alpha}\mathcal{L}_\beta\bar{d}_\phi}{\bar{\alpha}} - 2q\bar{\Phi}\mathcal{L}_\beta\bar{c}_\phi - \frac{\mathcal{L}_\beta\mathcal{L}_\beta\bar{d}_\phi}{\bar{\alpha}} \, .
\end{aligned} \tag{3.54}$$

If there is no electromagnetic coupling, these equations can be treated as completely separate fields. This would give the real scalar field equation, already derived in [10]. Regarding the conserved current (3.45), we expand it to

$$\tilde{q}_\phi = -q^2\bar{c}_\phi^2\Omega^2\bar{\Phi} - q^2\bar{d}_\phi^2\Omega^2\bar{\Phi} - q\bar{d}_\phi\Omega^2\mathcal{L}_n\bar{c}_\phi + q\bar{c}_\phi\Omega^2\mathcal{L}_n\bar{d}_\phi = \Omega^2\bar{q}_\phi \tag{3.55}$$

$$(\tilde{j}_\phi)_i = -q^2\bar{A}_{3i}\bar{c}_\phi^2\Omega^2 - q^2\bar{A}_{3i}\bar{d}_\phi^2\Omega^2 + q\bar{d}_\phi\Omega^2\bar{D}_i\bar{c}_\phi - q\bar{c}_\phi\Omega^2\bar{D}_i\bar{d}_\phi = \Omega^2(\bar{j}_\phi)_i \ . \tag{3.56}$$

The only evolution equation missing is the one for the scalar potential. We have some gauge freedom to do so, as we have already talked about. If we were to follow [28] and set the Lorentz gauge $\tilde{\nabla}_\mu\tilde{A}^\mu = 0$, this

reads:

$$\partial_t \bar{\Phi} = \bar{K}\bar{\alpha}\bar{\Phi} - \bar{\gamma}^{ij}\bar{\alpha}\bar{D}_i\bar{A}_{3j} - \bar{A}_3{}^i\bar{D}_i\bar{\alpha} + \frac{2\bar{A}_3{}^i\bar{\alpha}\bar{D}_i\Omega}{\Omega} + \frac{2\bar{\alpha}\bar{\Phi}\mathcal{L}_n\Omega}{\Omega} + \mathcal{L}_\beta\bar{\Phi} \ . \tag{3.57}$$

And with a choice of gauge for the scalar potential $\bar{\Phi}$, we complete the set of equations necessary to evolve our system. The Lorentz gauge could also be defined in the conformal world:

$$\partial_t \bar{\Phi} = \bar{K}\bar{\alpha}\bar{\Phi} - \bar{\gamma}^{ij}\bar{\alpha}\bar{D}_i\bar{A}_{3j} - \bar{A}_3{}^i\bar{D}_i\bar{\alpha} + \mathcal{L}_\beta\bar{\Phi} \ . \tag{3.58}$$

Whatever definition of the gauge we use for the electric field, the equation (3.48) will hold. During this work, it was useful to consider other gauge conditions, as will be shown later. One option taken into consideration was the light-cone gauge.

3.4.3 Light-Cone Gauge

In [27], it is shown that the Lorentz gauge does not hold under conformal transformations,

$$\tilde{g}^{\mu\nu}\tilde{\nabla}_\mu\tilde{A}_\nu = \bar{g}^{\mu\nu}\bar{\nabla}_\mu\bar{A}_\nu - 2\bar{g}^{\mu\nu}\bar{A}_\nu\bar{\nabla}_\mu \ln\Omega = 0\,, \tag{3.59}$$

This has been discussed in [39] as well, where the tails of the electromagnetic potentials are shown to be just gauge-tails. This contrasts with the late time tails of the scalar field [40, 4]. An alternative proposed in [27] is the light-cone gauge. It has been used in several contexts [41, 42], but more broadly in string theory [43]. The idea is to force,

$$l^\mu\tilde{A}_\mu = 0\,, \tag{3.60}$$

where l^μ is an outgoing null vector. This condition does not change under conformal transformations. Following the Newman-Penrose formalism [44], we start with a general spherically symmetric spacetime,

$$d\tilde{s}^2 = -f(\tilde{r})d\tilde{t}^2 + f(\tilde{r})^{-1}d\tilde{r}^2 + \tilde{r}^2d\tilde{\theta}^2 + \tilde{r}^2\sin^2\tilde{\theta}d\tilde{\phi}^2\,, \tag{3.61}$$

and the corresponding outgoing null vector can be given by,

$$l^\mu = \frac{1}{\sqrt{2}}(f(\tilde{r})^{-1/2}, f(\tilde{r})^{1/2}, 0, 0)\,. \tag{3.62}$$

The line element in terms of the lapse and the shift is described in the next section (3.70), but we write the result here for now, to proceed onwards with the derivation at hand:

$$d\tilde{s}^2 = -(\alpha^2 - \chi^{-1}\gamma_{rr}(\beta^r)^2)dt^2 + \chi^{-1}(2\gamma_{rr}\beta^r dtdr + \gamma_{rr}dr^2 + \gamma_{\theta\theta}r^2d\sigma^2).$$

In a spherically symmetric spacetime, as we are considering throughout this work, we can put $d\sigma = 0$. If we propose that $l^\mu = (B, C, 0, 0)$, where B and C are generic functions, and impose the null condition, we get:

$$\bar{g}_{\mu\nu}l^\mu l^\nu = 0 \iff -(\alpha^2 - \chi^{-1}\gamma_{rr}(\beta^r)^2)B^2 + \chi^{-1}(2\gamma_{rr}\beta^r BC + \gamma_{rr}C^2) = 0. \tag{3.63}$$

Imposing $B = 1$, we get a quadratic equation for C, with two solutions $C = -\beta^r \pm \alpha\sqrt{\frac{\chi}{\gamma_{rr}}}$. The outgoing speed [10] of the characteristics of our system is given by,

$$c_+ = -\beta^r + \alpha\sqrt{\frac{\chi}{\gamma_{rr}}},$$

so we will choose the positive sign. Going back to the decomposition of the four potential (3.41), we can rewrite it as (check (4.8) in the next section),

$$\bar{A}_\mu = \bar{\Phi}\bar{n}_\mu + \bar{A}_{3\mu} = (-\bar{\Phi}\alpha, \bar{\gamma}_{rr}\bar{A}_3{}^r, 0, 0)\,.$$

This means that the light-cone gauge imposes that,

$$l^\mu \tilde{A}_\mu = l^\mu \bar{A}_\mu = -\bar{\Phi}\alpha + c_+\gamma_{rr}\chi^{-1}A_3^r = 0 \iff \bar{\Phi} = A_3^r c_+\frac{\gamma_{rr}}{\chi\alpha} = \frac{\gamma_{rr}}{\chi\alpha}A_3^r\left(-\beta^r + \alpha\sqrt{\frac{\chi}{\gamma_{rr}}}\right). \tag{3.64}$$

With the light-cone gauge, we are removing one of the evolution equations and substituting it with a constraint equation. It is also possible to differentiate the condition with respect to time and derive an evolution equation for Φ. Note that this gauge, underneath, is imposing

$$A_\mu \propto l_\mu\,, \tag{3.65}$$

i.e., it is forcing the four-potential to evolve along the outgoing null geodesics. This is the physical intuition behind this gauge. We have tested this gauge in our simulation, and nothing conclusive was retrieved. This will be discussed in section 6.5.

3.4.4 Maxwell's and Klein-Gordon Equations in GBSSN Formulation

Regarding the electromagnetic quantities, we will propose that neither the electric potential, the magnetic vector potential nor the electric field change under this rescaling, i.e.,

$$\bar{A}_{3i} = A_{3i}\,,\quad \bar{\Phi} = \Phi\,,\quad \bar{E}_i = E_i\,.$$

We propose that the same happens for the current and charge densities, but we will continue showing them with a bar on top. We leave the details in Appendix A. The stress-energy components are also written explicitly in the Appendix. We remind the reader that the quantities above are dependent on the transformations derived in (3.35) and (3.36).

3.5 Coordinate Chart

To implement spherical symmetry in our code, we choose the standard spherical coordinates r, θ and ϕ, following [36],

$$\gamma_{ij} = \mathrm{Diag}(\gamma_{rr}, \gamma_{\theta\theta}r^2, \gamma_{\theta\theta}r^2\sin^2\theta) \tag{3.66}$$

Due to the extra degree of freedom coming from χ we can impose $\gamma_{\theta\theta} = \sqrt{\gamma_{rr}}$. For the background metric, we choose the Minkowski metric,

$$\hat{\gamma}_{ij} = \text{Diag}(\hat{\gamma}_{rr}, \hat{\gamma}_{\theta\theta} r^2, \hat{\gamma}_{\theta\theta} r^2 \sin^2\theta) \tag{3.67}$$

with $\hat{\gamma}_{rr} = \hat{\gamma}_{\theta\theta} = 1$. From the definition of the trace free part of the extrinsic curvature (3.26), together with the imposition of spherical symmetry, we can reduce the degrees of freedom of A_{ij} to 1, A_{rr}. We also get that,

$$A_{ij} = A_{rr} \cdot \text{Diag}\left(1, -\frac{r^2\gamma_{\theta\theta}}{2\gamma_{rr}}, -\frac{r^2\gamma_{\theta\theta}\sin^2\theta}{2\gamma_{rr}}\right) \tag{3.68}$$

and,

$$\Delta\Gamma^i = \left(\frac{2}{\gamma_{\theta\theta} r} - \frac{2}{\gamma_{rr} r} + \frac{\gamma'_{rr}}{2\gamma_{rr}^2} - \frac{\gamma'_{\theta\theta}}{\gamma_{rr}\gamma_{\theta\theta}}, \quad 0, \quad 0\right)^T. \tag{3.69}$$

The line element also becomes,

$$d\tilde{s}^2 = -(\alpha^2 - \chi^{-1}\gamma_{rr}(\beta^r)^2)dt^2 + \chi^{-1}(2\gamma_{rr}\beta^r dt dr + \gamma_{rr} dr^2 + \gamma_{\theta\theta} r^2 d\sigma^2). \tag{3.70}$$

Having a coordinate system, we can get the radial equations of motion. The reader can consult them in Appendix A.4.

3.6 Shift and Lapse Gauge Conditions

In addition to the equations of motion, we have to give evolution equations for the lapse and the shift (gauge conditions). These conditions are crucial for having stable simulations in numerical relativity. For the specificities of free evolution in hyperboloidal slices, the proposed conditions in [45] give stable long-running simulations. Therefore, we will use those to complete our PDE system:

$$\begin{aligned}
\partial_t \alpha &= \beta^r \alpha' - \hat{\beta}^r \hat{\alpha}' - \frac{(n_{cK} + \alpha^2)\Delta\tilde{K}}{\Omega} + \frac{\Omega'}{\Omega}(\hat{\beta}^r \hat{\alpha} - \beta^r \alpha) + \frac{\xi_{cK}(\hat{\alpha} - \alpha)}{\Omega} \\
\partial_t \beta^r &= \beta^r \beta^{r\prime} + \left(\lambda(r_{\mathscr{I}}^2 - r^2) + \frac{3}{4}\alpha^2\chi\right)\Lambda^r + \eta(\hat{\beta}^r - \beta^r) + \xi_{\beta^r}\left(\frac{\hat{\beta}^r}{\Omega} - \frac{\beta^r}{\Omega}\right),
\end{aligned} \tag{3.71}$$

where $r_{\mathscr{I}}$ is the location of $\mathscr{I}^+$ in our grid and $'$ denotes the partial derivative with respect to r, ∂_r. This is reminiscent of the 1+log condition used for the lapse and the generalized Gamma driver for the shift. There are only some extra source terms, and the coefficients in front of K and Λ_r have been modified. The source functions in the 1+log condition are here constructed from a 4D time-independent reference metric, which corresponds to the hatted quantities. These source functions are such that if $\partial_t \alpha = 0$, a solution for Minkowski spacetime is $\alpha = \hat{\alpha}$, $\beta^r = \hat{\beta}^r$ and $\Delta\tilde{K} = 0$. Their expressions are described better in the following section. The reader will note that there are some parameters: $n_{cK}, \lambda, \xi_{cK}, \eta, \xi_{\beta^r}$, which are to be chosen empirically, as the system to be evolved requires, in Chapter 6.

Chapter 4

Initial Data and Further Properties of the Setup

In this section, we provide initial data on a hyperboloidal slice as initially given on a Cauchy one. Further, we will discuss some necessary spacetime properties for the analysis during section 6.

4.1 Initial Data

Following [10], we first start with the generic line element given by,

$$d\tilde{s}^2 = -A(\tilde{r})d\tilde{t}^2 + \frac{1}{A(\tilde{r})}d\tilde{r}^2 + \tilde{r}^2 d\tilde{\sigma}^2. \tag{4.1}$$

When we introduce the height function (2.19), $t = \tilde{t} - h(\tilde{r})$, our line element becomes,

$$d\tilde{s}^2 = -A(\tilde{r})dt^2 - 2A(\tilde{r})h'(\tilde{r})dtd\tilde{r} + \frac{[1-(A(\tilde{r})h'(\tilde{r}))^2]}{A(\tilde{r})}d\tilde{r}^2 + \tilde{r}^2 d\sigma^2 \tag{4.2}$$

We now do a coordinate transformation through a compactifying factor called $\bar{\Omega}$. This allows us to define the compactified radial coordinate:

$$\tilde{r} = \frac{r}{\bar{\Omega}(r)}\,.$$

It will be particularly useful when deriving trumpet initial data. With this change, the line element becomes,

$$d\tilde{s}^2 = -Adt^2 - 2Ah'\frac{\bar{\Omega} - r\bar{\Omega}}{\bar{\Omega}^2}dtdr + \frac{[1-(Ah')^2]}{A}\frac{(\bar{\Omega} - r\bar{\Omega})^2}{\bar{\Omega}^4}dr^2 + \frac{r^2}{\bar{\Omega}^2}d\sigma^2 \tag{4.3}$$

Now that we are in hyperboloidal slices, we can proceed to the conformal rescaling of the whole metric by Ω, $d\tilde{s}^2 = \Omega^2 d\hat{s}^2$, which gets us to,

$$\begin{aligned} d\hat{s}^2 &= \Omega^2[-Adt^2 - 2Ah'\frac{\bar{\Omega} - r\bar{\Omega}}{\bar{\Omega}^2}dtdr + \frac{[1-(Ah')^2]}{A}\frac{(\bar{\Omega} - r\bar{\Omega})^2}{\bar{\Omega}^4}dr^2 + \frac{r^2}{\bar{\Omega}^2}d\sigma^2] \\ &= -A\Omega^2 dt^2 + \frac{\Omega^2}{\bar{\Omega}^2}\left[-2Ah'(\bar{\Omega} - r\bar{\Omega})dtdr + \frac{[1-(Ah')^2]}{A}\frac{(\bar{\Omega} - r\bar{\Omega})^2}{\bar{\Omega}^2}dr^2 + r^2 d\sigma^2\right] \end{aligned} \tag{4.4}$$

Looking back at (3.70), if we are to match both expressions, we get that the initial data for these variables must be,

$$\alpha_0 = \Omega\sqrt{\frac{A}{1-(Ah')^2}}\,, \quad \chi_0 = \frac{\bar{\Omega}^2}{\Omega^2}\,, \quad \beta^r_0 = -\frac{A^2\bar{\Omega}^2 h'}{[1-(Ah')^2][\bar{\Omega}-r\bar{\Omega}']}$$
$$\gamma_{rr0} = \frac{[1-(Ah')^2]}{A}\frac{(\bar{\Omega}-r\bar{\Omega}')^2}{\bar{\Omega}^2}\,, \quad \gamma_{\theta\theta_0} = 1 \tag{4.5}$$

For the Z4 variables, $\Theta_0 = 0$ and $Z_{r0} = 0$. We choose the background variables to be equal to the initial conditions of both metric components, $\hat{\gamma}_{rr} = \gamma_{rr0}$ and $\hat{\gamma}_{\theta\theta} = \gamma_{\theta\theta_0}$. This enforces $\Delta\Gamma^r_0 = 0$, which implies $\Lambda^r_0 = 0$. We are just left with indicating explicitly the values of Ω, $\bar{\Omega}$, and h. Let us first look at the height function.

4.1.1 Height Function

Here is where we will construct Constant Mean Curvature (CMC) slices [46]. Given that CMC slices are contracting/expanding at the same rate in all points of spacetime, this is suited for spherically symmetric codes. It has also been shown that for spherically symmetric black hole simulations, it results in stable numerical runs [10]. In [47], the authors compare the use of CMC slices vs. other formulations. Regarding the construction of these slices [48], we start with writing the trace of the extrinsic curvature as (check (3.10)),

$$\tilde{\bar{K}} = -\frac{1}{\sqrt{-\tilde{g}}}\partial_a(\sqrt{-\tilde{g}}\tilde{n}^a)\,. \tag{4.6}$$

CMC slices mean $\tilde{\bar{K}} = K_{\rm CMC}$. We now need to rewrite the RHS of the equation. For the metric, using (4.3), we have

$$\tilde{g}_{\mu\nu} = \begin{pmatrix} -A(\tilde{r}) & -A(\tilde{r})h'(\tilde{r}) & 0 & 0 \\ -A(\tilde{r})h'(\tilde{r}) & \frac{1-(-A(\tilde{r})h'(\tilde{r}))^2}{A(\tilde{r})} & 0 & 0 \\ 0 & 0 & \tilde{r}^2 & 0 \\ 0 & 0 & 0 & \tilde{r}^2\sin^2\theta \end{pmatrix}. \tag{4.7}$$

which means that $\tilde{g} = -\tilde{r}^4\sin^2\theta$. For the normal vector, using (3.4), we just pass the expression to spherical coordinates:

$$\tilde{n}^\mu = \frac{1}{\alpha}(1,-\tilde{\beta}^r,0,0)^T = \left(\sqrt{\frac{1-(A(\tilde{r})h'(\tilde{r}))^2}{A(\tilde{r})}}, \frac{A^{3/2}(\tilde{r})h'(\tilde{r})}{\sqrt{1-(A(\tilde{r})h'(\tilde{r}))^2}}, 0, 0\right)^T. \tag{4.8}$$

Thus, (4.6) becomes,

$$K_{\rm CMC} = -\frac{1}{r^2}\partial_r\left[r^2\frac{A^{3/2}(\tilde{r})h'(\tilde{r})}{\sqrt{1-(A(\tilde{r})h'(\tilde{r}))^2}}\right]. \tag{4.9}$$

Integrating with respect to r and admiting the constant of integration to be named $C_{\rm CMC}$, we get an expression for h',

$$h'(\tilde{r}) = -\frac{1}{A(\tilde{r})\sqrt{A(\tilde{r})+\left(\frac{K_{\rm CMC}\tilde{r}}{3}+\frac{C_{\rm CMC}}{\tilde{r}^2}\right)^2}}\left(\frac{K_{\rm CMC}\tilde{r}}{3}+\frac{C_{\rm CMC}}{\tilde{r}^2}\right). \tag{4.10}$$

If we now set this expression in (4.5), the initial data expressions turn into,

$$\alpha_0 = \Omega\sqrt{A\left(\frac{r}{\bar{\Omega}}\right)+\left(\frac{K_{\rm CMC}r}{3\bar{\Omega}}+\frac{C_{\rm CMC}\bar{\Omega}^2}{r^2}\right)^2}, \quad \gamma_{rr0} = \frac{(\bar{\Omega}-r\bar{\Omega}')^2}{\left[A\left(\frac{r}{\bar{\Omega}}\right)+\left(\frac{K_{\rm CMC}r}{3\bar{\Omega}}+\frac{C_{\rm CMC}\bar{\Omega}^2}{r^2}\right)^2\right]\bar{\Omega}^2},$$
$$\beta^r_0 = \frac{\bar{\Omega}^2\left(\frac{K_{\rm CMC}r}{3\bar{\Omega}}+\frac{C_{\rm CMC}\bar{\Omega}^2}{r^2}\right)\sqrt{A\left(\frac{r}{\bar{\Omega}}\right)+\left(\frac{K_{\rm CMC}r}{3\bar{\Omega}}+\frac{C_{\rm CMC}\bar{\Omega}^2}{r^2}\right)^2}}{(\bar{\Omega}-r\bar{\Omega}')}, \quad \chi_0 = \frac{\bar{\Omega}^2}{\Omega^2} \tag{4.11}$$

4.1.2 Compactification

The new conformal factor $\bar{\Omega}$ should be smooth, positive, and asymptotically behave as Ω. One option is to impose a conformally flat metric, i.e., $\gamma_{rr0} = 1$:

$$\gamma_{rr0} = \frac{[1-(Ah')^2]}{A}\frac{(\bar{\Omega}-r\bar{\Omega}')^2}{\bar{\Omega}^2} = 1\,. \tag{4.12}$$

This simplifies the rest of the expressions in (4.11). We now specify the initial data for the different scenarios to be studied.

4.1.3 Regular Initial Data

In flat spacetime, $A = 1$. We additionally assume $C_{\rm CMC} = 0$. This allows (4.10) to have an analytic solution,

$$h'(\tilde{r}) = -\frac{K_{\rm CMC}\tilde{r}}{3}\frac{1}{\sqrt{1+\left(\frac{K_{\rm CMC}\tilde{r}}{3}\right)^2}} \rightarrow h(\tilde{r}) = \sqrt{\tilde{r}^2+\left(\frac{3}{K_{\rm CMC}}\right)^2}+C, \tag{4.13}$$

where we are free to choose $C = 0$ without loss of generality and we assume $K_{\rm CMC} < 0$. This choice will give us slices that intersect $\mathscr{I}^+$. If $K_{\rm CMC} > 0$, then the height function, with an opposite sign as well, would lead the slices to $\mathscr{I}^-$. The condition that we imposed before (4.12), which assumes flat spacetime, also allows us to get an analytic expression for $\bar{\Omega}$,

$$\bar{\Omega} = -K_{\rm CMC}\frac{r_{\mathscr{I}^2}-r^2}{6r_{\mathscr{I}}}, \tag{4.14}$$

where recall that $r_{\mathscr{I}}$ is the position of $\mathscr{I}$ in our slice. (4.14) is also a suitable expression for the conformal factor Ω (and coincides with the compactification in Minkowski), so it will be used here and throughout the rest of the work. (4.11) now becomes,

$$\alpha_0 = \sqrt{\Omega^2+\left(\frac{K_{\rm CMC}r}{3}\right)^2}, \quad \chi_0 = 1, \quad \gamma_{rr0} = 1, \quad \beta^r_0 = \frac{K_{\rm CMC}r}{3}, \quad \gamma_{\theta\theta 0} = 1,$$
$$A_{rr0} = 0, \quad \bar{K}_0 = \frac{K_{\rm CMC}}{\Omega}+\frac{\Omega'}{\Omega}\frac{K_{\rm CMC}r}{\sqrt{\Omega^2+(\frac{K_{\rm CMC}r}{3})^2}}, \quad \Theta_0 = Z_{r0} = \Lambda_{r0} = 0. \tag{4.15}$$

4.1.4 Strong Field Initial Data

In this case, we cannot assume $C_{\mathrm{CMC}} = 0$ [10]. Technically, we can, but the slices that we would get would end up in the singularity, which we want to avoid. The purpose of introducing $\bar{\Omega}$ is exactly to avoid the singularity. This quantity is then introduced along with the isotropic radial coordinate r:

$$d\tilde{l}^2 = \frac{1}{A(\tilde{r}) + \left(\frac{K_{\mathrm{CMC}}\tilde{r}}{3} + \frac{C_{\mathrm{CMC}}}{\tilde{r}^2}\right)} d\tilde{r}^2 + \tilde{r}^2 d\sigma^2 = \frac{1}{\bar{\Omega}^2}(dr^2 + r^2 d\sigma^2), \tag{4.16}$$

which leads us to,

$$\frac{1}{A(\tilde{r}) + \left(\frac{K_{\mathrm{CMC}}\tilde{r}}{3} + \frac{C_{\mathrm{CMC}}}{\tilde{r}^2}\right)} d\tilde{r}^2 = \frac{1}{\bar{\Omega}^2} dr^2$$

Given that $\bar{\Omega}^2 = r^2/\tilde{r}^2$, we can simplify the expression and also integrate it to get the relation between r and $\tilde{r}$,

$$\pm \int \frac{dr}{r} = \int \frac{d\tilde{r}}{\tilde{r}\sqrt{A(\tilde{r}) + \left(\frac{K_{\mathrm{CMC}}\tilde{r}}{3} + \frac{C_{\mathrm{CMC}}}{\tilde{r}^2}\right)^2}}.$$

For a Reissner-Nördstrom metric, $A(\tilde{r}) = 1 - \frac{2M}{\tilde{r}} + \frac{Q^2}{\tilde{r}^2}$, with M and Q being the mass and charge of the black hole. To simplify the integral above, we can derive the value of C_{CMC} that makes the expression inside the square root have a double root [49, 50]. This is the procedure to get trumpet initial data. The condition is true if the discriminant of the expression inside the square root is set to 0,

$$\text{Discriminant}\left(\frac{1}{\tilde{r}^2}\left[\frac{K_{\mathrm{CMC}}^2\tilde{r}^6}{9} + \tilde{r}^4 + 2\left(\frac{K_{\mathrm{CMC}}C_{\mathrm{CMC}}}{3} - M\right)\tilde{r}^3 + Q^2\tilde{r}^2 + C_{\mathrm{CMC}}^2\right]\right) = 0. \tag{4.17}$$

The results for C_{CMC} are derived numerically, although there are extreme cases which provide us with analytic solutions ($M = 1$ or $Q = M$). For a charged black hole, with $M = 1$ and $Q = 0.8$, i.e., we get that $C_{\mathrm{CMC}} = 1.6256[...]$. There is also another solution ($C_{\mathrm{CMC}} = -0.2902[...]$), that goes into the white hole. In [10], there is a condition for C_{CMC} that gives horizon-penetrating slices,

$$C_{\mathrm{CMC}} > -\frac{1}{3}K_{\mathrm{CMC}}(M + \sqrt{M^2 - Q^2})^3, \tag{4.18}$$

that rules out the last solution. After having the value of C_{CMC}, we integrate numerically $\bar{\Omega}$ using (4.16). It will be just a matter of substituting everything in (4.11). The slices that the last subsections have given are shown in Fig. 4.1.

Trumpet Initial Data - A Clearer Representation

The idea of trumpet initial data is to be able to give data on a complete slice that avoids the singularity, while being horizon-penetrating. Looking back at (4.10), by substituting $A(\tilde{r}) = 1 - 2M/\tilde{r}$, we get that the derivative suddenly has a coordinate singularity at $\tilde{r} = 2M$ [51]. We leave a more detailed description of how to integrate the height function in C.3 or we refer you to [52]. There is a limit on how close we can get to the actual black hole's singularity, nonetheless, that corresponds to $\tilde{r} = R_0 < 2M$ (shown more explicitly in [53]). One could also have slices for $\tilde{r} < R_0$, but they would be trapped inside this surface.

Plotting the trumpet initial data, in hyperboloidal slices, one gets Fig. 4.1. In the figure, we filled with grey the area $0 < \tilde{r} < R_0$, that is, the region these slices never reach.

To better understand the full effects of using trumpet initial data, we should go into the maximal analytical extension of the Schwarzschild spacetime [54, 55]. This can be done by plotting with the negative domain of our Penrose diagram coordinates, giving the result shown in Fig. 4.2. By defining the correspondent infinities in the rest of the solution, we see that hyperboloidal slices in trumpet initial data (Fig. 4.1) connect the left-handed i_+ to $\mathscr{I}^+$ and, along $\tilde{r} = R_0$, it connects both i_+'s.

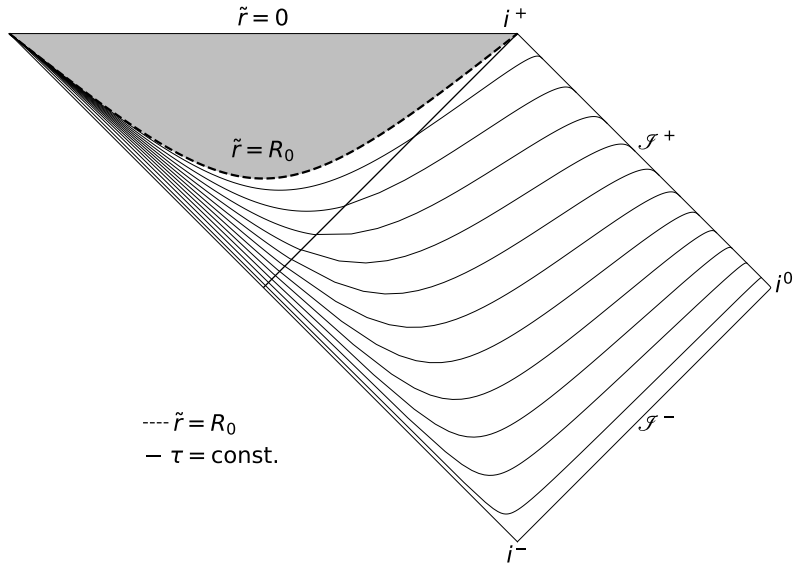

Figure 4.1: Hyperboloidal slices in trumpet initial data, in Schwarzschild spacetime. The grey area represents the part of the spacetime that the slices cannot reach.

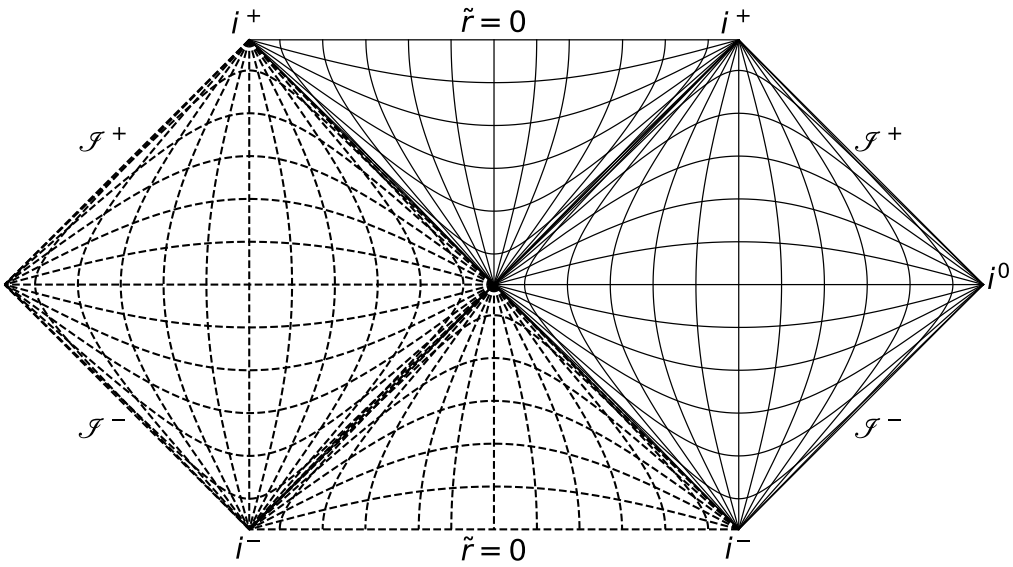

Figure 4.2: Maximal analytical extension of Schwarzschild spacetime. The dashed lines correspond to the extension of the original Schwarzschild solution.

4.2 Hyperbolicity and Well-Posedness

The Einstein-Klein-Gordon system of equations has already been studied in hyperboloidal slices, and successful numerical simulations have been performed with it in [10]. We will also require this for the new Einstein-KG-Maxwell system. The methods described henceforth follow [10, 56, 57]. In our PDEs, we have derivatives that are second order in space. Fortunately, our equations are linear with respect to the derivatives, not needing any approximation to look at the principal part of the equations to study the overall hyperbolicity of the system. What we mean by hyperbolicity will be made clear in a moment. Let us say our system can be written as a function of the vector $\mathbf{u}$, where $\mathbf{u}$ has in each entry one of the variables we are evolving. Therefore, by defining a linear operator P, we can say our system breaks down to,

$$\partial_t \mathbf{u} = P\mathbf{u}\,. \tag{4.19}$$

It will be useful to say that $\mathbf{u}$ can be written as $\mathbf{u} = \{u, v\}$, where v corresponds to the variables that are only derived once in space and u to the variables derived twice. This allows us to write the operator as,

$$P = \begin{pmatrix} A^i\partial_i + B & C \\ D^{ij}\partial_i\partial_j + E^i\partial_i + F & G^i\partial_i + J \end{pmatrix}. \tag{4.20}$$

Doing a Fourier transformation on the system (using $\omega_i = \omega n_i$ and $M^n = M^i n_i$), we get that P changes to its corresponding Fourier counterpart, $\hat{P}$,

$$\hat{P} = \begin{pmatrix} i\omega A^n + B & C \\ \omega^2 D^{nn} + i\omega E^n + F & i\omega G^n + J \end{pmatrix}. \tag{4.21}$$

The principal part of the system corresponds to the higher-order derivatives in each of the four blocks. However, before that, we do a pseudo-differential reduction, by defining a new variable, $\hat{w} = i\omega\hat{u}$, which also adds the trivial constraint $\mathscr{C} = \hat{w} - i\omega\hat{u}$. This implies the change of $\hat{u}$ to $\hat{u}_R = \{\hat{u}, \hat{v}, \hat{w}\}$, to accommodate the first order in space derived variables, in Fourier space. This makes the $\hat{P}$ matrix become,

$$\hat{P}_R = \begin{pmatrix} B & A^n & C \\ 0 & i\omega A^n + B & i\omega C \\ F & i\omega D^{nn} + E^n & i\omega G^n + J \end{pmatrix}. \tag{4.22}$$

Thus, the corresponding matrix to the principal part, called the principal symbol, can be written as,

$$\hat{P}'_R = \begin{pmatrix} 0 & 0 & 0 \\ 0 & i\omega A^n & i\omega C \\ 0 & i\omega D^{nn} & i\omega G^n \end{pmatrix}. \tag{4.23}$$

With this said, it means that our system will have a solution of the type, $\hat{u}_R(t) = e^{\hat{P}'_R t}\hat{u}_R(0)$, where $\hat{u}_R(0)$ is the initial data for the system vector. If $\hat{P}'_R$ is diagonalizable and has (a complete set of) only real eigenvalues, the solution just stated will be purely oscillatory and bounded by the initial data. This means

that the system is well posed and is strongly hyperbolic. Weak hyperbolicity would mean that the system still has real eigenvalues, but the diagonalization of the matrix $\hat{P}'_R$ would be incomplete (i.e., not a complete set of eigenvectors), giving a Jordan canonical form [58]. Another interesting fact about this analysis is that the eigenvalues that one extracts from this procedure correspond to the characteristic speeds or eigenspeeds, which are the speeds at which information travels in the system. A complete list of these speeds is shown in [10] for several formulations of Einstein's equations. We return to this in Section 6.5.

4.3 Misner-Sharp Mass and the Apparent Horizon finder

Although the concept of mass is hard to define in GR, in spherical symmetry, there is a way to do it. This concept of (quasi-local) mass we are going to discuss now is called the Misner-Sharp Mass [59]. For the case of the simplest black hole, Schwarzschild, it corresponds to the exact mass of the black hole. The first thing we must take notice of is how to write the physical radial coordinate (also called the areal radius), R_A, as a function of our rescaled variables [10]. In the usual physical metric, we will have that:

$$d\tilde{s}^2 = R_A^2 d\tilde{\sigma}^2 \,.$$

Comparing with (3.70), we get the expression:

$$R_A = \frac{r}{\Omega}\sqrt{\frac{\gamma_{\theta\theta}}{\chi}} \,. \tag{4.24}$$

The definition of the Misner-Sharp mass $M_{\rm MS}$ is then

$$\tilde{g}^{\mu\nu}(\tilde{\nabla}_\mu R_A)(\tilde{\nabla}_\nu R_A) = 1 - \frac{2M_{\rm MS}}{R_A} \,, \tag{4.25}$$

which can be rewritten directly in terms of the variables used in the equations shown in the previous sections,

$$\begin{aligned}
M_{\rm MS} = \frac{r}{2\Omega}\left(\frac{\gamma_{\theta\theta}}{\chi}\right)^{1/2}\Bigg(1 &- \frac{\gamma_{\theta\theta}}{\gamma_{rr}} + \frac{r^2\dot{\chi}^2\gamma_{\theta\theta}}{4(\alpha)^2(\chi)^3} - \frac{r^2\dot{\chi}\gamma_{\dot{\theta}\theta}}{2(\alpha)^2(\chi)^2} + \frac{r\dot{\chi}\gamma_{\theta\theta}\beta^r}{(\alpha)^2(\chi)^2} + \frac{r^2\gamma_{\dot{\theta}\theta}{}^2}{4\gamma_{\theta\theta}(\alpha)^2\chi} - \frac{r\gamma_{\dot{\theta}\theta}\beta^r}{(\alpha)^2\chi} + \frac{\gamma_{\theta\theta}(\beta^r)^2}{(\alpha)^2\chi} \\
&- \frac{r\gamma'_{\theta\theta}}{\gamma_{rr}} + \frac{r^2\dot{\chi}\beta^r\gamma'_{\theta\theta}}{2(\alpha)^2(\chi)^2} - \frac{r^2\gamma_{\dot{\theta}\theta}\beta^r\gamma'_{\theta\theta}}{2\gamma_{\theta\theta}(\alpha)^2\chi} + \frac{r(\beta^r)^2\gamma'_{\theta\theta}}{(\alpha)^2\chi} - \frac{r^2(\gamma'_{\theta\theta})^2}{4\gamma_{rr}\gamma_{\theta\theta}} + \frac{r^2(\beta^r)^2(\gamma'_{\theta\theta})^2}{4\gamma_{\theta\theta}(\alpha)^2\chi} - \frac{r^2\dot{\chi}\gamma_{\theta\theta}\beta^r\chi'}{2(\alpha)^2(\chi)^3} \\
&+ \frac{r^2\gamma_{\dot{\theta}\theta}\beta^r\chi'}{2(\alpha)^2(\chi)^2} - \frac{r\gamma_{\theta\theta}(\beta^r)^2\chi'}{(\alpha)^2(\chi)^2} + \frac{r\gamma_{\theta\theta}\chi'}{\gamma_{rr}\chi} - \frac{r^2(\beta^r)^2\gamma'_{\theta\theta}\chi'}{2(\alpha)^2(\chi)^2} + \frac{r^2\gamma'_{\theta\theta}\chi'}{2\gamma_{rr}\chi} + \frac{r^2\gamma_{\theta\theta}(\beta^r)^2(\chi')^2}{4(\alpha)^2(\chi)^3} - \frac{r^2\gamma_{\theta\theta}(\chi')^2}{4\gamma_{rr}(\chi)^2} \\
&+ \frac{2r\gamma_{\theta\theta}\Omega'}{\gamma_{rr}\Omega} - \frac{r^2\dot{\chi}\gamma_{\theta\theta}\beta^r\Omega'}{(\alpha)^2(\chi)^2\Omega} + \frac{r^2\gamma_{\dot{\theta}\theta}\beta^r\Omega'}{(\alpha)^2\chi\Omega} - \frac{2r\gamma_{\theta\theta}(\beta^r)^2\Omega'}{(\alpha)^2\chi\Omega} + \frac{r^2\gamma'_{\theta\theta}\Omega'}{\gamma_{rr}\Omega} - \frac{r^2(\beta^r)^2\gamma'_{\theta\theta}\Omega'}{(\alpha)^2\chi\Omega} + \frac{r^2\gamma_{\theta\theta}(\beta^r)^2\chi'\Omega'}{(\alpha)^2(\chi)^2\Omega} \\
&- \frac{r^2\gamma_{\theta\theta}\chi'\Omega'}{\gamma_{rr}\chi\Omega} - \frac{r^2\gamma_{\theta\theta}(\Omega')^2}{\gamma_{rr}(\Omega)^2} + \frac{r^2\gamma_{\theta\theta}(\beta^r)^2(\Omega')^2}{(\alpha)^2\chi(\Omega)^2}\Bigg) \,.
\end{aligned}$$

This mass coincides with the Bondi mass at null infinity, which will be useful for us. It also coincides with the ADM mass at spacelike infinity. In the cases we have a scalar field perturbation energetic enough to collapse into a black hole, it is important to have something that gives us an indication regarding the

formation of a black hole. The act of finding an event horizon can only be done after the simulation has ran. One can, however, use the apparent horizon finder. The apparent horizon is defined as the outermost marginally trapped surface, whose null geodesics have zero expansion and is located inside the event horizon, assuming that cosmic censorship holds. In spherical symmetry, it can be calculated in a very simple way, i.e., when the following expression equals zero:

$$1 - \frac{2M_{\rm MS}}{R_A} = \Omega^2 \bar{g}^{\mu\nu} (\bar{\nabla}_\mu R_A)(\bar{\nabla}_\nu R_A) = 0\,. \tag{4.26}$$

4.4 Quasi-Normal Modes and Power-law decay tails

As the last relevant topic for further discussion in the results, we focus now on quasi-normal modes (QNM) and power-law decay tails. One of the advantages of the hyperboloidal formulation is the ease with which one can show the ringing of QNM at scri+, [60]. Now, what are these modes? They describe how a perturbation of a scalar field in Schwarzschild (or other spacetimes) can lead to oscillating modes at timelike and future null infinities. The main idea is that the Klein-Gordon equation in one dimension has an extra term coming from the spheroidal decomposition of its solutions. The same happens, for example, when finding solutions to Schrödinger's equation. The asymptotic behaviour of the scalar field was first studied by Richard Price in his famous paper [61]. He also found out that after these modes stop being excited, it is expected that the scalar field decays with a power-law, i.e.,

$$\lim_{t\to+\infty} \phi(t, r) \propto t^p\,.$$

In our case, one expects the same for the real and the imaginary parts. The key aspect is that, along timelike surfaces, the p in the equation can be analytically derived to be -3, while along null surfaces, it is -2. This is only true for $l = 0$ poles. In our case, hyperboloidal slices, these asymptotically become null surfaces, so we can see this decay. For the case of a charged scalar field in a charged background, we refer to [16, 18, 62, 17], but we will discuss them in more detail during the results. With this, we finish off the necessary setup for the results and can proceed to the implementation.

Part II

Implementation and Results

Chapter 5

Numerical Methods

5.1 Spatial Discretization

First, we discretize space (we choose x instead of r for better readability). To avoid the origin ($x = 0$) and scri+ ($x = 1$), we will be using a shifted/staggered grid:

$$x_i = \left(\frac{1}{2} + i\right) \Delta x.$$

For the spatial derivatives, we use 4th-order finite differences (FD). Spectral discretization was also considered, but in this framework, local instabilities will propagate faster, which is not ideal for the development stage of the work we are performing.

5.2 Boundary Conditions

Because we are using a staggered grid, it is simpler to impose the boundary conditions through extrapolation at the ghost points of the grid. Ghost points are an extension of the grid we are using for our simulation, and they increase the higher convergence order we use. In 4th order FD, we have two ghost points at each edge of our grid, the origin and $\mathscr{I}^+$. Given the completely different nature of both of these places, we have to deal with them separately. Let us first look at the origin.

Boundary conditions at the origin

Following [10], we set the boundary conditions at the origin using the parity properties of each variable. In spherical symmetry, scalars are even, while vector components can have odd or even parity. Tensors, on the other hand, depend on the lower-order tensors one uses to construct them. This can be stated more clearly as follows,

$$\text{Even Parity: } A(-r) = A(r)\,, \quad \text{Odd Parity: } B(-r) = -B(r)\,.$$

For the variables of our model, we have the following boundary conditions at the origin [10]:

$$\text{Even Parity:} \quad \chi, \gamma_{rr}, \gamma_{\theta\theta}, A_{rr}, K, \Theta, \alpha, c_\phi, d_\phi, c_\Pi, d_\Pi, \Phi, \Psi \quad \text{Odd Parity:} \quad \Lambda^r, \beta^r, E^r, A^r_3$$

Boundary Conditions at $\mathscr{I}^+$

At $\mathscr{I}^+$, causality demands purely outgoing waves only. This comes from the fact that scri+ can only be reached through light rays. If there were any ingoing radiation, we would be getting information from the future. This outflow condition is then imposed through the ghost points [63], and the expressions for a generic variable A are given in [64]. They read:

$$\begin{aligned} \Delta x^5 D_-^5 A_{N+1} &= 0 \\ \Delta x^5 D_-^5 A_{N+2} &= 0 \end{aligned} \tag{5.1}$$

where A_{N+1} and A_{N+2} are the two ghost points, and D_+ is the backward finite difference operator, defined as,

$$D_- A_n = \frac{A_n - A_{n-1}}{\Delta x} .$$

We note that not all variables have to satisfy the above condition. The condition has to be imposed for the variables that appear derived twice in space in the evolution equations, to get 4th-order convergence. However, for a variable only once derived in space, the following conditions are enough to preserve 4th order convergence: $\Delta x^4 D_-^4 A_{N+1} = 0$, $\Delta x^4 D_-^4 A_{N+2} = 0$. In the code, however, condition (5.1) is used for all variables.

Boundary conditions at the origin

In the simulations where we have a black hole, the boundary conditions at the origin change. Given that we are using trumpet initial data, our origin corresponds to a puncture inside the black hole. The boundary conditions we use are then similar to the previous section, but assuming an inflow of information, instead of outflow. This is then equivalent to:

$$\begin{aligned} \Delta x^5 D_+^5 A_{-1} &= 0 \\ \Delta x^5 D_+^5 A_{-2} &= 0 , \end{aligned}$$

analogous to the previous subsection.

5.3 Method of Lines and Time Integration

The Method of Lines is a very common method to transform a partial differential equation into N ordinary differential equations (ODE), by discretizing first in space. In practice, it consists of having a system of equations whose LHSs are $\partial_t A$, with A being a generic variable, corresponding to a given expression on the respective RHS. We then discretize them in time, similar to what we did for space:

$$t_{i+1} = t_i + \Delta t .$$

In order to integrate in time, we use a 4th-order Runge-Kutta scheme. This way, the overall expected convergence order of our code is 4th order. Some things have still to be taken into account, however. One

of them is numerical dissipation.

5.4 Kreiss-Oliger Dissipation

We will follow [65, 66], where Kreiss-Oliger dissipation is added via the last term in,

$$\partial_t \mathbf{u} \rightarrow \partial_t \mathbf{u} + Q\mathbf{u} \tag{5.2}$$

where Q is a derivative operator of order $2r$, given by

$$Q = \sigma(-1)^r(\Delta x)^{2r-1}(D_+)^+\rho(D_-)^r/2^{2r}. \tag{5.3}$$

Here, σ represents the dissipation's strength, ρ is a weighting function. Inside the grid, $\rho = 1$, and outside the grid $\rho = 0$. This operator should be used for a $2r-2$ accurate scheme. In our case, we are aiming at a 4th-order accurate scheme. Thus, we need to have $r = 3$:

$$Q = -\sigma(\Delta x)^5(D_+)^3(D_-)^3/64.$$

It is useful to provide stable numerical evolution and is commonly used in the NR community.

5.5 Convergence Tests

To ensure that the system is evolving initial data that asymptotically goes to a physical result and we have stable simulations, we have to fulfill the Courant-Friedrich-Lewy (CFL) condition. It preserves correct information propagation and will be useful for convergence tests.

CFL condition

In a one-dimensional code, the CFL condition can be stated as,

$$C = u\frac{\Delta t}{\Delta x} \leq C_{max}, \tag{5.4}$$

where C is the Courant number and C_{max} is the maximum value C can attain for the code to remain stable. u is the magnitude of the velocity of a given wave in our PDE system. What this condition tells us is that if we decrease the spatial step, the time step has to go down accordingly. If not, the speed at which information propagates in our system can be bigger than what our discretization allows, and this will produce numerical instabilities. For the system modelled, we found roughly $C_{max} \approx 0.2$.

Pointwise Convergence

Following [67], we first consider a given method of convergence order p with a grid spacing h. We can relate the numerical solution that our code will produce to the exact solution as follows,

$$u_h = u_{\text{exact}} + \epsilon h^p,$$

where ϵ is an error function independent of h. If we now increase our step by f, this implies in the above equation that $h^p \to (fh)^p$. If we do three runs each with different grid spacing, u_h, u_{fh}, and u_{f^2h}, we can also calculate the following ratio:

$$\frac{u_{f^2h} - u_{fh}}{u_{fh} - u_h} = \frac{(u_{\text{exact}} + \epsilon f^{2p} h^p) - (u_{\text{exact}} + \epsilon f^p h^p)}{(u_{\text{exact}} + \epsilon f^p h^p) - (u_{\text{exact}} + \epsilon h^p)} = f^p \tag{5.5}$$

we get a result independent of any grid spacing. Further in the work, it will be usual to use $f = 3$ and $p = 4$, which provides $f^p = 81$. For the case of variables that have values very close to zero, checking convergence is trickier. This is the case for the constraints, because they vanish at the continuum level. For their case, then, we will opt for showing the 3 different resolutions and scale them accordingly.

5.6 Code

Given that the code developed is new, we will give a very brief description of how it works. The code is written in Mathematica, Python, and C++. In Mathematica, we used the package *xAct* [68] to systematize the derivation of the evolution equations and respective constraints (including the equations shown in previous sections). These are then copied to the C++ code, which evolves the evolution equations and is adapted to several scenarios. After the output is read with Python, using its graphic capabilities that are more versatile than C++. We expect to make the code public as soon as the implementation is more robust. The output of the code is given in code units and therefore we will refrain from showing units in the graphs, in Section 6.

Chapter 6

Results

6.1 Real Part of Scalar Field in Vacuum Spacetime

Here we will reproduce, with the new code, a result already shown in [10]. We remove the electromagnetic coupling and focus on the real part of the scalar field. The first step is solving the constraints. To tackle this, we carefully choose $\bar{c}_\Pi$, by looking at the momentum constraint (A.46). It is satisfied if

$$\bar{c}_\Pi = \beta^r \bar{c}'_\phi + \beta^r \bar{c}_\phi \frac{\Omega'}{\Omega} \,. \tag{6.1}$$

Inserting this condition into the Hamiltonian constraint (A.45), we solve the Hamiltonian constraint for χ:

$$\begin{aligned} \mathcal{H} = &-\frac{8}{9}\pi r^2 \bar{c}_\phi^2 \chi + \frac{24(1-r^2\chi)}{(1-r^2)^2} + \frac{8}{9}\pi r(1-r^2)\bar{c}_\phi \chi \bar{c}'_\phi - \frac{2}{9}\pi(1-r^2)^2\chi(\bar{c}'_\phi)^2 \\ &+ \frac{4\chi'}{r} - \frac{5(\chi')^2}{2\chi} + \frac{6(-4\chi + 2r\chi'/3)}{1-r^2} + 2\chi'' \end{aligned} \tag{6.2}$$

The Z-constraint is automatically satisfied, completing the setup. For $\bar{c}_\phi$, we choose it to be equal to a Gaussian-type distribution that goes to 0 fast enough at the origin and at $\mathscr{I}^+$ (enforcing numerical compact support),

$$\bar{c}_\phi = Ar^2 \exp\left(-\frac{(r^2-\mu^2)^2}{4\sigma^4}\right) , \tag{6.3}$$

and then solve the above ODE with respect to χ. This ODE, however, is lacking initial boundary conditions: at $r = r_{\mathscr{I}}$, the solution should be flat, which means $\chi = 1$ there. The other condition is given at $r = 0$: the derivative of χ there must be 0, due to the parity conditions. With this input, we had to develop an adapted shooting method, because the solutions (or local minima) of (6.2) are between volatile points that quickly blow up numerically. The results for the initial data for $\bar{c}_\phi$ and χ are shown in Fig. 6.1.

When we insert the initial data in Fig. 6.1, together with (4.5), we can then input everything in the code and see the system running. The results are shown in Fig. 6.2. We do not to show all of the variables being evolved because, otherwise, there would be too much information to be read from a single graphic. We also opted for showing separately the evolution for $\bar{c}_\phi$ and χ, given that χ has very subtle variations that can not be seen when compared to the scalar field's perturbation.

A similar procedure can be performed for the imaginary part of the scalar field, with the result being

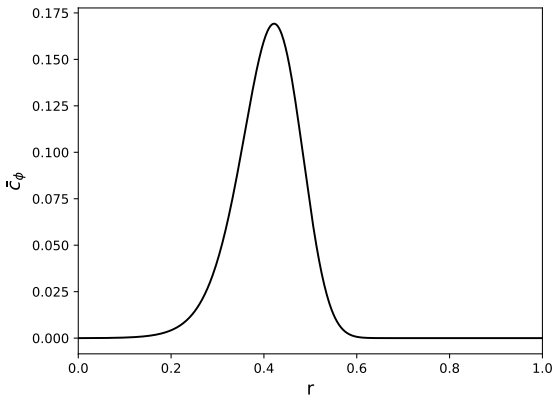

(a) Profile of $\bar{c}_\phi$ (6.3), with $A = 1$, $\mu = 0.4$ and $\sigma = 0.2$.

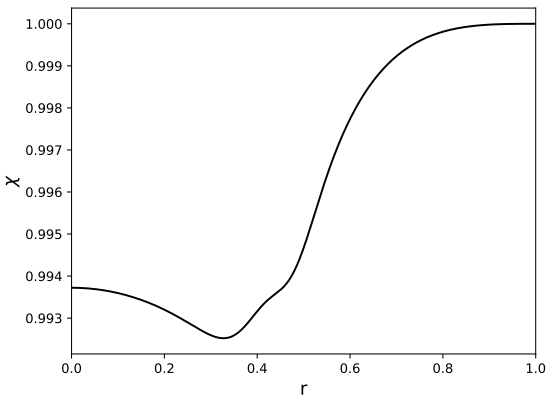

(b) Numerical result of χ.

Figure 6.1: Initial data for $\bar{c}_\phi$ and χ, on a regular spacetime.

equivalent. The initial conditions would only have to pass from the real part to the imaginary part, i.e., we would give a Gaussian perturbation to $\bar{d}_\phi$ and require,

$$\bar{d}_\Pi = \beta^r \bar{d}'_\phi + \beta^r \bar{d}_\phi \frac{\Omega'}{\Omega}$$

and then solve the Hamiltonian constraint for χ. Another possibility is to perturb both parts. This procedure, however, will imply an initial charge density, which will activate the coupling to Maxwell. If we were, however, to say that the scalar field's charge is 0, then we would not have this problem. Although we have all these possibilities, these are analogous to what we have in Fig. 6.2.

Going back to (5.5), we can show that the code is giving correct results if we recover the appropriate convergence order. In our case, given that we have a staggered grid, we cannot increase or decrease the resolution by even powers; otherwise, one of the runs will be evaluated at 0 (check Fig. 6.3 in [10]). If, on the other hand, we want the several runs to be evaluated at common points to all of them, we have to change the resolution by even powers. For example, increasing the grid precision by a factor of 3, together with a 4th order overall code (RK4 in time, 4th order FD in space), we expect a $3^4 = 81$ times more refined simulation. The time step has also to decrease by the same factor of 3, to keep the CFL condition constant. We still have to take into account that if we have too much resolution, the differences we will be seeing are just a product of machine precision. Thus, we chose a combination of resolutions that better shows the convergence: 720 points for the highest resolution, 480 points for the medium resolution, and 320 points for the lowest resolution (and the simulation in Fig. 6.2 used 320 points). The constraints' convergence is plotted in Fig. 6.3. One of the things we immediately see in the initial data for the Hamiltonian pointwise convergence plots is some imperfections at $r = r_{\mathscr{I}}$. These are caused by our shooting method, but these imperfections go away with time. Overall, the behavior of these pointwise convergence plots shows that the system is consistent, and we can be sure that we can trust our results.

Regarding the parameters used in this simulation, we have chosen similar ones to [10]. This implies: $k_1 = 1.5$, $k_2 = 0.1$, $\sigma_{KO} = 0.01$. This simulation could also be run without Kreiss-Oliger dissipation successfully. For the gauge conditions, we used $\eta = 0.1$, $\xi_{cK} = 1.0$, $n_{cK} = 1.0$, $\lambda = 0.75$ and $\xi_{\beta^r} = 0.0$.

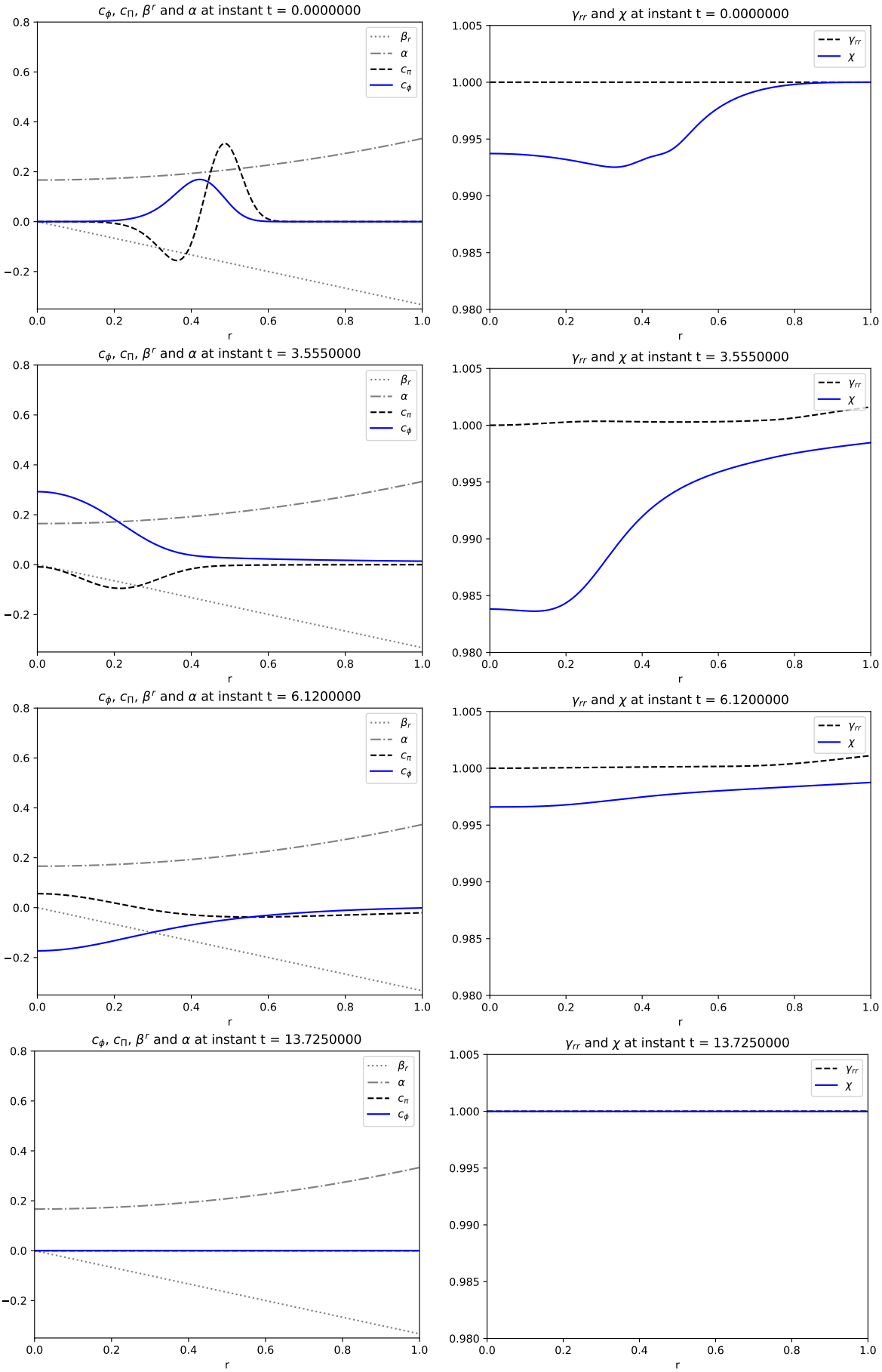

Figure 6.2: $\bar{c}_\phi$, $\bar{c}_\Pi$, β^r, α, χ and γ_{rr} evolving until the scalar field is radiated out through future null infinity, at $r_{\mathscr{I}} = 1$.

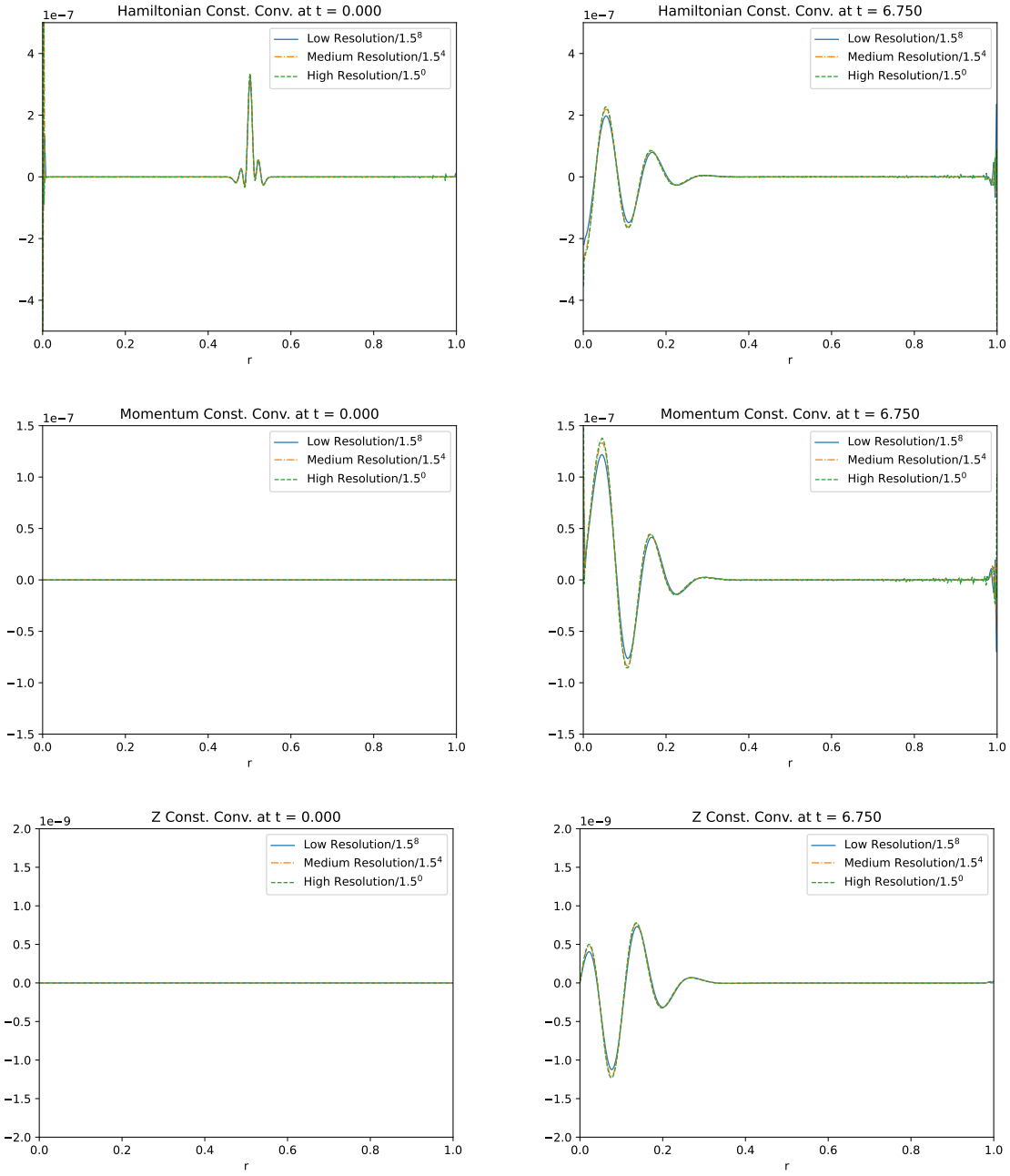

Figure 6.3: Pointwise constraint convergence. The "Low Resolution" lines are downscaled by the factor 1.5^4 and the "Medium Resolution" lines by 1.5^4, according to the convergence scheme chosen.

6.2 Four-Potential in Vacuum Spacetime

In regular spherically symmetric spacetime, there are no special configurations we could test besides the point charge at $r = 0$. (Interesting electrovacuum solutions can be found in axisymmetric models [69]. These are called geons, and they represent an unstable equilibrium between Maxwell's and Einstein's equations.) In electrovacuum, in spherical symmetry, there are only two types of solutions for the electric field, given the Gauss constraint: either a charge at $r = 0$ or no electric field. The last one is obvious; there is no charge density to create an electric field, and the trivial solution is setting the electric field to 0.

The other solution, of a charge at $r = 0$, we can get by looking back at the Gauss constraint,

$$\frac{2E\chi}{\gamma_{rr}r} + \frac{\chi E'}{\gamma_{rr}} - \frac{E\chi'}{2\gamma_{rr}} - \frac{E\chi\gamma'_{rr}}{(\gamma^2_{rr})} = 0\,,$$

and substituting γ_{rr} by 1 we can integrate it to get the solution,

$$E = \frac{\sqrt{\chi}Q}{r^2}\,, \tag{6.4}$$

which is the usual expression for the electric field in a curved spacetime [70, 71]. The constant Q appears during the integration, the physical relevance of which is given *a posteriori*. We will return to this afterward. Another option we can test for the electromagnetic part of our simulation is to look at the two components of the four-potential. They are physically irrelevant, so we should be able to evolve them freely without affecting the rest of the variables. Assuming $\Phi \neq 0$ and $A_{3r} \neq 0$, if we were to use the alternative derivation of our equations as shown in Appendix B, we would get that our constraints would be satisfied if,

$$\Phi = \delta\Phi\,, \quad A_{3r} = -\frac{1+r^2}{2r}\delta\Phi$$

where the perturbation in Φ could be any.

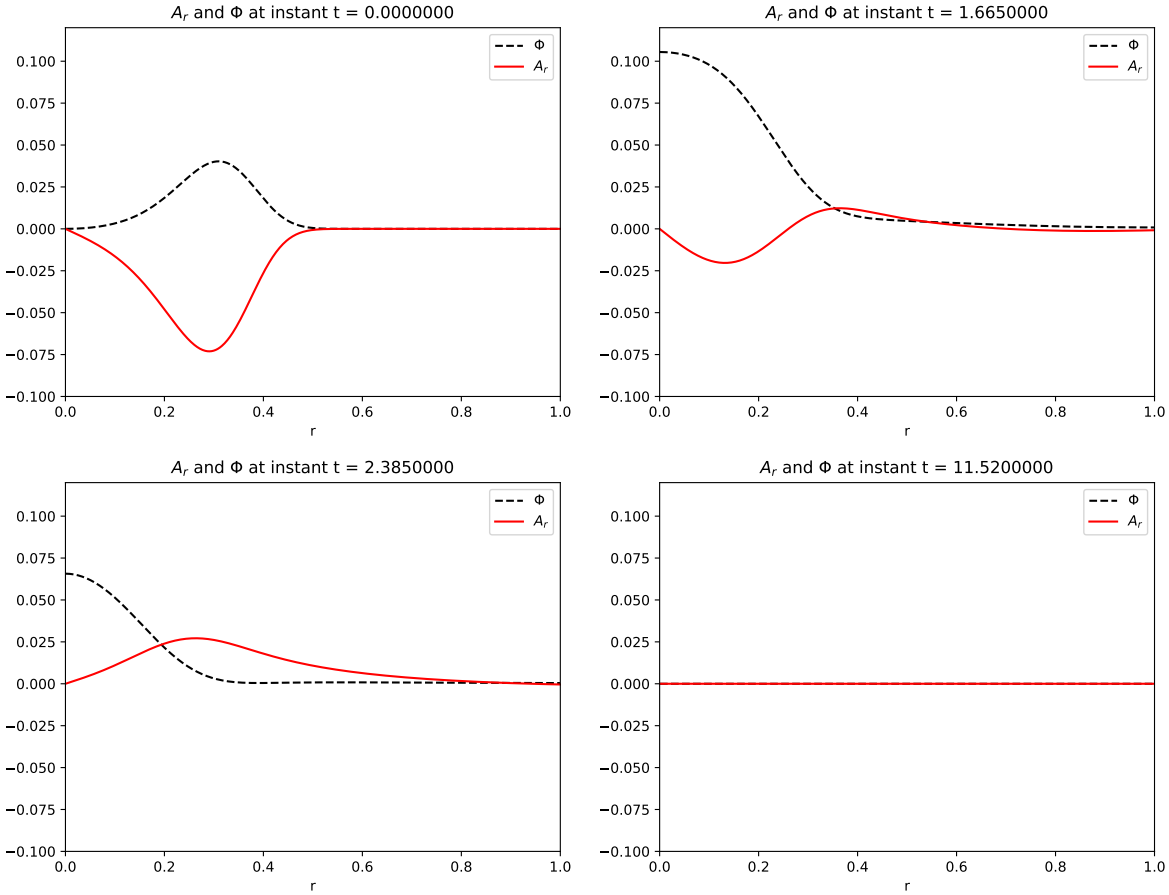

Figure 6.4: Evolution of the electromagnetic potentials, Φ and A_{3r}, until they leave through future null infinity.

Note, however, that the constraints only depend on these two quantities when they are coupled to the

scalar field. Thus, as one would expect, our system will not care about the values that Φ and A_{3_r} take, in the specific case of electrovacuum. This is especially true since the electric field's evolution equation is not directly coupled to the potentials, and it will not be evolved if it is set initially to 0. Thus, from the equations, we expect that the electromagnetic potentials, if they are excited initially, will not change the overall system. That is exactly what the simulation provides. We use the initial perturbation for Φ similar to the one for $\bar{c}_\phi$ in the previous section. This type of perturbation makes A_{3_r} go to 0 at the origin as well, something we require for vectorial quantities. The results for this are shown above in Fig. 6.4. The constraints do not see this behaviour, and they remain close to machine precision, as expected. Regarding the electric field, this will be discussed in greater detail in the following sections.

6.3 Charged Scalar Field in Regular Initial Data

Having checked the coupled behaviour of the KG equation and the four-potential in the code independently, we can now turn on the coupling between them. In the broader picture of the hyperboloidal formulation, this is something that has never been done before. First, we continue to do a perturbation on the real part of the scalar field. However, now that we have the electromagnetic part on, at some point in the simulation, we will excite the imaginary part of the scalar field. Having both the real and imaginary parts of the scalar field with non-zero values, there will be a nonzero charge and current densities that should excite the electric field. With this, all of the variables of our system should come into play, and we can now check the Gauss constraint convergence as well, as an additional consistency test of our code. Fortunately, the momentum constraint does not depend on any of the electromagnetic coupling (related to the vanishing trace of it), and thus the initial condition for it to be solved continues to be the same as before.

By setting $\Phi = E_r = 0$, initially, the Hamiltonian constraint appears with an extra term that comes from the coupling between the scalar field and the vector potential. This means that we have the freedom to choose any type of behavior for the vector potential. We will give it a similar bump as to the scalar field, but with a different positioning in space and a different amplitude, so they remain distinguishable. The Hamiltonian constraint thus becomes,

$$\mathcal{H} = -\tfrac{8}{9}\pi r^2\left(\bar{c}_\phi\right)^2\chi + \frac{24\left(1-r^2\chi\right)}{(1-r^2)^2} + \tfrac{8}{9}\pi r(1-r^2)\bar{c}_\phi\chi\bar{c}'_\phi - \tfrac{2}{9}\pi(1-r^2)^2\chi\left(q^2\left(A_{3_r}\right)^2\left(\bar{c}_\phi\right)^2 + \left(\bar{c}'_\phi\right)^2\right) + \frac{4\chi'}{r} - \frac{5\left(\chi'\right)^2}{2\chi} + \frac{6\left(-4\chi + \frac{2}{3}r\chi'\right)}{1-r^2} + 2\chi'' .$$

We have chosen the charge of the complex scalar field to be $q = -1$. The greater it is, the stronger the current and charge densities that source Maxwell's equations, and therefore stronger the bond between the real and imaginary parts. The initial profile of this part of the simulation is shown in Fig. 6.5.

To plot the evolution, we chose to show only the new dynamics: we leave the behavior of the real part of the scalar field out to focus on its imaginary part and the electromagnetic fields. This is shown in Fig. 6.7, together with the charge and current densities. The convergence of the Gauss constraint is plotted in Fig. 6.6. From a quick inspection, we see that there are some noticeable problems near the origin for the Gauss constraint. This shares some features with the momentum and Hamiltonian

constraints convergence, and quickly goes away as soon as the fields are reflected at the origin. Looking back at the overall behavior of the system (Fig. 6.7), we see an expected behavior, the imaginary part is excited, the charge and current densities arise, and the electric field comes into play as well. With this, we finish the overall tests of the system in regular spacetime, and we can pass on to Schwarzschild spacetime, which will involve an extra step.

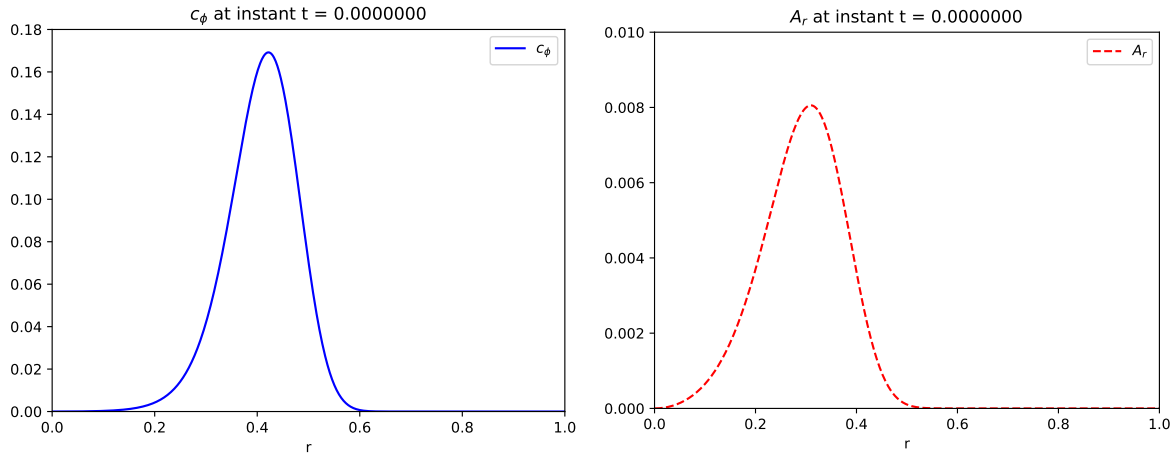

Figure 6.5: Initial profiles for $\bar{c}_\phi$ and A_{3r}. Note the different scales. We opted for a smaller perturbation in the vector potential and centered it more to the left.

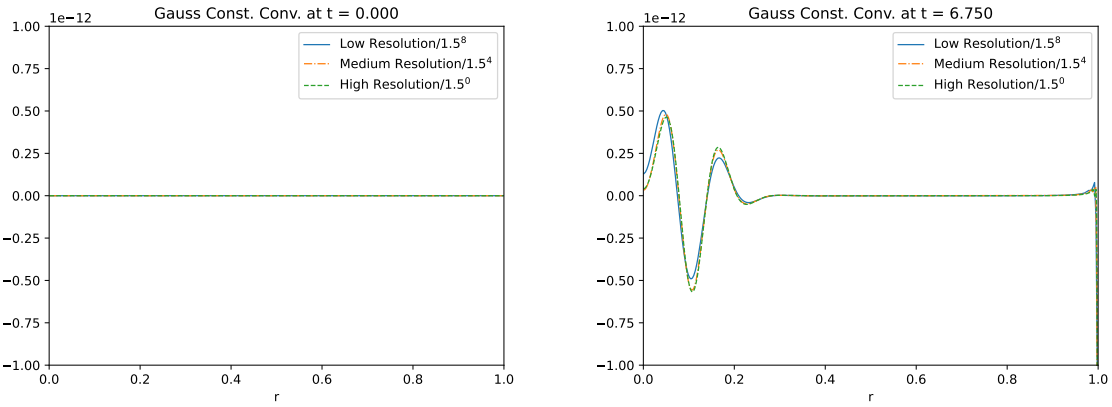

Figure 6.6: Gauss constraint convergence for an initial perturbation of the real scalar field and the radial component of the four-potential.

6.4 Real Part of Scalar Field in Schwarzschild Spacetime

To have the scalar field in a Schwarzschild spacetime, i.e., with a stationary black hole at $r = 0$, we will now consider trumpet initial data that goes through the event horizon (check Fig. 4.1). The initial conditions for all the variables are described in (4.11), but the one that will give us $\bar{\Omega}$ is (4.12), which we can rewrite to get the following ODE,

$$\bar{\Omega}' = \frac{\bar{\Omega}}{r} - \frac{\sqrt{9C_{\mathrm{CMC}}^2\bar{\Omega}^2 + 9Q^2\bar{\Omega}^4r^2 + 6(C_{\mathrm{CMC}}K_{\mathrm{CMC}} - 3M)\bar{\Omega}^3r^3 + 9\bar{\Omega}^2r^4 + K_{\mathrm{CMC}}^2r^6}}{3r^3}.$$

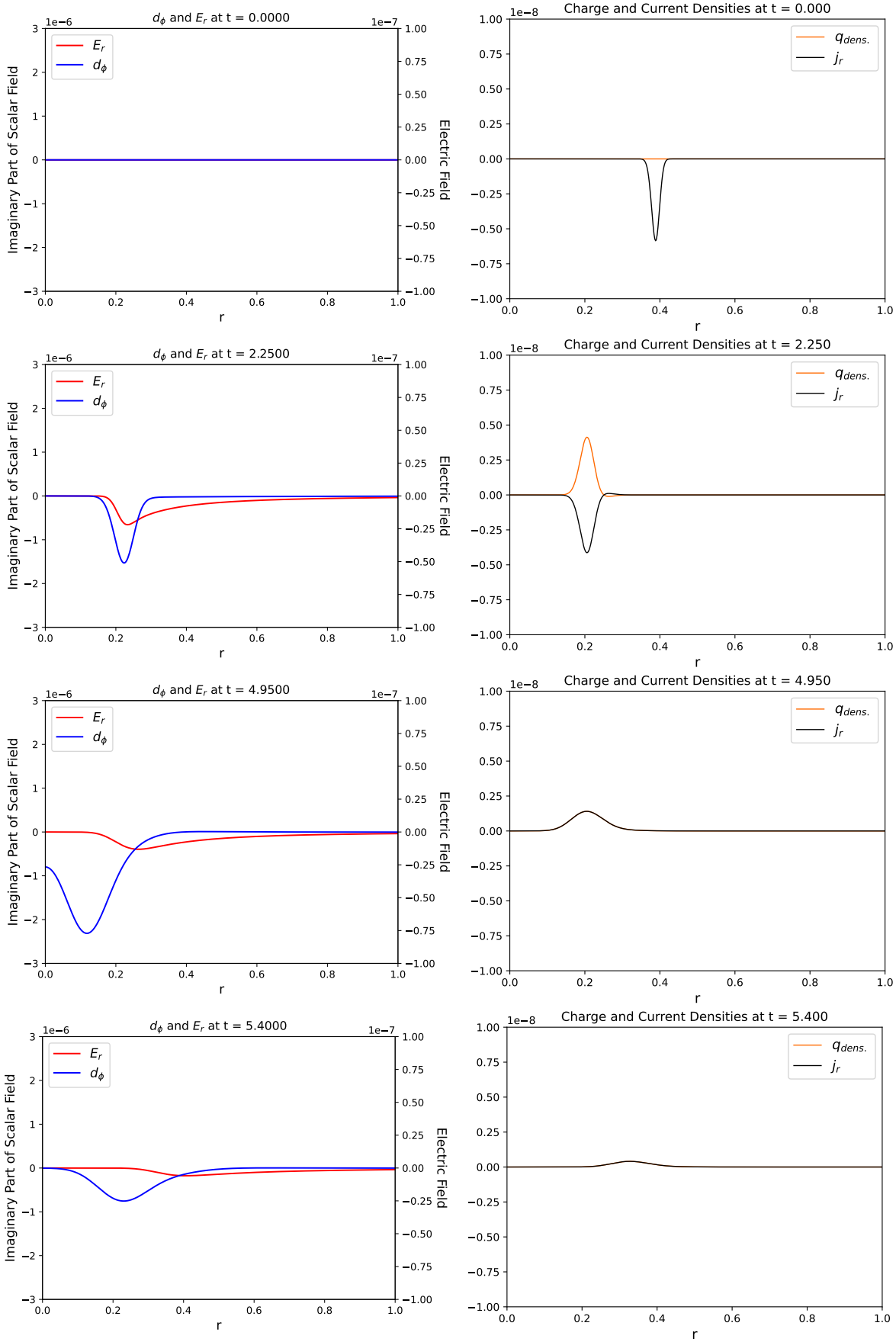

Figure 6.7: $\bar{d_\phi}$, E_r, $\bar{j_r}$ and $\bar{q}_{\text{dens.}}$ evolving until the scalar field is radiated out through future null infinity, at $r_{\mathscr{I}} = 1$.

Numerically, this equation makes it difficult to obtain a solution different from the trivial one equal to 0. This has to do with the fact that $\bar{\Omega}$ goes to 0 both at the origin and at future null infinity. We do the proposed transformation for this factor in [10],

$$\hat{\Omega} = \frac{R_0}{r}\bar{\Omega} - 1\,.$$

This way, our ODE becomes,

$$\begin{aligned}\hat{\Omega}' = \frac{1}{3R_0^2 r}\big[&9C_{\rm CMC}^2 + 6C_{\rm CMC}K_{\rm CMC}R_0^3 + R_0^2(9Q^2 - 18MR_0 + 9R_0^2 + K_{\rm CMC}^2R_0^4)\\ &- 18(3C_{\rm CMC}^2 + C_{\rm CMC}K_{\rm CMC}R_0^3 + R_0^2(2Q^2 - 3MR_0 + R_0^2))\hat{\Omega}\\ &+ 9(15C_{\rm CMC}^2 + 2C_{\rm CMC}K_{\rm CMC}R_0^3 + R_0^2(6Q^2 - 6MR_0 + R_0^2))\hat{\Omega}^2\\ &- 6(30C_{\rm CMC}^2 + 6Q^2R_0^2 + C_{\rm CMC}K_{\rm CMC}R_0^3 - 3MR_0^3)\hat{\Omega}^3 + 9(15C_{\rm CMC}^2 + Q^2R_0^2)\hat{\Omega}^4\\ &- 54C_{\rm CMC}^2\hat{\Omega}^5 + 9C_{\rm CMC}^2\hat{\Omega}^6\big]^{1/2}\,.\end{aligned} \tag{6.5}$$

The reader will notice that there is no explicit dependence on r inside the square root.

About reproducing these results in future works

If someone wants to replicate what will be shown below, one has to recall that: we are using a staggered grid, i.e., our grid starts at a half step from the origin and it also does not touch future null infinity, stopping at half a step before. Given that we are evolving our system with Runge-Kutta 4, we are also evaluating at each half-step between these grid points. Therefore, if one wants to use $\bar{\Omega}$, one has to change the grid to a regular one, with double the amount of points, to have it evaluated at all steps: not only of the "main" grid of the simulation but also the other intermediate steps of the rest of the system. This is remarkably different from the time-evolution RK4 we have been using, because this $\bar{\Omega}$ is going to be used for the shooting method to get a solution for χ. Furthermore, one also **has to use very high precision**. Since the programming language of choice in this work is C++, the minimum precision possible to have convergence is *long double* and very strict stopping conditions in the shooting method (we are talking of magnitudes of around 10^{-19}). Otherwise, all convergence tests will fail. However, *long double* is not standardized across all platforms. To get good constraint convergence, one has to use external libraries of C++ to have stricter tolerances in the shooting methods. In this case, we used the *Boost.Multiprecision* package, which also overwrites the standard functions of C++, to have general flexibility with the other precisions of the code. This allows the use of 128-bit floating-point precision points, which correspond to quad precision. The recommended tolerance for the shooting methods that worked best for me, to have well-behaved constraint convergence, was $10^{-21} - 10^{-25}$. The values for $C_{\rm CMC}$ and R_0 should be calculated with the same or higher precision. *Boost.Multiprecision* allows precision until 10^{-32}, and we therefore impose a stopping condition for the shooting methods of these last two variables to be close to that value.

The result of the numerical integration (already transformed back to $\bar{\Omega}$) and a convergence test are shown in Fig. 6.8. We opted for a L2 norm convergence plot, given that the behavior of the convergence of $\bar{\Omega}$ is more clearly pictured this way. The quantity plotted is $\sqrt{\left(\sum_{i=1}^{N}(\bar{\Omega}_{LR} - \bar{\Omega}_{MR})^2\right)} / \left(\sum_{i=1}^{N}(\bar{\Omega}_{MR} - \bar{\Omega}_{HR})^2\right)$. Note that $\bar{\Omega}$ has two distinct asymptotic behaviors: the clearest to understand is the one near future null

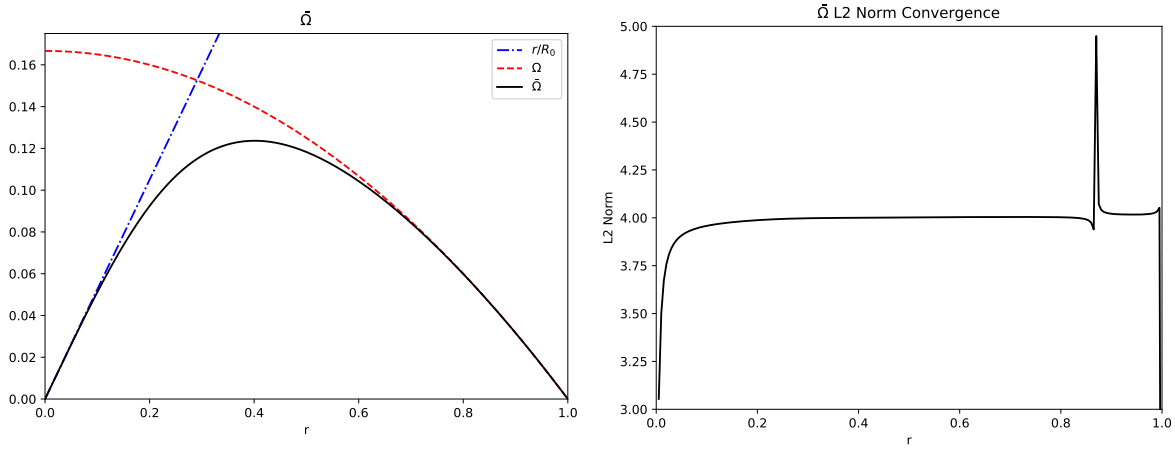

Figure 6.8: On the left: Numerical integration of $\bar{\Omega}$, together with its asymptotic behaviours: close to r/R_0 near the origin and close to Ω near future null infinity. This was done using $K_{\text{CMC}} = -1$, $M = 1$, $Q = 0$, $C_{\text{CMC}} \approx 3.115$ and $R_0 \approx 1.905$. On the right: convergence test for $\bar{\Omega}$, showing 4th order convergence, as expected.

infinity, where $\bar{\Omega} \to \Omega$, because $\chi \to 1$ asymptotically. The other one, nearer the origin, shows up when taking the limit $\tilde{r} \to R_0$ (recall that $\tilde{r}^2 = r^2/\bar{\Omega}^2$).

To satisfy the constraints, as we did before with only the real part of the scalar field, we continue having the same condition that $\bar{c}_\Pi = \beta^r \bar{c}'_\phi + \beta^r \bar{c}_\phi \frac{\Omega'}{\Omega}$. The Gauss constraint is automatically satisfied in this scenario because there is no charge density and no electric field. We only need to solve for χ. We had seen before that $\chi = \bar{\Omega}^2/\Omega^2$. In this scenario, we want a small perturbation of χ to get the Hamiltonian constraint to be satisfied. Following the Conformal Transverse Traceless method [48], we solve the momentum constraint by perturbing A_{rr} as well:

$$\chi \to \chi_0 \psi^{-4} = \frac{\bar{\Omega}^2}{\Omega^2}\psi^{-4} \quad A_{rr} \to A_{rr0}\psi^{-6} = -\frac{2C_{\text{CMC}}\bar{\Omega}^3}{r^3\Omega}\psi^{-6}. \tag{6.6}$$

When inserting this, together with the rest of the initial data in (4.11), we get the following ODE to solve,

$$\begin{aligned}\psi'' = &-\frac{\psi'\sqrt{9C_{\text{CMC}}^2\bar{\Omega}^6 + 6r^3\bar{\Omega}^3(C_{\text{CMC}}K_{\text{CMC}} - 3M) + 9r^4\bar{\Omega}^2 + K_{\text{CMC}}^2 r^6}}{3r^3\bar{\Omega}} + \frac{3C_{\text{CMC}}^2\bar{\Omega}^4\left(\psi^8 - 1\right)}{4r^6\psi^7} \\ &+ \frac{K_{\text{CMC}}^2\psi\left(\psi^4 - 1\right)}{12\bar{\Omega}^2} - \frac{\pi r\psi\left(\frac{1}{3}K_{\text{CMC}}r\bar{c}_\phi + \frac{1}{6}K_{\text{CMC}}(-1+r^2)\bar{c}'_\phi\right)^2 + \psi'}{r}.\end{aligned} \tag{6.7}$$

Note that this ψ has nothing to do with the one used in our version of Maxwell's equations. This is just a secondary variable that, as soon as its numerical solution is obtained, is reverted to χ. Solving this equation with the shooting method, we get the profiles for ψ and χ as shown in Fig. 6.9. The change in χ due to the scalar field perturbation seems almost indistinguishable when compared to the unperturbed χ, plotted in the red dashed line. The difference, although small, cannot be ignored for the constraints to be solved. The full evolution is shown in Fig. 6.10.

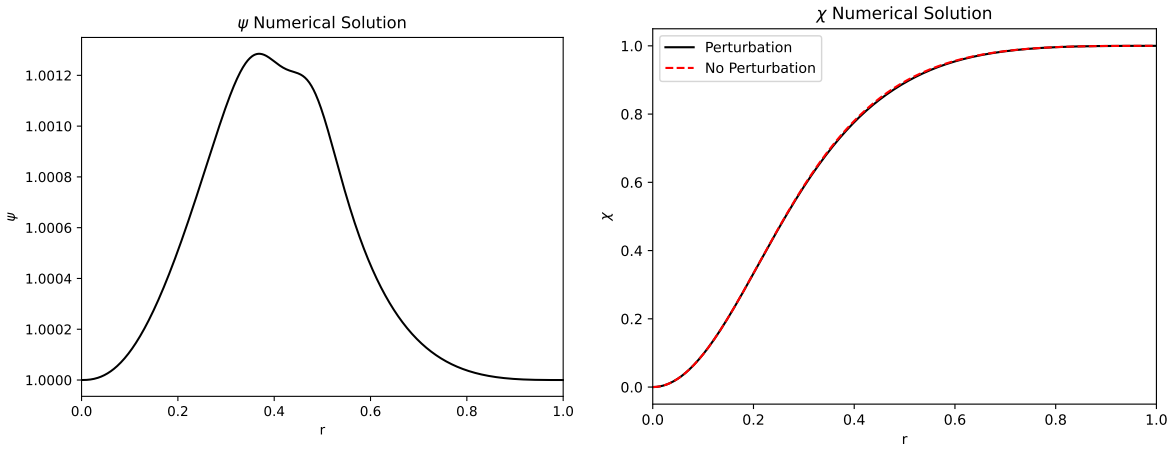

Figure 6.9: On the left: Numerical integration of ψ. On the right: Transformation of ψ into χ, in black, against the no perturbation reference in red, dashed line.

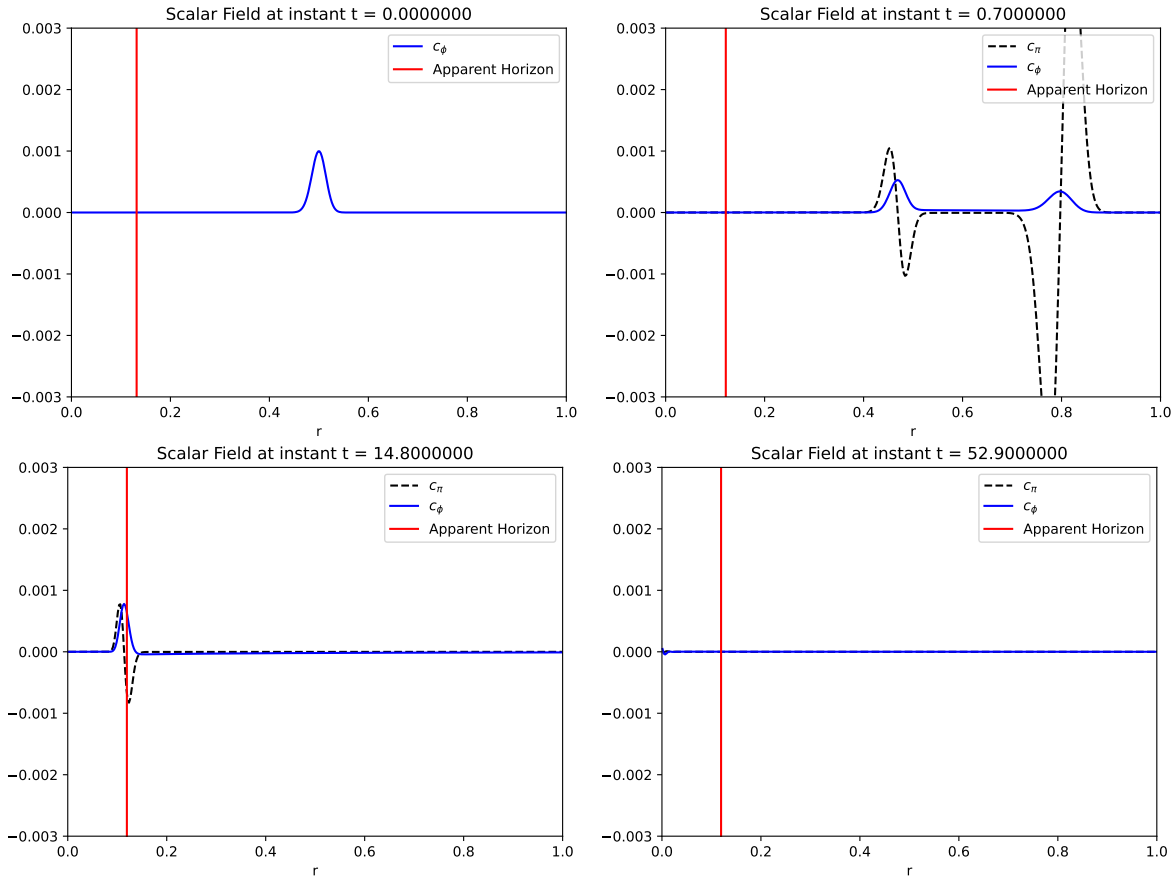

Figure 6.10: $\bar{c}_\phi$ and $\bar{c}_\Pi$ evolving until part of the initial perturbation is radiated out through future null infinity and the rest is absorbed into the black hole. The initial amplitude is 0.001, with $\sigma = 0.1$ and $\mu = 0.5$. The Kreiss-Oliger dissipation parameter had to be tuned to enhance the simulations' duration while keeping the interior of the BH well-behaved. $\sigma_{KO} = 0.08$ was used.

Only 200 points were necessary to have a stable run, and the Kreiss-Oliger dissipation was kept at 0.08. Values bigger than 1.5 would make the simulation crash too early (before $t = 1$) and smaller values would allow some high-frequency perturbations to show up inside the apparent horizon. Initially the apparent horizon presents some small variations but it stabilizes at $r \approx 0.13$ around $t \approx 2$. The scalar

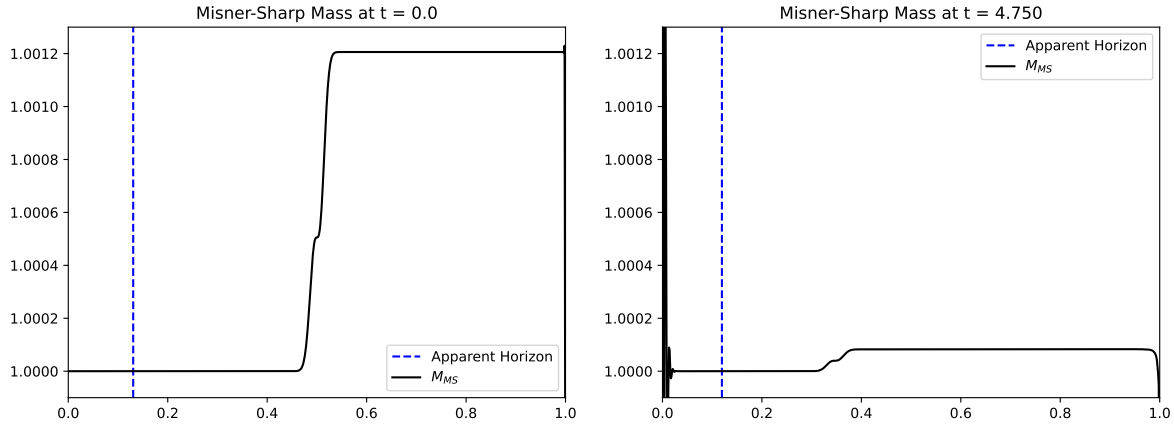

Figure 6.11: Change in the Misner-Sharp mass in the presence of a scalar field perturbation. The image on the left shows the initial state of the system, and on the right, the change coming from the incoming part of the initial perturbation.

field's perturbation does not seem to have a noticeable effect on the apparent horizon position. In terms of the Misner-Sharp mass, we see that most of the contents of our initial perturbation are radiated away, in Fig. 6.11, with a left-over ingoing part. The reader will notice some numerical errors nearer the origin, for the Misner-Sharp mass calculation, but these all happen inside the apparent horizon. Also it is worth noting that since we are perturbing the compactified scalar field, it is not exactly time symmetric and so most of the radiation is outgoing. That is why, on the right of Fig. 6.11, we only see a small fraction of the initial perturbation going in the black hole.

The constraint convergence is plotted in Fig. 6.12. The behavior obtained for the constraints resembles the one already shown in [10], although we are using a rescaling factor of 3 for each resolution, instead of only 1.5. The procedure has the advantage of not needing interpolation to compare the same points throughout the different resolutions, but there is another issue. The same Kreiss-Oliger dissipation for the different resolutions sometimes is not enough to dampen the high-frequencies that show up inside the apparent horizon or at $\mathscr{I}^+$. Therefore, we used a Kreiss-Oliger dissipation of $\sigma_{KO} = 0.08$, as used in the regular data scalar field evolution in regular spacetimes, but also added a linearly increasing dissipation, with the same magnitude. Overall, $\sigma = 0.08(1 + r)$. We should emphasize that the computational cost of these simulations is quite high. Access to a cluster or better computation power than the average computer is highly recommended if one wants to check late-time convergence. Using *long double* makes a noticeable difference in how the constraints look, but the computational cost due to this is even higher. Also, the initial data was calculated in *quad* precision, otherwise, no initial convergence is obtained. For the constraint convergence tests, again 1080 were used for the highest resolution, 360 for medium and 120 for the lowest one. Compared to the regular initial data, we now see that 120 points is not enough to get a similar behaviour to the other resolutions - see the dashed dark line in Fig. 6.12. To show that the code is converging, we did another run, with 270 points, which is 1080/4. Rescaling by 4^4, we should get comparable points and be able to see that the purple line is already closer to the highest resolution. Something worth commenting on as well is the apparent deviation from zero near the origin as time progresses. However, the highest and the medium resolutions agree, which means that we have convergence even there. The only region where convergence is lost is very near the origin, but this region

is already inside the apparent horizon. These again confirm what was seen in [10].

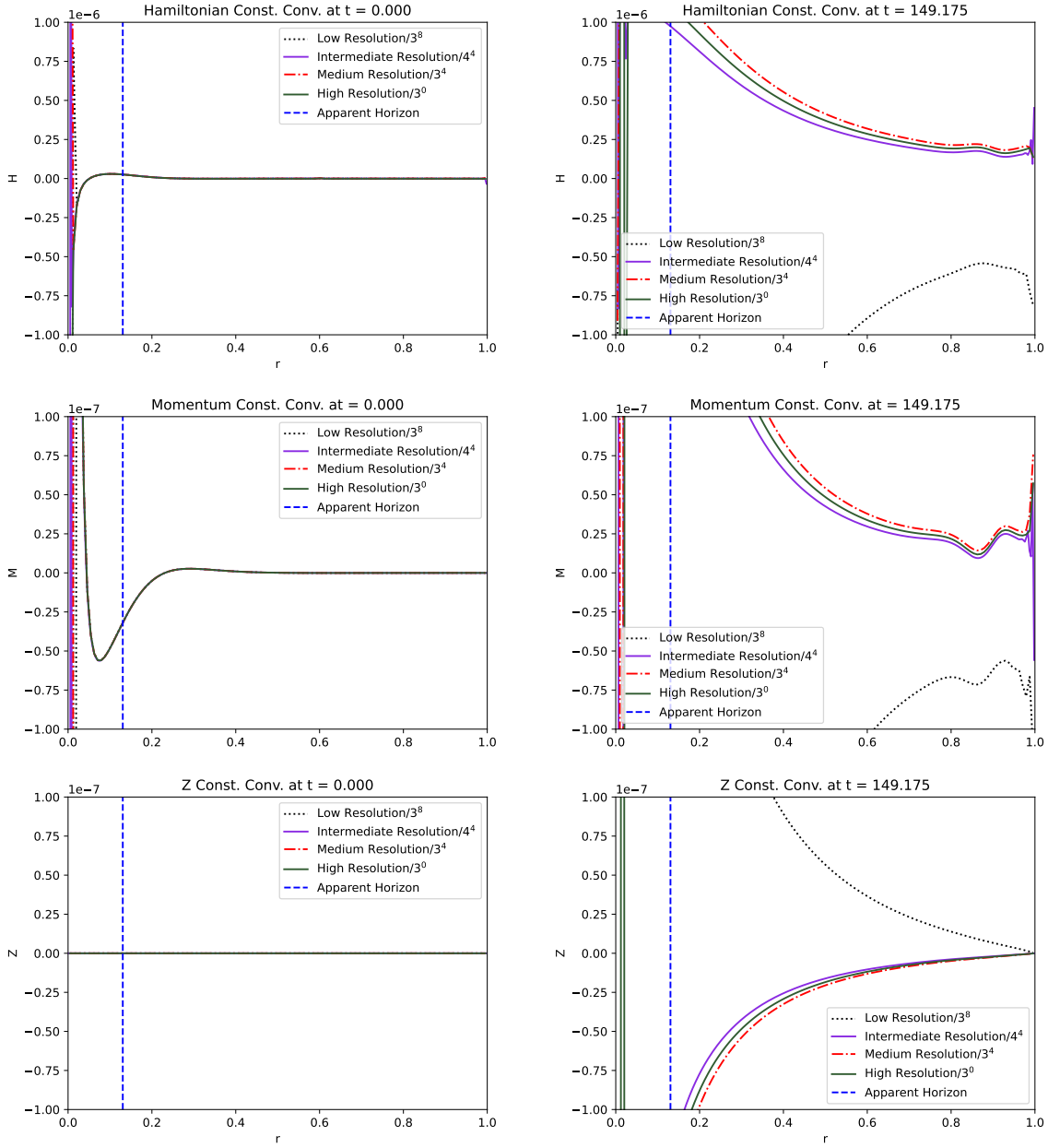

Figure 6.12: Convergence of the Hamiltonian, Momentum, and Z constraints, with a perturbation of the scalar field of Schwarzschild spacetime.

How $\bar{\Omega}$ behaves as a function of M, Q and $K_{\mathbf{CMC}}$

It is relevant for future work showing how $\bar{\Omega}$ changes according to its' free parameters: M, Q and K_{CMC}. Although K_{CMC} will remain -1 throughout the rest of the results and has a very noticeable effect on the convergence tests (the higher its absolute value, the higher the precision necessary for the code to converge), we nonetheless show the effect it has on $\bar{\Omega}$ in Fig. 6.13.

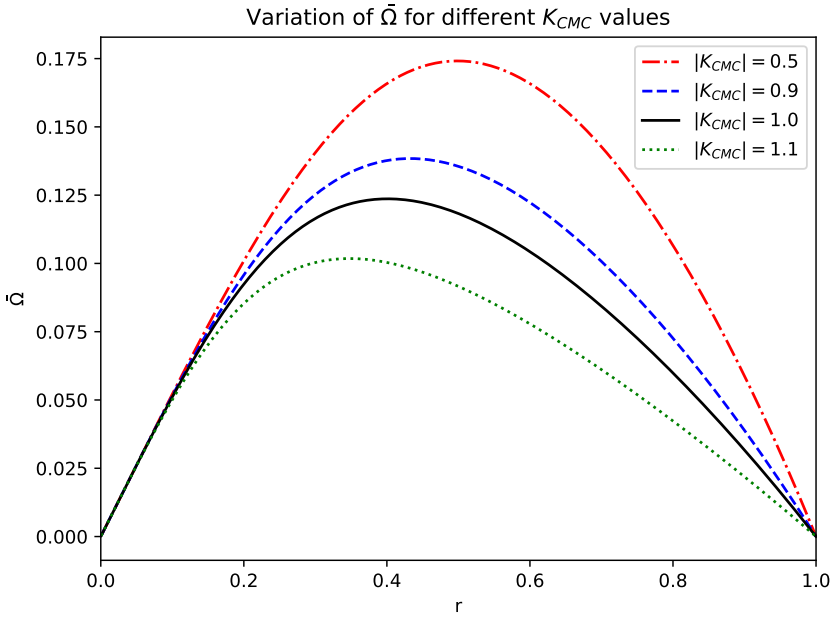

Figure 6.13: Variation of $\bar{\Omega}$ according to different values of K_{CMC}. M is set to 1 and Q to 0.

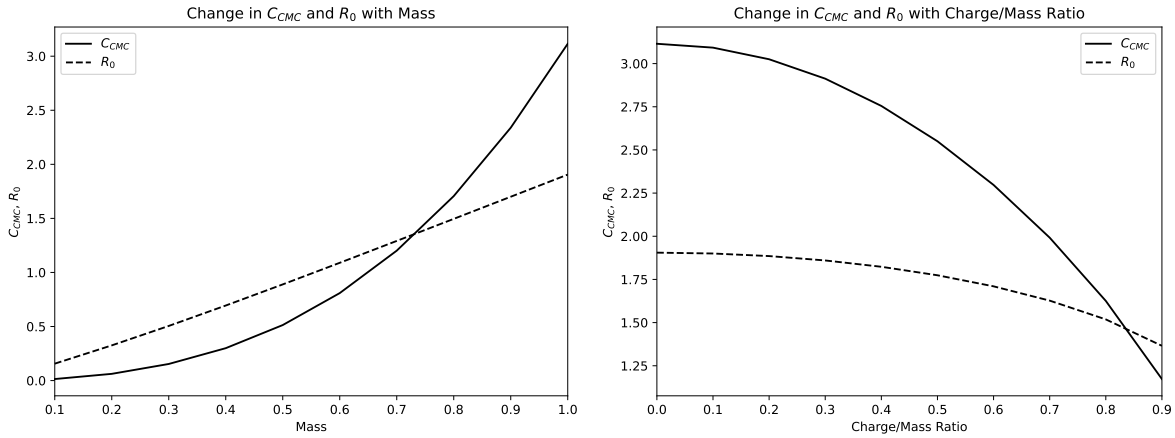

Figure 6.14: On the left: variation of C_{CMC} and R_0 with the black hole's mass M. On the right: variation of the same parameters with respect to the charge-to-mass ratio Q/M. M has been set to 1 and Q is changing.

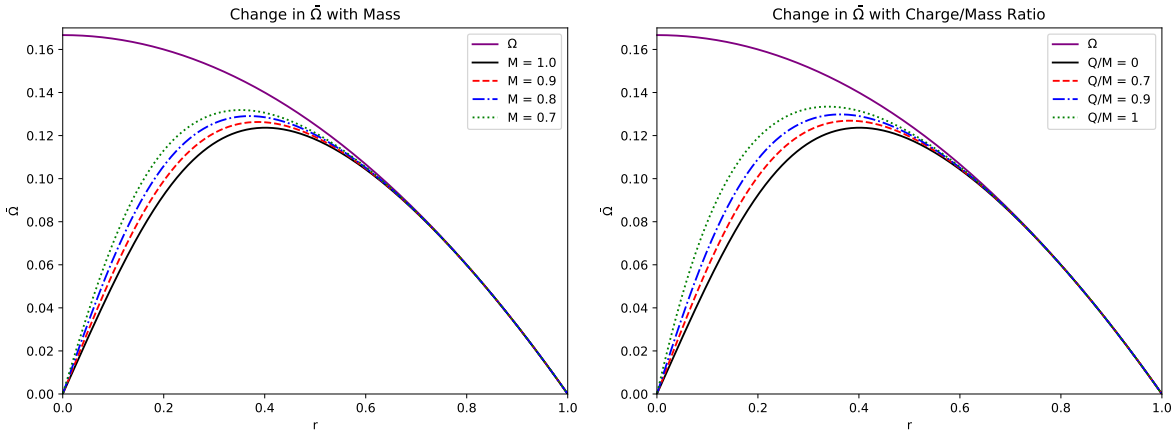

Figure 6.15: On the left: variation of $\bar{\Omega}$ according to different values of the mass M, without charge. On the right: variation of $\bar{\Omega}$ according to different values of the charge-to-mass ratio Q/M. M has been set to 1 and Q is changing.

We have left the solid line in the figure, such that it corresponds to the one plotted in Fig. 6.8. Higher absolute values of K_{CMC} revealed themselves very hard to solve for numerically, and thus we kept them out of the plot. To see the effect of the mass M in this compactification factor, we can go even further and study how C_{CMC} and R_0 change with it. Adding the charge of the black hole is relevant as well, more specifically in the charge-to-mass ratio. The effect of the mass alone and the effect of the charge-to-mass ratio are plotted in Fig. 6.14. Interpreting the results, one sees that the higher the mass, the higher C_{CMC} and R_0 are, which is expected: the more massive the black hole is, the less spacetime we can access. On the other hand, the higher the charge of the black hole, the smaller R_0 is, already noting here the "counter" effect of the charge with respect to the mass. The effect that M and Q/M have is plotted respectively in Fig. 6.15. $\bar{\Omega}$ shows the same conclusion as before: a decreasing mass seems to have a similar effect to an increasing charge-to-mass ratio. Having dealt with this, we can proceed to understand how the Reissner-Nördstrom solution behaves in our formulation and code.

6.5 Electrovacuum and Finding a Stable Gauge for Scalar Potential

6.5.1 Initial Data for Maxwell's Fields

The problem we have to tackle foremost now is that the electric field is formally divergent (6.4), but this goes against the idea of using trumpet initial data, which avoids the singularity. The problem has to do with the fact that we are using the covariant version of the electric field when it is more fruitful to work with the contravariant version [72], in this case. Its evolution equation is similar to the covariant one, just by raising one index in Maxwell's equations before the 3+1 decomposition. With that taken care of, we can look again at the Gauss constraint (A.57), now a function of E^r instead of E_r, without charge densities,

$$\mathcal{P} = -\frac{2E^r\alpha\Omega^2}{r} - \alpha\Omega^2 E^{r\prime} + \frac{3E^r\alpha\Omega^2\chi'}{2\chi} = 0 \iff -\frac{2E^r}{r} - E^{r\prime} + \frac{3E^r\chi'}{2\chi} = 0\,, \tag{6.8}$$

which has an immediate solution,

$$E^r = \frac{Q}{r^2}\chi^{3/2} \tag{6.9}$$

that is something we could already guess by immediately putting the index up with the 3+1 decomposed metric (before the compactification with χ). Knowing that $\chi \sim r^2$ near the origin, we see that the electric field now goes to 0 there, instead of blowing up to infinity. The same solution shows up when solving the Hamiltonian constraint, assuming that the black hole has charge. This, of course, is also valid for a massless charge. One should recall that the Gauss constraint in the absence of external charges requires only that the divergence of the electric field is 0. Therefore, a divergence-free electric field in this formulation has the above expression.

Now, although all of the equations are written as much as possible in terms of the electric field (as recommended in [28]), the electromagnetic potentials are still present in the equations for the real and imaginary parts of the scalar field. And these cannot be removed, so the first question to answer is, how do the scalar field components "know" of the black hole's presence? This should be implicit when giving

some initial conditions to these fields. However, this is not a necessary condition [73], due to the gauge freedom we have in the four-potential - $A_\mu \to A_\mu + \nabla_\mu f$, with f being a scalar function. We could give null initial conditions, and the system would find the same static solution, and this has been tested in the code. If we were working in flat space, we would have usual electrodynamics, and we would consider the potential, $V(r) = Q/r + c$, with c being a real constant scalar. However, we have not been working with this quantity. Instead, we have the evolution equation for Φ. After some pondering, one can impose a condition for Φ by setting the right-hand side of the equation for A_{3r} (A.49) to 0. Physically, it makes sense to impose $A_{3r} = 0$ initially. Therefore, we are left with

$$-E_r\alpha - \Phi\alpha' - \alpha\Phi' = 0 \iff E_r = -\Phi\frac{\alpha'}{\alpha} - \Phi' \,. \tag{6.10}$$

This is a bit different from the usual $E = -V'$. However, there is something interesting behind the equation: that a solution of the type $\Phi = C/\alpha$ is a homogeneous solution (it does not affect the electric field). Rewriting the equation, we get,

$$E_r = -\frac{\partial_r(\Phi\alpha)}{\alpha} \,,$$

that motivates us to define a new quantity, $V = \Phi\alpha$. If we substitute the expression for the electric field and write $\alpha = (\bar{\Omega} - r\bar{\Omega}')\frac{\Omega}{\bar{\Omega}}$ (check this using γ_{rr0} and α_0 in (4.5)), we get that,

$$V' = -\frac{Q}{r^2}\chi^{1/2}\alpha = -\frac{Q}{r^2}\frac{\bar{\Omega}}{\Omega}(\bar{\Omega} - r\bar{\Omega}')\frac{\Omega}{\bar{\Omega}} = -\frac{Q}{r^2}(\bar{\Omega} - r\bar{\Omega}') = \partial_r\left(\bar{\Omega}\frac{Q}{r}\right) \,. \tag{6.11}$$

This allows us to write the following,

$$V(r) = \bar{\Omega}\frac{Q}{r} + C \,.$$

This can be identified with the actual electric potential. Therefore, Φ **should not** be named an electric potential, but simply a scalar potential related to electrodynamics [72, 28]. This result also allows us to see that the potential does not have a singularity at $r = 0$, instead attaining a finite value, $V(0) = Q/R_0$, assuming $C = 0$. Going back to the definition of V, we have that,

$$\Phi = \frac{V}{\alpha} \,, \tag{6.12}$$

and note that $\alpha \to 0$ as $r \to 0$. Therefore, we cannot define freely the constant for V, otherwise, we will have a singularity at $r = 0$ for Φ. Thus, we have to "force" V to be 0 at the origin, by setting

$$V(r) = \bar{\Omega}\frac{Q}{r} - \frac{Q}{R_0} = \frac{Q}{r}\left(\bar{\Omega} - \frac{r}{R_0}\right) \,. \tag{6.13}$$

Therefore, we get that,

$$\Phi = \frac{Q}{r}\left(\bar{\Omega} - \frac{r}{R_0}\right)\frac{\bar{\Omega}}{\Omega}\frac{1}{\bar{\Omega} - r\bar{\Omega}'} \,. \tag{6.14}$$

To derive the limit of Φ as $r \to 0$, we should take into account two things: that $\bar{\Omega} \to r/R_0$, as $r \to 0$, and this implies that $\bar{\Omega}' \to 1/R_0$ and $\bar{\Omega}'' \to 0$, but nothing can be concluded with care about $\bar{\Omega}'''$. And the

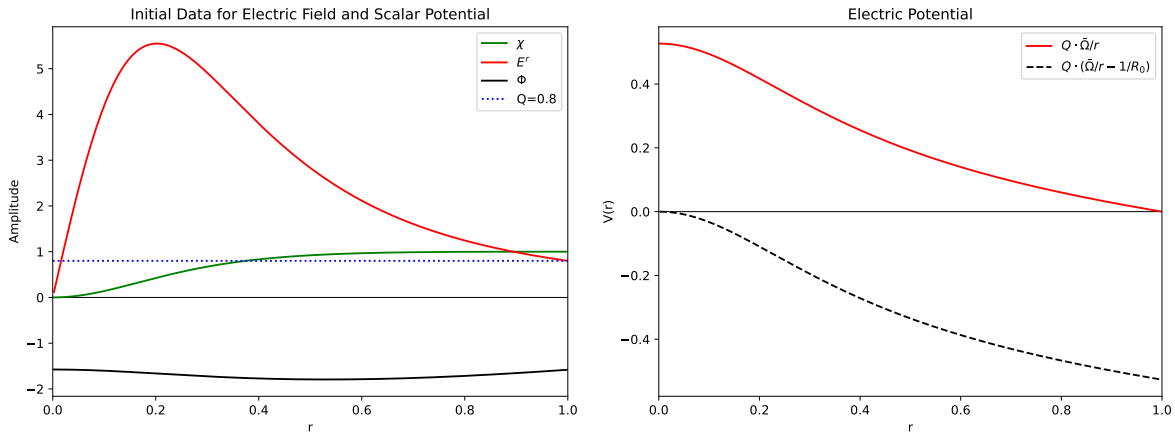

Figure 6.16: On the left: Initial data for the electric field E^r, (6.9), and the scalar potential Φ, (6.14). On the right: In red, the electric potential $V(r)$, assuming no additive constant. In dotted black, the adjusted $V(r)$, (6.13), is forced to go to 0 at the origin. On both graphs, $Q = 0.8$, $K_{\text{CMC}} = -1$ and $M = 1$.

Taylor expansions,

$$\bar{\Omega} = \bar{\Omega}(0) + r\bar{\Omega}'(0) + \frac{r^2}{2}\bar{\Omega}''(0) + \frac{r^3}{6}\bar{\Omega}'''(0) + O(r^4)$$
$$\bar{\Omega}' = \bar{\Omega}'(0) + r\bar{\Omega}''(0) + \frac{r^2}{2}\bar{\Omega}'''(0) + O(r^3)\,.$$

Substituting these expressions in (6.14), together with the fact that $\bar{\Omega}(0) = \bar{\Omega}''(0) = 0$ and $\bar{\Omega}'(0) = 1/R_0$,

$$\Phi(r \to 0) = \frac{1}{2}\frac{Q}{R_0}\frac{6}{K_{\text{CMC}}} = \frac{Q}{R_0}\frac{3}{K_{\text{CMC}}}\,. \tag{6.15}$$

For the usual values of our simulations, $Q = 0.8$, $K_{\text{CMC}} = -1$, $R_0 \approx 1.51$, we get $\Phi(0) \approx -1.57$ (see the first plot in Fig. 6.16). Therefore, we see that the correct imposition of the constant in the electric potential V gives a finite value of Φ throughout the whole domain of $r \in]0, 1[$. These considerations are useful, especially in our case, for numerical simulations, given that we had already concluded that these constants do not, in abstract, change the physical significance of the electric field being generated. The initial part of this derivation was inspired by [72, 73], and this has been carefully written here, for, as far as the author knows, it is the first time initial data is given for the four-potential in GR, in trumpet initial data. The result of the initial data is shown in Fig. 6.16. The generalization for a non-conformally flat initial data reads [73],

$$E_r = -\frac{\partial_r V}{\alpha\gamma_{rr}^2}\,.$$

6.5.2 Gauge Conditions for the Scalar Potential

The reason for reconsidering the gauge condition for the scalar potential Φ will be made clear in the following subsection. Until now, for regular initial data, the equations dealt well with the perturbations in $\bar{c}_\phi$ and A_{3_r}. However, when inputting Reissner-Nördstrom initial data to the whole system (recall Fig. 6.16), there is an unbounded behavior at $\mathscr{I}^+$ for Φ and A_{3_r} as the evolution continues. This behavior is shown more clearly in Fig. 6.17, where we present the system at $t \approx 160$, using the physical Lorenz gauge (3.57) and the conformal Lorenz gauge (3.58), respectively. We should note that, because we are not giving

any initial data for the scalar field, the evolution of the four-potential quantities does not affect the stability of the overall fields, i.e., we get a static solution for the electric field plus the variables coming from the Einstein's equations, which indeed tells us that we have reached a stable, charged black-hole solution.

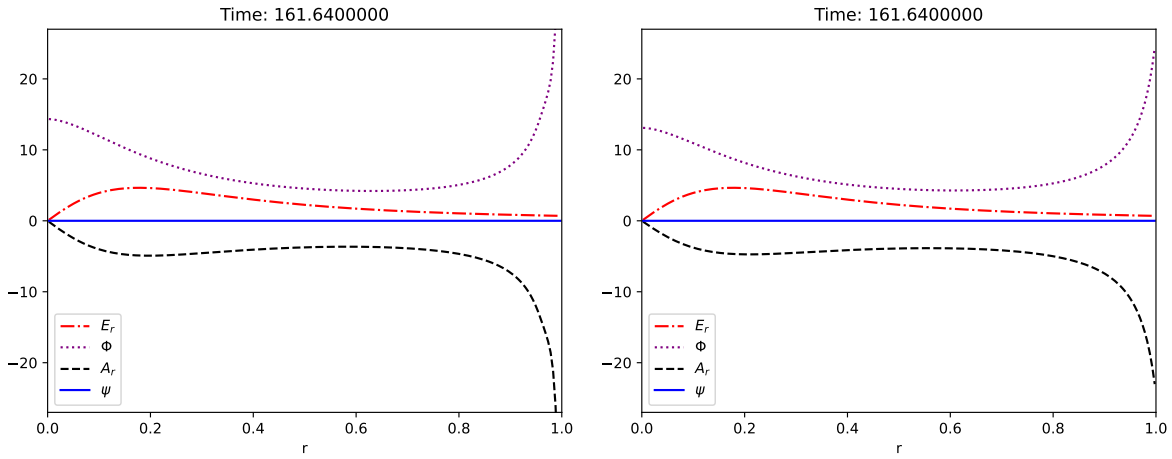

Figure 6.17: On the left: State of the system at $t = 161.64$, with initial data as shown in Fig. 6.16, using the physical Lorenz gauge (3.57). On the right: the same thing, but using the conformal Lorenz gauge (3.58).

This was evolved till $t \approx 500$ and the quantities' profiles remain unchanged. However, even if this should not cause any worries for electrovacuum, it will become problematic as soon as we want to investigate how the scalar field interacts with the black hole's electric field. Other than that, convergence tests will start to diverge at $\mathscr{I}^+$ due to the lack of precision as the potentials continue to augment. This will make it practically impossible to understand whether we are having a problem at $\mathscr{I}^+$ in terms of the outgoing radiation or not. Another thing to note is how the scalar potential goes from negative values (Fig. 6.16) to positive ones (Fig. 6.17). This behaviour is the same, independently of the initial data given for Φ, which agrees with the gauge invariance related to this quantity.

Fueled by this problem at $\mathscr{I}^+$, we decided to test some alternatives, inspired by [74]. Another important paper to understand the possible problems arising from this was [75], where the authors indicate the lack of strong hyperbolicity coming from the Lorenz gauge. Whatever choice is made for the Lorenz gauge, be it the physical or the conformal one, both should make the overall system lose its strong hyperboloidal property. However, this is usually related to the presence of a magnetic field, which involves the commutation of induced derivatives of A_{3r} in the electric field equation. An analysis of the characteristic speeds was done, following the prescriptions in Sec. 4.2, and it gave a set of only real eigenvalues, with a complete set of eigenvectors, which is required for strong hyperbolicity. Thus, our problem is well posed, but if further investigation is to be done, one will have to take care with adding another auxiliary variable, usually $\Gamma = D_i A_3{}^i$. Note that the Coulomb gauge would be equivalent to $\Gamma = 0$. The characteristic speeds of the system we are modeling are shown in Tab. 6.1. The constants n_{cK} and λ come from the gauge conditions for the shift and the lapse, in (3.8). If they are set both to 0, all of the speeds reduce to v_1 and v_2. One will recognize these speeds as the eigenspeeds when setting the line element $d\bar{s}^2$ to 0 and solving for $d\bar{r}/dt$: this means that $v_2 = c_+$, $v_3 = c_-$, i.e., the ingoing and outgoing speeds. They are plotted in Fig. 6.18 for better clarity. The speeds with the extra term coming from n_{cK} and λ are given the names

Number	Speed's label	Expression
v_1	0	0
v_2	c_+	$-\beta^r + \alpha\sqrt{\frac{\chi}{\gamma_{rr}}}$
v_3	c_-	$-\beta^r - \alpha\sqrt{\frac{\chi}{\gamma_{rr}}}$
v_4	$c_+ + n_{cK}$	$-\beta^r + \sqrt{\frac{\chi}{\gamma_{rr}}}\sqrt{n_{cK} + \alpha^2}$
v_5	$c_- + n_{cK}$	$-\beta^r - \sqrt{\frac{\chi}{\gamma_{rr}}}\sqrt{n_{cK} + \alpha^2}$
v_6	$c_+ + \lambda$	$-\beta^r + \sqrt{\frac{\chi}{\gamma_{rr}}}\sqrt{\lambda + \alpha^2}$
v_7	$c_- + \lambda$	$-\beta^r - \sqrt{\frac{\chi}{\gamma_{rr}}}\sqrt{\lambda + \alpha^2}$

Table 6.1: Characteristic speeds of the system.

$c_\pm + n_{cK}$ and $c_\pm + \lambda$. Looking back at Fig. 6.18, we see that the c_+'s speeds are in general positive and 0 at $r = 0$. Also, the c_-'s speeds are negative always, attaining a 0 value at the origin and at $\mathscr{I}^+$, which means that the overall system does not allow any incoming radiation at future null infinity. This has to be so to retain the physical significance of the region. Information can only go out, never go in, at $\mathscr{I}^+$.

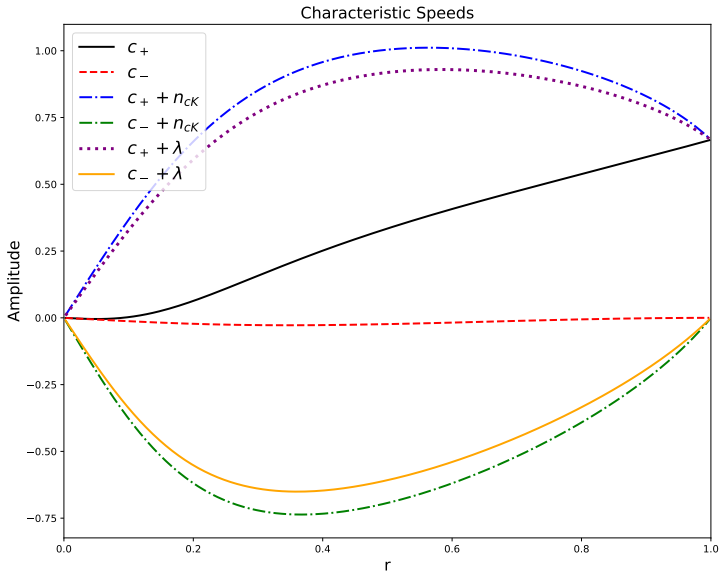

Figure 6.18: Characteristics of the system we are modeling. λ is set to 0.8 and n_{cK} to 1.0.

To find an alternative gauge condition for Φ, we tried using the light-cone gauge, but the simulation crashed right away. Some further investigation should be done to better understand why. We then went back to [74], where the author generalizes the Lorenz gauge to have an additional constant such that the (conformal) Lorenz gauge becomes,

$$\dot{\Phi} = \mu\left(-\frac{2A_3\alpha}{r} - \alpha A_3' - A_3\alpha' + \frac{3A_3\alpha\chi'}{2\chi}\right) + \frac{K_{\mathrm{CMC}}\alpha\Phi}{\Omega} + \frac{K\alpha\Phi}{\Omega} + \beta^r\Phi' + \frac{3\beta^r\Phi\Omega'}{\Omega}. \tag{6.16}$$

We should note that the proposal in the original paper is just an example, and it is used with no coupling of the Lorenz gauge to GR. Therefore, only the partial derivatives appear, not the covariant ones. The reader will then notice that the term inside the parentheses corresponds to the covariant derivative of the vector potential (multiplied by α). The conformal Lorenz gauge is recovered if one is to set $\mu = 1$. In terms of the overall hyperbolicity of the system, it remains unchanged, but there is a slight difference in

the eigenspeeds, which is to be expected because we are changing the principal part of our system. The additional speeds are shown in Tab. 6.2 and plotted against the previous known speeds in Fig. 6.19.

Number	Speed's label	Expression
v_8	$c_+ + \mu$	$-\frac{\beta^r}{2}(1+\mu) + \frac{1}{2\sqrt{\gamma_{rr}}}\sqrt{(-1+\mu)^2\gamma_{rr}\beta^{r2} + 4\mu\alpha^2\chi}$
v_9	$c_- + \mu$	$-\frac{\beta^r}{2}(1+\mu) - \frac{1}{2\sqrt{\gamma_{rr}}}\sqrt{(-1+\mu)^2\gamma_{rr}\beta^{r2} + 4\mu\alpha^2\chi}$

Table 6.2: Additional speeds coming from alternative Lorenz gauge.

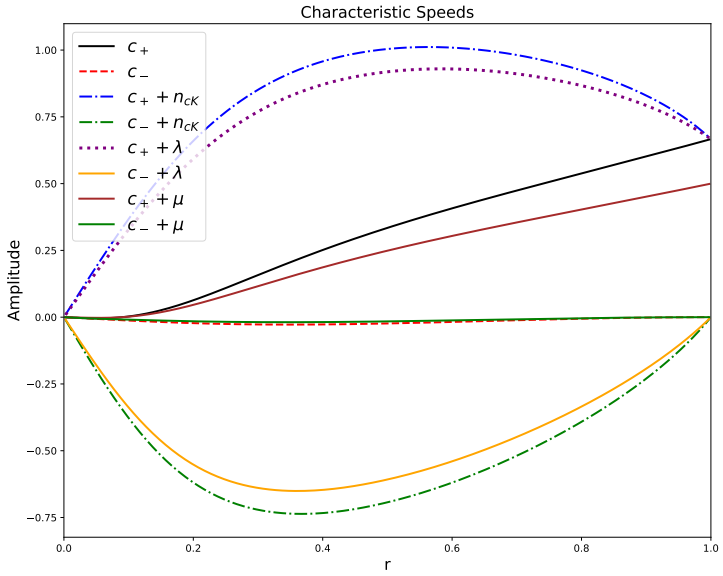

Figure 6.19: Characteristics of the system with the modified Lorenz gauge (6.16). λ is set to 0.8, n_{cK} to 1.0 and μ to 0.5.

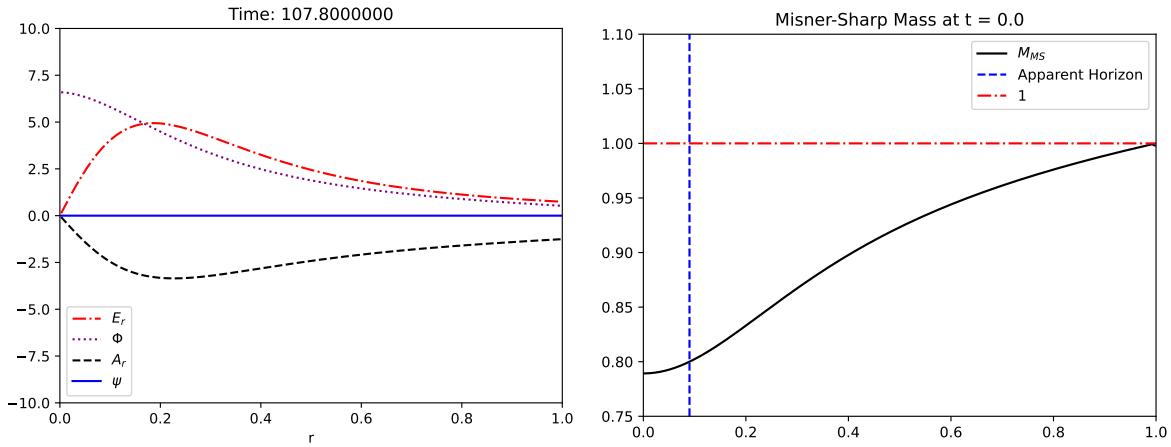

Figure 6.20: On the left: Long-term stationary solution of the system with the modified Lorenz gauge (6.16), at $t = 107.8$. Compare with Fig. 6.17. λ is set to 0.8, n_{cK} to 1.0 and μ to 0.5. On the right: Misner-Sharp mass relative to the electrovacuum solution of the system, at $t = 0.0$. The plot stays the same, with some negligible numerical changes, throughout the simulation.

The stationary solution that the simulation finds with this change is found on the left side of Fig. 6.20. On the right side of the figure, we also plot the Misner-Sharp mass, together with the apparent horizon. We have left the red line, which corresponds to the expected behavior of the Schwarzschild solution, i.e., a horizontal line at 1, for a $M = 1$ black hole. This goes according to the theoretical value for the Missner-Sharp mass of a charged black hole, $M_{\text{MS}} = M - Q^2/2r$, in physical units. The relevant thing

to understand here is that at the origin, we notice a very strong effect of the charge, and at $\mathscr{I}^+$ the contribution of the charge goes to 0 and we regain the asymptotic Schwarzschild-like behavior. Regarding convergence, the Gauss constraint converges as time progresses, as shown in Fig. 6.21, but a sanity check was done with *long double* precision to make sure that the constraints were not being violated. The Hamiltonian and momentum constraints behave in a very similar manner to the Schwarzschild solution with or without a scalar field perturbation, therefore, there is no need to show them. At the origin of Fig. 6.21, there is a loss of convergence, similar to what we have seen for the other constraints. This might have to do with the presence of the electric field, which has a very steep behavior at the origin.

We can now pass on to see how the charged scalar field interacts with the charged black hole.

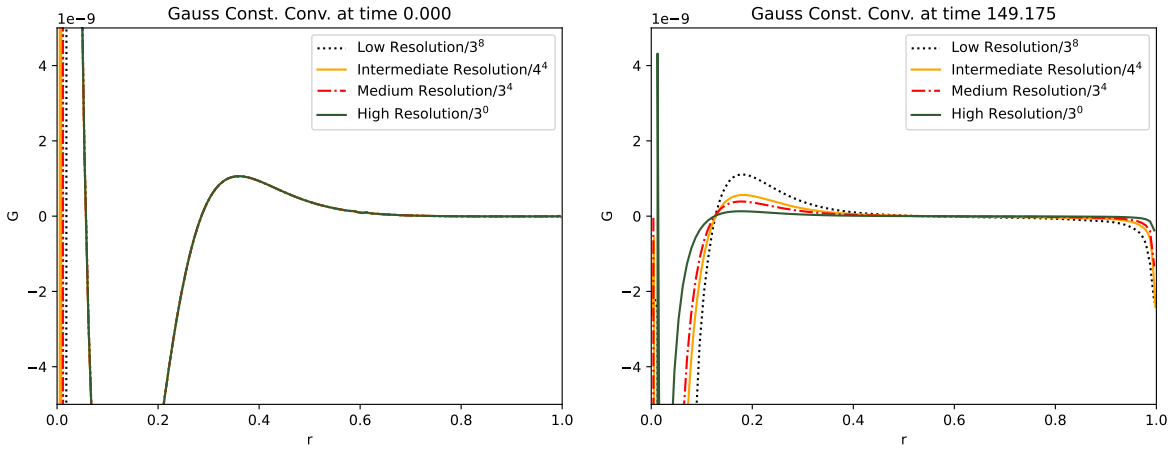

Figure 6.21: Evolution of the Gauss constraint of a Reissner-Nördstrom solution in our code.

6.6 Charged Scalar Field and Maxwell's Fields in Schwarzschild Spacetime

We will now go back to the Schwarzschild initial data and do the usual perturbations,

$$\delta\bar{c}_\phi = A_1 r^2 \exp\left(-\frac{r^2-\mu_1^2}{4\sigma_1^4}\right), \quad \delta A_{3_r} = A_2 r^2 \exp\left(-\frac{r^2-\mu_2^2}{4\sigma_2^4}\right).$$

The Hamiltonian equation now has an extra term related to the vector potential (compare with (6.7)),

$$\begin{aligned}\psi'' = &-\frac{\psi'\sqrt{9C_{\rm CMC}^2\bar{\Omega}^6 + 6r^3\bar{\Omega}^3(C_{\rm CMC}K_{\rm CMC}-3M) + 9r^4\bar{\Omega}^2 + K_{\rm CMC}^2 r^6}}{3r^3\bar{\Omega}} + \frac{3C_{\rm CMC}^2\bar{\Omega}^4\left(\psi^8-1\right)}{4r^6\psi^7} \\ &+ \frac{K_{\rm CMC}^2\psi\left(\psi^4-1\right)}{12\bar{\Omega}^2} - \frac{\pi r\psi\left(\frac{1}{3}K_{\rm CMC}r\bar{c}_\phi + \frac{1}{6}K_{\rm CMC}(-1+r^2)\bar{c}_\phi'\right)^2 + \psi'}{r} \\ &- \frac{1}{36}K_{\rm CMC}^2\pi q^2(-1+r^2)^2 A_{3_r}^2\bar{c}_\phi^2\psi\,. \end{aligned} \tag{6.17}$$

It is important to note that in this section, we have raised the charge of the scalar field to 3.0, instead of the usual 0.8. This was done to enhance the presence of the imaginary part. We have made the perturbation of the scalar field the same as shown in Fig. 6.10, and for the radial component of the vector

potential, we have made the following choices: $A_2 = 0.002$, $\mu_2 = 0.45$, and $\sigma_2 = 0.1$. The results are shown in Fig. 6.22.

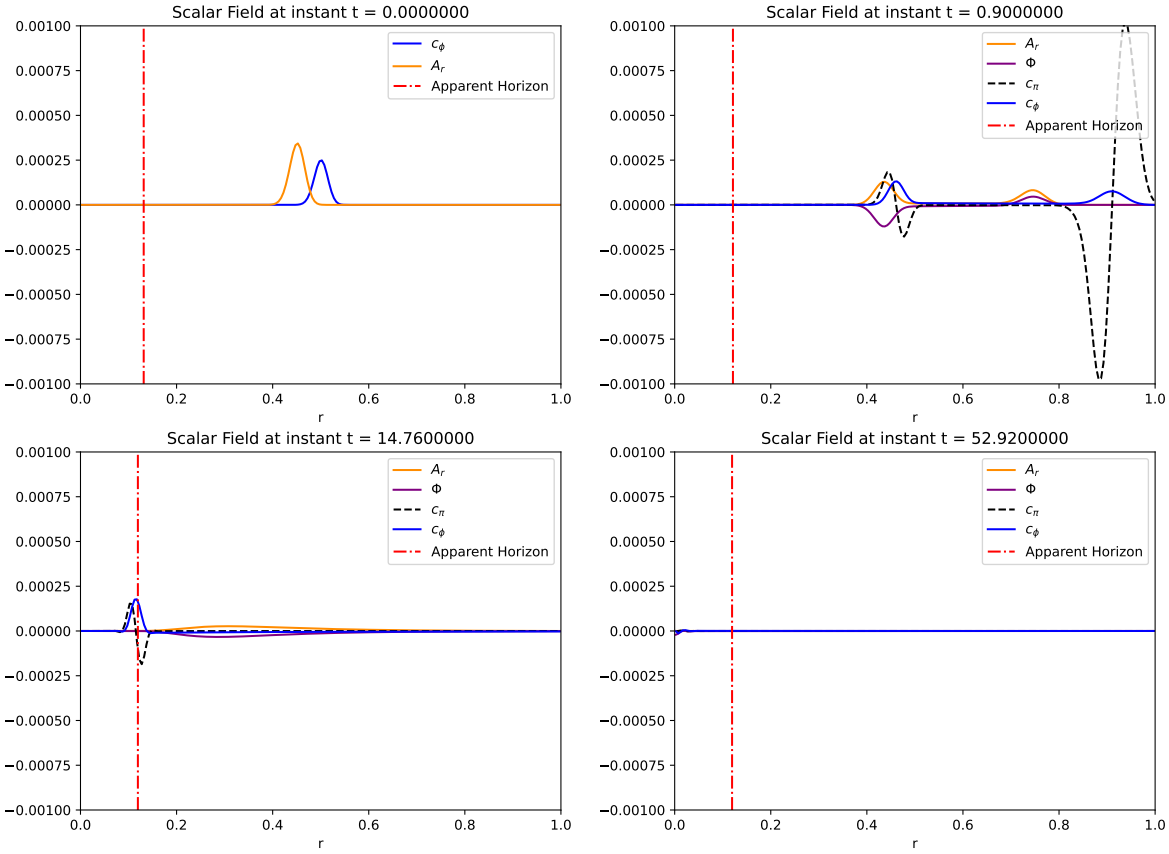

Figure 6.22: $\bar{c}_\phi$, $\bar{c}_\Pi$, A_{3r} and Φ evolving until part of the initial perturbation is radiated out through future null infinity and the rest is absorbed into the black hole. The initial amplitude for the scalar field is 0.001, with $\sigma = 0.1$ and $\mu = 0.5$. For A_{3r}, the amplitude is 0.002, $\sigma = 0.1$ and $\mu = 0.45$.

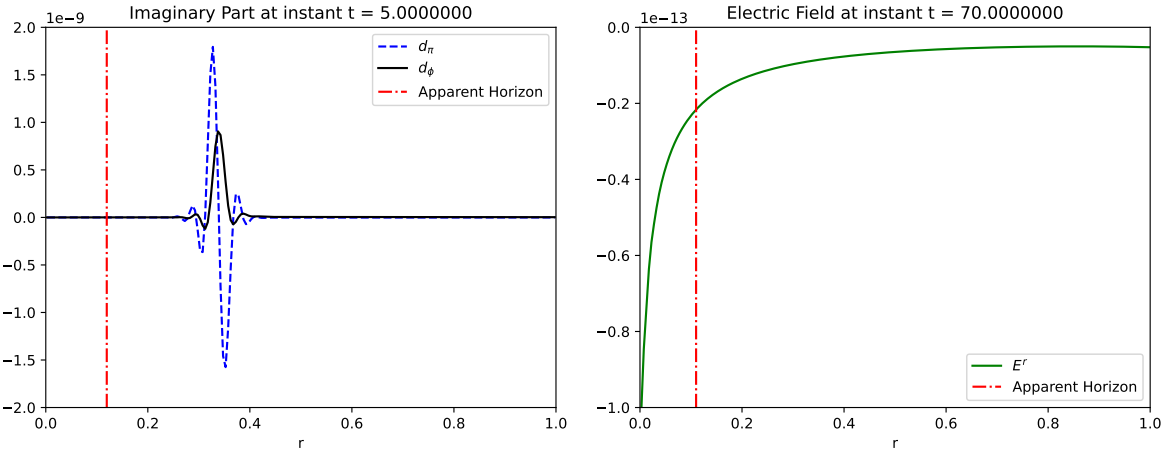

Figure 6.23: Zoom on Fig. 6.22. On the left: Imaginary part of the scalar field, which was excited due to the perturbation in the radial component of the vector potential. On the right: Electric field generated by the current density coming from the scalar field, which has been absorbed by the black hole. Compare with Fig. 6.16.

We see then that the electric potentials also go through the apparent horizon, and the real part of the scalar field behaves in a very similar way to when the charged part is ignored. To understand better how the imaginary part and the electric field behave, we have to zoom in on Fig. 6.22. This is shown

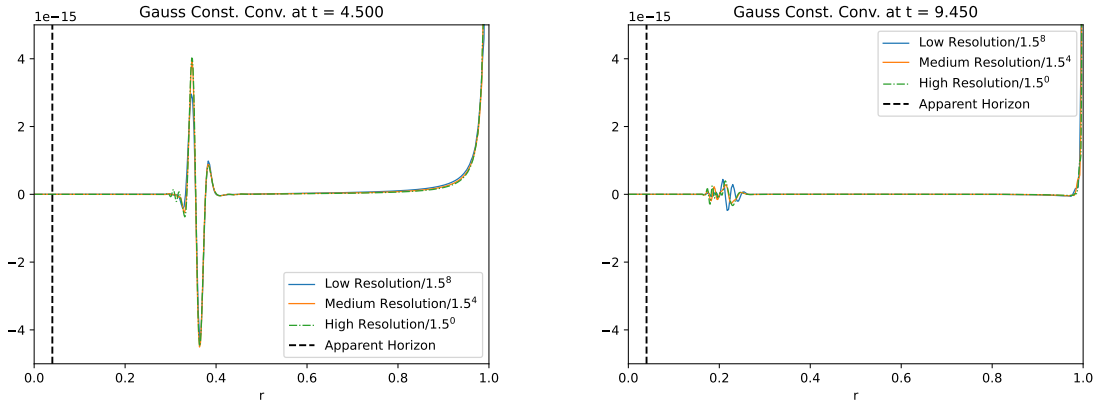

Figure 6.24: Gauss constraint convergence of a charged scalar field perturbation of Schwarzschild spacetime. As time progresses, it changes into a Reissner-Nördstrom solution.

in Fig. 6.23. In terms of how the imaginary part of the scalar field behaves, it is very similar to the real part. It slowly dissipates the closer it is to the origin, decreasing its speed accordingly. However, the electric field (with a very small amplitude, pay attention to the scale in Fig. 6.23) starts to stabilize by $t = 50$, acquiring a very similar curve to the one shown for the Reissner-Nördstrom spacetime in Fig. 6.16, with the appropriate scale. Therefore, we are already modeling, as soon as the scalar field is consumed by the black hole, an actual solution to the electrically charged black hole. This matches the physical expectations. In terms of how the constraints behave, it is very similar to what is shown in Fig. 6.12, but now we must also take into account the Gauss constraint. This is shown in Fig. 6.24. We see that there seems to exist a lack of convergence near $\mathscr{I}^+$, but again, this is still when the spacetime has not relaxed into a stationary solution. This lack of convergence is attenuated as time progresses, which again gives us some certainty that the stationary solution will be reached in the future if evolved for longer.

6.7 Charged Scalar Field in Reissner-Nördstrom Spacetime

Until now, we did not have to solve for a perturbation with the electric field initially "on", because we had $\Phi_0 = 0$. With $\Phi_0 \neq 0$, we have to follow the general prescription for these perturbations [73],

$$E^r \to E^r \psi^{-6}\,.$$

To not add any extra terms to solve for, we will do the following substitution,

$$E^r = \chi^{3/2}\frac{Q}{r^2} + \delta E^r \psi^{-6}, \quad \Phi \to \Phi\psi^{-6}\,. \tag{6.18}$$

This way, the Gauss constraint gives us an elliptic equation independent of ψ,

$$\delta E^{r\prime} = -\frac{2\delta E^r}{r} + \frac{3\delta E^r \bar{\Omega}'}{\bar{\Omega}} - \frac{3\delta E^r \Omega'}{\Omega} + 4\pi q^2 \bar{c}_\phi^2 \Phi\,,$$

where we recall that q is the scalar field's charge. Note that the last term in the equation comes from writing the charge density explicitly as a function of the non-null terms (A.55). Although we cannot say in general how the behavior of this portion of the electric field being generated by the charged scalar field will

be, we know for sure that at $r = 0$ it should be 0. Therefore, the initial condition will be $\delta E^r(0) = 0$. The result of this excitation is shown in Fig. 6.25, with a Gaussian perturbation of the scalar field as before.

The overall behavior matches the physical intuition: recall that our perturbations in the scalar field are spherical. Therefore, if they are to create an electric field, this can never attain a non-null value inside of this shell, only out of it. Similarly to the (compactified) electric field of the black hole, it attains a non-vanishing value at scri. The evolution is shown in Fig. 6.26. We only show two frames, because the general evolution of the scalar field remains the same as before. In this case, now we have that the imaginary part has an equal predominance very early in the simulation, due to the electromagnetic field coming from the black hole.

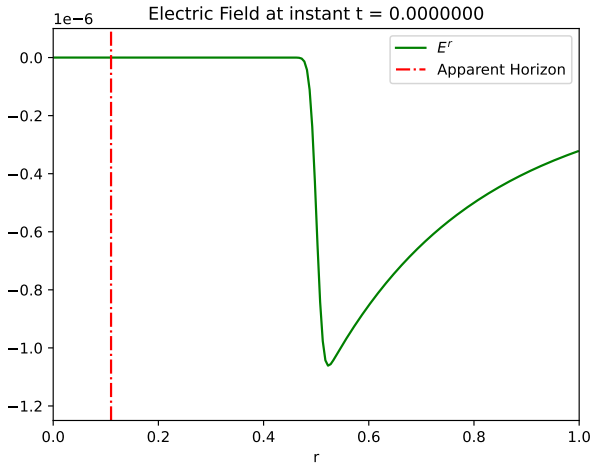

Figure 6.25: Additional electric field coming from the scalar field initial interaction with the scalar potential from the black hole.

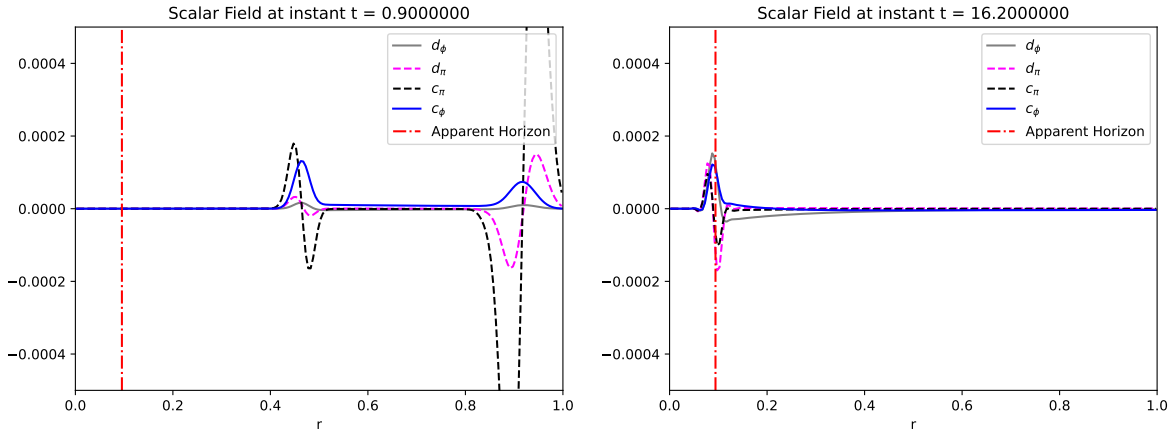

Figure 6.26: Charged scalar field interacting with a charged black hole. We have set the charge to 0.7. An initial perturbation in the real part of the scalar field was given.

6.8 Quasi-Normal Modes and Power-law decay tails

An expected feature of a scalar perturbation in a Schwarzschild background is the presence of quasi-normal modes (QNM) [40] and afterward a slow decay according to a given power-law, as was discussed in Sec. 4.4. However, if we were to use the initial data in Sec. 6.4, it takes until roughly $t \approx 3800$ to reach the beginning of the tail. Therefore, we have decided to take on a similar approach to [10] and force

the scalar field to be mostly ingoing, i.e., most of it is consumed by the black hole. This way, the QNM excitation is mostly suppressed, and it is easier to see the tails. To enforce this behavior, we need to have the freedom to choose the derivative of the scalar field, $\bar{c}_\Pi$. To do this, we add a new quantity, ψ_A, which will add a slight change to the initial data for A_{rr0} as

$$A_{rr0}\psi^{-6} \to (A_{rr0} + \psi_A)\psi^{-6}\,. \tag{6.19}$$

With this change, the momentum constraint can be solved to get an elliptic equation for ψ_A. In [10], a helper variable is defined,

$$\breve{\Pi} = \frac{\gamma_{\theta\theta}\sqrt{\gamma_{rr}}}{\alpha\chi^{3/2}}\left(\dot{\tilde{\Phi}} - \beta^r\tilde{\Phi}'\right),$$

which, when translated to the variables used here, means,

$$\breve{\bar{c}}_\Pi = \frac{\gamma_{\theta\theta}\sqrt{\gamma_{rr}}}{\alpha\chi^{3/2}}\left(\bar{c}_\Pi - \beta^r(\bar{c}'_\phi + \bar{c}_\phi\Omega'/\Omega)\right), \tag{6.20}$$

which can be reversed to get,

$$\bar{c}_\Pi = \frac{\alpha\chi^{3/2}}{\gamma_{\theta\theta}\sqrt{\gamma_{rr}}}\breve{\bar{c}}_\Pi + \beta^r(\bar{c}'_\phi + \bar{c}_\phi\Omega'/\Omega)\,.$$

I have written it this way to make it clearer what the actual change we are doing is. The reader will notice that the right-most factor is the term that appeared when we were solving the momentum constraint before. Now, with the helper variable, there is an extra term appearing. As initial data for this variable, $\breve{\bar{c}}_\Pi$, the choice made was,

$$\breve{\Pi}_0 = \sigma\frac{\gamma_{\theta\theta0}\sqrt{\gamma_{rr0}}}{\alpha_0\chi_0^{3/2}}\beta^r\tilde{\Phi}'_0 \iff \breve{\bar{c}}_{\Pi0} = \sigma\frac{\gamma_{\theta\theta0}\sqrt{\gamma_{rr0}}}{\alpha_0\chi_0^{3/2}}\beta^r(\bar{c}'_{\phi_0} + \bar{c}_{\phi_0}\Omega'/\Omega)\,,$$

with σ being ±1. It can take other constant values, however, but for simplicity we will use ±1 here as well. This condition means that the initial value for our original variable is,

$$\bar{c}_{\Pi0} = \beta^r(\bar{c}'_\phi + \bar{c}_\phi\Omega'/\Omega)\left(1 + \frac{\sigma}{\psi^6}\right). \tag{6.21}$$

Now, physically, this initial condition does not tell us much about what we are enforcing here. The new variable $\breve{\bar{c}}_\Pi$ is more helpful in this case since it is very reminiscent of the Lie derivative of $\tilde{c}_\phi$ (or $\tilde{\Phi}$ in [10]). Roughly, the condition we are imposing is equivalent to,

$$\mathcal{L}_n c_\Pi = \sigma\mathcal{L}_\beta c_\phi\,. \tag{6.22}$$

In abstract, the previous condition required to solve the momentum constraint was $\mathcal{L}_n c_\Pi = 0$. This is one of the reasons why people usually define the derivative of $\tilde{c}_\phi$ in this way. Going back to (6.22), the effect of σ is clearer in its effect. If we were to think of this in flat spacetime, this would correspond to $\partial_t c_\phi = \sigma\partial_r c_\phi$. If $\sigma = 1$, this means we want a pulse going to the right. If $\sigma = -1$, this means we want a pulse going to the left. In our case, an outgoing or ingoing pulse, respectively. We will never be able to

get a completely ingoing or outgoing pulse because the transformation involves χ, but the overall behavior will be similar to it. When we solve the momentum constraint with this extra formulation, we get,

$$\psi_A' = -\frac{8\pi\bar{\Omega}^3\breve{c}_0(\bar{c}_\phi'\Omega + \bar{c}_\phi\Omega')}{\Omega^3} - \psi_A\left(\frac{3}{r}\sqrt{\left(1 - \frac{2M\bar{\Omega}}{r} + \frac{Q^2\bar{\Omega}^2}{r^2}\right) + \left(\frac{K_{\text{CMC}}r}{3\bar{\Omega}} + \frac{C_{\text{CMC}}\bar{\Omega}^3}{r^2}\right)^2} + \frac{\Omega'}{\Omega}\right), \tag{6.23}$$

which is independent of ψ, a useful feature which allows us to get first ψ_A and then solve ψ already with this solution. This is the justification for the initial data used for $\breve{c}_\Pi$. The difference from (3.48b) in [10] is the presence of the charge Q. Assuming a Gaussian perturbation for the scalar field centered at 0.5, ψ_A (with $\sigma = 1$) takes the form shown in Fig. 6.27, with small changes regarding the charge of the black hole. If we were to choose the opposite sign, the solution would be reflected with respect to the x-axis.

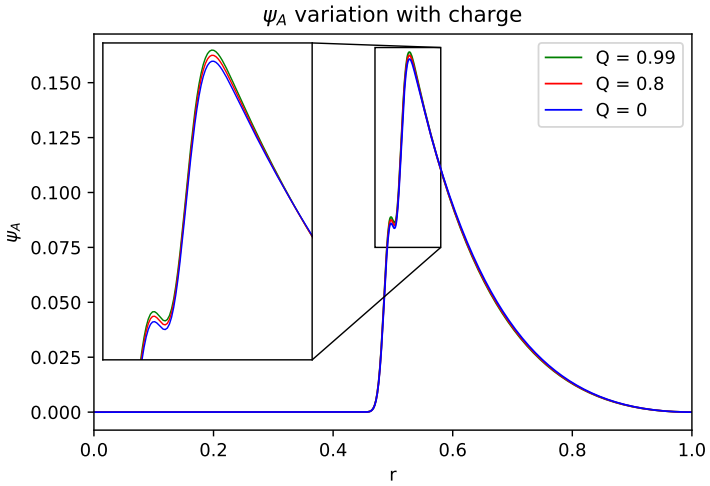

Figure 6.27: ψ_A numerical solution changing with the black hole's charge. We show a zoom-in on the region where it is easier to see the effect of the charge on ψ_A. M is set to 1 and K_{CMC} to -1.

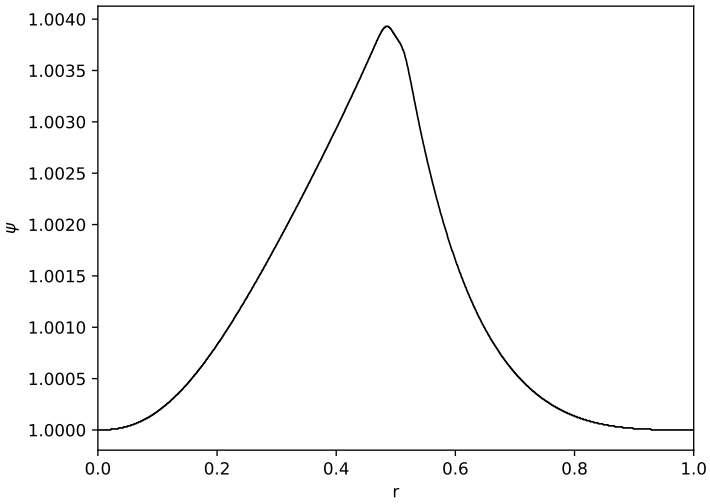

Figure 6.28: Integrating (6.24) to get the numerical solution for ψ. Compare with Fig. 6.9.

It is relevant to note that the initial condition for ψ_A is $\psi_A(0) = 0$, because the scalar field perturbation is 0 at the origin initially, and we also impose that the solution should go to 0 at future null infinity. We will

now have to separate between the two relevant cases, the real scalar field interacting with a Schwarzschild black hole and the charged scalar field interacting with a charged black hole. The real part has been done in [10], but we show them here with the gauge conditions chosen during the whole of this thesis, and also show that the new code can reproduce the same results.

6.8.1 Real Scalar Field in Schwarzschild

Regarding the real part of the scalar field, we also have to rederive the equation that solves the Hamiltonian constraint (6.2), to include ψ_A. This now gives us,

$$\begin{aligned}\psi'' = &-\frac{3C_{\rm CMC}^2\bar{\Omega}^4}{4r^6\psi^7} - \frac{K_{\rm CMC}^2\psi}{12\bar{\Omega}^2} + \frac{3C_{\rm CMC}^2\bar{\Omega}^4\psi}{4r^6} + \frac{K_{\rm CMC}^2\psi^5}{12\bar{\Omega}^2} - \frac{\pi\bar{\Omega}^4\breve{c}_0^2}{\psi^7\Omega^4} + \frac{C_{\rm CMC}\bar{\Omega}\psi_A\Omega}{4r^3\psi^7} - \frac{3\psi_A^2\Omega^2}{16\Omega^2\psi^7} \\ &- \pi\psi\Omega^2\bar{c}_\phi'^{\,2} - \frac{\psi'}{r} - \frac{\psi'}{3r^3\bar{\Omega}}\sqrt{K_{\rm CMC}^2r^6 + 9r^4\bar{\Omega}^2 + 6(C_{\rm CMC}K_{\rm CMC} - 3M)r^3\bar{\Omega}^3 + 9C_{\rm CMC}^2\bar{\Omega}^6} \\ &- 2\pi\bar{c}_\phi\psi\Omega\bar{c}_\phi'\Omega' - \pi\bar{c}_\phi^2\psi\Omega'^2\,.\end{aligned} \tag{6.24}$$

The numerical evolution of the system with this new initial data is shown in Fig. 6.28. Comparing with Fig. 6.9, we get a slightly different solution, due to the inclusion of ψ_A. In terms of the overall evolution of the system, it is very similar to how the usual perturbation behaves in Sec. 6.2, so it will not be shown again.

Recalling that hyperboloidal slices are spacelike curves and become tangent to null rays at infinity, this means that there should be a continuous change from an observer that is situated along a timelike worldtube at $r = 0.5$ or $r = 0.8$, where the tail decay should go with t^{-3}, to an observer placed at $\mathscr{I}^+$, where the decay should go with t^{-2}. Fig. 6.29 shows the profile of the scalar field perturbation changing with time, extracted at several values of the compactified radius.

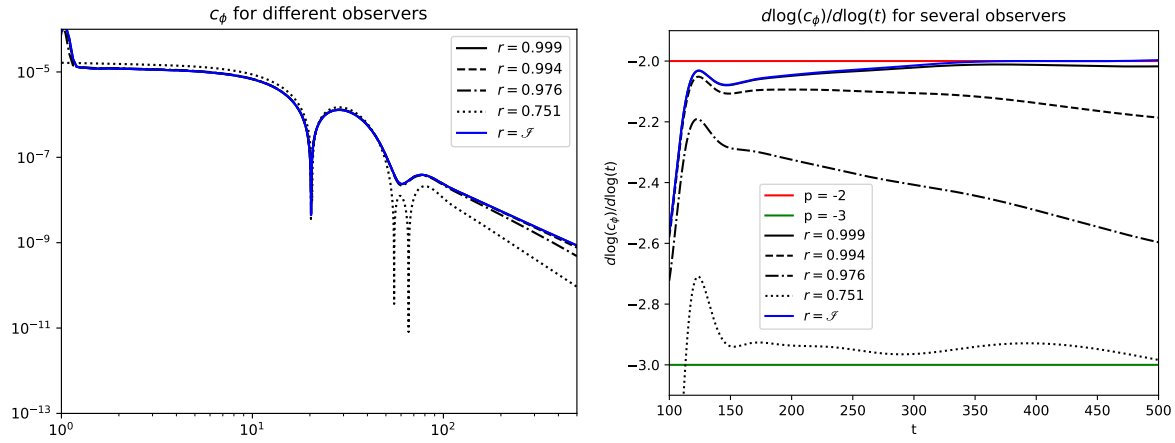

Figure 6.29: On the left: scalar field's behavior (absolute value) as time progresses for observers placed at several radii. We extrapolate the radiation at $\mathscr{I}^+$, because the staggered grid stops at half a spatial step before. The plot is on a logarithmic scale. On the right: derivative of the absolute value of the scalar field with respect to the logarithmic time. This corresponds to the exponent of the decay tail. In the tail regime, we get values that asymptote to -3 at $\mathscr{I}^+$ and to -2 along timelike hypersurfaces.

The plot is shown on a logarithmic scale to make it easier to see the change from the quasi-normal

modes regime to the tail decay regime. On the right plot, we also show the derivative of the logarithm of the absolute value of the scalar field with respect to logarithmic time. In the tail regime, this should provide the exponent of the decay and, indeed, for observers nearer scri+, the decay exponent is closer to -2 and nearer timelike curves, i.e., for smaller radii, it quickly approaches the expected -3. Doing a linear regression on the extrapolated points at $\mathscr{I}^+$, between $t = 350$ and $t = 500$, gives us $p = -2.000107 \pm 3\times10^{-6}$.

6.8.2 Charged Scalar Field in Reissner-Nördstrom

For the Reissner-Nördstrom case, we make similar changes as were done in Sec. 6.7, together with the ψ_A variable introduced in the previous section. Solving for the Hamiltonian constraint, we get

$$\begin{aligned}\psi'' = &-\frac{3C_{\rm CMC}^2\bar{\Omega}^4}{4r^6\psi^7} - \frac{K_{\rm CMC}^2\psi}{12\bar{\Omega}^2} + \frac{3C_{\rm CMC}^2\bar{\Omega}^4\psi}{4r^6} + \frac{K_{\rm CMC}^2\psi^5}{12\bar{\Omega}^2} - \frac{\pi\bar{\Omega}^4\Pi^2}{\psi^7\Omega^4} + \frac{C_{\rm CMC}\bar{\Omega}\psi_A\Omega}{4r^3\psi^7} - \frac{3\psi_A^2\Omega^2}{16\Omega^2\psi^7} \\ &- \pi\psi\Omega^2\bar{c}_\phi'^{\,2} - \frac{\psi'}{r} - \frac{\psi'}{3r^3\bar{\Omega}}\sqrt{K_{\rm CMC}^2r^6 + 9r^4\bar{\Omega}^2 + 6(C_{\rm CMC}K_{\rm CMC} - 3M)r^3\bar{\Omega}^3 + 9Q^2r^2\bar{\Omega}^4 + 9C_{\rm CMC}^2\bar{\Omega}^6} \\ &- 2\pi\bar{c}_\phi\psi\Omega\bar{c}_\phi'\Omega' - \pi\bar{c}_\phi^2\psi\Omega'^2 - \frac{Q^2\bar{\Omega}^2}{4r^4\psi^3} + \frac{Q^2\bar{\Omega}^2\psi}{4r^4} - \frac{Q\delta E^r\Omega^3}{2r^2\bar{\Omega}\psi^3} - \frac{\pi q^2\bar{c}_\phi\Phi^2\Omega^4}{\bar{\Omega}^2\psi^7} - \frac{(\delta E^r)^2\Omega^6}{4\bar{\Omega}^4\psi^3}\,.\end{aligned} \tag{6.25}$$

Regarding the charged scalar field interacting with a charged black hole, some research has been done already [16, 76, 77, 18]. More specifically, in [77], there is a table that describes the power-law decays of a scalar field in Schwarzschild and Reissner-Nördstrom backgrounds. There, they also consider the case of a massive scalar field, so we just take the relevant part for us in Tab. 6.3.

q	$Q = 0$	$Q \leq M$
0	t^{-2l-3}	t^{-2l-3}
$q \neq 0$	–	t^{-2l-2}

Table 6.3: Summary of power-law decays of a scalar field in Schwarzschild and Reissner-Nördstrom backgrounds [77]. q is the scalar field's charge, Q the black hole's charge and M the latter's mass. The entries describe the late-time decay tails behavior for timelike hypersurfaces. l comes from the spherical harmonic decomposition of the scalar field.

However, this table is far from complete, as we will see later. Also, in the third part of a series of 3 papers [18, 62, 17], it is shown that this should be otherwise. The authors of [77] cite the first paper of the series [18], and they even say that the considered case in these papers is for a very small electromagnetic interaction between the charged scalar field and the black hole, i.e., $|qQ| \lll 1$. Although they say that they have found analytical descriptions of the late time tails for the case we are considering, these are only valid for the same conditions of electromagnetic interaction that they said they were expanding on. The second and third papers of the series we just mentioned [62, 17] show analytically and numerically that the actual late time tails of the charged scalar field in a Reissner-Nördstrom background are given by,

$$t^{-(2\beta+2)}\,, \tag{6.26}$$

for timelike infinity and

$$t^{-(\beta+1-iqQ)}\,, \tag{6.27}$$

for future null infinity. The parameter β is given by,

$$\beta = \frac{-1+\sqrt{(2l+1)^2-4(qQ)^2}}{2}\,. \tag{6.28}$$

Spherical symmetry is restricted to $l = 0$. If there is no electromagnetic interaction, $qQ = 0$ and $\beta = 0$, and the tail decay exponents will be those corresponding to the real scalar field case. If, however, as we increase the value of the charge, we get $4(qQ)^2 > 1$, the square root becomes imaginary and the exponents that we expect for the late time tails become $p = -1$ for timelike infinity and $p = -0.5$ at $\mathscr{I}^+$. To test this, we have run 4 different scenarios. The mass of the black hole and the charge of the scalar field remained constant, equal to 1, and only changed the black hole's charge: 0.001, 0.3, 0.6, and 1.0. The scalar field's behavior is shown in Fig. 6.30. In this case, the quantity where we can appreciate the tails is the modulus of the scalar field, which is plotted in black in all graphs.

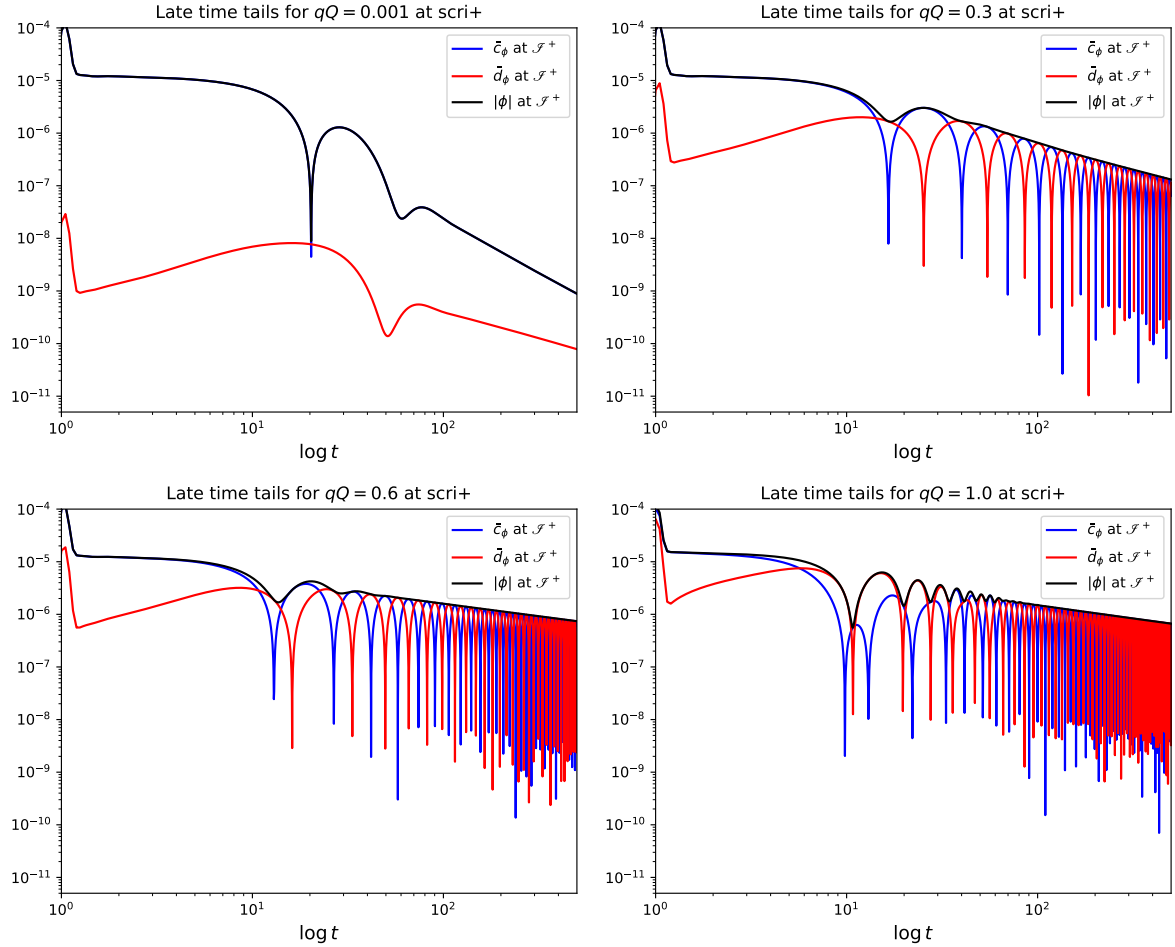

Figure 6.30: Value of the real and imaginary parts of the scalar field, together with its amplitude, at $\mathscr{I}^+$, as a function of time. The charge of the scalar field is set to 1, the mass of the black hole as well, and we only change the black hole's charge throughout the several graphs: 0.001, 0.3, 0.6, and 1.0.

As the charge of the black hole increases, the decay of the field's amplitude becomes slower. This has to do with the fact that the late time effects we see are progressively dominated by the electromagnetic

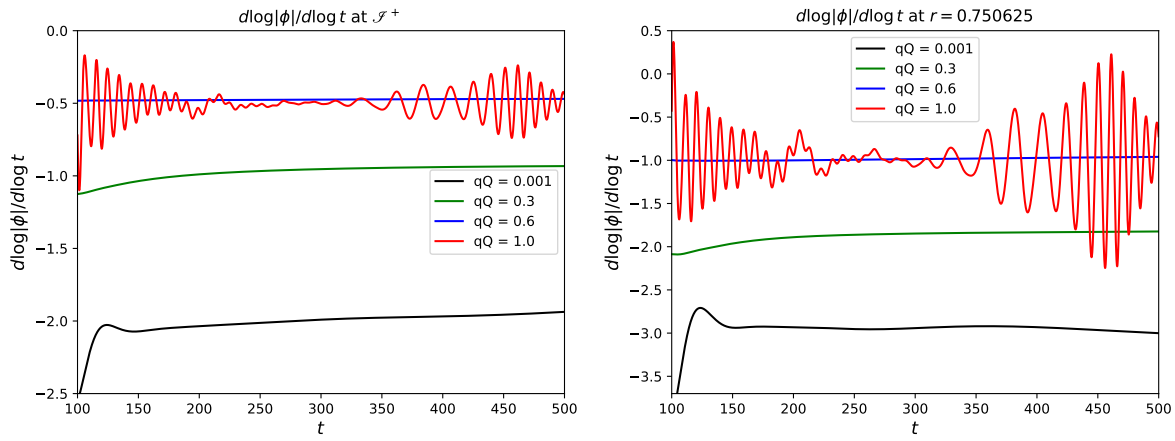

Figure 6.31: Derivative of the log of the absolute value of the scalar field with respect to the log of time. This gives the changing time exponent as we increase the charge. On the left, for $\mathscr{I}^+$. On the right, for $r \approx 0.75$.

interaction instead of the curvature [18]. We also see that as the charge increases, the oscillation frequency in the tail regime increases, which also matches the prediction in (6.27). Fig. 6.31 shows equivalent information to the right plot in Fig. 6.29, but including the exponents of the decay at scri+ on the left and along a timelike hypersurface on the right.

If we compare with the β exponent proposed in [18] and the prediction of [77], we get the plot Fig. 6.32, where we have run for other values of the charge for a clearer picture. The results agree with [18] and, in the limit $Qq \ll 0.001$, they agree with [77].

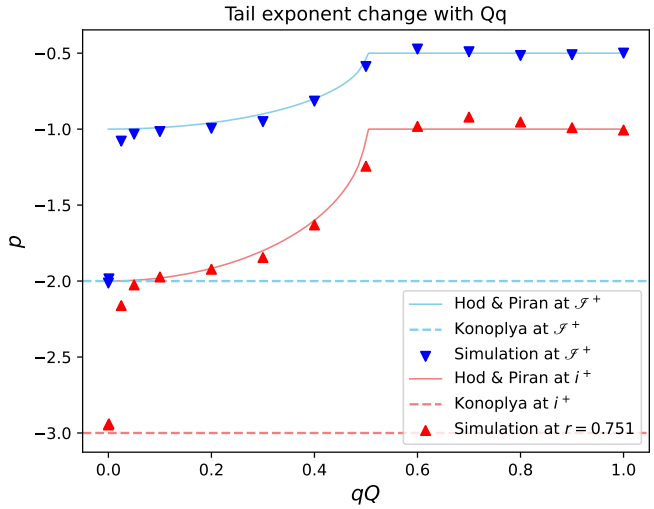

Figure 6.32: Comparison of the results from our simulation (the triangles) with the analytical results coming from Konoplya [77] and from Hod & Piran [18].

Fig. 6.30, during the tail decay regime, also shows an increasing frequency of oscillation of the real and imaginary parts. Analytically, this comes from the imaginary part in the definition of β in (6.28) and the other exponent in (6.27). Performing a Fourier Transform on the tail regime (we consider data only after $t = 300$ in each simulation), we get a linear correlation between the frequency of oscillation and the parameter Qq. This linear correlation is off by a factor of 10 from the prediction (6.28), by [62]. Therefore, we show the analytical prediction rescaled by a factor of 10 together with the frequencies that came

from the simulation in Fig. 6.33. We also compare with the function $f = Qq/10$, because the results coincide very well with this linear correlation between the oscillation frequency and the Qq parameter. The simulation does not agree, however, with the diverging behavior for $Qq \geq 0.5$. One could propose that the charge parameter we are using is incorrect by a factor of 10 as well, but then Fig. 6.32 should not agree with the analytical predictions as well. The Fourier Transform was applied to the imaginary part as well, giving the same result.

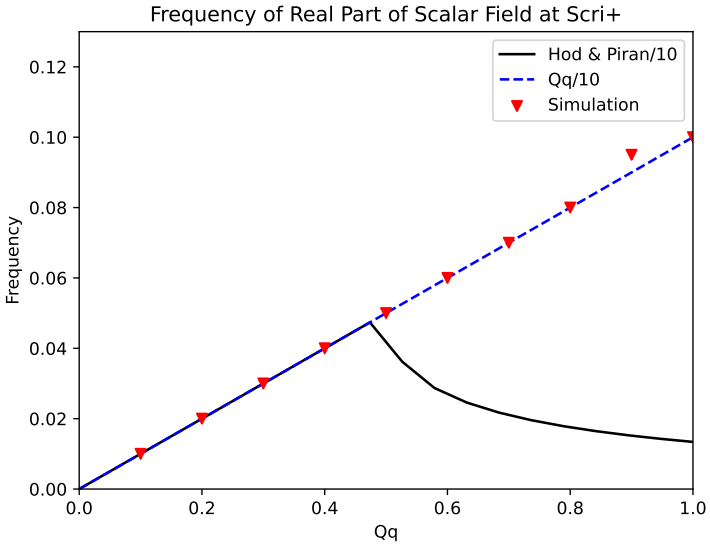

Figure 6.33: Frequency comparison of the results from our simulation (the triangles) with the analytical results coming from Hod and Piran [18] (the black line). The blue line corresponds to the function $f = Qq/10$, an empirical guess that shows better agreement.

6.8.3 Real Scalar Field in Reissner-Nördstrom

Here we take the charge of the scalar field to be 0 and see how it behaves late in time interacting with a Reissner-Nördstrom black hole. There has been some discussion about it: the authors of [78] contest the results of Bicak in [16], for the extremal RN case. However, Bicak and Price helped the authors of [79] to extract, for the extremal case, the power law t^{-2l-2}. This confirms what was shown in Tab. 6.3, from [77]. Therefore, the conclusion is that even for the extremal case, the tail decay of the real scalar field in a Reissner-Nördstrom background should be the same as in a Schwarzschild background. We have tested this for $Q = 0.1$ and $Q = 0.5$. The results are almost indistinguishable from Fig. 6.29, so no need to show the figures again. When tested for the extreme RN black hole, nothing conclusive could be interpreted, because there was no tail decay by $t = 500$, as had happened for all other simulations shown here.

6.9 Scalar Field Collapse

As the last section describing the results, we experiment with including a scalar field perturbation so strong that it produces a black hole [40, 80, 81]. The black hole's creation can be detected if the compactification factor χ goes to zero at the origin in a smooth way and finds a static solution there, a behavior that the lapse should also share, to freeze the evolution and avoid reaching the singularity. Furthermore, the apparent horizon can be used to give additional evidence that indeed there is black hole formation.

After much tuning, we found that the gauge conditions we have been using throughout this whole work

do not seem to withstand, in a consistent way, a collapsing scalar field. This would make it impossible to do convergence tests after the collapse, because at least one of the resolutions would blow up. To tackle this, I decided to change the gauge conditions (3.71) for the ones used in [52, 82]. This led me to the following expressions:

$$\begin{aligned}\dot{\alpha} &= \beta^r \alpha' - \hat{\beta}^r \hat{\alpha}' - \frac{\alpha^2 K}{\Omega} + \frac{\Omega'}{\Omega}(\hat{\beta}^r \hat{\alpha} - \beta^r \alpha) + \frac{\xi_{cK}(\hat{\alpha} - \alpha)}{\Omega} \\ \dot{\beta} &= \beta^r \beta^{r\prime} + \eta(\hat{\beta}^r - \beta^r) + \xi_{\beta^r}\left(\frac{\hat{\beta}^r}{\Omega} - \frac{\beta^r}{\Omega}\right) + \frac{3}{4}\alpha^2 \chi\lambda - 2\lambda\frac{3\Omega}{K_{\mathrm{CMC}}}\Lambda_r - \frac{K_{CMC}^2 r}{9}.\end{aligned} \tag{6.29}$$

These conditions are equivalent to (3.71) with $n_{cK} = 0$. We focus now on the results.

6.9.1 Collapse into a Schwarzschild Black Hole

For the case of the collapse of a real scalar field, this has been shown already in [10], using the tuned 1+log condition and the integrated Gamma-driver gauge conditions. To see how well this code can withstand this type of simulation, we decided to reproduce the result, with the adapted gauge conditions (6.29). Here, we continue using $K_{\mathrm{CMC}} = -1$ and a time-symmetric Gaussian perturbation for the (physical) scalar field, with $A = 0.05$, $\mu = 0.5$, and $\sigma = 0.1$. The Kreiss-Oliger dissipation amplitude had to be carefully tuned to provide for a long-lasting simulation. A good value was $\sigma_{\mathrm{KO}} = 0.15$. The evolution of the system is shown in Fig. 6.34, with the apparent horizon forming around $t \approx 7.1$.

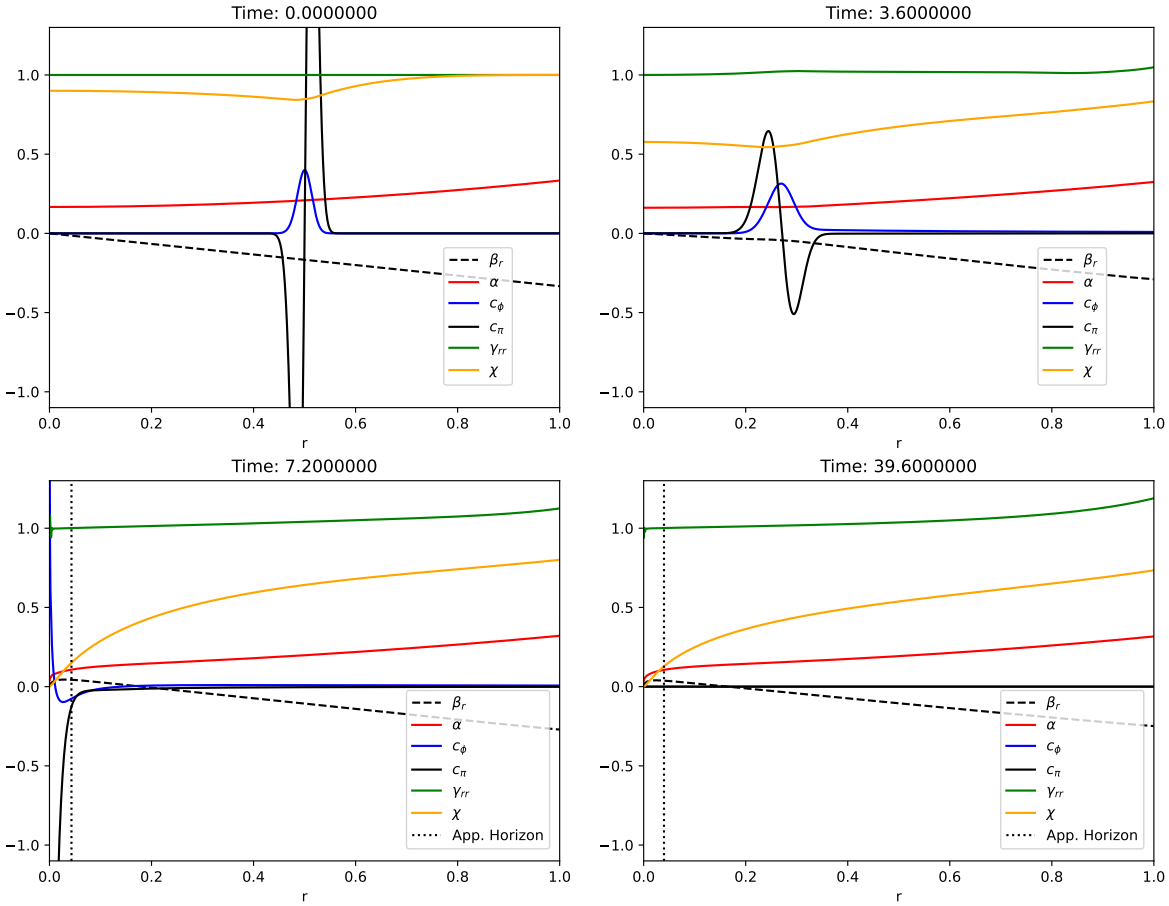

Figure 6.34: $\bar{c}_\phi$, $\bar{c}_\Pi$, β^r, α, χ, γ_{rr} evolving as the scalar field collapses into a black hole.

By looking at Fig. 6.34, we can see that on the bottom two frames, the lapse and χ have gone to

0 at the origin, the location of the trumpet. Simultaneously, β^r becomes positive at the horizon, which qualitatively mirrors the negative values it takes at scri+. The reason for this is that future null infinity is an ingoing null surface, while the event horizon is an outgoing one. The behavior of the shift allows us to preserve the resolution of our simulation in the region outside of the black hole. The apparent horizon appears around $r \approx 0.04$, and the Missner-Sharp mass indicates that the black hole's mass is about $M \approx 0.33$. This is shown in Fig. 6.35. The constraint convergence after the collapse is shown in Fig. 6.36. Regarding the scalar field, the reader will see that most of the perturbation in Fig. 6.35 radiates away through future null infinity. The ingoing part, on the other hand, when it hits the origin, it rapidly dissipates away, without reflection. Regarding the constraints (Fig. 6.36), as soon as the collapse happens, the constraints lose convergence near the origin. We also plotted the apparent horizon in the figures to better understand the region of space where this loss of convergence happens, and most of it happens inside the apparent horizon. This region does not affect constraint convergence in the rest of the domain, remaining in that fixed region of spacetime. There also seems to exist a small convergence loss at $\mathscr{I}^+$, but it attenuates with time. This latter part seems to be an improvement on the results obtained in [10].

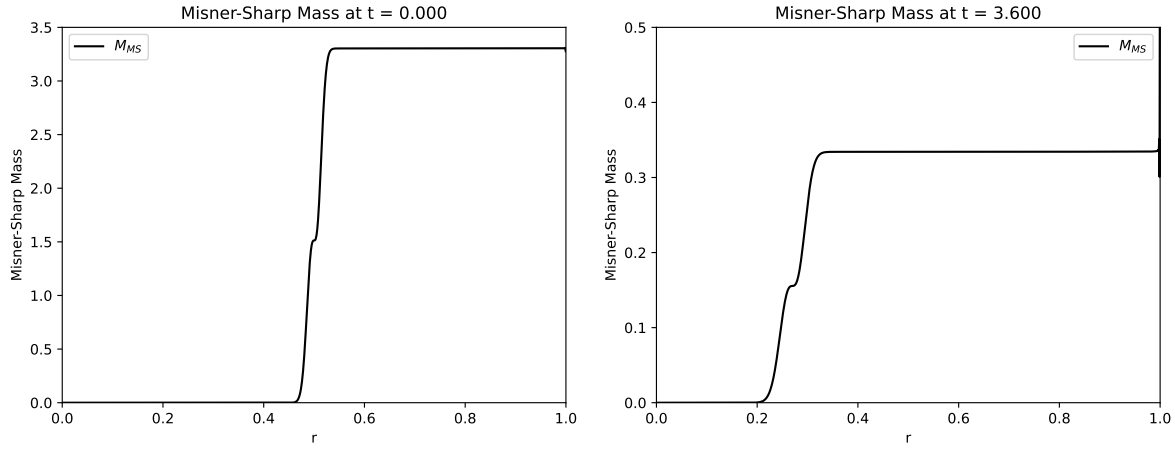

Figure 6.35: Misner-Sharp mass corresponding to the evolution in Fig. 6.34. The y-axis is rescaled appropriately for each picture. The first frame shows that initially we have a 3.5 (in mass units) scalar field perturbation. On the second frame, we see that most of it has radiated out through future null infinity, and the ingoing part (around 0.33 mass units) will become the black hole's mass.

6.9.2 Collapse into a Reissner-Nördstrom Black Hole

Regarding the charged scalar field collapse, this has also been of interest throughout the last decades [16, 30] and hence we shall do a similar perturbation in the same way as was done in Sec. 6.3. We continue using, for the physical scalar field, $A = 0.05$, $\mu = 0.5$, and $\sigma = 0.1$. For $\delta {A_3}^r$, we use $A = 0.02$, $\mu = 0.46$ and $\sigma = 0.2$. In this case, we decided to increase the charge of the scalar field, $q = 5.0$, to get a stronger electric field for the black hole. The result is shown in Fig. 6.37. We are plotting only the electromagnetic part, together with the real part of the scalar field. We have left this latter one for a better understanding of when the black hole is formed, but the rest of the variables have a very similar behavior as the one shown in Fig. 6.34. The conclusion is that a static electric field is formed after the collapse, matching the physical expectations. The apparent horizon is formed at around $r \approx 0.039$, closer to the origin than with the real scalar field due to the presence of charge. The electric field generated by the ingoing charged scalar

field is negative, due to the negative sign in the current density (A.55), but it continues to go to 0 near the origin, analogous to Fig. 6.17. The constraints converge similarly to Fig. 6.36, so here we only plot the Gauss constraint convergence (Fig. 6.38). In [83], we also show the convergence of the scalar field at $\mathscr{I}^+$. To the best of our knowledge, this is the first time that a collapse of a charged scalar field to a RN black hole has been carried out on hyperboloidal slices, with a common formulation such as BSSN/Z4.

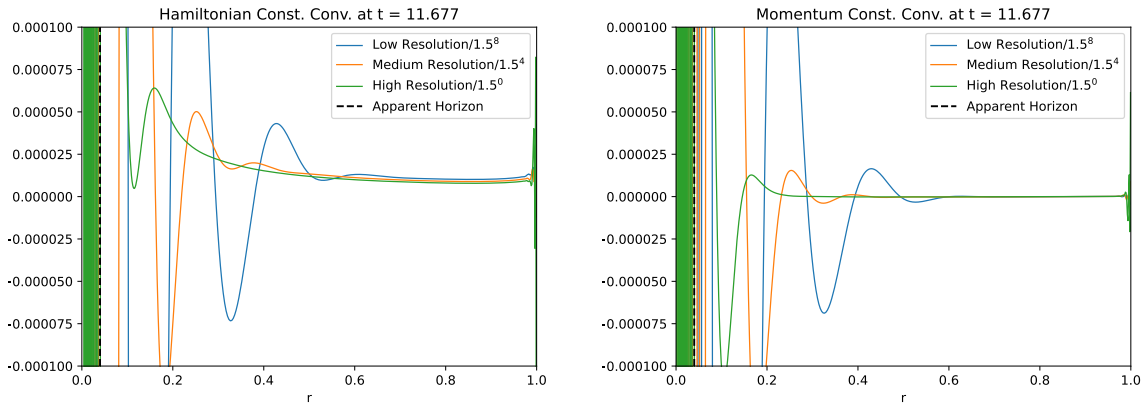

Figure 6.36: Constraint Convergence at $t = 11.677$, corresponding to the evolution shown in Fig. 6.34. Collapse has occurred at around $t \approx 7.1$.

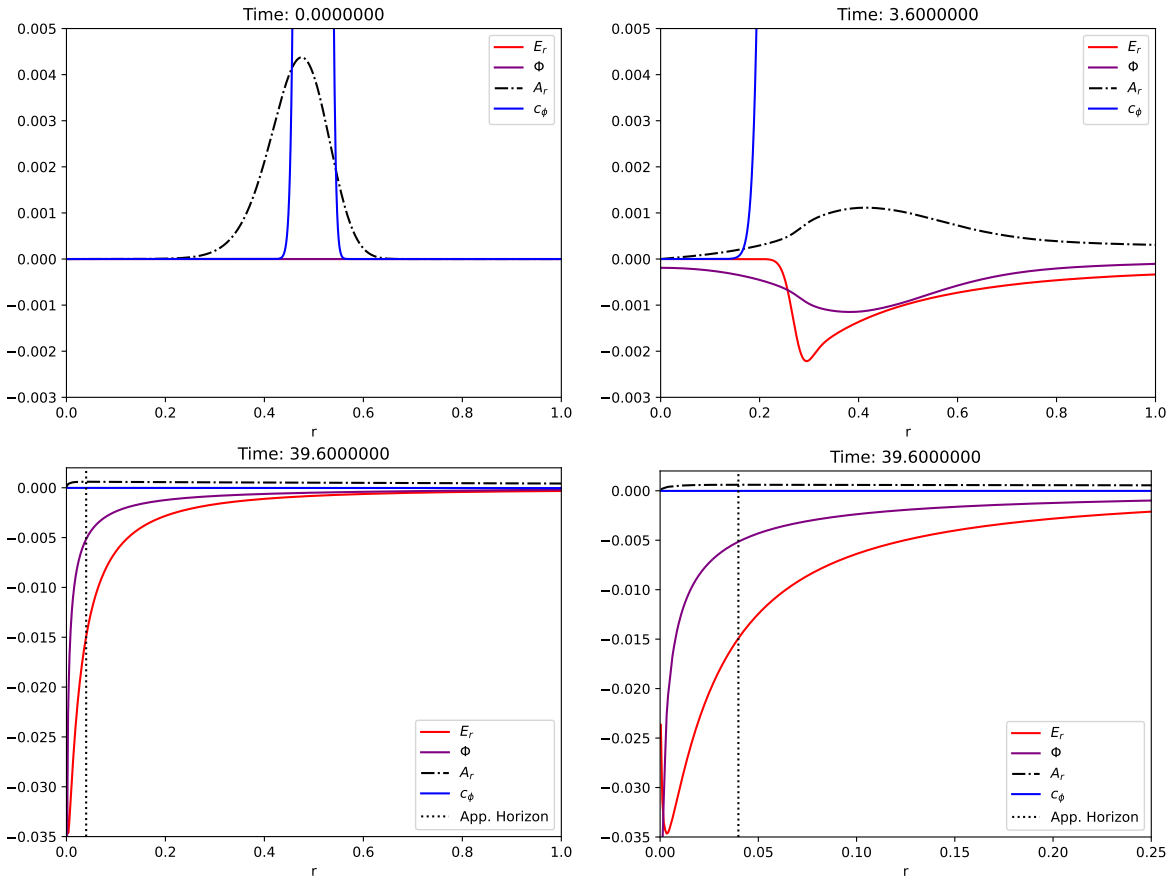

Figure 6.37: $\bar{c}_\phi$, E_r, Φ and A_{3_r} evolving until the charged scalar field collapses into a black hole at the origin. The last plot is a zoom-in of the first-to-last plot, for a clearer picture of the electromagnetic fields near the origin. The y-axis on the top figures is different from the lower ones.

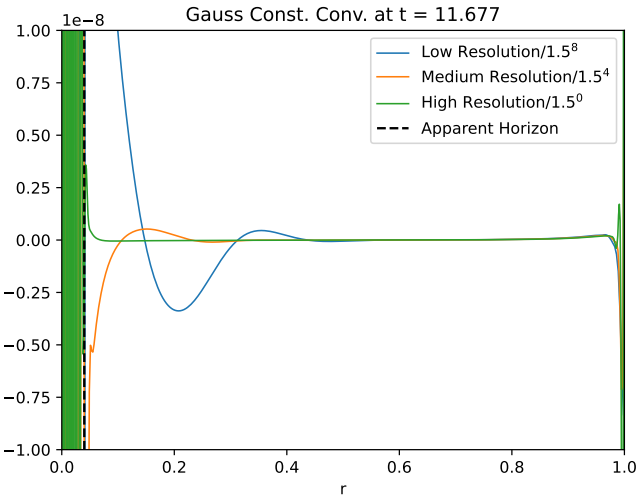

Figure 6.38: Gauss constraint convergence at $t = 11.677$, corresponding to the evolution shown in Fig. 6.37. Collapse has occured at around $t \approx 7.1$

Chapter 7

Conclusions and Future Work

7.1 Conclusions

With this work, we were able to piece together the Einstein-Maxwell-Klein-Gordon system of equations in hyperboloidal slices. This was done using BSSN/Z4 for the EFEs, and for Maxwell's equations we added a scalar ψ, following [37]. It is analogous to the role of Z4 in EFE but for Maxwell's equations. We also had to find a gauge condition for the scalar potential Φ that did not cause the electromagnetic potentials to grow unbounded at scri+. We were able to do this using a similar trick to what was done for α and β. Additionally, the constraints converge as expected, meaning the code and the system are steadily converging to the exact solutions as we increase the grid precision.

We also derived initial data for the Reissner-Nördstrom black hole background, adapted to trumpet initial data, in the hyperboloidal framework. This led to the correct modelling of a RN black hole interacting with a charged scalar field. After having this problem settled, we introduced a strong enough scalar field perturbation that collapsed into a black hole. This was done for the real scalar field, producing a Schwarzschild black hole, and for a charged scalar field, producing a Reissner-Nördstrom black hole.

Regarding the power-law tail decays, we were able to extract, for the first time, in hyperboloidal slices, how the decay exponent changes with different qQ without assuming a constant background. We checked that the exponent changes in accordance with previous analytical results, albeit with some systematic differences. The frequency of the real and imaginary parts of the scalar field, in the tail regime, was also compared with the analytical results from [17], and we got an almost linear relation between the parameter qQ and the frequency f, off by a factor of 10. This linear relation was expected, but from $qQ \geq 0.5$ onwards the analytical results diverge from the simulations' results.

7.2 Future Work

In the long run, one of the aims of the hyperboloidal approach is to be used in NR for extraction of gravitational waves right at scri+ from simulations of compact binary coalescences, to avoid systematic errors associated with extraction. This is crucial to reach higher accuracy in the waveform models

to prepare data analysis for the next generation of earth-based GW interferometers, like the Einstein Telescope and the Cosmic Explorer, and the space-based ones, like LISA, Taiji, TianQin, DECIGO, etc.

This work then comes as a relevant step in expanding the use of hyperboloidal slices to charged spacetimes and to the possibility of simulating with extremal RN BHs as a proxy for rotating Kerr ones. The next important objective will be putting this formalism in 3D. Before 3D, however, it would be interesting to expand to 2D and simulate the magnetic field that we discarded here because of spherical symmetry. In 2D, we could generalize the black hole we are considering, from RN to Kerr. Something that is still a matter of debate is simulating the massive Klein-Gordon equation on hyperboloidal slices. This would be particularly interesting because a massive scalar field can be interpreted as a boson star. The problem regarding this implementation is that the massive term does not fall off fast enough at future null infinity [84]. We say fast enough because, from a physical point of view, a massive object cannot travel at the speed of light and therefore should never reach scri+.

Part III

Bibliography and Appendices

Bibliography

[1] N. Aimar et al. *GYOTO 2.0: a polarized relativistic ray-tracing code*. arXiv:2311.18802 [astro-ph]. Nov. 2023. DOI: 10.48550/arXiv.2311.18802. URL: http://arxiv.org/abs/2311.18802 (visited on 02/10/2025).

[2] Frederic H. Vincent et al. "GYOTO: a new general relativistic ray-tracing code". In: *Classical and Quantum Gravity* 28.22 (Nov. 2011). arXiv:1109.4769 [gr-qc], p. 225011. ISSN: 0264-9381, 1361-6382. DOI: 10.1088/0264-9381/28/22/225011. URL: http://arxiv.org/abs/1109.4769 (visited on 02/10/2025).

[3] J. Frauendiener. "Numerical treatment of the hyperboloidal initial value problem for the vacuum Einstein equations. III. On the determination of radiation". In: *Class. Quantum Grav.* 17.2 (Jan. 2000). arXiv:gr-qc/9808072, pp. 373–387. ISSN: 0264-9381, 1361-6382. DOI: 10.1088/0264-9381/17/2/308. URL: http://arxiv.org/abs/gr-qc/9808072 (visited on 12/16/2023).

[4] Edward W. Leaver. "Spectral decomposition of the perturbation response of the Schwarzschild geometry". In: *Phys. Rev. D* 34.2 (July 1986). Publisher: American Physical Society, pp. 384–408. DOI: 10.1103/PhysRevD.34.384. URL: https://link.aps.org/doi/10.1103/PhysRevD.34.384 (visited on 12/17/2023).

[5] Michael Pürrer, Sascha Husa, and Peter C. Aichelburg. "News from Critical Collapse: Bondi Mass, Tails and Quasinormal Modes". In: *Phys. Rev. D* 71.10 (May 2005). arXiv:gr-qc/0411078, p. 104005. ISSN: 1550-7998, 1550-2368. DOI: 10.1103/PhysRevD.71.104005. URL: http://arxiv.org/abs/gr-qc/0411078 (visited on 12/16/2023).

[6] Sizheng Ma et al. "Merging black holes with Cauchy-characteristic matching: Computation of late-time tails". In: (Dec. 2024). arXiv: 2412.06906 [gr-qc].

[7] N. Bishop et al. *Cauchy-characteristic extraction in numerical relativity*. arXiv:gr-qc/9705033. May 1997. DOI: 10.48550/arXiv.gr-qc/9705033. URL: http://arxiv.org/abs/gr-qc/9705033 (visited on 07/29/2024).

[8] Anıl Zenginoğlu. "Hyperboloidal foliations and scri-fixing". In: *Class. Quantum Grav.* 25.14 (July 2008). arXiv:0712.4333 [gr-qc], p. 145002. ISSN: 0264-9381, 1361-6382. DOI: 10.1088/0264-9381/25/14/145002. URL: http://arxiv.org/abs/0712.4333 (visited on 12/16/2023).

[9] Anıl Zenginoğlu. “A hyperboloidal study of tail decay rates for scalar and Yang-Mills fields”. In: *Class. Quantum Grav.* 25.17 (Sept. 2008). arXiv:0803.2018 [gr-qc], p. 175013. ISSN: 0264-9381, 1361-6382. DOI: 10.1088/0264-9381/25/17/175013. URL: http://arxiv.org/abs/0803.2018 (visited on 12/16/2023).

[10] Alex Vañó-Viñuales. *Free evolution of the hyperboloidal initial value problem in spherical symmetry*. arXiv:1512.00776 [gr-qc]. Nov. 2015. DOI: 10.48550/arXiv.1512.00776. URL: http://arxiv.org/abs/1512.00776 (visited on 12/16/2023).

[11] José Damián López and Miguel Alcubierre. *Charged boson stars revisited*. arXiv:2303.04066 [gr-qc]. Mar. 2023. DOI: 10.48550/arXiv.2303.04066. URL: http://arxiv.org/abs/2303.04066 (visited on 12/16/2023).

[12] Ph. Jetzer and J. J. Van Der Bij. “Charged boson stars”. In: *Physics Letters B* 227.3 (Aug. 1989), pp. 341–346. ISSN: 0370-2693. DOI: 10.1016/0370-2693(89)90941-6. URL: https://www.sciencedirect.com/science/article/pii/0370269389909416 (visited on 12/17/2023).

[13] LIGO Scientific Collaboration and Virgo Collaboration et al. “Observation of Gravitational Waves from a Binary Black Hole Merger”. In: *Physical Review Letters* 116.6 (Feb. 2016). Publisher: American Physical Society, p. 061102. DOI: 10.1103/PhysRevLett.116.061102. URL: https://link.aps.org/doi/10.1103/PhysRevLett.116.061102 (visited on 07/30/2024).

[14] LIGO Scientific Collaboration and Virgo Collaboration et al. “GW151226: Observation of Gravitational Waves from a 22-Solar-Mass Binary Black Hole Coalescence”. In: *Physical Review Letters* 116.24 (June 2016). Publisher: American Physical Society, p. 241103. DOI: 10.1103/PhysRevLett.116.241103. URL: https://link.aps.org/doi/10.1103/PhysRevLett.116.241103 (visited on 07/30/2024).

[15] Stuart L. Shapiro and Saul A. Teukolsky. *Black holes, white dwarfs and neutron stars. The physics of compact objects*. Publication Title: A Wiley-Interscience Publication ADS Bibcode: 1983bhwd.book.....S. Jan. 1983. DOI: 10.1002/9783527617661. URL: https://ui.adsabs.harvard.edu/abs/1983bhwd.book.....S (visited on 07/29/2024).

[16] Jiří Bičák. “Gravitational collapse with charge and small asymmetries I. Scalar perturbations”. en. In: *General Relativity and Gravitation* 3.4 (Dec. 1972), pp. 331–349. ISSN: 0001-7701, 1572-9532. DOI: 10.1007/BF00759172. URL: http://link.springer.com/10.1007/BF00759172 (visited on 03/01/2025).

[17] Shahar Hod and Tsvi Piran. “Late-Time Evolution of Charged Gravitational Collapse and Decay of Charged Scalar Hair - III. Nonlinear Analysis”. In: *Physical Review D* 58.2 (June 1998). arXiv:gr-qc/9801060, p. 024019. ISSN: 0556-2821, 1089-4918. DOI: 10.1103/PhysRevD.58.024019. URL: http://arxiv.org/abs/gr-qc/9801060 (visited on 03/05/2025).

[18] Shahar Hod and Tsvi Piran. “Late-Time Evolution of Charged Gravitational Collapse and Decay of Charged Scalar Hair - I”. In: *Physical Review D* 58.2 (June 1998). arXiv:gr-qc/9712041, p. 024017.

ISSN: 0556-2821, 1089-4918. DOI: 10.1103/PhysRevD.58.024017. URL: http://arxiv.org/abs/gr-qc/9712041 (visited on 03/05/2025).

[19] Ray d'Inverno et al. *Introducing Einstein's Relativity: A Deeper Understanding*. Second Edition, Second Edition. Oxford, New York: Oxford University Press, June 2022. ISBN: 978-0-19-886202-4.

[20] H. Reissner. "Über die Eigengravitation des elektrischen Feldes nach der Einsteinschen Theorie". In: (Jan. 1916). DOI: 10.1002/andp.19163550905. URL: https://zenodo.org/records/1447315 (visited on 07/30/2024).

[21] Thomas Mädler, Radouane Gannouj, and Emanuel Gallo. *Characteristic initial value problems for the Einstein-Maxwell-scalar field equations in spherical symmetry*. arXiv:2503.24162 [gr-qc]. Mar. 2025. DOI: 10.48550/arXiv.2503.24162. URL: http://arxiv.org/abs/2503.24162 (visited on 04/01/2025).

[22] "Zero rest-mass fields including gravitation: asymptotic behaviour". EN. In: *Proceedings of the Royal Society of London. Series A. Mathematical and Physical Sciences* (Feb. 1965). Publisher: The Royal SocietyLondon. DOI: 10.1098/rspa.1965.0058. URL: https://royalsocietypublishing.org/doi/10.1098/rspa.1965.0058 (visited on 07/30/2024).

[23] Robert M. Wald. *General Relativity*. English. UK ed. edition. Chicago: University of Chicago Press, June 1984. ISBN: 978-0-226-87033-5.

[24] C. Bona et al. "A symmetry-breaking mechanism for the Z4 general-covariant evolution system". In: *Physical Review D* 69.6 (Mar. 2004). arXiv:gr-qc/0307067, p. 064036. ISSN: 1550-7998, 1550-2368. DOI: 10.1103/PhysRevD.69.064036. URL: http://arxiv.org/abs/gr-qc/0307067 (visited on 08/27/2024).

[25] C. Bona et al. "General-covariant evolution formalism for numerical relativity". en. In: *Physical Review D* 67.10 (May 2003), p. 104005. ISSN: 0556-2821, 1089-4918. DOI: 10.1103/PhysRevD.67.104005. URL: https://link.aps.org/doi/10.1103/PhysRevD.67.104005 (visited on 08/27/2024).

[26] A.I. Arbab. "Conformal electrodynamics in curved space". en. In: *Optik* 241 (Sept. 2021), p. 167009. ISSN: 00304026. DOI: 10.1016/j.ijleo.2021.167009. URL: https://linkinghub.elsevier.com/retrieve/pii/S0030402621006975 (visited on 08/06/2024).

[27] Jeremy Côté, Valerio Faraoni, and Andrea Giusti. "Revisiting the conformal invariance of Maxwell's equations in curved spacetime". In: *Gen Relativ Gravit* 51.9 (Sept. 2019). arXiv:1905.09968 [gr-qc, physics:hep-th], p. 117. ISSN: 0001-7701, 1572-9532. DOI: 10.1007/s10714-019-2599-x. URL: http://arxiv.org/abs/1905.09968 (visited on 12/16/2023).

[28] Miguel Alcubierre, Juan Carlos Degollado, and Marcelo Salgado. "The Einstein-Maxwell system in 3+1 form and initial data for multiple charged black holes". In: *Phys. Rev. D* 80.10 (Nov. 2009). arXiv:0907.1151 [gr-qc], p. 104022. ISSN: 1550-7998, 1550-2368. DOI: 10.1103/PhysRevD.80.104022. URL: http://arxiv.org/abs/0907.1151 (visited on 12/16/2023).

[29] Thomas W. Baumgarte and Stuart L. Shapiro. *Numerical Relativity: Solving Einstein's Equations on the Computer*. Cambridge: Cambridge University Press, 2010. ISBN: 978-0-521-51407-1. DOI: 10.1017/CBO9781139193344. URL: https://www.cambridge.org/core/books/numerical-relativity/72D4F6D791BC6F8F9CF87A60FC354D6A (visited on 12/16/2023).

[30] Jose M. Torres and Miguel Alcubierre. "Gravitational collapse of charged scalar fields". In: *Gen Relativ Gravit* 46.9 (Sept. 2014). arXiv:1407.7885 [gr-qc], p. 1773. ISSN: 0001-7701, 1572-9532. DOI: 10.1007/s10714-014-1773-4. URL: http://arxiv.org/abs/1407.7885 (visited on 12/16/2023).

[31] John David Jackson. *Classical Electrodynamics, 2nd Edition*. eng. Oct. 1975. URL: http://archive.org/details/ClassicalElectrodynamics2nd (visited on 08/27/2024).

[32] Rishabh Jha. "Introduction to Hamiltonian formulation of general relativity and homogeneous cosmologies". en. In: *SciPost Physics Lecture Notes* (Aug. 2023), p. 73. ISSN: 2590-1990. DOI: 10.21468/SciPostPhysLectNotes.73. URL: https://scipost.org/10.21468/SciPostPhysLectNotes.73 (visited on 05/27/2025).

[33] Lawrence E. Kidder, Mark A. Scheel, and Saul A. Teukolsky. "Extending the lifetime of 3D black hole computations with a new hyperbolic system of evolution equations". In: *Physical Review D* 64.6 (Aug. 2001). arXiv:gr-qc/0105031, p. 064017. ISSN: 0556-2821, 1089-4918. DOI: 10.1103/PhysRevD.64.064017. URL: http://arxiv.org/abs/gr-qc/0105031 (visited on 08/31/2024).

[34] Thomas W. Baumgarte and Stuart L. Shapiro. "Numerical integration of Einstein's field equations". In: *Physical Review D* 59.2 (Dec. 1998). Publisher: American Physical Society, p. 024007. DOI: 10.1103/PhysRevD.59.024007. URL: https://link.aps.org/doi/10.1103/PhysRevD.59.024007 (visited on 08/31/2024).

[35] Masaru Shibata and Takashi Nakamura. "Evolution of three-dimensional gravitational waves: Harmonic slicing case". In: *Physical Review D* 52.10 (Nov. 1995). Publisher: American Physical Society, pp. 5428–5444. DOI: 10.1103/PhysRevD.52.5428. URL: https://link.aps.org/doi/10.1103/PhysRevD.52.5428 (visited on 08/31/2024).

[36] David Brown. "BSSN in Spherical Symmetry". In: *Classical and Quantum Gravity* 25.20 (Oct. 2008). arXiv:0705.3845 [gr-qc], p. 205004. ISSN: 0264-9381, 1361-6382. DOI: 10.1088/0264-9381/25/20/205004. URL: http://arxiv.org/abs/0705.3845 (visited on 08/31/2024).

[37] Carles Bona, Carlos Palenzuela-Luque, and Carles Bona-Casas. *Elements of Numerical Relativity and Relativistic Hydrodynamics: From Einstein's Equations to Astrophysical Simulations*. en. Vol. 783. Lecture Notes in Physics. Berlin, Heidelberg: Springer, 2009. ISBN: 978-3-642-01163-4 978-3-642-01164-1. DOI: 10.1007/978-3-642-01164-1. URL: https://link.springer.com/10.1007/978-3-642-01164-1 (visited on 12/17/2023).

[38] David J. Griffiths. *Introduction to electrodynamics*. en. Fourth edition. Boston: Pearson, 2013. ISBN: 978-0-321-85656-2.

[39] S. Sonego and V. Faraoni. “Huygens’ principle and characteristic propagation property for waves in curved space-times”. en. In: *Journal of Mathematical Physics* 33.2 (Feb. 1992). Publisher: AIP Publishing, pp. 625–632. ISSN: 0022-2488, 1089-7658. DOI: 10.1063/1.529798. URL: https://pubs.aip.org/jmp/article/33/2/625/229720/Huygens-principle-and-characteristic-propagation (visited on 01/14/2025).

[40] Richard H. Price. *Nonspherical Perturbations of Relativistic Gravitational Collapse. I. Scalar and Gravitational Perturbations | Phys. Rev. D*. URL: https://journals.aps.org/prd/abstract/10.1103/PhysRevD.5.2419 (visited on 01/14/2025).

[41] Sucheta Majumdar. “Residual gauge symmetry in light-cone electromagnetism”. In: *Journal of High Energy Physics* 2023.2 (Feb. 2023). arXiv:2212.10637 [hep-th]. ISSN: 1029-8479. DOI: 10.1007/JHEP02(2023)215. URL: http://arxiv.org/abs/2212.10637 (visited on 01/14/2025).

[42] Gary McCartor and David G. Robertson. “Light-Cone Quantization of Gauge Fields”. In: *Zeitschrift für Physik C Particles and Fields* 62.2 (June 1994). arXiv:hep-th/9311065, pp. 349–355. ISSN: 0170-9739, 1434-6052. DOI: 10.1007/BF01560250. URL: http://arxiv.org/abs/hep-th/9311065 (visited on 01/14/2025).

[43] Yuji Ando et al. *A consistent light-cone-gauge superstring field theory*. arXiv:2411.19570 [hep-th]. Nov. 2024. DOI: 10.48550/arXiv.2411.19570. URL: http://arxiv.org/abs/2411.19570 (visited on 01/14/2025).

[44] Michele Maggiore. *Gravitational Waves. Vol. 2: Astrophysics and Cosmology*. Oxford University Press, Mar. 2018. ISBN: 978-0-19-857089-9.

[45] Alex Vañó-Viñuales. “Spherically symmetric black hole spacetimes on hyperboloidal slices”. In: *Frontiers in Applied Mathematics and Statistics* 9 (Aug. 2023). arXiv:2304.05384 [gr-qc], p. 1206017. ISSN: 2297-4687. DOI: 10.3389/fams.2023.1206017. URL: http://arxiv.org/abs/2304.05384 (visited on 01/10/2025).

[46] Adrian P. Gentle et al. “Constant Crunch Coordinates for Black Hole Simulations”. In: *Physical Review D* 63.6 (Feb. 2001). arXiv:gr-qc/0005113, p. 064024. ISSN: 0556-2821, 1089-4918. DOI: 10.1103/PhysRevD.63.064024. URL: http://arxiv.org/abs/gr-qc/0005113 (visited on 09/22/2024).

[47] Alex Vañó-Viñuales and Tiago Valente. “Height-function-based 4D reference metrics for hyperboloidal evolution”. In: *General Relativity and Gravitation* 56.11 (Nov. 2024). arXiv:2408.08952 [gr-qc], p. 135. ISSN: 0001-7701, 1572-9532. DOI: 10.1007/s10714-024-03323-8. URL: http://arxiv.org/abs/2408.08952 (visited on 03/26/2025).

[48] Miguel Alcubierre. “Introduction to 3+1 Numerical Relativity”. In: *Introduction to 3+1 Numerical Relativity* (Apr. 2006). ISSN: 9780199205677. DOI: 10.1093/acprof:oso/9780199205677.001.0001.

[49] Thomas W. Baumgarte and Stephen G. Naculich. “Analytical representation of a black hole puncture solution”. en. In: *Physical Review D* 75.6 (Mar. 2007), p. 067502. ISSN: 1550-7998, 1550-2368. DOI: 10.1103/PhysRevD.75.067502. URL: https://link.aps.org/doi/10.1103/PhysRevD.75.067502 (visited on 12/09/2024).

[50] Helmut Friedrich and Alan Rendall. “The Cauchy Problem for the Einstein Equations”. en. In: *Einstein’s Field Equations and Their Physical Implications*. Ed. by Bernd G. Schmidt. Berlin, Heidelberg: Springer, 2000, pp. 127–223. ISBN: 978-3-540-46580-5. DOI: 10.1007/3-540-46580-4_2.

[51] Kyle Slinker, Charles R. Evans, and Mark Hannam. “Trumpet Initial Data for Boosted Black Holes”. In: *Physical Review D* 98.4 (Aug. 2018). arXiv:1806.08364 [gr-qc], p. 044014. ISSN: 2470-0010, 2470-0029. DOI: 10.1103/PhysRevD.98.044014. URL: http://arxiv.org/abs/1806.08364 (visited on 12/09/2024).

[52] Alex Vañó-Viñuales. “Conformal diagrams for stationary and dynamical strong-field hyperboloidal slices”. In: *Classical and Quantum Gravity* 41.10 (May 2024). arXiv:2311.04972 [gr-qc], p. 105003. ISSN: 0264-9381, 1361-6382. DOI: 10.1088/1361-6382/ad3aca. URL: http://arxiv.org/abs/2311.04972 (visited on 12/09/2024).

[53] Mark Hannam et al. “Wormholes and trumpets: Schwarzschild spacetime for the moving-puncture generation”. en. In: *Physical Review D* 78.6 (Sept. 2008), p. 064020. ISSN: 1550-7998, 1550-2368. DOI: 10.1103/PhysRevD.78.064020. URL: https://link.aps.org/doi/10.1103/PhysRevD.78.064020 (visited on 12/09/2024).

[54] M. D. Kruskal. “Maximal Extension of Schwarzschild Metric”. In: *Physical Review* 119.5 (Sept. 1960). Publisher: American Physical Society, pp. 1743–1745. DOI: 10.1103/PhysRev.119.1743. URL: https://link.aps.org/doi/10.1103/PhysRev.119.1743 (visited on 12/09/2024).

[55] José P. S. Lemos and Diogo L. F. G. Silva. “Maximal extension of the Schwarzschild metric: From Painlevé-Gullstrand to Kruskal-Szekeres”. In: *Annals of Physics* 430 (July 2021). arXiv:2005.14211 [gr-qc], p. 168497. ISSN: 00034916. DOI: 10.1016/j.aop.2021.168497. URL: http://arxiv.org/abs/2005.14211 (visited on 12/09/2024).

[56] Gioel Calabrese, Ian Hinder, and Sascha Husa. “Numerical stability for finite difference approximations of Einstein’s equations”. In: *Journal of Computational Physics* 218.2 (Nov. 2006). arXiv:gr-qc/0503056, pp. 607–634. ISSN: 00219991. DOI: 10.1016/j.jcp.2006.02.027. URL: http://arxiv.org/abs/gr-qc/0503056 (visited on 02/03/2025).

[57] Sascha Husa. “Numerical modeling of black holes as sources of gravitational waves in a nutshell”. In: *The European Physical Journal Special Topics* 152.1 (Dec. 2007). arXiv:0812.4395 [gr-qc], pp. 183–207. ISSN: 1951-6355, 1951-6401. DOI: 10.1140/epjst/e2007-00381-6. URL: http://arxiv.org/abs/0812.4395 (visited on 02/03/2025).

[58] Luis Magalhães. *Álgebra Linear Como Introdução à Matemática Aplicada*. Texto Editora, 1993. ISBN: 972-47-0007-0.

[59] Charles W. Misner and David H. Sharp. “Relativistic Equations for Adiabatic, Spherically Symmetric Gravitational Collapse”. In: *Physical Review* 136.2B (Oct. 1964). Publisher: American Physical Society, B571–B576. DOI: 10.1103/PhysRev.136.B571. URL: https://link.aps.org/doi/10.1103/PhysRev.136.B571 (visited on 02/09/2025).

[60] Anıl Zenginoğlu, Dario Nunez, and Sascha Husa. “Gravitational perturbations of Schwarzschild spacetime at null infinity and the hyperboloidal initial value problem”. In: *Classical and Quantum Gravity* 26 (Nov. 2008). DOI: 10.1088/0264-9381/26/3/035009.

[61] *Nonspherical Perturbations of Relativistic Gravitational Collapse. I. Scalar and Gravitational Perturbations | Phys. Rev. D*. URL: https://journals.aps.org/prd/abstract/10.1103/PhysRevD.5.2419 (visited on 02/09/2025).

[62] Shahar Hod and Tsvi Piran. “Late-Time Evolution of Charged Gravitational Collapse and Decay of Charged Scalar Hair - II”. In: *Physical Review D* 58.2 (June 1998). arXiv:gr-qc/9801001, p. 024018. ISSN: 0556-2821, 1089-4918. DOI: 10.1103/PhysRevD.58.024018. URL: http://arxiv.org/abs/gr-qc/9801001 (visited on 03/05/2025).

[63] J.M. Carcione. “Boundary conditions for wave propagation problems”. en. In: *Finite Elements in Analysis and Design* 16.3-4 (June 1994), pp. 317–327. ISSN: 0168874X. DOI: 10.1016/0168-874X(94)90074-4. URL: https://linkinghub.elsevier.com/retrieve/pii/0168874X94900744 (visited on 08/17/2024).

[64] Gioel Calabrese and Carsten Gundlach. *Discrete boundary treatment for the shifted wave equation*. arXiv:gr-qc/0509119 version: 2. July 2006. DOI: 10.48550/arXiv.gr-qc/0509119. URL: http://arxiv.org/abs/gr-qc/0509119 (visited on 06/28/2024).

[65] M. C. Babiuc et al. “Implementation of standard testbeds for numerical relativity”. In: *Classical and Quantum Gravity* 25.12 (June 2008). arXiv:0709.3559 [gr-qc], p. 125012. ISSN: 0264-9381, 1361-6382. DOI: 10.1088/0264-9381/25/12/125012. URL: http://arxiv.org/abs/0709.3559 (visited on 08/17/2024).

[66] Manuel Kindelan, Miguel Moscoso, and Pedro Gonzalez-Rodriguez. “Optimized Finite Difference Formulas for Accurate High Frequency Components”. In: *Mathematical Problems in Engineering* 2016 (Jan. 2016), pp. 1–15. DOI: 10.1155/2016/7860618.

[67] Alex Vañó-Viñuales. *Wave equation: analysis and discretization*. en. 2023.

[68] *xAct: Efficient tensor computer algebra for the Wolfram Language*. URL: http://www.xact.es/index.html (visited on 12/27/2023).

[69] John Archibald Wheeler. “Geons”. In: *Physical Review* 97.2 (Jan. 1955). Publisher: American Physical Society, pp. 511–536. DOI: 10.1103/PhysRev.97.511. URL: https://link.aps.org/doi/10.1103/PhysRev.97.511 (visited on 11/17/2024).

[70] H. P. de Oliveira. “Non-linear charged black holes”. en. In: *Classical and Quantum Gravity* 11.6 (June 1994), p. 1469. ISSN: 0264-9381. DOI: 10.1088/0264-9381/11/6/012. URL: https://dx.doi.org/10.1088/0264-9381/11/6/012 (visited on 12/16/2024).

[71] Gonzalo J. Olmo and D. Rubiera-Garcia. “Reissner-Nordström black holes in extended Palatini theories”. In: *Physical Review D* 86.4 (Aug. 2012). arXiv:1207.6004 [gr-qc], p. 044014. ISSN: 1550-7998, 1550-2368. DOI: 10.1103/PhysRevD.86.044014. URL: http://arxiv.org/abs/1207.6004 (visited on 12/16/2024).

[72] Víctor Jaramillo et al. *Full 3D nonlinear dynamics of charged and magnetized boson stars*. arXiv:2411.07284 [gr-qc]. Nov. 2024. DOI: 10.48550/arXiv.2411.07284. URL: http://arxiv.org/abs/2411.07284 (visited on 01/20/2025).

[73] Miguel Zilhão, Helvi Witek, and Vitor Cardoso. "Nonlinear interactions between black holes and Proca fields". In: *Classical and Quantum Gravity* 32.23 (Dec. 2015). arXiv:1505.00797 [gr-qc], p. 234003. ISSN: 0264-9381, 1361-6382. DOI: 10.1088/0264-9381/32/23/234003. URL: http://arxiv.org/abs/1505.00797 (visited on 01/25/2025).

[74] David Hilditch. "An Introduction to Well-posedness and Free-evolution". In: *International Journal of Modern Physics A* 28.22n23 (Sept. 2013). arXiv:1309.2012 [gr-qc], p. 1340015. ISSN: 0217-751X, 1793-656X. DOI: 10.1142/S0217751X13400150. URL: http://arxiv.org/abs/1309.2012 (visited on 01/20/2025).

[75] A. M. Knapp, E. J. Walker, and T. W. Baumgarte. "Illustrating Stability Properties of Numerical Relativity in Electrodynamics". In: *Physical Review D* 65.6 (Feb. 2002). arXiv:gr-qc/0201051, p. 064031. ISSN: 0556-2821, 1089-4918. DOI: 10.1103/PhysRevD.65.064031. URL: http://arxiv.org/abs/gr-qc/0201051 (visited on 01/21/2025).

[76] R. A. Konoplya. "Massive charged scalar field in a Reissner-Nordstrom black hole background: quasinormal ringing". In: *Physics Letters B* 550.1-2 (Dec. 2002). arXiv:gr-qc/0210105, pp. 117–120. ISSN: 03702693. DOI: 10.1016/S0370-2693(02)02974-X. URL: http://arxiv.org/abs/gr-qc/0210105 (visited on 02/17/2025).

[77] R. A. Konoplya and A. Zhidenko. "Massive charged scalar field in the Kerr-Newman background: Quasinormal modes, late-time tails and stability". In: *Physical Review D* 88.2 (July 2013). Publisher: American Physical Society, p. 024054. DOI: 10.1103/PhysRevD.88.024054. URL: https://link.aps.org/doi/10.1103/PhysRevD.88.024054 (visited on 03/03/2025).

[78] Amos Ori. *Late-time tails in extremal Reissner-Nordstrom spacetime*. arXiv:1305.1564 [gr-qc]. May 2013. DOI: 10.48550/arXiv.1305.1564. URL: http://arxiv.org/abs/1305.1564 (visited on 03/03/2025).

[79] Carl J. Blaksley and Lior M. Burko. "The late-time tails in the Reissner-Nordström spacetime revisited". In: *Physical Review D* 76.10 (Nov. 2007). arXiv:0710.2915 [gr-qc], p. 104035. ISSN: 1550-7998, 1550-2368. DOI: 10.1103/PhysRevD.76.104035. URL: http://arxiv.org/abs/0710.2915 (visited on 03/03/2025).

[80] Matthew W. Choptuik. "Universality and scaling in gravitational collapse of a massless scalar field". en. In: *Physical Review Letters* 70.1 (Jan. 1993), pp. 9–12. ISSN: 0031-9007. DOI: 10.1103/PhysRevLett.70.9. URL: https://link.aps.org/doi/10.1103/PhysRevLett.70.9 (visited on 02/28/2025).

[81] Jun-Qi Guo. "Dynamics near the central singularity in spherical collapse". In: *Journal of Physics Communications* 5.7 (July 2021). arXiv:2011.14853 [gr-qc], p. 075015. ISSN: 2399-6528. DOI: 10.1088/2399-6528/ac1505. URL: http://arxiv.org/abs/2011.14853 (visited on 03/01/2025).

[82] Alex Vañó-Viñuales and Sascha Husa. “Spherical symmetry as a test case for unconstrained hyperboloidal evolution II: gauge conditions”. In: *Classical and Quantum Gravity* 35.4 (Feb. 2018). arXiv:1705.06298 [gr-qc], p. 045014. ISSN: 0264-9381, 1361-6382. DOI: 10.1088/1361-6382/aaa4e2. URL: http://arxiv.org/abs/1705.06298 (visited on 01/10/2025).

[83] João D. Álvares and Alex Vaño-Viñuales. *Free Hyperboloidal Evolution of the Einstein-Maxwell-Klein-Gordon System*. arXiv:2505.17176 [gr-qc]. May 2025. DOI: 10.48550/arXiv.2505.17176. URL: http://arxiv.org/abs/2505.17176 (visited on 05/26/2025).

[84] Shalabh Gautam et al. “Summation by Parts and Truncation Error Matching on Hyperboloidal Slices”. In: *Physical Review D* 103.8 (Apr. 2021). arXiv:2101.05038 [gr-qc], p. 084045. ISSN: 2470-0010, 2470-0029. DOI: 10.1103/PhysRevD.103.084045. URL: http://arxiv.org/abs/2101.05038 (visited on 04/09/2025).

[85] Oscar Reula and Olivier Sarbach. “The Initial-Boundary Value Problem in General Relativity”. In: *International Journal of Modern Physics D* 20.05 (May 2011). arXiv:1009.0589 [gr-qc], pp. 767–783. ISSN: 0218-2718, 1793-6594. DOI: 10.1142/S0218271811019116. URL: http://arxiv.org/abs/1009.0589 (visited on 09/19/2024).

[86] Juliusz Doboszewski. “Relativistic spacetimes and definitions of determinism”. en. In: *European Journal for Philosophy of Science* 9.2 (Feb. 2019), p. 24. ISSN: 1879-4920. DOI: 10.1007/s13194-019-0248-6. URL: https://doi.org/10.1007/s13194-019-0248-6 (visited on 09/19/2024).

[87] Albert Einstein. “Relativity: The Special and General Theory”. en. In: *Albert Einstein* ().

[88] Bryan W. Roberts. *Notes on Holes*. URL: https://personal.lse.ac.uk/robert49/teaching/einstein/BWR-Holes.html (visited on 09/19/2024).

[89] Israel Quiros. *Selected topics in scalar-tensor theories and beyond*. arXiv:1901.08690. May 2019. URL: http://arxiv.org/abs/1901.08690 (visited on 10/17/2024).

[90] Valerio Faraoni, Edgard Gunzig, and Pasquale Nardone. *Conformal transformations in classical gravitational theories and in cosmology*. arXiv:gr-qc/9811047. Nov. 1998. URL: http://arxiv.org/abs/gr-qc/9811047 (visited on 10/17/2024).

[91] The ATLAS Collaboration. *Observation of a new particle in the search for the Standard Model Higgs boson with the ATLAS detector at the LHC*. arXiv:1207.7214. Aug. 2012. URL: http://arxiv.org/abs/1207.7214 (visited on 10/17/2024).

[92] Xavier Calmet, Iberê Kuntz, and Ian G. Moss. *Non-Minimal Coupling of the Higgs Boson to Curvature in an Inflationary Universe*. arXiv:1701.02140. Jan. 2017. URL: http://arxiv.org/abs/1701.02140 (visited on 10/17/2024).

[93] D. Kazanas. “Dynamics of the universe and spontaneous symmetry breaking”. In: *The Astrophysical Journal* 241 (Oct. 1980). Publisher: IOP ADS Bibcode: 1980ApJ...241L..59K, pp. L59–L63. ISSN: 0004-637X. DOI: 10.1086/183361. URL: https://ui.adsabs.harvard.edu/abs/1980ApJ...241L..59K (visited on 10/17/2024).

[94] Shinji Tsujikawa. *Introductory review of cosmic inflation*. arXiv:hep-ph/0304257. Apr. 2003. URL: http://arxiv.org/abs/hep-ph/0304257 (visited on 10/17/2024).

[95] Igor G. Irastorza. *An introduction to axions and their detection*. arXiv:2109.07376. Nov. 2021. DOI: 10.48550/arXiv.2109.07376. URL: http://arxiv.org/abs/2109.07376 (visited on 10/17/2024).

[96] Stephen Blundell and Katherine M. Blundell. *Concepts in thermal physics*. en. 2nd ed. Oxford: Oxford university press, 2010. ISBN: 978-0-19-956209-1.

[97] Daniel Naegels. *An introduction to Goldstone boson physics and to the coset construction*. arXiv:2110.14504. Oct. 2021. URL: http://arxiv.org/abs/2110.14504 (visited on 10/18/2024).

Appendix A

GBSSN system of equations

A.1 PDE system

The EFEs, when written in the GBSSN formalism, together with the Z4 quantities, give the following set of equations (check the variables in Sec. 3.3.3):

$$\partial_\perp \chi = \frac{2}{3}\alpha\chi(K+2\Theta) + \frac{1}{3}\chi\partial_\perp \ln\gamma, \tag{A.1}$$

$$\partial_\perp \gamma_{ab} = -2\alpha A_{ab} + \frac{1}{3}\gamma_{ab}\partial_\perp \ln\gamma \tag{A.2}$$

$$\begin{aligned}\partial_\perp A_{ab} = \Bigg[&\alpha\chi\left(R_{ab} + 2D_{(a}Z_{b)}\right) - \chi D_a D_b\alpha - D_{(a}\alpha D_{b)}\chi - \frac{\alpha D_a\chi D_b\chi}{4\chi} + \frac{1}{2}\alpha D_a D_b\chi \\ &+ 2Z_{(a}\alpha D_{b)}\chi + \frac{2\alpha D_{(a}\chi D_{b)}\Omega}{\Omega} + \frac{2\alpha\chi D_a D_b\Omega}{\Omega} + \frac{4\alpha\chi Z_{(a}D_{b)}\Omega}{\Omega} - 8\pi\alpha S_{ab}\Bigg]^{\mathrm{TF}},\end{aligned} \tag{A.3}$$

$$\begin{aligned}\partial_\perp K = &\alpha\left(A^{ab}A_{ab} + \frac{1}{3}(K+2\Theta)^2 + \frac{\kappa_1(1-\kappa_2)\Theta}{\Omega}\right) - \chi\Delta\alpha + \frac{1}{2}D^a\alpha D_a\chi + 2C_{Z_4c}Z^a D_a\alpha \\ &+ \frac{3[(\partial_\perp\Omega)^2 - \alpha^2\chi D^a\Omega D_a\Omega]}{\Omega^2\alpha} - \frac{2C_{Z_4c}\alpha Z_a D_a\Omega}{\Omega} + \frac{3\chi D^a\alpha D_a\Omega}{\Omega} - \frac{\alpha D^a\chi D_a\Omega}{2\Omega} \\ &+ \frac{\alpha\chi\Delta\Omega}{\Omega} + \frac{[K+4\Theta]\partial_\perp\Omega}{\Omega} + \frac{3\partial_\perp\alpha\partial_\perp\Omega}{\Omega\alpha^2} - \frac{3\partial_\perp\partial_\perp\Omega}{\Omega\alpha} + 4\pi\alpha(\rho+S),\end{aligned} \tag{A.4}$$

$$\begin{aligned}\partial_\perp \Lambda_a = &\frac{2Z^b\tilde{D}_b\beta^a}{\chi} + \alpha\left(2A^{bc}\Delta\Gamma^a_{bc} - \frac{2}{3}D^a(K+2\Theta) - \frac{3A^{ab}D_b\chi}{\chi} - \frac{4Z^a(K+2\Theta)}{3\chi} - \frac{2\kappa_1 Z^a}{\Omega\chi}\right) \\ &+ \gamma^{bc}\hat{D}_b\hat{D}_c\beta_a - \gamma^{bc}R[\hat{\gamma}]^a_{bcd}\beta^d - 2A^{ab}D_b\alpha - 2C_{Z_4c}\Theta D^a\alpha - \frac{4\alpha A^{ab}D_b\Omega}{\Omega} \\ &- \frac{2\alpha(2K+\Theta)D^a\Omega}{3\Omega} + \frac{2C_{Z4c}\alpha\Theta D^a\Omega}{\Omega} - \frac{4D^a\partial_\perp\Omega}{\Omega} + \frac{4D^a\alpha\partial_\perp\Omega}{\Omega\alpha} - \frac{4Z^a\partial_\perp\Omega}{\Omega\chi} \\ &- \frac{1}{6}D^a\partial_\perp\ln\gamma - \frac{1}{3}\Delta\Gamma^a\partial_\perp\ln\gamma - \frac{2Z^a\partial_\perp\ln\gamma}{3\chi} - \frac{16\pi J^a\alpha}{\chi}\end{aligned} \tag{A.5}$$

$$\begin{aligned}\partial_\perp\Theta = &\frac{\alpha}{2}\left[\chi(R[\gamma] + 2D^aZ_a) - A^{ab}A_{ab} + \frac{2}{3}(K+2\Theta)^2 - 2C_{Z_4c}\Theta(K+2\Theta) - \frac{2\kappa_1(2+\kappa_2)\Theta}{\Omega}\right] \\ &+ \alpha\Delta\chi - \frac{5\alpha D^a\chi D_a\chi}{4\chi} - C_{Z4c}Z^aD_a\alpha - \frac{C_{Z4c}\alpha Z_aD_a\chi}{2\chi} + \frac{2\alpha\chi\Delta\Omega}{\Omega} - \frac{\alpha D^a\chi D_a\Omega}{\Omega} \\ &\frac{3[(\partial_\perp\Omega)^2 - \alpha^2\chi D^a\Omega D_a\Omega]}{\Omega^2\alpha} + \frac{2K\partial_\perp\Omega}{\Omega} - 8\pi\alpha\rho,\end{aligned} \tag{A.6}$$

together with the constraints,

$$\mathcal{H} = \chi R[\gamma] - A_{ab}A^{ab} + \frac{2}{3}(K+2\Theta)^2 + 2\triangle\chi - \frac{5D^a\chi D_a\chi}{2\chi} + \frac{6[(\partial_\perp\Omega)^2 - \alpha^2\chi D^a\Omega D_a\Omega]}{\Omega^2\alpha^2} - \frac{2D^a\chi D_a\Omega}{\Omega} + \frac{4\chi\Delta\Omega}{\Omega} + \frac{4(K+2\Theta)\partial_\perp\Omega}{\Omega\alpha} - 16\pi\rho, \tag{A.7}$$

$$\mathcal{M}_a = D_bA^b_a - \frac{2}{3}D_a(K+2\Theta) - \frac{3A^b_aD_b\chi}{2\chi} - \frac{2A^b_aD_b\Omega}{\Omega} - \frac{2(K+2\Theta)D_a\Omega}{3\Omega} - \frac{2D_a\partial_\perp\Omega}{\Omega\alpha} + \frac{2D_a\alpha\partial_\perp\Omega}{\Omega\alpha^2} - 8\pi J_a, \tag{A.8}$$

$$Z_a = \frac{\gamma_{ab}}{2}\left(\Lambda^b - \Delta\Gamma^b\right), \tag{A.9}$$

where the third constraint comes from writing the Z4 quantity Z_a in terms of Λ^a and $\Delta\Gamma^a$. The equations we evolved in this work used the physical trace of extrinsic curvature, $\tilde{K}$, and the "physical" $\tilde{\Theta}$ variable, as is done in [10]. Regarding Maxwell's and Klein-Gordon equations, they become (written already as functions of the physical extrinsic curvature and the physical Θ):

$$\partial_tE_j = 4\pi\bar{j}_j\alpha + \frac{K_{CMC}E_j\alpha}{3\Omega} + \frac{\tilde{K}E_j\alpha}{3\Omega} + \frac{2C_{Z4}E_j\tilde{\Theta}\alpha}{3\Omega} + \beta^iD_iE_j - E_iD_j\beta^i - \frac{\alpha D_j\psi}{\Omega^2} - \frac{\alpha E_j\mathcal{L}_n\Omega}{\Omega} \tag{A.10}$$

$$\partial_t\psi = -4\pi\bar{q}_{\text{dens.}}\alpha + 4\pi k\alpha\Omega^2\psi - \alpha\Omega^2D_iE^i + \frac{3E^i\alpha\Omega^2D_i\chi}{2\chi} + \beta^iD_i\psi \tag{A.11}$$

$$\partial_tA_{3j} = E_j\alpha + \beta^iD_iA_{3j} - \Phi D_j\alpha + A_{3i}D_j\beta^i - \alpha D_j\Phi \tag{A.12}$$

$$\partial_t\Phi = \frac{K_{CMC}\alpha\Phi}{\Omega} + \frac{K\alpha\Phi}{\Omega} + \frac{2C_{Z4}\tilde{\Theta}\alpha\Phi}{\Omega} - \alpha D_kA_3{}^k - A_3{}^kD_k\alpha + \beta^kD_k\Phi + \frac{3A_3{}^k\alpha D_k\chi}{2\chi} - \frac{3\Phi\partial_\perp\Omega}{\Omega} \tag{A.13}$$

$$\partial_t\bar{c}_\phi = \bar{c}_\Pi \tag{A.14}$$

$$\partial_t\bar{d}_\phi = \bar{d}_\Pi \tag{A.15}$$

$$\begin{aligned}\partial_t\bar{c}_\Pi =& \frac{\bar{c}_\Pi\partial_t\alpha}{\alpha} - q\bar{d}_\phi\partial_t\Phi\alpha - q^2A_{3m}A_3{}^m\bar{c}_\phi\alpha^2 + \frac{K_{CMC}\bar{c}_\Pi\alpha}{\Omega} + \frac{\bar{c}_\Pi\tilde{K}\alpha}{\Omega} + \frac{2C_{Z4}\bar{c}_\Pi\tilde{\Theta}\alpha}{\Omega} - 2q\bar{d}_\Pi\alpha\Phi \\ &+ \frac{K_{CMC}q\bar{d}_\phi\alpha^2\Phi}{\Omega} + \frac{q\tilde{K}\bar{d}_\phi\alpha^2\Phi}{\Omega} + \frac{2qC_{Z4}\bar{d}_\phi\tilde{\Theta}\alpha^2\Phi}{\Omega} + q^2\bar{c}_\phi\alpha^2\Phi^2 + 2\beta^iD_i\bar{c}_\Pi + \partial_t\beta^iD_i\bar{c}_\phi \\ &- \frac{\partial_t\alpha\beta^iD_i\bar{c}_\phi}{\alpha} - \frac{K_{CMC}\alpha\beta^iD_i\bar{c}_\phi}{\Omega} - \frac{\tilde{K}\alpha\beta^iD_i\bar{c}_\phi}{\Omega} - \frac{2C_{Z4}\tilde{\Theta}\alpha\beta^iD_i\bar{c}_\phi}{\Omega} + 2q\alpha\beta^i\Phi D_i\bar{d}_\phi \\ &- \frac{\bar{c}_\Pi\beta^iD_i\alpha}{\alpha} - \frac{K_{CMC}\bar{c}_\phi\alpha\beta^iD_i\Omega}{\Omega^2} - \frac{\bar{c}_\phi\tilde{K}\alpha\beta^iD_i\Omega}{\Omega^2} - \frac{2C_{Z4}\bar{c}_\phi\tilde{\Theta}\alpha\beta^iD_i\Omega}{\Omega^2} + \frac{\bar{c}_\phi\partial_t\beta^iD_i\Omega}{\Omega} \\ &- \frac{\bar{c}_\phi\partial_t\alpha\beta^iD_i\Omega}{\alpha\Omega} + q\bar{d}_\phi\alpha\beta^iD_i\Phi + \frac{3qA_3{}^i\bar{d}_\phi\alpha^2D_i\chi}{2\chi} + \frac{\beta^i\beta^jD_i\alpha D_j\bar{c}_\phi}{\alpha} + \frac{\beta^i\beta^jD_i\Omega D_j\bar{c}_\phi}{\Omega} \\ &- \beta^jD_i\bar{c}_\phi D_j\beta^i - \frac{\bar{c}_\phi\beta^jD_i\Omega D_j\beta^i}{\Omega} - \frac{\beta^i\beta^jD_i\bar{c}_\phi D_j\Omega}{\Omega} + \frac{\bar{c}_\phi\beta^i\beta^jD_i\alpha D_j\Omega}{\alpha\Omega} + \frac{2\bar{c}_\phi\beta^i\beta^jD_i\Omega D_j\Omega}{\Omega^2} \\ &- \tfrac{3}{2}\gamma^{ij}\alpha^2D_i\bar{c}_\phi D_j\chi - \frac{3\bar{c}_\phi\gamma^{ij}\alpha^2D_i\Omega D_j\chi}{2\Omega} - \beta^i\beta^jD_jD_i\bar{c}_\phi - \frac{\bar{c}_\phi\beta^i\beta^jD_jD_i\Omega}{\Omega} - qA_3{}^k\bar{d}_\phi\alpha D_k\alpha \\ &+ \frac{4qA_3{}^k\bar{d}_\phi\alpha^2D_k\Omega}{\Omega} + \gamma^{lk}\alpha\chi D_k\alpha D_l\bar{c}_\phi - \frac{4\gamma^{kl}\alpha^2\chi D_k\bar{c}_\phi D_l\Omega}{\Omega} + \frac{\bar{c}_\phi\gamma^{lk}\alpha\chi D_k\alpha D_l\Omega}{\Omega} \\ &- \frac{4\bar{c}_\phi\gamma^{kl}\alpha^2\chi D_k\Omega D_l\Omega}{\Omega^2} - q\bar{d}_\phi\gamma^{mn}\alpha^2\chi D_mA_{3n} - 2qA_3{}^m\alpha^2D_m\bar{d}_\phi - \frac{4qA_3{}^m\bar{d}_\phi\alpha^2D_m\Omega}{\Omega} \\ &- \frac{qA_3{}^m\bar{d}_\phi\alpha^2D_m\chi}{2\chi} + \frac{2\gamma^{mn}\alpha^2\chi D_m\Omega D_n\bar{c}_\phi}{\Omega} + \tfrac{1}{2}\gamma^{mn}\alpha^2D_m\chi D_n\bar{c}_\phi + \frac{2\gamma^{mn}\alpha^2\chi D_m\bar{c}_\phi D_n\Omega}{\Omega}\end{aligned}$$

$$
\begin{aligned}
&+\frac{2\bar{c}_\phi \gamma^{mn}\alpha^2\chi D_m\Omega D_n\Omega}{\Omega^2}+\frac{\bar{c}_\phi\gamma^{mn}\alpha^2 D_m\chi D_n\Omega}{2\Omega}-\frac{qA_3{}^n\bar{d}_\phi\alpha^2 D_n\chi}{2\chi}+\tfrac{1}{2}\gamma^{mn}\alpha^2 D_m\bar{c}_\phi D_n\chi\\
&+\frac{\bar{c}_\phi\gamma^{mn}\alpha^2 D_m\Omega D_n\chi}{2\Omega}+\gamma^{mn}\alpha^2\chi D_nD_m\bar{c}_\phi+\frac{\bar{c}_\phi\gamma^{mn}\alpha^2\chi D_nD_m\Omega}{\Omega}-\frac{3\bar{c}_\Pi\partial_\perp\Omega}{\Omega}-\frac{3q\bar{d}_\phi\alpha\Phi\partial_\perp\Omega}{\Omega}\\
&+\frac{3\beta^i D_i\bar{c}_\phi\partial_\perp\Omega}{\Omega}+\frac{3\bar{c}_\phi\beta^i D_i\Omega\partial_\perp\Omega}{\Omega^2}
\end{aligned}
\tag{A.16}
$$

$$
\begin{aligned}
\partial_t\bar{d}_\Pi=&\frac{\bar{d}_\Pi\partial_t\alpha}{\alpha}+q\bar{c}_\phi\partial_t\Phi\alpha-q^2A_{3m}A_3{}^m\bar{d}_\phi\alpha^2+\frac{K_{CMC}\bar{d}_\Pi\alpha}{\Omega}+\frac{\tilde{K}\bar{d}_\Pi\alpha}{\Omega}+\frac{2C_{Z4}\bar{d}_\Pi\tilde{\Theta}\alpha}{\Omega}+2q\bar{c}_\Pi\alpha\Phi\\
&-\frac{K_{CMC}q\bar{c}_\phi\alpha^2\Phi}{\Omega}-\frac{q\bar{c}_\phi\tilde{K}\alpha^2\Phi}{\Omega}-\frac{2qC_{Z4}\bar{c}_\phi\tilde{\Theta}\alpha^2\Phi}{\Omega}+q^2\bar{d}_\phi\alpha^2\Phi^2-2q\alpha\beta^i\Phi D_i\bar{c}_\phi+2\beta^i D_i\bar{d}_\Pi\\
&+\partial_t\beta^i D_i\bar{d}_\phi-\frac{\partial_t\alpha\beta^i D_i\bar{d}_\phi}{\alpha}-\frac{K_{CMC}\alpha\beta^i D_i\bar{d}_\phi}{\Omega}-\frac{\tilde{K}\alpha\beta^i D_i\bar{d}_\phi}{\Omega}-\frac{2C_{Z4}\tilde{\Theta}\alpha\beta^i D_i\bar{d}_\phi}{\Omega}-\frac{\bar{d}_\Pi\beta^i D_i\alpha}{\alpha}\\
&-\frac{K_{CMC}\bar{d}_\phi\alpha\beta^i D_i\Omega}{\Omega^2}-\frac{\tilde{K}\bar{d}_\phi\alpha\beta^i D_i\Omega}{\Omega^2}-\frac{2C_{Z4}\bar{d}_\phi\tilde{\Theta}\alpha\beta^i D_i\Omega}{\Omega^2}+\frac{\bar{d}_\phi RHS\beta^i D_i\Omega}{\Omega}-\frac{\bar{d}_\phi\partial_t\alpha\beta^i D_i\Omega}{\alpha\Omega}\\
&-q\bar{c}_\phi\alpha\beta^i D_i\Phi-\frac{3qA_3{}^i\bar{c}_\phi\alpha^2 D_i\chi}{2\chi}+\frac{\beta^i\beta^j D_i\alpha D_j\bar{d}_\phi}{\alpha}+\frac{\beta^i\beta^j D_i\Omega D_j\bar{d}_\phi}{\Omega}-\beta^j D_i\bar{d}_\phi D_j\beta^i\\
&-\frac{\bar{d}_\phi\beta^j D_i\Omega D_j\beta^i}{\Omega}-\frac{\beta^i\beta^j D_i\bar{d}_\phi D_j\Omega}{\Omega}+\frac{\bar{d}_\phi\beta^i\beta^j D_i\alpha D_j\Omega}{\alpha\Omega}+\frac{2\bar{d}_\phi\beta^i\beta^j D_i\Omega D_j\Omega}{\Omega^2}-\tfrac{3}{2}\gamma^{ij}\alpha^2 D_i\bar{d}_\phi D_j\chi\\
&-\frac{3\bar{d}_\phi\gamma^{ij}\alpha^2 D_i\Omega D_j\chi}{2\Omega}-\beta^i\beta^j D_jD_i\bar{d}_\phi-\frac{\bar{d}_\phi\beta^i\beta^j D_jD_i\Omega}{\Omega}+qA_3{}^k\bar{c}_\phi\alpha D_k\alpha-\frac{4qA_3{}^k\bar{c}_\phi\alpha^2 D_k\Omega}{\Omega}\\
&+\gamma^{lk}\alpha\chi D_k\alpha D_l\bar{d}_\phi-\frac{4\gamma^{kl}\alpha^2\chi D_k\bar{d}_\phi D_l\Omega}{\Omega}+\frac{\bar{d}_\phi\gamma^{lk}\alpha\chi D_k\alpha D_l\Omega}{\Omega}-\frac{4\bar{d}_\phi\gamma^{kl}\alpha^2\chi D_k\Omega D_l\Omega}{\Omega^2}\\
&+q\bar{c}_\phi\gamma^{mn}\alpha^2\chi D_mA_{3n}+2qA_3{}^m\alpha^2 D_m\bar{c}_\phi+\frac{4qA_3{}^m\bar{c}_\phi\alpha^2 D_m\Omega}{\Omega}+\frac{qA_3{}^m\bar{c}_\phi\alpha^2 D_m\chi}{2\chi}+\frac{2\gamma^{mn}\alpha^2\chi D_m\Omega D_n\bar{d}_\phi}{\Omega}\\
&+\tfrac{1}{2}\gamma^{mn}\alpha^2 D_m\chi D_n\bar{d}_\phi+\frac{2\gamma^{mn}\alpha^2\chi D_m\bar{d}_\phi D_n\Omega}{\Omega}+\frac{2\bar{d}_\phi\gamma^{mn}\alpha^2\chi D_m\Omega D_n\Omega}{\Omega^2}+\frac{\bar{d}_\phi\gamma^{mn}\alpha^2 D_m\chi D_n\Omega}{2\Omega}\\
&+\frac{qA_3{}^n\bar{c}_\phi\alpha^2 D_n\chi}{2\chi}+\tfrac{1}{2}\gamma^{mn}\alpha^2 D_m\bar{d}_\phi D_n\chi+\frac{\bar{d}_\phi\gamma^{mn}\alpha^2 D_m\Omega D_n\chi}{2\Omega}+\gamma^{mn}\alpha^2\chi D_nD_m\bar{d}_\phi+\frac{\bar{d}_\phi\gamma^{mn}\alpha^2\chi D_nD_m\Omega}{\Omega}\\
&-\frac{3\bar{d}_\Pi\partial_\perp\Omega}{\Omega}+\frac{3q\bar{c}_\phi\alpha\Phi\partial_\perp\Omega}{\Omega}+\frac{3\beta^i D_i\bar{d}_\phi\partial_\perp\Omega}{\Omega}+\frac{3\bar{d}_\phi\beta^i D_i\Omega\partial_\perp\Omega}{\Omega^2}.
\end{aligned}
\tag{A.17}
$$

The Gauss constraint (3.49) becomes,

$$
\mathcal{G}=D_iE^i+\frac{3E^iD_i\chi}{2\chi}+4\pi\bar{q}_{\text{dens.}} \tag{A.18}
$$

A.2 Stress-energy Tensor

As we saw during the 3+1 decomposition of Einstein's equations, the way we incorporate the Maxwell and Scalar Field contributions is through the projections of the stress-energy tensor. Recapping, we have,

$$
\begin{aligned}
\bar{\rho}&=\bar{n}^a\bar{n}^b\bar{T}_{ab}\\
\bar{J}^a&=-\bar{B}^{ab}\bar{n}^c\bar{T}_{bc}\\
\bar{S}_{ab}&=\bar{B}^c_a\bar{B}^d_b\bar{T}_{cd}\\
\bar{S}&=\bar{\gamma}^{ab}\bar{S}_{ab}
\end{aligned}
$$

We recall that $\bar{T}_{ab}$ is just the stress-energy written as a function of the already conformally compactified variables, it is not a rescaled quantity. We will now display these projections separately for Maxwell and

Klein-Gordon parts, for better readability. Some cross terms will appear in the Klein-Gordon equations, due to the natural coupling arising from the charge. We will directly show them already in the GBSSN+Z4 formulation.

Scalar Field Part

$$
\begin{aligned}
\bar{\rho} = &\frac{\bar{c}_\Pi^2\Omega^2}{2\alpha^2} + \frac{q^2\bar{d}_\Pi^2\Omega^2}{2\alpha^2} + \tfrac{1}{2}q^2 A_{3i}A_3{}^i\bar{c}_\phi^2\Omega^6 + \tfrac{1}{2}q^4 A_{3i}A_3{}^i\bar{d}_\phi^2\Omega^6 - \frac{q^2\bar{c}_\phi\bar{d}_\Pi\Omega^4\Phi}{\alpha} + \frac{q^2\bar{c}_\Pi\bar{d}_\phi\Omega^4\Phi}{\alpha} \\
&+ \tfrac{1}{2}q^2\bar{c}_\phi^2\Omega^6\Phi^2 + \tfrac{1}{2}q^4\bar{d}_\phi^2\Omega^6\Phi^2 - \frac{\bar{c}_\Pi\beta^i\Omega^2 D_i\bar{c}_\phi}{\alpha^2} - q^2 A_3{}^i\bar{d}_\phi\Omega^4 D_i\bar{c}_\phi - \frac{q^2\bar{d}_\phi\beta^i\Omega^4\Phi D_i\bar{c}_\phi}{\alpha} \\
&- \frac{q^2\bar{d}_\Pi\beta^i\Omega^2 D_i\bar{d}_\phi}{\alpha^2} + q^2 A_3{}^i\bar{c}_\phi\Omega^4 D_i\bar{d}_\phi + \frac{q^2\bar{c}_\phi\beta^i\Omega^4\Phi D_i\bar{d}_\phi}{\alpha} - \frac{\bar{c}_\Pi\bar{c}_\phi\beta^i\Omega D_i\Omega}{\alpha^2} - \frac{q^2\bar{d}_\Pi\bar{d}_\phi\beta^i\Omega D_i\Omega}{\alpha^2} \\
&+ \frac{\beta^i\beta^j\Omega^2 D_i\bar{c}_\phi D_j\bar{c}_\phi}{2\alpha^2} + \tfrac{1}{2}\gamma^{ji}\Omega^2\chi D_i\bar{c}_\phi D_j\bar{c}_\phi + \frac{q^2\beta^i\beta^j\Omega^2 D_i\bar{d}_\phi D_j\bar{d}_\phi}{2\alpha^2} + \tfrac{1}{2}q^2\gamma^{ji}\Omega^2\chi D_i\bar{d}_\phi D_j\bar{d}_\phi \\
&+ \frac{\bar{c}_\phi\beta^i\beta^j\Omega D_i\bar{c}_\phi D_j\Omega}{\alpha^2} + \bar{c}_\phi\gamma^{ji}\Omega\chi D_i\bar{c}_\phi D_j\Omega + \frac{q^2\bar{d}_\phi\beta^i\beta^j\Omega D_i\bar{d}_\phi D_j\Omega}{\alpha^2} + q^2\bar{d}_\phi\gamma^{ji}\Omega\chi D_i\bar{d}_\phi D_j\Omega \\
&+ \frac{\bar{c}_\phi^2\beta^i\beta^j D_i\Omega D_j\Omega}{2\alpha^2} + \frac{q^2\bar{d}_\phi^2\beta^i\beta^j D_i\Omega D_j\Omega}{2\alpha^2} + \tfrac{1}{2}\bar{c}_\phi^2\gamma^{ji}\chi D_i\Omega D_j\Omega + \tfrac{1}{2}q^2\bar{d}_\phi^2\gamma^{ji}\chi D_i\Omega D_j\Omega
\end{aligned} \tag{A.19}
$$

$$
\begin{aligned}
\bar{J}^i = &-\frac{q^2 A_3{}^i\bar{c}_\phi\bar{d}_\Pi\Omega^4}{\alpha} + \frac{q^2 A_3{}^i\bar{c}_\Pi\bar{d}_\phi\Omega^4}{\alpha} + q^2 A_3{}^i\bar{c}_\phi^2\Omega^6\Phi + q^4 A_3{}^i\bar{d}_\phi^2\Omega^6\Phi - \frac{q^2 A_3{}^i\bar{d}_\phi\beta^j\Omega^4 D_j\bar{c}_\phi}{\alpha} \\
&- \frac{\bar{c}_\Pi\gamma^{ij}\Omega^2\chi D_j\bar{c}_\phi}{\alpha} - q^2\bar{d}_\phi\gamma^{ij}\Omega^4\Phi\chi D_j\bar{c}_\phi + \frac{q^2 A_3{}^i\bar{c}_\phi\beta^j\Omega^4 D_j\bar{d}_\phi}{\alpha} - \frac{q^2\bar{d}_\Pi\gamma^{ij}\Omega^2\chi D_j\bar{d}_\phi}{\alpha} \\
&+ q^2\bar{c}_\phi\gamma^{ij}\Omega^4\Phi\chi D_j\bar{d}_\phi - \frac{\bar{c}_\Pi\bar{c}_\phi\gamma^{ij}\Omega\chi D_j\Omega}{\alpha} - \frac{q^2\bar{d}_\Pi\bar{d}_\phi\gamma^{ij}\Omega\chi D_j\Omega}{\alpha} + \frac{\gamma^{ij}\beta^k\Omega^2\chi D_j\bar{c}_\phi D_k\bar{c}_\phi}{\alpha} \\
&+ \frac{\bar{c}_\phi\gamma^{ij}\beta^k\Omega\chi D_j\Omega D_k\bar{c}_\phi}{\alpha} + \frac{q^2\gamma^{ij}\beta^k\Omega^2\chi D_j\bar{d}_\phi D_k\bar{d}_\phi}{\alpha} + \frac{q^2\bar{d}_\phi\gamma^{ij}\beta^k\Omega\chi D_j\Omega D_k\bar{d}_\phi}{\alpha} + \frac{\bar{c}_\phi\gamma^{ij}\beta^k\Omega\chi D_j\bar{c}_\phi D_k\Omega}{\alpha} \\
&+ \frac{q^2\bar{d}_\phi\gamma^{ij}\beta^k\Omega\chi D_j\bar{d}_\phi D_k\Omega}{\alpha} + \frac{\bar{c}_\phi^2\gamma^{ij}\beta^k\chi D_j\Omega D_k\Omega}{\alpha} + \frac{q^2\bar{d}_\phi^2\gamma^{ij}\beta^k\chi D_j\Omega D_k\Omega}{\alpha}
\end{aligned} \tag{A.20}
$$

$$
\begin{aligned}
\bar{S}_{ij} = &q^2 A_{3i}A_{3j}\bar{c}_\phi^2\Omega^6 + q^4 A_{3i}A_{3j}\bar{d}_\phi^2\Omega^6 + \frac{\bar{c}_\Pi^2\gamma_{ij}\Omega^2}{2\alpha^2\chi} + \frac{q^2\bar{d}_\Pi^2\gamma_{ij}\Omega^2}{2\alpha^2\chi} - \frac{q^2 A_{3k}A_3{}^k\bar{c}_\phi^2\gamma_{ij}\Omega^6}{2\chi} - \frac{q^4 A_{3k}A_3{}^k\bar{d}_\phi^2\gamma_{ij}\Omega^6}{2\chi} \\
&- \frac{q^2\bar{c}_\phi\bar{d}_\Pi\gamma_{ij}\Omega^4\Phi}{\alpha\chi} + \frac{q^2\bar{c}_\Pi\bar{d}_\phi\gamma_{ij}\Omega^4\Phi}{\alpha\chi} + \frac{q^2\bar{c}_\phi^2\gamma_{ij}\Omega^6\Phi^2}{2\chi} + \frac{q^4\bar{d}_\phi^2\gamma_{ij}\Omega^6\Phi^2}{2\chi} - q^2 A_{3j}\bar{d}_\phi\Omega^4 D_i\bar{c}_\phi \\
&+ q^2 A_{3j}\bar{c}_\phi\Omega^4 D_i\bar{d}_\phi - q^2 A_{3i}\bar{d}_\phi\Omega^4 D_j\bar{c}_\phi + \Omega^2 D_i\bar{c}_\phi D_j\bar{c}_\phi + \bar{c}_\phi\Omega D_i\Omega D_j\bar{c}_\phi + q^2 A_{3i}\bar{c}_\phi\Omega^4 D_j\bar{d}_\phi \\
&+ q^2\Omega^2 D_i\bar{d}_\phi D_j\bar{d}_\phi + q^2\bar{d}_\phi\Omega D_i\Omega D_j\bar{d}_\phi + \bar{c}_\phi\Omega D_i\bar{c}_\phi D_j\Omega + q^2\bar{d}_\phi\Omega D_i\bar{d}_\phi D_j\Omega + \bar{c}_\phi^2 D_i\Omega D_j\Omega \\
&+ q^2\bar{d}_\phi^2 D_i\Omega D_j\Omega - \frac{\bar{c}_\Pi\gamma_{ij}\beta^k\Omega^2 D_k\bar{c}_\phi}{\alpha^2\chi} + \frac{q^2 A_3{}^k\bar{d}_\phi\gamma_{ij}\Omega^4 D_k\bar{c}_\phi}{\chi} - \frac{q^2\bar{d}_\phi\gamma_{ij}\beta^k\Omega^4\Phi D_k\bar{c}_\phi}{\alpha\chi} \\
&- \frac{q^2\bar{d}_\Pi\gamma_{ij}\beta^k\Omega^2 D_k\bar{d}_\phi}{\alpha^2\chi} - \frac{q^2 A_3{}^k\bar{c}_\phi\gamma_{ij}\Omega^4 D_k\bar{d}_\phi}{\chi} + \frac{q^2\bar{c}_\phi\gamma_{ij}\beta^k\Omega^4\Phi D_k\bar{d}_\phi}{\alpha\chi} - \frac{\bar{c}_\Pi\bar{c}_\phi\gamma_{ij}\beta^k\Omega D_k\Omega}{\alpha^2\chi} \\
&- \frac{q^2\bar{d}_\Pi\bar{d}_\phi\gamma_{ij}\beta^k\Omega D_k\Omega}{\alpha^2\chi} - \tfrac{1}{2}\gamma_{ij}\gamma^{kl}\Omega^2 D_k\bar{c}_\phi D_l\bar{c}_\phi + \frac{\gamma_{ij}\beta^k\beta^l\Omega^2 D_k\bar{c}_\phi D_l\bar{c}_\phi}{2\alpha^2\chi} - \tfrac{1}{2}q^2\gamma_{ij}\gamma^{kl}\Omega^2 D_k\bar{d}_\phi D_l\bar{d}_\phi \\
&+ \frac{q^2\gamma_{ij}\beta^k\beta^l\Omega^2 D_k\bar{d}_\phi D_l\bar{d}_\phi}{2\alpha^2\chi} - \bar{c}_\phi\gamma_{ij}\gamma^{kl}\Omega D_k\bar{c}_\phi D_l\Omega + \frac{\bar{c}_\phi\gamma_{ij}\beta^k\beta^l\Omega D_k\bar{c}_\phi D_l\Omega}{\alpha^2\chi} - q^2\bar{d}_\phi\gamma_{ij}\gamma^{kl}\Omega D_k\bar{d}_\phi D_l\Omega \\
&+ \frac{q^2\bar{d}_\phi\gamma_{ij}\beta^k\beta^l\Omega D_k\bar{d}_\phi D_l\Omega}{\alpha^2\chi} - \tfrac{1}{2}\bar{c}_\phi^2\gamma_{ij}\gamma^{kl}D_k\Omega D_l\Omega - \tfrac{1}{2}q^2\bar{d}_\phi^2\gamma_{ij}\gamma^{kl}D_k\Omega D_l\Omega + \frac{\bar{c}_\phi^2\gamma_{ij}\beta^k\beta^l D_k\Omega D_l\Omega}{2\alpha^2\chi} \\
&+ \frac{q^2\bar{d}_\phi^2\gamma_{ij}\beta^k\beta^l D_k\Omega D_l\Omega}{2\alpha^2\chi}
\end{aligned} \tag{A.21}
$$

$$
\begin{aligned}
\bar{S} = & \frac{3\bar{c}_\Pi^2\Omega^2}{2\alpha^2} + \frac{3q^2\bar{d}_\Pi^2\Omega^2}{2\alpha^2} - \tfrac{1}{2}q^2 A_{3i}A_3{}^i\bar{c}_\phi^2\Omega^6 - \tfrac{1}{2}q^4 A_{3i}A_3{}^i\bar{d}_\phi^2\Omega^6 - \frac{3q^2\bar{c}_\phi\bar{d}_\Pi\Omega^4\Phi}{\alpha} + \frac{3q^2\bar{c}_\Pi\bar{d}_\phi\Omega^4\Phi}{\alpha} \\
& + \tfrac{3}{2}q^2\bar{c}_\phi^2\Omega^6\Phi^2 + \tfrac{3}{2}q^4\bar{d}_\phi^2\Omega^6\Phi^2 - \frac{3\bar{c}_\Pi\beta^i\Omega^2 D_i\bar{c}_\phi}{\alpha^2} + q^2 A_3{}^i\bar{d}_\phi\Omega^4 D_i\bar{c}_\phi - \frac{3q^2\bar{d}_\phi\beta^i\Omega^4\Phi D_i\bar{c}_\phi}{\alpha} \\
& - \frac{3q^2\bar{d}_\Pi\beta^i\Omega^2 D_i\bar{d}_\phi}{\alpha^2} - q^2 A_3{}^i\bar{c}_\phi\Omega^4 D_i\bar{d}_\phi + \frac{3q^2\bar{c}_\phi\beta^i\Omega^4\Phi D_i\bar{d}_\phi}{\alpha} - \frac{3\bar{c}_\Pi\bar{c}_\phi\beta^i\Omega D_i\Omega}{\alpha^2} - \frac{3q^2\bar{d}_\Pi\bar{d}_\phi\beta^i\Omega D_i\Omega}{\alpha^2} \\
& - \tfrac{3}{2}\Omega^2\chi D_i\bar{c}_\phi D^i\bar{c}_\phi - 3\bar{c}_\phi\Omega\chi D_i\Omega D^i\bar{c}_\phi - \tfrac{3}{2}q^2\Omega^2\chi D_i\bar{d}_\phi D^i\bar{d}_\phi - 3q^2\bar{d}_\phi\Omega\chi D_i\Omega D^i\bar{d}_\phi - \tfrac{3}{2}\bar{c}_\phi^2\chi D_i\Omega D^i\Omega \\
& - \tfrac{3}{2}q^2\bar{d}_\phi^2\chi D_i\Omega D^i\Omega + \frac{3\beta^i\beta^j\Omega^2 D_i\bar{c}_\phi D_j\bar{c}_\phi}{2\alpha^2} + \gamma^{ij}\Omega^2\chi D_i\bar{c}_\phi D_j\bar{c}_\phi + \bar{c}_\phi\gamma^{ij}\Omega\chi D_i\Omega D_j\bar{c}_\phi + \frac{3q^2\beta^i\beta^j\Omega^2 D_i\bar{d}_\phi D_j\bar{d}_\phi}{2\alpha^2} \\
& + q^2\gamma^{ij}\Omega^2\chi D_i\bar{d}_\phi D_j\bar{d}_\phi + q^2\bar{d}_\phi\gamma^{ij}\Omega\chi D_i\Omega D_j\bar{d}_\phi + \frac{3\bar{c}_\phi\beta^i\beta^j\Omega D_i\bar{c}_\phi D_j\Omega}{\alpha^2} + \bar{c}_\phi\gamma^{ij}\Omega\chi D_i\bar{c}_\phi D_j\Omega \\
& + \frac{3q^2\bar{d}_\phi\beta^i\beta^j\Omega D_i\bar{d}_\phi D_j\Omega}{\alpha^2} + q^2\bar{d}_\phi\gamma^{ij}\Omega\chi D_i\bar{d}_\phi D_j\Omega + \frac{3\bar{c}_\phi^2\beta^i\beta^j D_i\Omega D_j\Omega}{2\alpha^2} + \frac{3q^2\bar{d}_\phi^2\beta^i\beta^j D_i\Omega D_j\Omega}{2\alpha^2} \\
& + \bar{c}_\phi^2\gamma^{ij}\chi D_i\Omega D_j\Omega + q^2\bar{d}_\phi^2\gamma^{ij}\chi D_i\Omega D_j\Omega
\end{aligned} \tag{A.22}
$$

Maxwell Part

Maxwell's part has a difficulty and we leave the note for anyone who tries to attempt something similar to what is being done here. There are two ways to write Faraday's tensor, $F_{\mu\nu}$, one, which is the more standard way, is saying, $F_{\mu\nu} = \nabla_\mu A_\nu - \nabla_\nu A_\mu$. The other way is to write it as a function of the electric field, as we have already seen. When writing out the stress-energy tensor part related to electromagnetism, this latter definition simplifies more the expressions. This works out better also because we are looking at a spherical symmetric world and so we discard the more problematic term related to the magnetic field. We will work with the definition in terms of the electric field, but we leave the alternative derivation in Appendix B. We have tested it in the code and it is equivalent (as expected), but numerically the definition we will show now behaves better. This has been thoroughly discussed in [28] and the authors of the paper even advise against using the electric and magnetic potentials, given that they will make the whole system of equations only weakly hyperbolic. We, however, have to evolve these potentials because they enter directly into the scalar field. Hence, the best we can do is, at least, reduce the dependency on A_3 and Φ. Note that the stress-energy tensor, when using the definition in terms of the electric field becomes simply,

$$
(\bar{T}_{\mu\nu})_{\text{Max}} = \Omega^2\left(-\frac{E_\mu E_\nu}{4\pi} + \frac{E_\alpha E^\alpha\bar{g}_{\mu\nu}}{8\pi} + \frac{E_\alpha E^\alpha n_\mu n_\nu}{4\pi}\right). \tag{A.23}
$$

The projections then become,

$$
\bar{\rho} = \frac{E_i E^i\Omega^2}{8\pi} \tag{A.24}
$$

$$
\bar{J}^i = 0 \tag{A.25}
$$

$$
\bar{S}_{ij} = -\frac{E_i E_j\Omega^2}{4\pi} + \frac{E_k E^k\gamma_{ij}\Omega^2}{8\pi\chi} \tag{A.26}
$$

$$
\bar{S} = \frac{E_i E^i\Omega^2}{8\pi}. \tag{A.27}
$$

Note that $\bar{S} = \bar{\rho}$, which is according to the fact that the electromagnetic part of the stress-energy tensor is trace-free.

A.3 Alternative Formulation for the KG Secondary Variable

We leave here the alternative formulation of the scalar field, albeit it is equivalent to the one above: instead of defining $\bar{\Pi} = \partial_t \bar{\phi}$, we have the Lie derivative of $\bar{\phi}$, such as done in [30], together with the respective complex decomposition,

$$\bar{\Pi} = -\mathcal{L}_{\bar{n}}\bar{\phi} = -\frac{1}{\bar{\alpha}}\left[\partial_\perp \bar{\phi} - \mathcal{L}_\beta \bar{\phi}\right] \quad , \qquad \bar{\Pi} = \bar{c}_\Pi + i\bar{d}_\Pi \quad . \tag{A.28}$$

This makes $\bar{c}_\Pi$ the lie derivative along $\bar{n}_\mu$ of $\bar{c}_\phi$ and the same holds for $\bar{d}_\Pi$ and $\bar{d}_\phi$. Now writing (3.52) with the new definition for $\bar{c}_\Pi$ we get

$$\begin{aligned}
\partial_\perp \bar{c}_\Pi =& q^2 \bar{A}_3^a (\bar{A}_3)_a \bar{c}_\phi \bar{\alpha} + \bar{c}_\Pi \bar{K}\bar{\alpha} - \frac{2\bar{c}_\phi (\mathcal{L}_{\bar{n}}\Omega)^2 \bar{\alpha}}{\Omega^2} + \frac{\bar{c}_\phi \mathcal{L}_{\bar{n}}\mathcal{L}_{\bar{n}}\Omega\bar{\alpha}}{\Omega} \\
& - \frac{\bar{c}_\phi \bar{K}\mathcal{L}_{\bar{n}}\Omega\bar{\alpha}}{\Omega} - 2q\bar{d}_\Pi \bar{\alpha}\bar{\Phi} - q\bar{d}_\phi \bar{K}\bar{\alpha}\bar{\Phi} - q^2 \bar{c}_\phi \bar{\alpha}\bar{\Phi}^2 + q\bar{d}_\phi \bar{\alpha}\bar{D}_a (A_3)^a \\
& + 2qA_3^a \bar{\alpha}\bar{D}_a \bar{d}_\phi + qA_3^a \bar{d}_\phi \bar{D}_a \bar{\alpha} - \bar{\alpha}\bar{D}_a \bar{D}^a \bar{c}_\phi - \frac{\bar{c}_\phi \bar{\alpha}\bar{D}_a \bar{D}^a \Omega}{\Omega} \\
& - \bar{D}_a \bar{\alpha}(\bar{D}^a \bar{c}_\phi) - \frac{\bar{c}_\phi \bar{D}_a \bar{\alpha}\bar{D}^a \Omega}{\Omega} + \frac{2\bar{c}_\phi \bar{\alpha}\bar{D}_a \Omega \bar{D}^a \Omega}{\Omega^2} + q\bar{d}_\phi \bar{\alpha}\mathcal{L}_{\bar{n}}\bar{\Phi} + \mathcal{L}_\beta \bar{c}_\Pi
\end{aligned} \tag{A.29}$$

and $\bar{d}_\Pi$,

$$\begin{aligned}
\partial_\perp \bar{d}_\Pi =& q^2 \bar{A}_3^a (\bar{A}_3)_a \bar{d}_\phi \bar{\alpha} + \bar{d}_\Pi \bar{K}\bar{\alpha} - \frac{2\bar{d}_\phi (\mathcal{L}_{\bar{n}}\Omega)^2 \bar{\alpha}}{\Omega^2} + \frac{\bar{d}_\phi \mathcal{L}_{\bar{n}}\mathcal{L}_{\bar{n}}\Omega\bar{\alpha}}{\Omega} \\
& - \frac{\bar{d}_\phi \bar{K}\mathcal{L}_{\bar{n}}\Omega\bar{\alpha}}{\Omega} + 2q\bar{c}_\Pi \bar{\alpha}\bar{\Phi} + q\bar{c}_\phi \bar{K}\bar{\alpha}\bar{\Phi} - \bar{q}^2 \bar{d}_\phi \bar{\alpha}\bar{\Phi}^2 - q\bar{c}_\phi \bar{\alpha}\bar{D}_a (A_3)^a \\
& - 2qA_3^a \bar{\alpha}\bar{D}_a \bar{c}_\phi - qA_3^a \bar{c}_\phi \bar{D}_a \bar{\alpha} - \bar{\alpha}\bar{D}_a \bar{D}^a \bar{d}_\phi - \frac{\bar{d}_\phi \bar{\alpha}\bar{D}_a \bar{D}^a \Omega}{\Omega} \\
& - \bar{D}_a \bar{\alpha}(\bar{D}^a \bar{d}_\phi) - \frac{\bar{d}_\phi \bar{D}_a \bar{\alpha}\bar{D}^a \Omega}{\Omega} + \frac{2\bar{d}_\phi \bar{\alpha}\bar{D}_a \Omega \bar{D}^a \Omega}{\Omega^2} - q\bar{c}_\phi \bar{\alpha}\mathcal{L}_{\bar{n}}\bar{\Phi} + \mathcal{L}_\beta \bar{d}_\Pi
\end{aligned} \tag{A.30}$$

It is easily noticed that the expressions are much simpler than with the above definition, but we prefer to use the definition $\partial_t \bar{\phi} = \bar{\Pi}$ so that there is no transformation of $\bar{\alpha}$ missing. This is just a personal preference, it does not affect the overall behavior of the system. The rest of the equations would then follow from this, but we leave this aside and go on to the reduction to spherical symmetry.

A.4 Spherically Symmetric Form of the Equations

A.4.1 Field Equations (without Maxwell+KG)

Now that we have the basic definitions in terms of the coordinate system we will work with, we can go to the equations of motion. Looking back at (A.1)-(A.6), these become, (without any electromagnetic or

scalar field part yet)

$$\dot{\chi} = \beta^r \chi' + \frac{2}{3}\alpha\chi(K + 2\Theta) - \frac{\beta^r \gamma'_{rr}\chi}{3\gamma_{rr}} - \frac{2\beta^r \gamma'_{\theta\theta}\chi}{3\gamma_{\theta\theta}} - \frac{4\beta^r \chi}{3r} - 2\frac{(\beta^r)'\chi}{3}, \tag{A.31}$$

$$\dot{\gamma}_{rr} = \frac{2\beta^r \gamma'_{rr}}{3} - 2A_{rr}\alpha - \frac{2\gamma_{rr}\beta^r \gamma'_{\theta\theta}}{3\gamma_{\theta\theta}} + \frac{4\gamma_{rr}(\beta^r)'}{3r} - \frac{4\gamma_{rr}\beta^r}{3}, \tag{A.32}$$

$$\dot{\gamma}_{\theta\theta} = \frac{\beta^r \gamma'_{\theta\theta}}{3} + \frac{A_{rr}\gamma_{\theta\theta}\alpha}{\gamma_{rr}} - \frac{\gamma_{\theta\theta}\beta^r \gamma'_{rr}}{3\gamma_{rr}} + \frac{2\gamma_{\theta\theta}\beta^r}{3r} - \frac{2\gamma_{\theta\theta}(\beta^r)'}{3}, \tag{A.33}$$

$$\begin{aligned}
\dot{A}_{rr} = {} & \beta^r A'_{rr} + \frac{2}{3}\gamma_{rr}\alpha\chi(\Lambda^r)' - \frac{\alpha\gamma''_{rr}\chi}{3\gamma_{\theta\theta}} + \frac{\alpha\gamma''_{\theta\theta}\chi}{3\gamma_{\theta\theta}} - \frac{2\alpha''\chi}{3} + \frac{\alpha\chi''}{3} + \alpha A_{rr}[K + 2(1 - CZ_{4c})\Theta] \\
& - \frac{2\alpha A_{rr}^2}{\gamma_{rr}} + \frac{4(\beta^r)' A_{rr}}{3} - \frac{4\beta^r A_{rr}}{3r} - \frac{\beta^r \gamma'_{rr} A_{rr}}{3\gamma_{\theta\theta}} - \frac{2\beta^r \gamma'_{\theta\theta} A_{rr}}{3\gamma_{\theta\theta}} + \frac{\alpha\chi(\gamma'_{rr})^2}{2\gamma_{rr}^2} - \frac{2\alpha\chi(\gamma'_{\theta\theta})^2}{3\gamma_{\theta\theta}^2 r} \\
& - \frac{\alpha(\chi')^2}{6\chi} + \frac{2\gamma_{rr}\alpha\chi}{\gamma_{\theta\theta}r^2} - \frac{2\alpha\chi}{r^2} - \frac{2\alpha\Lambda^r\chi\gamma_{rr}}{3r} + \frac{\alpha\Lambda^r\chi\gamma'_{rr}}{3} - \frac{\alpha\Lambda^r\chi\gamma_{rr}\gamma'_{\theta\theta}}{3\gamma_{\theta\theta}} + \frac{2\alpha\chi\gamma_{rr}\gamma_{\theta\theta}}{3\gamma_{\theta\theta}^2} \\
& - \frac{2\alpha\gamma'_{rr}\chi}{3\gamma_{\theta\theta}r} - \frac{4\alpha\gamma'_{\theta\theta}\chi}{3\gamma_{\theta\theta}r} + \frac{2\alpha'\chi}{3r} + \frac{\chi\gamma'_{rr}\alpha'}{3\gamma_{rr}} + \frac{\chi\gamma'_{\theta\theta}\alpha'}{3\gamma_{\theta\theta}} - \frac{\alpha\chi'}{3r} - \frac{\alpha\gamma'_{rr}\chi'}{6\gamma_{rr}} - \frac{\alpha\gamma'_{\theta\theta}\chi'}{6\gamma_{\theta\theta}} - \frac{2\alpha'\chi'}{3} \\
& + \frac{4}{3}Z_r\alpha\chi' - \frac{2\alpha\chi\gamma'_{rr}\Omega'}{3\gamma_{rr}\Omega} - \frac{2\alpha\chi\gamma'_{\theta\theta}\Omega'}{3\gamma_{\theta\theta}\Omega} + \frac{4\alpha\chi'\Omega'}{3\Omega} - \frac{4\alpha\chi\Omega'}{3r\Omega} - \frac{2A_{rr}\beta^r\Omega'}{\Omega} + \frac{4\alpha\chi\Omega''}{3\Omega} \\
& + \frac{8Z_r\alpha\chi\Omega'}{3\Omega}
\end{aligned} \tag{A.34}$$

$$\begin{aligned}
\dot{K} = {} & \beta^r K' - \frac{\chi\alpha''}{\gamma_{rr}} + \frac{\alpha}{3}(K + 2\Theta)^2 + \frac{3\alpha A_{rr}^2}{2\gamma_{rr}^2} - \frac{2\chi\alpha'}{\gamma_{rr}r} + \frac{\chi\gamma'_{rr}\alpha'}{2\gamma_{rr}^2} - \frac{\chi\gamma'_{\theta\theta}\alpha'}{\gamma_{rr}\gamma_{\theta\theta}} + \frac{\alpha'\chi'}{2\gamma_{rr}} - \frac{3\beta^r\dot{\alpha}\Omega'}{\alpha^2\Omega} \\
& + \frac{3\dot{\beta}^r\Omega'}{\alpha\Omega} + \frac{\kappa_1(1-\kappa_2)\alpha\Theta}{\Omega} - \frac{2CZ_{4c}Z_r\alpha'\chi}{\gamma_{rr}} - \frac{\alpha\chi\gamma'_{rr}\Omega'}{2\gamma_{rr}^2\Omega} + \frac{\alpha\chi\gamma_{\theta\theta}\Omega'}{\gamma_{rr}\gamma_{\theta\theta}\Omega} + \frac{3\chi\alpha'\Omega'}{\gamma_{rr}\Omega} - \frac{\alpha\chi'\Omega'}{2\gamma_{rr}\Omega} \\
& + \frac{2\alpha\chi\Omega' r}{\gamma_{rr}r} + \frac{\alpha\chi\Omega''}{\gamma_{rr}\Omega} - \frac{2C_{Z4c}Z_r\alpha\chi\Omega'}{\gamma_{rr}\Omega} + \frac{3\alpha(\Omega')^2}{\Omega^2}\left(\frac{(\beta^r)^2}{\alpha^2} - \frac{\chi}{\gamma_{rr}}\right) + \frac{3(\beta^r)^2\alpha'\Omega'}{\alpha^2\Omega} - \frac{3\beta^r(\beta^r)'\Omega'}{\alpha\Omega} \\
& - \frac{3(\beta^r)^2\Omega''}{\alpha\Omega} - \frac{(K + 4\Theta)\beta^r\Omega'}{\Omega}
\end{aligned} \tag{A.35}$$

$$\begin{aligned}
\dot{\Lambda}^r = {} & \beta^r(\Lambda^r)' - \frac{2\alpha(2K' + \Theta')}{3\gamma_{rr}} + \frac{\beta^r\gamma''_{rr}}{6\gamma_{rr}^2} + \frac{\beta^r\gamma''_{\theta\theta}}{3\gamma_{rr}\gamma_{\theta\theta}} + \frac{4(\beta^r)''}{3\gamma_{rr}r} + \frac{2A_{rr}\alpha}{\gamma_{rr}^2 r} - \frac{2A_{rr}\alpha}{\gamma_{rr}\gamma_{\theta\theta}r} - \frac{2A_{rr}\alpha'}{\gamma_{rr}^2} \\
& - \frac{3A_{rr}\alpha\chi'}{\gamma_{rr}^2\chi} + \frac{A_{rr}\alpha\gamma'_{rr}}{\gamma_{rr}^3} + \frac{A_{rr}\alpha\gamma'_{\theta\theta}}{\gamma_{rr}^2\gamma_{\theta\theta}} - \frac{\beta^r(\gamma'_{\theta\theta})^2}{\gamma_{rr}^2\gamma_{\theta\theta}^2} + \frac{2\beta^r\gamma'_{rr}}{3\gamma_{rr}\gamma_{\theta\theta}r} - \frac{8\beta^r\gamma'_{\theta\theta}}{3\gamma_{rr}\gamma_{\theta\theta}r} + \frac{4\beta^r\gamma'_{\theta\theta}}{3\gamma_{\theta\theta}^2 r} \\
& + \frac{2\gamma'_{\theta\theta}(\beta^r)'}{3\gamma_{rr}\gamma_{\theta\theta}} - \frac{10\beta^r}{3\gamma_{rr}r^2} + \frac{2\beta^r}{3\gamma_{\theta\theta}r^2} + \frac{4(\beta^r)'}{3\gamma_{rr}r} + \frac{4(\beta^r)'}{3\gamma_{\theta\theta}r} - \frac{4(K + 2\Theta)Z_r\alpha}{3\gamma_{rr}} + \frac{2Z_r\beta^r\gamma'_{rr}}{3\gamma_{rr}^2} \\
& + \frac{4Z_r\beta^r\gamma'_{\theta\theta}}{3\gamma_{rr}\gamma_{\theta\theta}} + \frac{8Z_r\beta^r}{3\gamma_{rr}r} + \frac{4Z_r(\beta^r)'}{3\gamma_{rr}} - \frac{2C_{Z4c}\Theta\alpha'}{\gamma_{rr}} - \frac{2\alpha(2K + \Theta)\Omega'}{3\gamma_{rr}\Omega} + \frac{2C_{Z4c}\alpha\Theta\Omega'}{\gamma_{rr}\Omega} \\
& - \frac{4A_{rr}\Omega'\alpha}{\gamma_{rr}^2\Omega} - \frac{4\beta^r\alpha'\Omega'}{\alpha\gamma_{rr}\Omega} + \frac{4(\beta^r)'\Omega'}{\gamma_{rr}\Omega} + \frac{4\beta^r\Omega''}{\gamma_{rr}\Omega} + \frac{4Z_r\beta^r\Omega'}{\gamma_{rr}\Omega} - \frac{2\kappa_1\alpha Z_r}{\gamma_{rr}\Omega}
\end{aligned} \tag{A.36}$$

$$\begin{aligned}
\dot{\Theta} = {} & \beta^r\Theta' + \frac{1}{2}\alpha\chi(\Lambda^r)' - \frac{\alpha\chi\gamma''_{rr}}{4\gamma_{rr}^2} - \frac{\alpha\chi\gamma''_{\theta\theta}}{2\gamma_{rr}\gamma_{\theta\theta}} + \frac{\alpha\chi'}{\gamma_{rr}} + \frac{\alpha}{3}(K + 2\Theta)^2 - CZ_{4c}\alpha\Theta(K + 2\Theta) \\
& - \frac{C_{Z4c}Z_r\alpha'\chi}{\gamma_{rr}} - \frac{C_{Z4c}Z_r\alpha\chi'}{2\gamma_{rr}} - \frac{\kappa_1(2+\kappa_2)\alpha\Theta}{\Omega} - \frac{3\alpha A_{rr}^2}{4\gamma_{rr}^2} + \frac{\alpha\Lambda^r\chi}{r} + \frac{3\alpha\chi(\gamma'_{rr})^2}{8\gamma_{rr}^3} \\
& + \frac{\alpha\chi(\gamma'_{\theta\theta})^2}{4\gamma_{rr}\gamma_{\theta\theta}} - \frac{5\alpha(\chi')^2}{4\gamma_{rr}\chi} - \frac{\alpha\chi\gamma'_{rr}}{2\gamma_{rr}\gamma_{\theta\theta}r} + \frac{\alpha\Lambda^r\chi\gamma'_{rr}}{4\gamma_{rr}} - \frac{\alpha\chi\gamma'_{\theta\theta}}{\gamma_{rr}\gamma_{\theta\theta}r} + \frac{\alpha\Lambda^r\chi\gamma'_{\theta\theta}}{2\gamma_{\theta\theta}} + \frac{2\alpha\chi'}{\gamma_{rr}r} \\
& - \frac{\alpha\gamma'_{rr}\chi'}{2\gamma_{rr}^2} + \frac{\alpha\gamma'_{\theta\theta}\chi'}{\gamma_{rr}\gamma_{\theta\theta}} - \frac{\alpha\chi\gamma'_{rr}\Omega'}{\gamma_{rr}^2\Omega} + \frac{2\alpha\chi\gamma'_{\theta\theta}\Omega'}{\gamma_{rr}\gamma_{\theta\theta}\Omega} - \frac{\alpha\chi'\Omega'}{\gamma_{rr}\Omega} + \frac{4\alpha\chi\Omega'}{\gamma_{rr}r\Omega} + \frac{2\alpha\chi\Omega''}{\gamma_{rr}\Omega} \\
& + \frac{3\alpha(\Omega')^2}{\Omega^2}\left(\frac{(\beta^r)^2}{\alpha^2} - \frac{\chi}{\gamma_{rr}}\right) - \frac{2K\beta^r\Omega'}{\Omega},
\end{aligned} \tag{A.37}$$

Where the variable K in these equations corresponds to the $\tilde{K}$ when used in the equations in the tensorial form. We have taken out the tilde here for better readibility. The same happens for Θ. The constraints also become,

$$\begin{aligned}\mathcal{H} = &-\frac{3A_r^2}{2\gamma_{rr}^2}+\frac{2(K+2\Theta)^2}{3}+\frac{\chi(\gamma'_{\theta\theta})^2}{2\gamma_{\theta\theta}^2}-\frac{5(\chi')^2}{2\chi\gamma_{rr}}-\frac{2\chi}{\gamma_{rr}r^2}+\frac{2\chi}{\gamma_{\theta\theta}r^2}+\frac{2\chi\gamma'_{rr}}{\gamma_{rr}^2 r}-\frac{6\chi\gamma'_{\theta\theta}}{\gamma_{rr}\gamma_{\theta\theta}r}\\&+\frac{\chi\gamma'_{rr}\gamma'_{\theta\theta}}{\gamma_{rr}^2}-\frac{\gamma'_{rr}\chi'}{\gamma_{rr}^2}+\frac{2\gamma'_{\theta\theta}\chi'}{\gamma_{rr}\gamma_{\theta\theta}}+\frac{4\chi'}{\gamma_{rr}r}-\frac{2\chi\gamma''_{\theta\theta}}{\gamma_{rr}\gamma_{\theta\theta}}+\frac{2\chi''}{\gamma_{rr}}-\frac{2\chi\gamma'_{rr}\Omega'}{\gamma_{rr}^2\Omega}+\frac{4\chi\gamma'_{\theta\theta}\Omega'}{\gamma_{rr}\gamma_{\theta\theta}\Omega}-\frac{2\chi'\Omega'}{\gamma_{rr}\Omega}\\&-\frac{6\chi(\Omega')^2}{\gamma_{rr}\Omega^2}+\frac{8\chi(\Omega')^2}{\gamma_{rr}r\Omega}+\frac{4\chi\Omega''}{\gamma_{rr}\Omega},\end{aligned}\tag{A.38}$$

$$\mathcal{M}_r = -\frac{\gamma'_{rr}A_{rr}}{\gamma_{rr}^2}+\frac{3\gamma'_{\theta\theta}A_{rr}}{2\gamma_{rr}\gamma_{\theta\theta}}-\frac{3\chi'A_{rr}}{2\chi\gamma_{rr}}+\frac{A'_{rr}}{\gamma_{rr}}-\frac{2}{3}(K'+2\Theta')-\frac{2A_{rr}\Omega'}{\gamma_{rr}\Omega}\tag{A.39}$$

$$Z_r = \frac{1}{2}\gamma_{rr}\Lambda^r+\frac{1}{r}-\frac{\gamma_{rr}}{\gamma_{\theta\theta}r}-\frac{\gamma'_{rr}}{4\gamma_{rr}}+\frac{\gamma'_{\theta\theta}}{2\gamma_{\theta\theta}}.\tag{A.40}$$

A.4.2 Field Equations (with Maxwell+KG)

In order to incorporate the Maxwell and Klein-Gordon part, we have to add the following terms to each of the equations and this will make the whole system complete:

$$\begin{aligned}(\dot{A}_{rr})_{\text{Max+KG}} = &-\tfrac{16}{3}\pi q^2(A_3)^2(\bar{c}_\phi)^2\alpha\chi(\Omega)^2-\tfrac{16}{3}\pi q^4(A_3)^2(\bar{d}_\phi)^2\alpha\chi(\Omega)^2+\tfrac{4}{3}(E)^2\alpha\chi(\Omega)^2\\&+\tfrac{32}{3}\pi q^2A_3\bar{d}_\phi\alpha\chi(\Omega)^2\bar{c}'_\phi-\tfrac{16}{3}\pi\alpha\chi(\Omega)^2(\bar{c}'_\phi)^2-\tfrac{32}{3}\pi q^2A_3\bar{c}_\phi\alpha\chi(\Omega)^2\bar{d}'_\phi-\tfrac{16}{3}\pi q^2\alpha\chi(\Omega)^2(\bar{d}'_\phi)^2\\&-\tfrac{32}{3}\pi\bar{c}_\phi\alpha\chi\Omega\bar{c}'_\phi\Omega'-\tfrac{32}{3}\pi q^2\bar{d}_\phi\alpha\chi\Omega\bar{d}'_\phi\Omega'-\tfrac{16}{3}\pi(\bar{c}_\phi)^2\alpha\chi(\Omega')^2-\tfrac{16}{3}\pi q^2(\bar{d}_\phi)^2\alpha\chi(\Omega')^2\end{aligned}\tag{A.41}$$

$$\begin{aligned}(\dot{K})_{\text{Max+KG}} = &\frac{8\pi(\bar{c}_\Pi)^2(\Omega)^3}{\alpha}+\frac{8\pi q^2(\bar{d}_\Pi)^2(\Omega)^3}{\alpha}-16\pi q^2\bar{c}_\phi\bar{d}_\Pi\Phi(\Omega)^3+16\pi q^2\bar{c}_\Pi\bar{d}_\phi\Phi(\Omega)^3\\&+8\pi q^2(\bar{c}_\phi)^2\alpha(\Phi)^2(\Omega)^3+8\pi q^4(\bar{d}_\phi)^2\alpha(\Phi)^2(\Omega)^3+\frac{(E)^2\alpha\chi(\Omega)^3}{\gamma_{rr}}-\frac{16\pi\bar{c}_\Pi\beta^r(\Omega)^3\bar{c}'_\phi}{\alpha}\\&-16\pi q^2\bar{d}_\phi\beta^r\Phi(\Omega)^3\bar{c}'_\phi+\frac{8\pi(\beta^r)^2(\Omega)^3(\bar{c}'_\phi)^2}{\alpha}-\frac{16\pi q^2\bar{d}_\Pi\beta^r(\Omega)^3\bar{d}'_\phi}{\alpha}+16\pi q^2\bar{c}_\phi\beta^r\Phi(\Omega)^3\bar{d}'_\phi\\&+\frac{8\pi q^2(\beta^r)^2(\Omega)^3(\bar{d}'_\phi)^2}{\alpha}-\frac{16\pi\bar{c}_\Pi\bar{c}_\phi\beta^r(\Omega)^2\Omega'}{\alpha}-\frac{16\pi q^2\bar{d}_\Pi\bar{d}_\phi\beta^r(\Omega)^2\Omega'}{\alpha}+\frac{16\pi\bar{c}_\phi(\beta^r)^2(\Omega)^2\bar{c}'_\phi\Omega'}{\alpha}\\&+\frac{16\pi q^2\bar{d}_\phi(\beta^r)^2(\Omega)^2\bar{d}'_\phi\Omega'}{\alpha}+\frac{8\pi(\bar{c}_\phi)^2(\beta^r)^2\Omega(\Omega')^2}{\alpha}+\frac{8\pi q^2(\bar{d}_\phi)^2(\beta^r)^2\Omega(\Omega')^2}{\alpha}\end{aligned}\tag{A.42}$$

$$\begin{aligned}(\dot{\Lambda}_r)_{\text{Max+KG}} = &\frac{16\pi q^2A_3\bar{c}_\phi\bar{d}_\Pi(\Omega)^4}{\gamma_{rr}}-\frac{16\pi q^2A_3\bar{c}_\Pi\bar{d}_\phi(\Omega)^4}{\gamma_{rr}}-\frac{16\pi q^2A_3(\bar{c}_\phi)^2\alpha\Phi(\Omega)^6}{\gamma_{rr}}-\frac{16\pi q^4A_3(\bar{d}_\phi)^2\alpha\Phi(\Omega)^6}{\gamma_{rr}}\\&+\frac{16\pi\bar{c}_\Pi(\Omega)^2\bar{c}'_\phi}{\gamma_{rr}}+\frac{16\pi q^2A_3\bar{d}_\phi\beta^r(\Omega)^4\bar{c}'_\phi}{\gamma_{rr}}+\frac{16\pi q^2\bar{d}_\phi\alpha\Phi(\Omega)^4\bar{c}'_\phi}{\gamma_{rr}}-\frac{16\pi\beta^r(\Omega)^2(\bar{c}'_\phi)^2}{\gamma_{rr}}\\&+\frac{16\pi q^2\bar{d}_\Pi(\Omega)^2\bar{d}'_\phi}{\gamma_{rr}}-\frac{16\pi q^2A_3\bar{c}_\phi\beta^r(\Omega)^4\bar{d}'_\phi}{\gamma_{rr}}-\frac{16\pi q^2\bar{c}_\phi\alpha\Phi(\Omega)^4\bar{d}'_\phi}{\gamma_{rr}}-\frac{16\pi q^2\beta^r(\Omega)^2(\bar{d}'_\phi)^2}{\gamma_{rr}}\\&+\frac{16\pi\bar{c}_\Pi\bar{c}_\phi\Omega\Omega'}{\gamma_{rr}}+\frac{16\pi q^2\bar{d}_\Pi\bar{d}_\phi\Omega\Omega'}{\gamma_{rr}}-\frac{32\pi\bar{c}_\phi\beta^r\Omega\bar{c}'_\phi\Omega'}{\gamma_{rr}}-\frac{32\pi q^2\bar{d}_\phi\beta^r\Omega\bar{d}'_\phi\Omega'}{\gamma_{rr}}\\&-\frac{16\pi(\bar{c}_\phi)^2\beta^r(\Omega')^2}{\gamma_{rr}}-\frac{16\pi q^2(\bar{d}_\phi)^2\beta^r(\Omega')^2}{\gamma_{rr}}\end{aligned}\tag{A.43}$$

$$
\begin{aligned}
(\dot{\Theta})_{\text{Max+KG}} = & -\frac{4\pi(\bar{c}_\Pi)^2(\Omega)^3}{\alpha} - \frac{4\pi q^2(\bar{d}_\Pi)^2(\Omega)^3}{\alpha} + 8\pi q^2\bar{c}_\phi\bar{d}_\Pi\Phi(\Omega)^3 - 8\pi q^2\bar{c}_\Pi\bar{d}_\phi\Phi(\Omega)^3 \\
& - 4\pi q^2(\bar{c}_\phi)^2\alpha(\Phi)^2(\Omega)^3 - 4\pi q^4(\bar{d}_\phi)^2\alpha(\Phi)^2(\Omega)^3 - \frac{4\pi q^2(A_3)^2(\bar{c}_\phi)^2\alpha\chi(\Omega)^3}{\gamma_{rr}} \\
& - \frac{4\pi q^4(A_3)^2(\bar{d}_\phi)^2\alpha\chi(\Omega)^3}{\gamma_{rr}} - \frac{(E)^2\alpha\chi(\Omega)^3}{\gamma_{rr}} + \frac{8\pi\bar{c}_\Pi\beta^r(\Omega)^3\bar{c}'_\phi}{\alpha} \\
& + 8\pi q^2\bar{d}_\phi\beta^r\Phi(\Omega)^3\bar{c}'_\phi + \frac{8\pi q^2A_3\bar{d}_\phi\alpha\chi(\Omega)^3\bar{c}'_\phi}{\gamma_{rr}} - \frac{4\pi(\beta^r)^2(\Omega)^3(\bar{c}'_\phi)^2}{\alpha} - \frac{4\pi\alpha\chi(\Omega)^3(\bar{c}'_\phi)^2}{\gamma_{rr}} \\
& + \frac{8\pi q^2\bar{d}_\Pi\beta^r(\Omega)^3\bar{d}'_\phi}{\alpha} - 8\pi q^2\bar{c}_\phi\beta^r\Phi(\Omega)^3\bar{d}'_\phi - \frac{8\pi q^2A_3\bar{c}_\phi\alpha\chi(\Omega)^3\bar{d}'_\phi}{\gamma_{rr}} - \frac{4\pi q^2(\beta^r)^2(\Omega)^3(\bar{d}'_\phi)^2}{\alpha} \\
& - \frac{4\pi q^2\alpha\chi(\Omega)^3(\bar{d}'_\phi)^2}{\gamma_{rr}} + \frac{8\pi\bar{c}_\Pi\bar{c}_\phi\beta^r(\Omega)^2\Omega'}{\alpha} + \frac{8\pi q^2\bar{d}_\Pi\bar{d}_\phi\beta^r(\Omega)^2\Omega'}{\alpha} - \frac{8\pi\bar{c}_\phi(\beta^r)^2(\Omega)^2\bar{c}'_\phi\Omega'}{\alpha} \\
& - \frac{8\pi\bar{c}_\phi\alpha\chi(\Omega)^2\bar{c}'_\phi\Omega'}{\gamma_{rr}} - \frac{8\pi q^2\bar{d}_\phi(\beta^r)^2(\Omega)^2\bar{d}'_\phi\Omega'}{\alpha} - \frac{8\pi q^2\bar{d}_\phi\alpha\chi(\Omega)^2\bar{d}'_\phi\Omega'}{\gamma_{rr}} \\
& - \frac{4\pi(\bar{c}_\phi)^2(\beta^r)^2\Omega(\Omega')^2}{\alpha} - \frac{4\pi q^2(\bar{d}_\phi)^2(\beta^r)^2\Omega(\Omega')^2}{\alpha} - \frac{4\pi(\bar{c}_\phi)^2\alpha\chi\Omega(\Omega')^2}{\gamma_{rr}} \\
& - \frac{4\pi q^2(\bar{d}_\phi)^2\alpha\chi\Omega(\Omega')^2}{\gamma_{rr}} .
\end{aligned}
\tag{A.44}
$$

In the case of the constraints, the extra terms that one must add are:

$$
\begin{aligned}
(\mathcal{H})_{\text{Max+KG}} = & -\frac{8\pi(\bar{c}_\Pi)^2(\Omega)^2}{(\alpha)^2} - \frac{8\pi q^2(\bar{d}_\Pi)^2(\Omega)^2}{(\alpha)^2} + \frac{16\pi q^2\bar{c}_\phi\bar{d}_\Pi\Phi(\Omega)^2}{\alpha} - \frac{16\pi q^2\bar{c}_\Pi\bar{d}_\phi\Phi(\Omega)^2}{\alpha} \\
& - 8\pi q^2(\bar{c}_\phi)^2(\Phi)^2(\Omega)^2 - 8\pi q^4(\bar{d}_\phi)^2(\Phi)^2(\Omega)^2 - \frac{8\pi q^2(A_3)^2(\bar{c}_\phi)^2\chi(\Omega)^2}{\gamma_{rr}} \\
& - \frac{8\pi q^4(A_3)^2(\bar{d}_\phi)^2\chi(\Omega)^2}{\gamma_{rr}} - \frac{2(E)^2\chi(\Omega)^2}{\gamma_{rr}} + \frac{16\pi\bar{c}_\Pi\beta^r(\Omega)^2\bar{c}'_\phi}{(\alpha)^2} + \frac{16\pi q^2\bar{d}_\phi\beta^r\Phi(\Omega)^2\bar{c}'_\phi}{\alpha} \\
& + \frac{16\pi q^2A_3\bar{d}_\phi\chi(\Omega)^2\bar{c}'_\phi}{\gamma_{rr}} - \frac{8\pi(\beta^r)^2(\Omega)^2(\bar{c}'_\phi)^2}{(\alpha)^2} - \frac{8\pi\chi(\Omega)^2(\bar{c}'_\phi)^2}{\gamma_{rr}} + \frac{16\pi q^2\bar{d}_\Pi\beta^r(\Omega)^2\bar{d}'_\phi}{(\alpha)^2} \\
& - \frac{16\pi q^2\bar{c}_\phi\beta^r\Phi(\Omega)^2\bar{d}'_\phi}{\alpha} - \frac{16\pi q^2A_3\bar{c}_\phi\chi(\Omega)^2\bar{d}'_\phi}{\gamma_{rr}} - \frac{8\pi q^2(\beta^r)^2(\Omega)^2(\bar{d}'_\phi)^2}{(\alpha)^2} - \frac{8\pi q^2\chi(\Omega)^2(\bar{d}'_\phi)^2}{\gamma_{rr}} \\
& + \frac{16\pi\bar{c}_\Pi\bar{c}_\phi\beta^r\Omega\Omega'}{(\alpha)^2} + \frac{16\pi q^2\bar{d}_\Pi\bar{d}_\phi\beta^r\Omega\Omega'}{(\alpha)^2} - \frac{16\pi\bar{c}_\phi(\beta^r)^2\Omega\bar{c}'_\phi\Omega'}{(\alpha)^2} - \frac{16\pi\bar{c}_\phi\chi\Omega\bar{c}'_\phi\Omega'}{\gamma_{rr}} \\
& - \frac{16\pi q^2\bar{d}_\phi(\beta^r)^2\Omega\bar{d}'_\phi\Omega'}{(\alpha)^2} - \frac{16\pi q^2\bar{d}_\phi\chi\Omega\bar{d}'_\phi\Omega'}{\gamma_{rr}} - \frac{8\pi(\bar{c}_\phi)^2(\beta^r)^2(\Omega')^2}{(\alpha)^2} - \frac{8\pi q^2(\bar{d}_\phi)^2(\beta^r)^2(\Omega')^2}{(\alpha)^2} \\
& - \frac{8\pi(\bar{c}_\phi)^2\chi(\Omega')^2}{\gamma_{rr}} - \frac{8\pi q^2(\bar{d}_\phi)^2\chi(\Omega')^2}{\gamma_{rr}}
\end{aligned}
\tag{A.45}
$$

$$
\begin{aligned}
(\mathcal{M}_r)_{\text{Max+KG}} = & \frac{8\pi q^2A_3\bar{c}_\phi\bar{d}_\Pi(\Omega)^4}{\alpha} - \frac{8\pi q^2A_3\bar{c}_\Pi\bar{d}_\phi(\Omega)^4}{\alpha} - 8\pi q^2A_3(\bar{c}_\phi)^2\Phi(\Omega)^6 - 8\pi q^4A_3(\bar{d}_\phi)^2\Phi(\Omega)^6 \\
& + \frac{8\pi\bar{c}_\Pi(\Omega)^2\bar{c}'_\phi}{\alpha} + \frac{8\pi q^2A_3\bar{d}_\phi\beta^r(\Omega)^4\bar{c}'_\phi}{\alpha} + 8\pi q^2\bar{d}_\phi\Phi(\Omega)^4\bar{c}'_\phi - \frac{8\pi\beta^r(\Omega)^2(\bar{c}'_\phi)^2}{\alpha} \\
& + \frac{8\pi q^2\bar{d}_\Pi(\Omega)^2\bar{d}'_\phi}{\alpha} - \frac{8\pi q^2A_3\bar{c}_\phi\beta^r(\Omega)^4\bar{d}'_\phi}{\alpha} - 8\pi q^2\bar{c}_\phi\Phi(\Omega)^4\bar{d}'_\phi - \frac{8\pi q^2\beta^r(\Omega)^2(\bar{d}'_\phi)^2}{\alpha}
\end{aligned}
$$

$$+\frac{8\pi\bar{c}_\Pi\bar{c}_\phi\Omega\Omega'}{\alpha}+\frac{8\pi q^2\bar{d}_\Pi\bar{d}_\phi\Omega\Omega'}{\alpha}-\frac{16\pi\bar{c}_\phi\beta^r\Omega\bar{c}'_\phi\Omega'}{\alpha}-\frac{16\pi q^2\bar{d}_\phi\beta^r\Omega\bar{d}'_\phi\Omega'}{\alpha}-\frac{8\pi\left(\bar{c}_\phi\right)^2\beta^r\left(\Omega'\right)^2}{\alpha}$$
$$-\frac{8\pi q^2\left(\bar{d}_\phi\right)^2\beta^r\left(\Omega'\right)^2}{\alpha}. \tag{A.46}$$

The reader probably has already taken note of this, but notice that the momentum constraint and the Λ_r equations have no factors that come directly from electromagnetism only. This has to do with the fact that both depend on the $\bar{J}^i$ projection of the stress-energy tensor which in spherical symmetry vanishes completely. Only the terms that are coupled to the scalar field survive.

A.4.3 GBSSN Maxwell and Scalar Field in Spherical Symmetry

The equations (A.11)-(A.17) now become,

$$\dot{E}=-\frac{2A_{rr}E\alpha}{\gamma_{rr}}+4\pi\bar{j}_r\alpha+\frac{K_{\text{CMC}}E\alpha}{3\Omega}+\frac{KE\alpha}{3\Omega}+\frac{2C_{Z4}E\Theta\alpha}{3\Omega}+\beta^rE'+E\beta'-\frac{\alpha\psi'}{\left(\Omega\right)^2}+\frac{E\beta^r\Omega'}{\Omega} \tag{A.47}$$

$$\dot{\psi}=-4\pi q_{\text{dens.}}\alpha-\frac{2E\alpha\chi\left(\Omega\right)^2}{\gamma_{rr}r}+4\pi k\alpha\psi(r)\left(\Omega\right)^2-\frac{\alpha\chi\left(\Omega\right)^2E'}{\gamma_{rr}}+\frac{E\alpha\chi\left(\Omega\right)^2\gamma'_{rr}}{\left(\gamma_{rr}\right)^2}+\frac{E\alpha\left(\Omega\right)^2\chi'}{2\gamma_{rr}}+\beta^r\psi' \tag{A.48}$$

$$\dot{A}_3=-E\alpha+\beta^rA'_3-\Phi\alpha'+A_3\beta'-\alpha\Phi' \tag{A.49}$$

$$\dot{\Phi}=-\frac{2A_3\alpha\chi}{\gamma_{rr}r}+\frac{K_{\text{CMC}}\alpha\Phi}{\Omega}+\frac{K\alpha\Phi}{\Omega}+\frac{2C_{Z4}\Theta\alpha\Phi}{\Omega}-\frac{\alpha\chi A'_3}{\gamma_{rr}}+\frac{A_3\alpha\chi\gamma'_{rr}}{\left(\gamma_{rr}\right)^2}-\frac{A_3\chi\alpha'}{\gamma_{rr}}+\beta^r\Phi'$$
$$+\frac{A_3\alpha\chi'}{2\gamma_{rr}}+\frac{\beta^r\Phi\Omega'}{\Omega}+\frac{2A_3\alpha\chi\Omega'}{\gamma_{rr}\Omega} \tag{A.50}$$

$$\dot{\bar{c}}_\phi=\bar{c}_\Pi \tag{A.51}$$

$$\dot{\bar{d}}_\phi=\bar{d}_\Pi \tag{A.52}$$

$$\dot{\bar{c}}_\Pi=\frac{\bar{c}_\Pi\partial_t\alpha}{\alpha}-q\bar{d}_\phi\partial_t\Phi\alpha-2q\bar{d}_\Pi\alpha\Phi+q^2\bar{c}_\phi\left(\alpha\right)^2\left(\Phi\right)^2-\frac{q^2\left(A_3\right)^2\bar{c}_\phi\left(\alpha\right)^2\chi}{\gamma_{rr}}-\frac{2qA_3\bar{d}_\phi\left(\alpha\right)^2\chi}{\gamma_{rr}r}$$
$$+\frac{K_{\text{CMC}}\bar{c}_\Pi\alpha}{\Omega}+\frac{\bar{c}_\Pi K\alpha}{\Omega}+\frac{2C_{Z4}\bar{c}_\Pi\Theta\alpha}{\Omega}+\frac{K_{\text{CMC}}q\bar{d}_\phi\left(\alpha\right)^2\Phi}{\Omega}+\frac{qK\bar{d}_\phi\left(\alpha\right)^2\Phi}{\Omega}+\frac{2qC_{Z4}\bar{d}_\phi\Theta\left(\alpha\right)^2\Phi}{\Omega}$$
$$-\frac{q\bar{d}_\phi\left(\alpha\right)^2\chi A'_3}{\gamma_{rr}}+2\beta^r\frac{\partial\bar{c}_\Pi}{\partial r}+\partial_t\beta^r\bar{c}'_\phi-\frac{\partial_t\alpha\beta^r\bar{c}'_\phi}{\alpha}+\frac{2\left(\alpha\right)^2\chi\bar{c}'_\phi}{\gamma_{rr}r}-\frac{K_{\text{CMC}}\alpha\beta^r\bar{c}'_\phi}{\Omega}-\frac{K\alpha\beta^r\bar{c}'_\phi}{\Omega}$$
$$-\frac{2C_{Z4}\Theta\alpha\beta^r\bar{c}'_\phi}{\Omega}+2q\alpha\beta^r\Phi\bar{d}'_\phi-\frac{2qA_3\left(\alpha\right)^2\chi\bar{d}'_\phi}{\gamma_{rr}}+\frac{qA_3\bar{d}_\phi\left(\alpha\right)^2\chi\gamma'_{rr}}{\left(\gamma_{rr}\right)^2}-\frac{\left(\alpha\right)^2\chi\bar{c}'_\phi\gamma'_{rr}}{\left(\gamma_{rr}\right)^2}-\frac{\bar{c}_\Pi\beta^r\alpha'}{\alpha}$$
$$-\frac{qA_3\bar{d}_\phi\alpha\chi\alpha'}{\gamma_{rr}}+\frac{\left(\beta^r\right)^2\bar{c}'_\phi\alpha'}{\alpha}+\frac{\alpha\chi\bar{c}'_\phi\alpha'}{\gamma_{rr}}-\beta^r\bar{c}'_\phi\beta'+q\bar{d}_\phi\alpha\beta^r\Phi'+\frac{qA_3\bar{d}_\phi\left(\alpha\right)^2\chi'}{2\gamma_{rr}}-\frac{\left(\alpha\right)^2\bar{c}'_\phi\chi'}{2\gamma_{rr}}$$
$$-\frac{K_{\text{CMC}}\bar{c}_\phi\alpha\beta^r\Omega'}{\left(\Omega\right)^2}-\frac{\bar{c}_\phi K\alpha\beta^r\Omega'}{\left(\Omega\right)^2}-\frac{2C_{Z4}\bar{c}_\phi\Theta\alpha\beta^r\Omega'}{\left(\Omega\right)^2}+\frac{\bar{c}_\phi\partial_t\beta^r\Omega'}{\Omega}+\frac{3\bar{c}_\Pi\beta^r\Omega'}{\Omega}-\frac{\bar{c}_\phi\partial_t\alpha\beta^r\Omega'}{\alpha\Omega}$$
$$+\frac{3q\bar{d}_\phi\alpha\beta^r\Phi\Omega'}{\Omega}+\frac{2\bar{c}_\phi\left(\alpha\right)^2\chi\Omega'}{\gamma_{rr}r\Omega}-\frac{3\left(\beta^r\right)^2\bar{c}'_\phi\Omega'}{\Omega}-\frac{\bar{c}_\phi\left(\alpha\right)^2\chi\gamma'_{rr}\Omega'}{\left(\gamma_{rr}\right)^2\Omega}+\frac{\bar{c}_\phi\left(\beta^r\right)^2\alpha'\Omega'}{\alpha\Omega}+\frac{\bar{c}_\phi\alpha\chi\alpha'\Omega'}{\gamma_{rr}\Omega}$$
$$-\frac{\bar{c}_\phi\beta^r\beta'\Omega'}{\Omega}-\frac{\bar{c}_\phi\left(\alpha\right)^2\chi'\Omega'}{2\gamma_{rr}\Omega}-\frac{\bar{c}_\phi\left(\beta^r\right)^2\left(\Omega'\right)^2}{\left(\Omega\right)^2}-\frac{2\bar{c}_\phi\left(\alpha\right)^2\chi\left(\Omega'\right)^2}{\gamma_{rr}\left(\Omega\right)^2}-\left(\beta^r\right)^2\frac{\partial^2\bar{c}_\phi}{\partial r^2}+\frac{\left(\alpha\right)^2\chi\bar{c}''_\phi}{\gamma_{rr}}$$
$$-\frac{\bar{c}_\phi\left(\beta^r\right)^2\Omega''}{\Omega}+\frac{\bar{c}_\phi\left(\alpha\right)^2\chi\Omega''}{\gamma_{rr}\Omega} \tag{A.53}$$

$$
\begin{aligned}
\dot{\bar{d}}_\Pi = & \frac{\bar{d}_\Pi \partial_t \alpha}{\alpha} + q\bar{c}_\phi \partial_t \Phi \alpha + 2q\bar{c}_\Pi \alpha \Phi + q^2 \bar{d}_\phi (\alpha)^2 (\Phi)^2 - \frac{q^2 (A_3)^2 \bar{d}_\phi (\alpha)^2 \chi}{\gamma_{rr}} + \frac{2qA_3 \bar{c}_\phi (\alpha)^2 \chi}{\gamma_{rr} r} \\
& + \frac{K_{\mathrm{CMC}} \bar{d}_\Pi \alpha}{\Omega} + \frac{K \bar{d}_\Pi \alpha}{\Omega} + \frac{2C_{Z4} \bar{d}_\Pi \Theta \alpha}{\Omega} - \frac{K_{\mathrm{CMC}} q \bar{c}_\phi (\alpha)^2 \Phi}{\Omega} - \frac{q\bar{c}_\phi K (\alpha)^2 \Phi}{\Omega} - \frac{2qC_{Z4} \bar{c}_\phi \Theta (\alpha)^2 \Phi}{\Omega} \\
& + \frac{q\bar{c}_\phi (\alpha)^2 \chi A_3'}{\gamma_{rr}} - 2q\alpha\beta^r \Phi \bar{c}_\phi' + \frac{2qA_3 (\alpha)^2 \chi \bar{c}_\phi'}{\gamma_{rr}} + 2\beta^r \frac{\partial \bar{d}_\Pi}{\partial r} + \partial_t \beta^r \bar{d}_\phi' - \frac{\partial_t \alpha \beta^r \bar{d}_\phi'}{\alpha} + \frac{2(\alpha)^2 \chi \bar{d}_\phi'}{\gamma_{rr} r} \\
& - \frac{K_{\mathrm{CMC}} \alpha \beta^r \bar{d}_\phi'}{\Omega} - \frac{K\alpha\beta^r \bar{d}_\phi'}{\Omega} - \frac{2C_{Z4} \Theta \alpha \beta^r \bar{d}_\phi'}{\Omega} - \frac{qA_3 \bar{c}_\phi (\alpha)^2 \chi \gamma_{rr}'}{(\gamma_{rr})^2} - \frac{(\alpha)^2 \chi \bar{d}_\phi' \gamma_{rr}'}{(\gamma_{rr})^2} - \frac{\bar{d}_\Pi \beta^r \alpha'}{\alpha} \\
& + \frac{qA_3 \bar{c}_\phi \alpha \chi \alpha'}{\gamma_{rr}} + \frac{(\beta^r)^2 \bar{d}_\phi' \alpha'}{\alpha} + \frac{\alpha \chi \bar{d}_\phi' \alpha'}{\gamma_{rr}} - \beta^r \bar{d}_\phi' \beta' - q\bar{c}_\phi \alpha \beta^r \Phi' - \frac{qA_3 \bar{c}_\phi (\alpha)^2 \chi'}{2\gamma_{rr}} - \frac{(\alpha)^2 \bar{d}_\phi' \chi'}{2\gamma_{rr}} \\
& - \frac{K_{\mathrm{CMC}} \bar{d}_\phi \alpha \beta^r \Omega'}{(\Omega)^2} - \frac{K\bar{d}_\phi \alpha \beta^r \Omega'}{(\Omega)^2} - \frac{2C_{Z4} \bar{d}_\phi \Theta \alpha \beta^r \Omega'}{(\Omega)^2} + \frac{\bar{d}_\phi \partial_t \beta^r \Omega'}{\Omega} + \frac{3\bar{d}_\Pi \beta^r \Omega'}{\Omega} - \frac{\bar{d}_\phi \partial_t \alpha \beta^r \Omega'}{\alpha \Omega} \\
& - \frac{3q\bar{c}_\phi \alpha \beta^r \Phi \Omega'}{\Omega} + \frac{2\bar{d}_\phi (\alpha)^2 \chi \Omega'}{\gamma_{rr} r \Omega} - \frac{3(\beta^r)^2 \bar{d}_\phi' \Omega'}{\Omega} - \frac{\bar{d}_\phi (\alpha)^2 \chi \gamma_{rr}' \Omega'}{(\gamma_{rr})^2 \Omega} + \frac{\bar{d}_\phi (\beta^r)^2 \alpha' \Omega'}{\alpha \Omega} + \frac{\bar{d}_\phi \alpha \chi \alpha' \Omega'}{\gamma_{rr} \Omega} \\
& - \frac{\bar{d}_\phi \beta^r \beta' \Omega'}{\Omega} - \frac{\bar{d}_\phi (\alpha)^2 \chi' \Omega'}{2\gamma_{rr} \Omega} - \frac{\bar{d}_\phi (\beta^r)^2 (\Omega')^2}{(\Omega)^2} - \frac{2\bar{d}_\phi (\alpha)^2 \chi (\Omega')^2}{\gamma_{rr} (\Omega)^2} - (\beta^r)^2 \frac{\partial^2 \bar{d}_\phi}{\partial r^2} + \frac{(\alpha)^2 \chi \bar{d}_\phi''}{\gamma_{rr}} \\
& - \frac{\bar{d}_\phi (\beta^r)^2 \Omega''}{\Omega} + \frac{\bar{d}_\phi (\alpha)^2 \chi \Omega''}{\gamma_{rr} \Omega},
\end{aligned}
\tag{A.54}
$$

and the physical charge and current densities take the form,

$$
\begin{aligned}
\tilde{q}_{\mathrm{dens.}} = & \frac{q\bar{c}_\phi \bar{d}_\Pi (\Omega)^2}{\alpha} - \frac{q\bar{c}_\Pi \bar{d}_\phi (\Omega)^2}{\alpha} - q^2 (\bar{c}_\phi)^2 \Phi (\Omega)^2 - q^2 (\bar{d}_\phi)^2 \Phi (\Omega)^2 \\
& + \frac{q\bar{d}_\phi \beta^r (\Omega)^2 \bar{c}_\phi'}{\alpha} - \frac{q\bar{c}_\phi \beta^r (\Omega)^2 \bar{d}_\phi'}{\alpha}
\end{aligned}
\tag{A.55}
$$

$$
\tilde{j}_r = -q^2 A_3 (\bar{c}_\phi)^2 (\Omega)^2 - q^2 A_3 (\bar{d}_\phi)^2 (\Omega)^2 + q\bar{d}_\phi (\Omega)^2 \bar{c}_\phi' - q\bar{c}_\phi (\Omega)^2 \bar{d}_\phi'. \tag{A.56}
$$

We again recall that to get the compactified currents, one only has to divide by Ω^2. Finally, the Gauss constraint (A.18) becomes,

$$
\mathcal{P} = \frac{2E\chi}{\gamma_{rr} r} + \frac{\chi E'}{\gamma_{rr}} - \frac{E\chi \gamma_{rr}'}{(\gamma_{rr})^2} - \frac{E\chi'}{2\gamma_{rr}} + 4\pi \bar{q}_{\mathrm{dens.}} \tag{A.57}
$$

Appendix B

Alternative Formulation of Electromagnetic part of the Stress Energy Tensor

If we are to write the Faraday tensor as a function of the four-potential, A_μ, we get that the projections become,

$$\begin{aligned}\bar{\rho} = &\frac{E_i E^i \Omega^6}{8\pi} + \frac{E^i \Omega^5 \Phi D_i \Omega}{2\pi} - \frac{\gamma^{ki}\Omega^6 \chi D_i A_3{}^j D_j A_{3k}}{8\pi} - \frac{A_3{}^k \gamma^{ji}\Omega^6 D_i \chi D_j A_{3k}}{16\pi} - \frac{A_3{}^i E_i \beta^j \Omega^5 D_j \Omega}{2\pi\alpha} \\ &- \frac{A_3{}^i \Omega^5 D_i A_3{}^j D_j \Omega}{2\pi} - \frac{A_3{}^i A_3{}^j \Omega^4 D_i \Omega D_j \Omega}{2\pi} - \frac{A_3{}^i \beta^j \Omega^4 \Phi D_i \Omega D_j \Omega}{\pi\alpha} + \frac{\gamma^{ji}\Omega^4 \Phi^2 \chi D_i \Omega D_j \Omega}{2\pi} \\ &+ \frac{A_3{}^i A_3{}^j \Omega^5 D_i \chi D_j \Omega}{2\pi\chi} + \frac{\gamma^{ki}\Omega^6 \chi D_i A_3{}^j D_k A_{3j}}{8\pi} + \frac{A_3{}^j \gamma^{ki}\Omega^5 \chi D_i A_{3j} D_k \Omega}{2\pi} + \frac{A_{3j} A_3{}^j \gamma^{ki}\Omega^4 \chi D_i \Omega D_k \Omega}{2\pi} \\ &+ \frac{A_{3i} A_3{}^i \beta^j \beta^k \Omega^4 D_j \Omega D_k \Omega}{2\pi\alpha^2} - \frac{A_3{}^j \gamma^{ik}\Omega^6 D_i A_{3j} D_k \chi}{16\pi} + \frac{A_3{}^j \gamma^{ik}\Omega^6 D_j A_{3i} D_k \chi}{8\pi}\end{aligned} \tag{B.1}$$

$$\begin{aligned}\bar{J}^i = &\frac{E^j \Omega^6 D_j A_3{}^i}{4\pi} - \frac{E^k \gamma^{ij}\Omega^6 \chi D_j A_{3k}}{4\pi} + \frac{A_3{}^i E^j \Omega^5 D_j \Omega}{2\pi} - \frac{A_3{}^k E_k \gamma^{ij}\Omega^5 \chi D_j \Omega}{2\pi} - \frac{A_3{}^i E^j \Omega^6 D_j \chi}{4\pi\chi} \\ &- \frac{A_3{}^j \beta^k \Omega^5 D_j A_3{}^i D_k \Omega}{2\pi\alpha} + \frac{\gamma^{kj}\Omega^5 \Phi \chi D_j A_3{}^i D_k \Omega}{2\pi} - \frac{\gamma^{ij}\Omega^5 \Phi \chi D_j A_3{}^k D_k \Omega}{2\pi} - \frac{A_3{}^i A_3{}^j \beta^k \Omega^4 D_j \Omega D_k \Omega}{\pi\alpha} \\ &- \frac{A_3{}^k \gamma^{ij}\Omega^4 \Phi \chi D_j \Omega D_k \Omega}{\pi} + \frac{A_3{}^i \gamma^{kj}\Omega^4 \Phi \chi D_j \Omega D_k \Omega}{\pi} - \frac{A_3{}^i \gamma^{kj}\Omega^5 \Phi D_j \chi D_k \Omega}{2\pi} + \frac{A_3{}^k \gamma^{ji}\Omega^5 \Phi D_j \Omega D_k \chi}{2\pi} \\ &+ \frac{A_3{}^i A_3{}^k \beta^j \Omega^5 D_j \Omega D_k \chi}{2\pi\alpha\chi} + \frac{A_3{}^k \gamma^{ij}\beta^l \Omega^5 \chi D_j A_{3k} D_l \Omega}{2\pi\alpha} + \frac{A_{3k} A_3{}^k \gamma^{ij}\beta^l \Omega^4 \chi D_j \Omega D_l \Omega}{\pi\alpha}\end{aligned} \tag{B.2}$$

$$\begin{aligned}\bar{S}_{ij} = &-\frac{E_i E_j \Omega^6}{4\pi} + \frac{E_k E^k \gamma_{ij}\Omega^6}{8\pi\chi} - \frac{E_j \Omega^5 \Phi D_i \Omega}{2\pi} + \frac{A_3{}^k \Omega^5 D_i \Omega D_j A_{3k}}{2\pi} + \frac{\gamma^{lk}\Omega^6 \chi D_i A_{3k} D_j A_{3l}}{4\pi} \\ &- \frac{A_{3k} A_{3l}\Omega^6 D_i \beta^l D_j \beta^k}{4\pi\alpha^2} + \frac{A_{3k} A_{3l}\Omega^6 D_i \beta^k D_j \beta^l}{4\pi\alpha^2} - \frac{E_i \Omega^5 \Phi D_j \Omega}{2\pi} + \frac{A_3{}^k \Omega^5 D_i A_{3k} D_j \Omega}{2\pi} \\ &+ \frac{A_{3k} A_3{}^k \Omega^4 D_i \Omega D_j \Omega}{\pi} - \frac{\Omega^4 \Phi^2 D_i \Omega D_j \Omega}{\pi} - \frac{A_{3l}\beta^k \Omega^6 D_j \beta^l D_k A_{3i}}{4\pi\alpha^2} - \frac{A_3{}^k \Omega^5 D_j \Omega D_k A_{3i}}{2\pi} \\ &- \frac{A_3{}^k \Omega^5 D_i \Omega D_k A_{3j}}{2\pi} + \frac{A_{3j} E_i \beta^k \Omega^5 D_k \Omega}{2\pi\alpha} + \frac{A_{3i} E_j \beta^k \Omega^5 D_k \Omega}{2\pi\alpha} + \frac{E^k \gamma_{ij}\Omega^5 \Phi D_k \Omega}{2\pi\chi} - \frac{A_{3j} A_3{}^k \Omega^4 D_i \Omega D_k \Omega}{\pi}\end{aligned}$$

$$
\begin{aligned}
&+\frac{A_{3j}\beta^k\Omega^4\Phi D_i\Omega D_k\Omega}{\pi\alpha}-\frac{A_{3i}A_3{}^k\Omega^4 D_j\Omega D_k\Omega}{\pi}+\frac{A_{3i}\beta^k\Omega^4\Phi D_j\Omega D_k\Omega}{\pi\alpha}-\frac{\gamma^{kl}\Omega^6\chi D_jA_{3k}D_lA_{3i}}{4\pi}\\
&+\frac{A_{3k}\beta^l\Omega^6D_j\beta^kD_lA_{3i}}{4\pi\alpha^2}-\frac{\beta^k\beta^l\Omega^6D_kA_{3j}D_lA_{3i}}{4\pi\alpha^2}-\frac{\gamma^{kl}\Omega^6\chi D_iA_{3k}D_lA_{3j}}{4\pi}+\frac{\beta^k\beta^l\Omega^6D_kA_{3i}D_lA_{3j}}{4\pi\alpha^2}\\
&+\frac{\gamma^{kl}\Omega^6\chi D_kA_{3i}D_lA_{3j}}{4\pi}+\frac{A_{3i}\gamma^{kl}\Omega^6D_k\chi D_lA_{3j}}{8\pi}-\frac{A_3{}^kE_k\gamma_{ij}\beta^l\Omega^5D_l\Omega}{2\pi\alpha\chi}-\frac{A_{3j}\gamma^{lk}\Omega^5\chi D_iA_{3k}D_l\Omega}{2\pi}\\
&-\frac{A_{3i}\gamma^{lk}\Omega^5\chi D_jA_{3k}D_l\Omega}{2\pi}+\frac{A_{3j}\gamma^{kl}\Omega^5\chi D_kA_{3i}D_l\Omega}{2\pi}+\frac{A_{3i}\gamma^{kl}\Omega^5\chi D_kA_{3j}D_l\Omega}{2\pi}-\frac{A_{3i}A_{3j}\beta^k\beta^l\Omega^4D_k\Omega D_l\Omega}{\pi\alpha^2}\\
&+\frac{\gamma_{ij}\gamma^{kl}\Omega^4\Phi^2D_k\Omega D_l\Omega}{2\pi}+\frac{A_3{}^kA_3{}^l\gamma_{ij}\Omega^4D_k\Omega D_l\Omega}{2\pi\chi}-\frac{A_3{}^k\gamma_{ij}\beta^l\Omega^4\Phi D_k\Omega D_l\Omega}{\pi\alpha\chi}+\frac{A_{3i}A_{3j}\gamma^{kl}\Omega^4\chi D_k\Omega D_l\Omega}{\pi}\\
&-\frac{A_{3j}\gamma^{kl}\Omega^6D_iA_{3k}D_l\chi}{8\pi}+\frac{A_{3j}\gamma^{lk}\Omega^6D_iA_{3k}D_l\chi}{8\pi}-\frac{A_{3i}\gamma^{kl}\Omega^6D_kA_{3j}D_l\chi}{8\pi}-\frac{A_3{}^k\gamma_{ij}\gamma^{lm}\Omega^6D_l\chi D_mA_{3k}}{8\pi\chi}\\
&+\frac{A_3{}^l\gamma_{ij}\gamma^{km}\Omega^6D_k\chi D_mA_{3l}}{8\pi\chi}-\frac{A_3{}^k\gamma_{ij}\gamma^{lm}\Omega^5D_lA_{3k}D_m\Omega}{2\pi}+\frac{A_3{}^l\gamma_{ij}\gamma^{mk}\Omega^5D_lA_{3k}D_m\Omega}{2\pi}\\
&-\frac{A_{3k}A_3{}^k\gamma_{ij}\gamma^{lm}\Omega^4D_l\Omega D_m\Omega}{2\pi}+\frac{A_{3k}A_3{}^k\gamma_{ij}\beta^l\beta^m\Omega^4D_l\Omega D_m\Omega}{2\pi\alpha^2\chi}+\frac{A_3{}^k\gamma_{ij}\gamma^{lm}\Omega^6D_kA_{3l}D_m\chi}{8\pi\chi}\\
&-\frac{A_3{}^l\gamma_{ij}\gamma^{km}\Omega^6D_lA_{3k}D_m\chi}{8\pi\chi}+\frac{\gamma_{ij}\gamma^{lk}\gamma^{mn}\Omega^6\chi D_lA_{3m}D_nA_{3k}}{8\pi}-\frac{\gamma_{ij}\gamma^{lk}\gamma^{mn}\Omega^6\chi D_mA_{3k}D_nA_{3l}}{8\pi}
\end{aligned}
\tag{B.3}
$$

$$
\begin{aligned}
\bar{S}=&\frac{E_iE^i\Omega^6}{8\pi}+\frac{E^i\Omega^5\Phi D_i\Omega}{2\pi}+\frac{3\Omega^4\Phi^2\chi D_i\Omega D^i\Omega}{2\pi}+\frac{3A_3{}^j\Omega^5\chi D^i\Omega D_jA_{3i}}{2\pi}-\frac{3A_3{}^j\Omega^6D^i\chi D_jA_{3i}}{8\pi}\\
&+\frac{A_3{}^k\gamma^{ij}\Omega^5\chi D_i\Omega D_jA_{3k}}{2\pi}+\frac{\gamma^{ij}\gamma^{lk}\Omega^6\chi^2D_iA_{3k}D_jA_{3l}}{4\pi}-\frac{A_{3k}A_{3l}\gamma^{ij}\Omega^6\chi D_i\beta^lD_j\beta^k}{4\pi\alpha^2}\\
&+\frac{A_{3k}A_{3l}\gamma^{ij}\Omega^6\chi D_i\beta^kD_j\beta^l}{4\pi\alpha^2}-\frac{A_3{}^iE_i\beta^j\Omega^5D_j\Omega}{2\pi\alpha}+\frac{A_3{}^k\gamma^{ij}\Omega^5\chi D_iA_{3k}D_j\Omega}{2\pi}-\frac{A_3{}^iA_3{}^j\Omega^4D_i\Omega D_j\Omega}{2\pi}\\
&-\frac{A_3{}^i\beta^j\Omega^4\Phi D_i\Omega D_j\Omega}{\pi\alpha}+\frac{A_{3k}A_3{}^k\gamma^{ij}\Omega^4\chi D_i\Omega D_j\Omega}{\pi}-\frac{\gamma^{ij}\Omega^4\Phi^2\chi D_i\Omega D_j\Omega}{\pi}+\frac{3\Omega^6\chi^2D^iA_{3j}D^jA_{3i}}{8\pi}\\
&-\frac{A_3{}^i\Omega^5\chi D_j\Omega D^jA_{3i}}{2\pi}-\frac{A_3{}^i\Omega^6D_j\chi D^jA_{3i}}{8\pi}-\frac{A_3{}^i\Omega^5\chi D_iA_{3j}D^j\Omega}{\pi}-\frac{A_{3i}A_3{}^i\Omega^4\chi D_j\Omega D^j\Omega}{2\pi}\\
&+\frac{3A_3{}^i\Omega^6D_iA_{3j}D^j\chi}{8\pi}+\frac{A_3{}^i\Omega^6D_jA_{3i}D^j\chi}{8\pi}-\frac{A_{3l}\gamma^{ij}\beta^k\Omega^6\chi D_j\beta^lD_kA_{3i}}{4\pi\alpha^2}-\frac{A_3{}^k\gamma^{ij}\Omega^5\chi D_j\Omega D_kA_{3i}}{2\pi}\\
&-\frac{A_3{}^k\gamma^{ij}\Omega^5\chi D_i\Omega D_kA_{3j}}{2\pi}+\frac{A_{3i}A_3{}^i\beta^j\beta^k\Omega^4D_j\Omega D_k\Omega}{2\pi\alpha^2}-\frac{\gamma^{ij}\Omega^6\chi^2D_jA_{3k}D^kA_{3i}}{4\pi}+\frac{\gamma^{ij}\Omega^6\chi^2D_kA_{3j}D^kA_{3i}}{4\pi}\\
&-\frac{3\gamma^{ji}\Omega^6\chi^2D_kA_{3j}D^kA_{3i}}{8\pi}-\frac{\gamma^{ij}\Omega^6\chi^2D_iA_{3k}D^kA_{3j}}{4\pi}+\frac{A_{3k}\gamma^{ij}\beta^l\Omega^6\chi D_j\beta^kD_lA_{3i}}{4\pi\alpha^2}-\frac{\gamma^{ij}\beta^k\beta^l\Omega^6\chi D_kA_{3j}D_lA_{3i}}{4\pi\alpha^2}\\
&+\frac{\gamma^{ij}\beta^k\beta^l\Omega^6\chi D_kA_{3i}D_lA_{3j}}{4\pi\alpha^2},
\end{aligned}
\tag{B.4}
$$

which is significantly more complicated than expected. When passed down to spherically symmetric coordinates, the expressions get more simplified. At the same time, matching these expressions with the ones obtained with writing the Faraday tensor only as a function of the electric field is easier to do. The factors we have to add to the evolution equations, given the above projections, become instead,

$$
\begin{aligned}
(\dot{A}_{rr})_{\text{Max+KG}}=&-\tfrac{16}{3}\pi q^2(A_3)^2(\bar{c}_\phi)^2\alpha\chi(\Omega)^6-\tfrac{16}{3}\pi q^4(A_3)^2(\bar{d}_\phi)^2\alpha\chi(\Omega)^6+\tfrac{4}{3}(E)^2\alpha\chi(\Omega)^6+\tfrac{32}{3}\pi q^2A_3\bar{d}_\phi\alpha\chi(\Omega)^4\bar{c}'_\phi\\
&-\tfrac{16}{3}\pi\alpha\chi(\Omega)^2(\bar{c}'_\phi)^2-\tfrac{32}{3}\pi q^2A_3\bar{c}_\phi\alpha\chi(\Omega)^4\bar{d}'_\phi-\tfrac{16}{3}\pi q^2\alpha\chi(\Omega)^2(\bar{d}'_\phi)^2-\tfrac{16}{3}A_3E\beta^r\chi(\Omega)^5\Omega'\\
&+\tfrac{16}{3}E\alpha\Phi\chi(\Omega)^5\Omega'-\tfrac{32}{3}\pi\bar{c}_\phi\alpha\chi\Omega\bar{c}'_\phi\Omega'-\tfrac{32}{3}\pi q^2\bar{d}_\phi\alpha\chi\Omega\bar{d}'_\phi\Omega'-\tfrac{16}{3}\pi(\bar{c}_\phi)^2\alpha\chi(\Omega')^2
\end{aligned}
$$

$$- \tfrac{16}{3}\pi q^2 \left(\bar{d}_\phi\right)^2 \alpha \chi \left(\Omega'\right)^2 + \frac{16 \left(A_3\right)^2 \left(\beta^r\right)^2 \chi \left(\Omega\right)^4 \left(\Omega'\right)^2}{3\alpha} - \tfrac{32}{3} A_3 \beta^r \Phi \chi \left(\Omega\right)^4 \left(\Omega'\right)^2 + \tfrac{16}{3}\alpha \left(\Phi\right)^2 \chi \left(\Omega\right)^4 \left(\Omega'\right)^2 \tag{B.5}$$

$$\begin{aligned}
\left(\dot{K}\right)_{\text{Max+KG}} = {} & \frac{8\pi \left(\bar{c}_\Pi\right)^2 \left(\Omega\right)^3}{\alpha} + \frac{8\pi q^2 \left(\bar{d}_\Pi\right)^2 \left(\Omega\right)^3}{\alpha} - 16\pi q^2 \bar{c}_\phi \bar{d}_\Pi \Phi \left(\Omega\right)^5 + 16\pi q^2 \bar{c}_\Pi \bar{d}_\phi \Phi \left(\Omega\right)^5 + 8\pi q^2 \left(\bar{c}_\phi\right)^2 \alpha \left(\Phi\right)^2 \left(\Omega\right)^7 \\
& + 8\pi q^4 \left(\bar{d}_\phi\right)^2 \alpha \left(\Phi\right)^2 \left(\Omega\right)^7 + \frac{\left(E\right)^2 \alpha \chi \left(\Omega\right)^7}{\gamma_{rr}} - \frac{16\pi \bar{c}_\Pi \beta^r \left(\Omega\right)^3 \bar{c}'_\phi}{\alpha} - 16\pi q^2 \bar{d}_\phi \beta^r \Phi \left(\Omega\right)^5 \bar{c}'_\phi \\
& + \frac{8\pi \left(\beta^r\right)^2 \left(\Omega\right)^3 \left(\bar{c}'_\phi\right)^2}{\alpha} - \frac{16\pi q^2 \bar{d}_\Pi \beta^r \left(\Omega\right)^3 \bar{d}'_\phi}{\alpha} + 16\pi q^2 \bar{c}_\phi \beta^r \Phi \left(\Omega\right)^5 \bar{d}'_\phi + \frac{8\pi q^2 \left(\beta^r\right)^2 \left(\Omega\right)^3 \left(\bar{d}'_\phi\right)^2}{\alpha} \\
& - \frac{16\pi \bar{c}_\Pi \bar{c}_\phi \beta^r \left(\Omega\right)^2 \Omega'}{\alpha} - \frac{16\pi q^2 \bar{d}_\Pi \bar{d}_\phi \beta^r \left(\Omega\right)^2 \Omega'}{\alpha} - \frac{4 A_3 E \beta^r \chi \left(\Omega\right)^6 \Omega'}{\gamma_{rr}} + \frac{4E\alpha\Phi\chi \left(\Omega\right)^6 \Omega'}{\gamma_{rr}} \\
& + \frac{16\pi \bar{c}_\phi \left(\beta^r\right)^2 \left(\Omega\right)^2 \bar{c}'_\phi \Omega'}{\alpha} + \frac{16\pi q^2 \bar{d}_\phi \left(\beta^r\right)^2 \left(\Omega\right)^2 \bar{d}'_\phi \Omega'}{\alpha} + \frac{8\pi \left(\bar{c}_\phi\right)^2 \left(\beta^r\right)^2 \Omega \left(\Omega'\right)^2}{\alpha} \\
& + \frac{8\pi q^2 \left(\bar{d}_\phi\right)^2 \left(\beta^r\right)^2 \Omega \left(\Omega'\right)^2}{\alpha} + \frac{4 \left(A_3\right)^2 \left(\beta^r\right)^2 \chi \left(\Omega\right)^5 \left(\Omega'\right)^2}{\gamma_{rr}\alpha} - \frac{8 A_3 \beta^r \Phi \chi \left(\Omega\right)^5 \left(\Omega'\right)^2}{\gamma_{rr}} \\
& + \frac{4\alpha \left(\Phi\right)^2 \chi \left(\Omega\right)^5 \left(\Omega'\right)^2}{\gamma_{rr}}
\end{aligned} \tag{B.6}$$

$$\begin{aligned}
\left(\dot{\Lambda}_r\right)_{\text{Max+KG}} = {} & \frac{16\pi q^2 A_3 \bar{c}_\phi \bar{d}_\Pi \left(\Omega\right)^4}{\gamma_{rr}} - \frac{16\pi q^2 A_3 \bar{c}_\Pi \bar{d}_\phi \left(\Omega\right)^4}{\gamma_{rr}} - \frac{16\pi q^2 A_3 \left(\bar{c}_\phi\right)^2 \alpha \Phi \left(\Omega\right)^6}{\gamma_{rr}} - \frac{16\pi q^4 A_3 \left(\bar{d}_\phi\right)^2 \alpha \Phi \left(\Omega\right)^6}{\gamma_{rr}} \\
& + \frac{16\pi \bar{c}_\Pi \left(\Omega\right)^2 \bar{c}'_\phi}{\gamma_{rr}} + \frac{16\pi q^2 A_3 \bar{d}_\phi \beta^r \left(\Omega\right)^4 \bar{c}'_\phi}{\gamma_{rr}} + \frac{16\pi q^2 \bar{d}_\phi \alpha \Phi \left(\Omega\right)^4 \bar{c}'_\phi}{\gamma_{rr}} - \frac{16\pi \beta^r \left(\Omega\right)^2 \left(\bar{c}'_\phi\right)^2}{\gamma_{rr}} \\
& + \frac{16\pi q^2 \bar{d}_\Pi \left(\Omega\right)^2 \bar{d}'_\phi}{\gamma_{rr}} - \frac{16\pi q^2 A_3 \bar{c}_\phi \beta^r \left(\Omega\right)^4 \bar{d}'_\phi}{\gamma_{rr}} - \frac{16\pi q^2 \bar{c}_\phi \alpha \Phi \left(\Omega\right)^4 \bar{d}'_\phi}{\gamma_{rr}} - \frac{16\pi q^2 \beta^r \left(\Omega\right)^2 \left(\bar{d}'_\phi\right)^2}{\gamma_{rr}} \\
& + \frac{16\pi \bar{c}_\Pi \bar{c}_\phi \Omega \Omega'}{\gamma_{rr}} + \frac{16\pi q^2 \bar{d}_\Pi \bar{d}_\phi \Omega \Omega'}{\gamma_{rr}} - \frac{32\pi \bar{c}_\phi \beta^r \Omega \bar{c}'_\phi \Omega'}{\gamma_{rr}} - \frac{32\pi q^2 \bar{d}_\phi \beta^r \Omega \bar{d}'_\phi \Omega'}{\gamma_{rr}} \\
& - \frac{16\pi \left(\bar{c}_\phi\right)^2 \beta^r \left(\Omega'\right)^2}{\gamma_{rr}} - \frac{16\pi q^2 \left(\bar{d}_\phi\right)^2 \beta^r \left(\Omega'\right)^2}{\gamma_{rr}}
\end{aligned} \tag{B.7}$$

$$\begin{aligned}
\left(\dot{\Theta}\right)_{\text{Max+KG}} = {} & - \frac{4\pi \left(\bar{c}_\Pi\right)^2 \left(\Omega\right)^3}{\alpha} - \frac{4\pi q^2 \left(\bar{d}_\Pi\right)^2 \left(\Omega\right)^3}{\alpha} + 8\pi q^2 \bar{c}_\phi \bar{d}_\Pi \Phi \left(\Omega\right)^5 - 8\pi q^2 \bar{c}_\Pi \bar{d}_\phi \Phi \left(\Omega\right)^5 \\
& - 4\pi q^2 \left(\bar{c}_\phi\right)^2 \alpha \left(\Phi\right)^2 \left(\Omega\right)^7 - 4\pi q^4 \left(\bar{d}_\phi\right)^2 \alpha \left(\Phi\right)^2 \left(\Omega\right)^7 - \frac{4\pi q^2 \left(A_3\right)^2 \left(\bar{c}_\phi\right)^2 \alpha \chi \left(\Omega\right)^7}{\gamma_{rr}} \\
& - \frac{4\pi q^4 \left(A_3\right)^2 \left(\bar{d}_\phi\right)^2 \alpha \chi \left(\Omega\right)^7}{\gamma_{rr}} - \frac{\left(E\right)^2 \alpha \chi \left(\Omega\right)^7}{\gamma_{rr}} + \frac{8\pi \bar{c}_\Pi \beta^r \left(\Omega\right)^3 \bar{c}'_\phi}{\alpha} + 8\pi q^2 \bar{d}_\phi \beta^r \Phi \left(\Omega\right)^5 \bar{c}'_\phi \\
& + \frac{8\pi q^2 A_3 \bar{d}_\phi \alpha \chi \left(\Omega\right)^5 \bar{c}'_\phi}{\gamma_{rr}} - \frac{4\pi \left(\beta^r\right)^2 \left(\Omega\right)^3 \left(\bar{c}'_\phi\right)^2}{\alpha} - \frac{4\pi \alpha \chi \left(\Omega\right)^3 \left(\bar{c}'_\phi\right)^2}{\gamma_{rr}} + \frac{8\pi q^2 \bar{d}_\Pi \beta^r \left(\Omega\right)^3 \bar{d}'_\phi}{\alpha} \\
& - 8\pi q^2 \bar{c}_\phi \beta^r \Phi \left(\Omega\right)^5 \bar{d}'_\phi - \frac{8\pi q^2 A_3 \bar{c}_\phi \alpha \chi \left(\Omega\right)^5 \bar{d}'_\phi}{\gamma_{rr}} - \frac{4\pi q^2 \left(\beta^r\right)^2 \left(\Omega\right)^3 \left(\bar{d}'_\phi\right)^2}{\alpha} - \frac{4\pi q^2 \alpha \chi \left(\Omega\right)^3 \left(\bar{d}'_\phi\right)^2}{\gamma_{rr}} \\
& + \frac{8\pi \bar{c}_\Pi \bar{c}_\phi \beta^r \left(\Omega\right)^2 \Omega'}{\alpha} + \frac{8\pi q^2 \bar{d}_\Pi \bar{d}_\phi \beta^r \left(\Omega\right)^2 \Omega'}{\alpha} + \frac{4 A_3 E \beta^r \chi \left(\Omega\right)^6 \Omega'}{\gamma_{rr}} - \frac{4E\alpha\Phi\chi \left(\Omega\right)^6 \Omega'}{\gamma_{rr}} \\
& - \frac{8\pi \bar{c}_\phi \left(\beta^r\right)^2 \left(\Omega\right)^2 \bar{c}'_\phi \Omega'}{\alpha} - \frac{8\pi \bar{c}_\phi \alpha \chi \left(\Omega\right)^2 \bar{c}'_\phi \Omega'}{\gamma_{rr}} - \frac{8\pi q^2 \bar{d}_\phi \left(\beta^r\right)^2 \left(\Omega\right)^2 \bar{d}'_\phi \Omega'}{\alpha} \\
& - \frac{8\pi q^2 \bar{d}_\phi \alpha \chi \left(\Omega\right)^2 \bar{d}'_\phi \Omega'}{\gamma_{rr}} - \frac{4\pi \left(\bar{c}_\phi\right)^2 \left(\beta^r\right)^2 \Omega \left(\Omega'\right)^2}{\alpha} - \frac{4\pi q^2 \left(\bar{d}_\phi\right)^2 \left(\beta^r\right)^2 \Omega \left(\Omega'\right)^2}{\alpha} \\
& - \frac{4\pi \left(\bar{c}_\phi\right)^2 \alpha \chi \Omega \left(\Omega'\right)^2}{\gamma_{rr}} - \frac{4\pi q^2 \left(\bar{d}_\phi\right)^2 \alpha \chi \Omega \left(\Omega'\right)^2}{\gamma_{rr}} - \frac{4 \left(A_3\right)^2 \left(\beta^r\right)^2 \chi \left(\Omega\right)^5 \left(\Omega'\right)^2}{\gamma_{rr}\alpha}
\end{aligned}$$

$$+\frac{8A_3\beta^r\Phi\chi(\Omega)^5(\Omega')^2}{\gamma_{rr}}-\frac{4\alpha(\Phi)^2\chi(\Omega)^5(\Omega')^2}{\gamma_{rr}}\,. \tag{B.8}$$

Finally, the constraints become,

$$\begin{aligned}(\mathcal{H})_{\text{Max+KG}} =& -\frac{8\pi(\bar{c}_\Pi)^2(\Omega)^2}{(\alpha)^2}-\frac{8\pi q^2(\bar{d}_\Pi)^2(\Omega)^2}{(\alpha)^2}+\frac{16\pi q^2\bar{c}_\phi\bar{d}_\Pi\Phi(\Omega)^4}{\alpha}-\frac{16\pi q^2\bar{c}_\Pi\bar{d}_\phi\Phi(\Omega)^4}{\alpha}-8\pi q^2(\bar{c}_\phi)^2(\Phi)^2(\Omega)^6\\
&-8\pi q^4(\bar{d}_\phi)^2(\Phi)^2(\Omega)^6-\frac{8\pi q^2(A_3)^2(\bar{c}_\phi)^2\chi(\Omega)^6}{\gamma_{rr}}-\frac{8\pi q^4(A_3)^2(\bar{d}_\phi)^2\chi(\Omega)^6}{\gamma_{rr}}-\frac{2(E)^2\chi(\Omega)^6}{\gamma_{rr}}\\
&+\frac{16\pi\bar{c}_\Pi\beta^r(\Omega)^2\bar{c}'_\phi}{(\alpha)^2}+\frac{16\pi q^2\bar{d}_\phi\beta^r\Phi(\Omega)^4\bar{c}'_\phi}{\alpha}+\frac{16\pi q^2A_3\bar{d}_\phi\chi(\Omega)^4\bar{c}'_\phi}{\gamma_{rr}}-\frac{8\pi(\beta^r)^2(\Omega)^2(\bar{c}'_\phi)^2}{(\alpha)^2}\\
&-\frac{8\pi\chi(\Omega)^2(\bar{c}'_\phi)^2}{\gamma_{rr}}+\frac{16\pi q^2\bar{d}_\Pi\beta^r(\Omega)^2\bar{d}'_\phi}{(\alpha)^2}-\frac{16\pi q^2\bar{c}_\phi\beta^r\Phi(\Omega)^4\bar{d}'_\phi}{\alpha}-\frac{16\pi q^2A_3\bar{c}_\phi\chi(\Omega)^4\bar{d}'_\phi}{\gamma_{rr}}\\
&-\frac{8\pi q^2(\beta^r)^2(\Omega)^2(\bar{d}'_\phi)^2}{(\alpha)^2}-\frac{8\pi q^2\chi(\Omega)^2(\bar{d}'_\phi)^2}{\gamma_{rr}}+\frac{16\pi\bar{c}_\Pi\bar{c}_\phi\beta^r\Omega\Omega'}{(\alpha)^2}+\frac{16\pi q^2\bar{d}_\Pi\bar{d}_\phi\beta^r\Omega\Omega'}{(\alpha)^2}\\
&+\frac{8A_3E\beta^r\chi(\Omega)^5\Omega'}{\gamma_{rr}\alpha}-\frac{8E\Phi\chi(\Omega)^5\Omega'}{\gamma_{rr}}-\frac{16\pi\bar{c}_\phi(\beta^r)^2\Omega\bar{c}'_\phi\Omega'}{(\alpha)^2}-\frac{16\pi\bar{c}_\phi\chi\Omega\bar{c}'_\phi\Omega'}{\gamma_{rr}}\\
&-\frac{16\pi q^2\bar{d}_\phi(\beta^r)^2\Omega\bar{d}'_\phi\Omega'}{(\alpha)^2}-\frac{16\pi q^2\bar{d}_\phi\chi\Omega\bar{d}'_\phi\Omega'}{\gamma_{rr}}-\frac{8\pi(\bar{c}_\phi)^2(\beta^r)^2(\Omega')^2}{(\alpha)^2}-\frac{8\pi q^2(\bar{d}_\phi)^2(\beta^r)^2(\Omega')^2}{(\alpha)^2}\\
&-\frac{8\pi(\bar{c}_\phi)^2\chi(\Omega')^2}{\gamma_{rr}}-\frac{8\pi q^2(\bar{d}_\phi)^2\chi(\Omega')^2}{\gamma_{rr}}-\frac{8(A_3)^2(\beta^r)^2\chi(\Omega)^4(\Omega')^2}{\gamma_{rr}(\alpha)^2}+\frac{16A_3\beta^r\Phi\chi(\Omega)^4(\Omega')^2}{\gamma_{rr}\alpha}\\
&-\frac{8(\Phi)^2\chi(\Omega)^4(\Omega')^2}{\gamma_{rr}}\end{aligned} \tag{B.9}$$

$$\begin{aligned}(\mathcal{M}_r)_{\text{Max+KG}} =& \frac{8\pi q^2A_3\bar{c}_\phi\bar{d}_\Pi(\Omega)^4}{\alpha}-\frac{8\pi q^2A_3\bar{c}_\Pi\bar{d}_\phi(\Omega)^4}{\alpha}-8\pi q^2A_3(\bar{c}_\phi)^2\Phi(\Omega)^6-8\pi q^4A_3(\bar{d}_\phi)^2\Phi(\Omega)^6\\
&+\frac{8\pi\bar{c}_\Pi(\Omega)^2\bar{c}'_\phi}{\alpha}+\frac{8\pi q^2A_3\bar{d}_\phi\beta^r(\Omega)^4\bar{c}'_\phi}{\alpha}+8\pi q^2\bar{d}_\phi\Phi(\Omega)^4\bar{c}'_\phi-\frac{8\pi\beta^r(\Omega)^2(\bar{c}'_\phi)^2}{\alpha}\\
&+\frac{8\pi q^2\bar{d}_\Pi(\Omega)^2\bar{d}'_\phi}{\alpha}-\frac{8\pi q^2A_3\bar{c}_\phi\beta^r(\Omega)^4\bar{d}'_\phi}{\alpha}-8\pi q^2\bar{c}_\phi\Phi(\Omega)^4\bar{d}'_\phi-\frac{8\pi q^2\beta^r(\Omega)^2(\bar{d}'_\phi)^2}{\alpha}\\
&+\frac{8\pi\bar{c}_\Pi\bar{c}_\phi\Omega\Omega'}{\alpha}+\frac{8\pi q^2\bar{d}_\Pi\bar{d}_\phi\Omega\Omega'}{\alpha}-\frac{16\pi\bar{c}_\phi\beta^r\Omega\bar{c}'_\phi\Omega'}{\alpha}-\frac{16\pi q^2\bar{d}_\phi\beta^r\Omega\bar{d}'_\phi\Omega'}{\alpha}-\frac{8\pi(\bar{c}_\phi)^2\beta^r(\Omega')^2}{\alpha}\\
&-\frac{8\pi q^2(\bar{d}_\phi)^2\beta^r(\Omega')^2}{\alpha}\,.\end{aligned} \tag{B.10}$$

Appendix C

Notes on Penrose Diagrams

Before starting this appendix, the following must be said: the first two sections are more related to the aesthetic of Penrose diagrams and the third section has more in-depth calculations for trumpet initial data.

C.1 Cauchy Slices

When doing this work, I was confronted with a not-so-clear difficulty in making a Penrose diagram that suited my aesthetic preferences. From talking with several people, what usually is done is one chooses some values of $\tilde{t}$ and $\tilde{r}$, and then, by eye, one gradually builds the diagram. However, there is a way to do this more systematically.

The way I consider a Penrose diagram to be more aesthetic is by having equally spaced slices when crossing the axis of the Penrose diagram, i.e., variables T and R (see Fig. C.1). To express this in practice, we choose adapted coordinates to write the Schwarzschild and Reissner-Nördstrom spacetimes and afterward apply the thought process.

For Schwarzschild, we opt to use Kruskal-Szekeres coordinates. If the reader is interested, I redirect you to Appendix A in [10]. The expressions we are interested in using are,

$\tilde{r} > 2M$,

$$\tilde{T} = e^{\tilde{r}/4M}\sqrt{\frac{\tilde{r}}{2M} - 1}\sinh\left(\frac{\tilde{t}}{4M}\right) \tag{C.1}$$

$$\tilde{R} = e^{\tilde{r}/4M}\sqrt{\frac{\tilde{r}}{2M} - 1}\cosh\left(\frac{\tilde{t}}{4M}\right) \tag{C.2}$$

$\tilde{r} < 2M$,

$$\tilde{T} = e^{\tilde{r}/4M}\sqrt{1 - \frac{\tilde{r}}{2M}}\cosh\left(\frac{\tilde{t}}{4M}\right) \tag{C.3}$$

$$\tilde{R} = e^{\tilde{r}/4M}\sqrt{1 - \frac{\tilde{r}}{2M}}\sinh\left(\frac{\tilde{t}}{4M}\right) \tag{C.4}$$

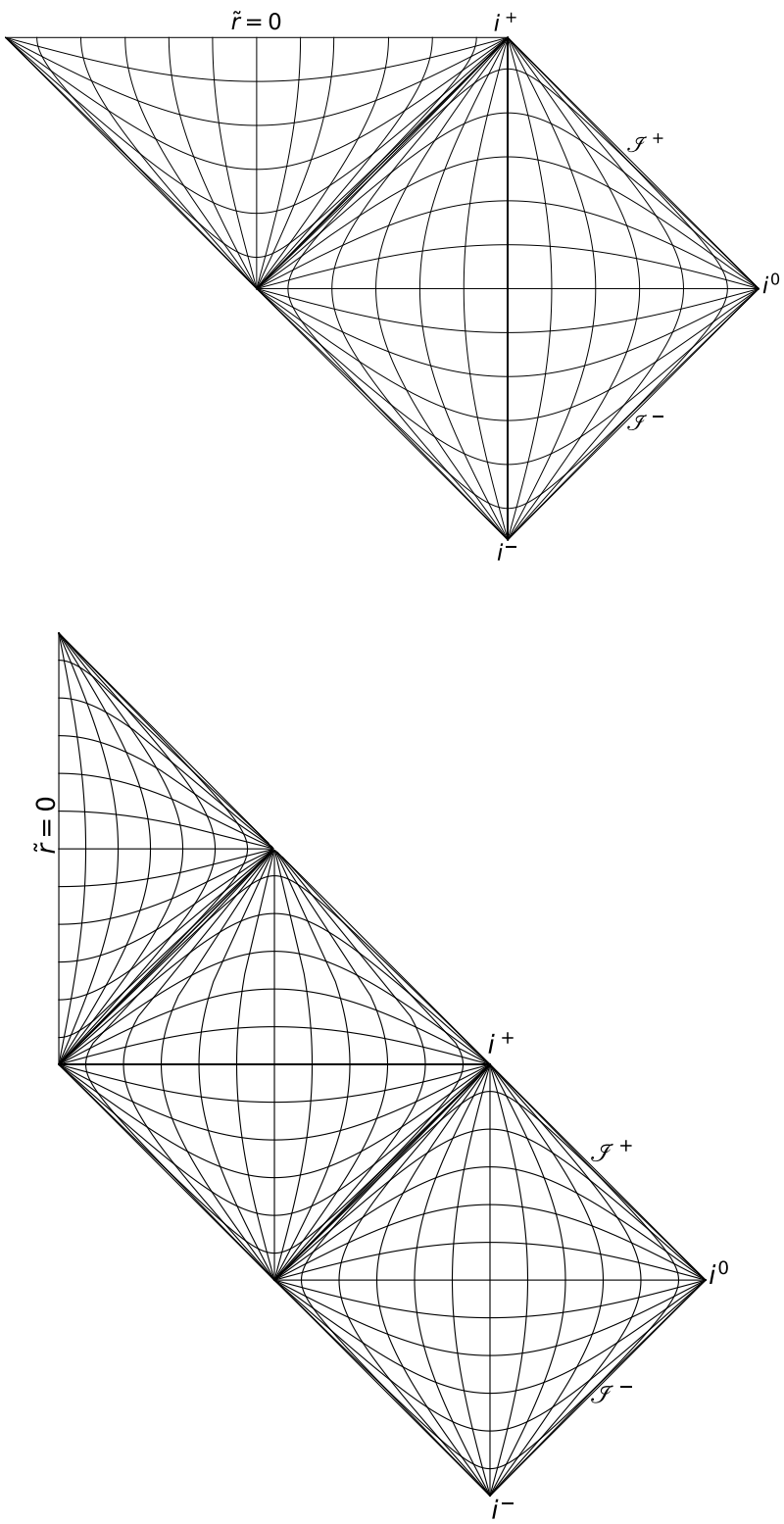

Figure C.1: Schwarzschild and Reissner-Nördstrom Penrose diagrams with lines of constant $\tilde{t}$ and constant $\tilde{r}$.

Recall that the coordinates in which the Penrose diagram is usually written are,

$$T = \arctan(\tilde{T} + \tilde{R}) + \arctan(\tilde{T} - \tilde{R}), \quad R = \arctan(\tilde{T} + \tilde{R}) - \arctan(\tilde{T} - \tilde{R}). \tag{C.5}$$

We can now proceed to translate the aesthetics into the coordinates.

Looking back to (C.5), these coordinates are the ones in which our Schwarzschild Penrose Diagram will be written. If we look only at the part of domain where $\tilde{r} > 2M$, we get that $\tilde{T} \in]-\infty, +\infty[$ and $\tilde{R} \in]0, +\infty[$. This means that $T \in]-\pi/2, \pi/2[$ and $R \in]0, \pi[$. To have the slices equally spaced, we define the following: the amount of slices, N, and the spacing between each, Δ. To have a slice in the middle of the diagram, N has to be odd. With that settled, let us first say we want,

$$R = i \cdot \Delta, \; i \in [1, N].$$

Furthermore, we want them specifically to be equally spaced when $T = 0$. If we put these conditions back into (C.2), we get,

$$\begin{aligned} 0 &= e^{\tilde{r}/4M}\sqrt{\frac{\tilde{r}}{2M} - 1}\sinh\left(\frac{\tilde{t}}{4M}\right) \\ i \cdot \Delta &= e^{\tilde{r}/4M}\sqrt{\frac{\tilde{r}}{2M} - 1}\cosh\left(\frac{\tilde{t}}{4M}\right). \end{aligned}$$

Given that $\tilde{r} > 2M$, the only option that suits the first requirement is if $\tilde{t} = 0$. We are only left with,

$$i \cdot \Delta = e^{\tilde{r}/4M}\sqrt{\frac{\tilde{r}}{2M} - 1}, \tag{C.6}$$

which is an implicit function of $\tilde{r}$. One needs to find the roots of the right-hand side minus the left-hand side of the equation. The initial guess should always be near $2M$, given that most of the slices will have an $\tilde{r}$ close to that value.

If we are to look at the other type of slices (Cauchy Slices),

$$T = i \cdot \Delta, \; i \in [1, N]$$

R should also be in the middle of the diagram, i.e., $R = \frac{\pi}{2}$, so that the Cauchy slices are equally spaced in the middle. The thing is not as clear cut as before. We rewrite the tilded variables as a function of the untilded variables and immediately get,

$$\tilde{T} = \frac{1}{2}\left(\tan\left(\frac{T+R}{2}\right) + \tan\left(\frac{T-R}{2}\right)\right) \tag{C.7}$$

$$\tilde{R} = \frac{1}{2}\left(\tan\left(\frac{T+R}{2}\right) - \tan\left(\frac{T-R}{2}\right)\right) \tag{C.8}$$

This will get us non-zero values for the tilded variables. Afterward, we want to invert back to the physical

variables and so we pick the two equations in (C.2) and divide one by the other, to get,

$$\frac{\tilde{T}}{\tilde{R}} = \frac{\sinh(\tilde{t}/(4M))}{\cosh(\tilde{t}/(4M))},$$

that can be rewritten as,

$$\tilde{T}\cosh(\tilde{t}/(4M)) - \tilde{R}\sinh(\tilde{t}/(4M)) = 0, \tag{C.9}$$

and again we have an implicit function. This one is better behaved and the initial guess is irrelevant. Something close to 0 works fine.

For the Reissner-Nördstrom case, the thought process is identical, but some problems might appear when trying to draw the innermost region of the spacetime, given that $\tilde{r}$ has very small values there. This can also be applied to Schwarzschild spacetime if $2M$ is very small when we are trying to draw the region inside the event horizon. Something helpful for numerical stability is using the logarithmic version of these functions. For example, going back to (C.6), applying log to both sides gives,

$$\log(i\cdot\Delta) = \frac{\tilde{r}}{4M} + \frac{1}{2}\log\left(\frac{\tilde{r}}{2M} - 1\right),$$

and this function is "slower" behaved for $\tilde{r}$ near $2M$. I had to resort to this when plotting the region $\tilde{r} < \tilde{r}_-$ in the Reissner-Nördstrom spacetime.

C.2 Hyperboloidal Slices

We can do something similar to hyperboloidal slices, it only requires a bit more work. To have hyperboloidal slices of Minkowski spacetime, we do a change of time coordinate, like,

$$\tau = \tilde{t} - \sqrt{\tilde{r}^2 + \left(\frac{3}{K_{\text{CMC}}}\right)^2}.$$

In order to have things equally spaced along the line $R = \pi/2$, we can start from the lines of constant $\tilde{t}$, in (C.9). This equation gives us the times $\tilde{t}$ we want, but it is not enough for us to find the constant τ: the $\tilde{r}$ is missing. Thus, we have to find the $\tilde{r}$'s, to have the pairs of coordinates that correspond to the points in the Penrose diagram of the type $(R,T) = (\pi/2, i\cdot\Delta)$. If we go to (C.8), we can substitute directly the values for T and R,

$$\tilde{T} = \frac{1}{2}\left(\tan\left(\frac{i\cdot\Delta+\pi/2}{2}\right) + \tan\left(\frac{i\cdot\Delta-\pi/2}{2}\right)\right).$$

If we also use (C.2), we can already substitute the value for $\tilde{t}$, leaving us, again, with an implicit function for $\tilde{r}$:

$$e^{\tilde{r}/4M}\sqrt{\frac{\tilde{r}}{2M} - 1}\sinh\left(\frac{\tilde{t}}{4M}\right) = \frac{1}{2}\left(\tan\left(\frac{i\cdot\Delta+\pi/2}{2}\right) + \tan\left(\frac{i\cdot\Delta-\pi/2}{2}\right)\right).$$

Finding the root of this function, we get the desired value for $\tilde{r}$. Note that you do not have to solve this function for each pair of values $(\tilde{t},\tilde{T}) = (\tilde{t}, i\cdot\Delta)$. The $\tilde{r}$ that we want will be the same for all points, along the middle line of the Penrose diagram (roughly equal to 1.2784). With all this work, we get the red points

plotted in Fig. C.2.

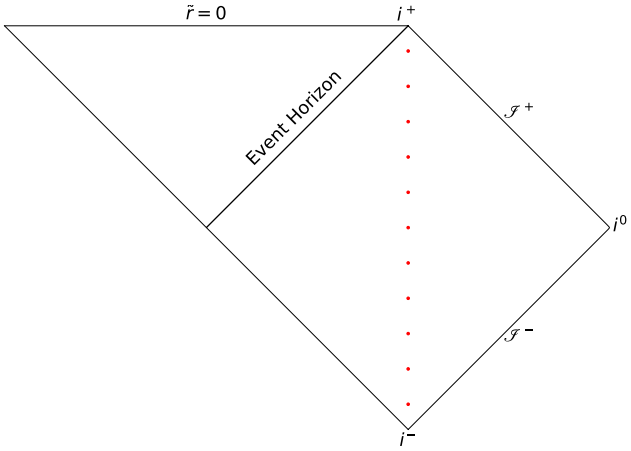

Figure C.2: Schwarzschild spacetime Penrose Diagram with red points equally spaced along the middle line of diagram, in the region outside the event horizon.

Ideally, the hyperboloidal slices should pass through these points.

C.3 Trumpet Initial Data

In order to get trumpet initial data in our Penrose diagrams [52], we have to go back to (4.10), which we present again here,

$$h'(\tilde{r}) = -\frac{1}{A(\tilde{r})\sqrt{A(\tilde{r}) + \left(\frac{K_{CMC}\tilde{r}}{3} + \frac{C_{CMC}}{\tilde{r}^2}\right)^2}} \left(\frac{K_{CMC}\tilde{r}}{3} + \frac{C_{CMC}}{\tilde{r}^2}\right).$$

Trumpet initial data is useful to avoid the black hole's singularity by a clever choice of slicing. Let us pick the Schwarzschild solution, which means we have to choose,

$$A(\tilde{r}) = 1 - \frac{2M}{\tilde{r}},$$

where M is the black hole's mass. Making this substitution in the equation before, it is impossible to get an analytic expression. Furthermore, the derivative of the height function suddenly has a (coordinate) singularity at $\tilde{r} = 2M$. If we were to rewrite the metric as a function of the tortoise coordinate for Schwarzschild spacetime,

$$\tilde{r}_* = \tilde{r} + 2M \log\left(\frac{\tilde{r}}{2M} - 1\right),$$

this singularity would vanish, as the horizon is pushed to infinity. But we do not need to get into that. Given that we want trumpet initial data, we have to choose C_{CMC} accordingly, which provides a double root for the square root in the denominator, R_0. This R_0 will correspond to the minimum Schwarzschild radius that the hyperboloidal slices can reach. Going back to the height function: if we try to integrate it numerically, one gets Fig. C.3. Two things worth discussing about the figure: the initial value of h and the way the

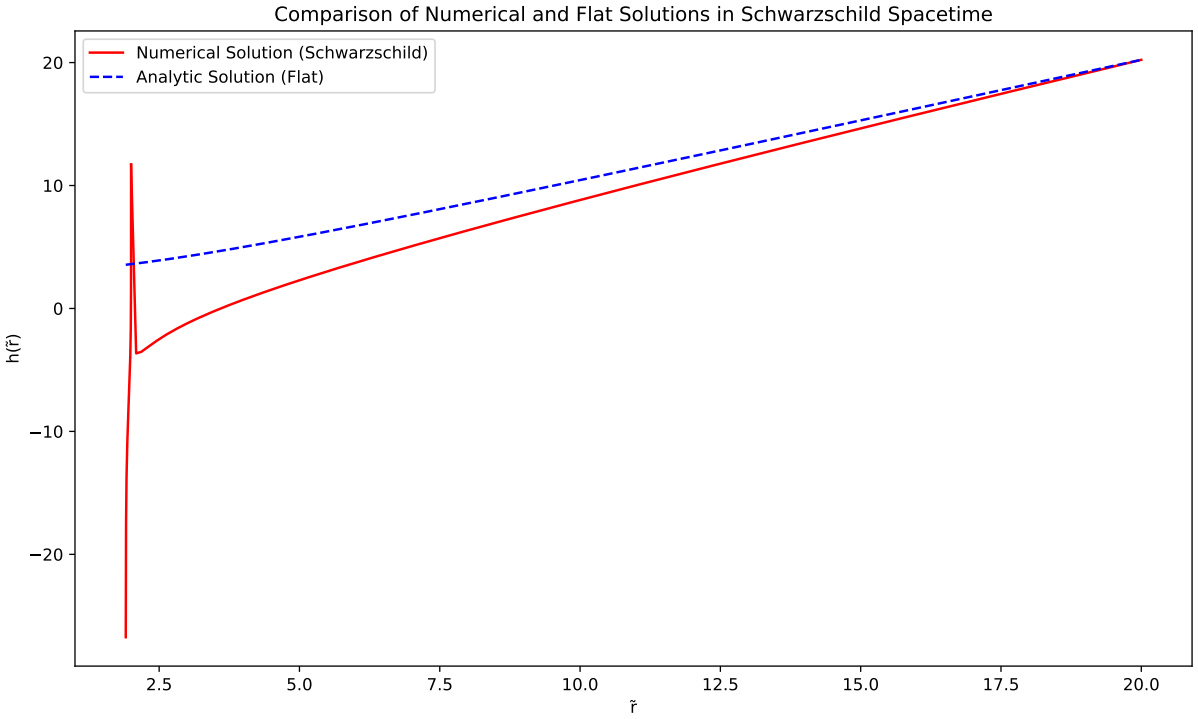

Figure C.3: Numerical integration of (4.10), with $K_{\text{CMC}} = -1$ and $C_{\text{CMC}} \approx 3.11483$. The initial value of h is chosen so that asymptotically the solution approaches the one we chose for flat spacetime.

coordinate singularity is dealt with. Recalling the height function we had chosen for flat spacetime,

$$h(r) = \sqrt{\tilde{r}^2 + \left(\frac{3}{K_{CMC}}\right)^2},$$

we note that our trumpet initial data should, asymptotically, reach this behavior. Therefore, we chose the initial value of h such that the last point between our numerically integrated solution and the flat spacetime one were the same. This makes it easier to see that the asymptotic behavior of both solutions is the same. The other problem is how to treat the coordinate singularity: starting the integration at $\tilde{r} = R_0$, as it approaches $\tilde{r} = 2M$, the function blows up. We stop the integration at a given $2M - \epsilon$ and restart the ingretation at $2M + \epsilon$. This ϵ is chosen to be as small as possible before the any NaNs showed up. A good enough value was $\epsilon \approx 0.001$. Having dealt with this, we can go back to the Penrose diagrams. We have the same points we want to cross, as shown in Fig. C.2, so we simply interpolate the numerical solution we had in order to have the value of h there, put it together with the value for $\tilde{t}$ and get the τ that indicates the hyperboloidal slice that should go through the point. The result is plotted in Fig. C.4.

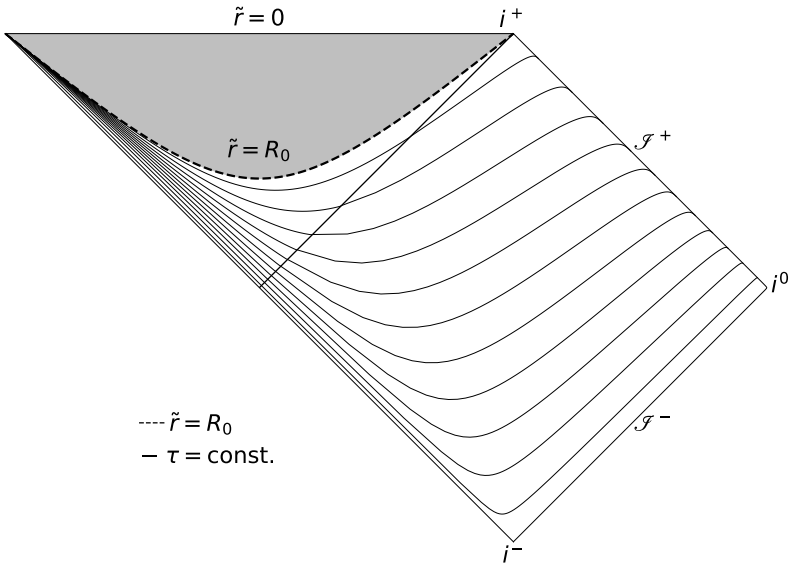

Figure C.4: Hyperboloidal slices in trumpet initial data, in Schwarzschild spacetime. The grey area represents the part of the spacetime that the outer slices do not reach. There are inner slices that connect the singularity to i^+, that we are not plotting here.

Appendix D

Metaphysical Considerations

D.1 On Space and Time

The following text is not a scientific one. One can even regard it as being unnecessary for the work, but it was important to get some ideas straight about what I was doing and thus I will leave them here for it might be of use to someone who reads this document.

Throughout this work, we have focused on what people had done before, asserted, and studied, never questioning why we did that. I am not speaking about the motivation for each step done, which was always given, but it was given with a further lack of metaphysical motivation.

> "The fact that curiosity always holds by what is coming next, and has forgotten what has gone before, is not a result that ensues only from curiosity, but is the ontological condition for curiosity itself.", Martin Heidegger, Being and Time, 1927

Curiosity has to be the essential motivation behind this work, although it is not this work in particular that is curious, it is the Being of human beings (Dasein) that is curious. Otherwise, by being sentient, we would face ourselves with the absence of reason in life. Curiosity is the primordial tool for keeping oneself alive and caring, as defined by Heidegger, is the reason behind it.

> “There is a wish for completeness inherent to human logic, a contempt for the particular case, a constant fight for the general case. Why should the general case be more interesting than the particular case?”, Ludwig Wittgenstein, On Certainty, 1969

Taking off from curiosity, Wittgenstein shows us a way to describe it: the constant fight for something general, for something more abstract, which is not tangible just by mere sight. Curiosity is only kept alive when the run is after something that does not exist without the presence of Dasein. So, we have touched the surface of why one should be motivated to investigate whatever topic: it is an a priori condition of human life. In our case, the science to be studied is mathematical physics, which serves a very distinct purpose.

> "The classical example of the historical development of a science and even for its ontological genesis is the rise of mathematical physics. What is decisive for its development does not lie

> in its rather high esteem for the observation of facts, nor in its 'application' of mathematics in determining the character of natural processes; it lies rather in the way in which Nature herself is mathematically projected. In this projection, something constantly present-at-hand (matter) is uncovered beforehand, and the horizon is opened so that one may be guided by looking at those constitutive items in it which are quantitatively determinable (motion, force, location, and time). [...] In the mathematical projection of Nature what is decisive is not primarily the mathematical as such; what is decisive is that this projection discloses something that is a priori.", Martin Heidegger, Being and Time, 1927

Mathematics is the system we, as a species, have developed to understand nature. The bare necessity of mathematics comes from the fact that languages lack rigor: they are ever-changing. "It is the particular use of a word that gives it meaning", according to Wittgenstein. Thus, by the creation of abstract symbols that have a precise definition, which are not natural and thus need study to be understood, humans have developed a space upon which they can project nature. Nothing that is defined in physics really exists, it is just an interpretation of this projection and we, given the natural constraint of our understanding, will never be sure whether what we have defined is true. Like philosophy, physics and mathematics are a collection of definitions and tools that delve into human understanding and, in the end, must produce exactly what we expect them to produce. We will never understand what we cannot understand.

> "Why can we not imagine a white transparent glass?", Ludwig Wittgenstein, Remarks on Colours, 1950

We have until now talked about why this work was created in the first place, fueled by curiosity; we have described what is the assumption that mathematical physics makes, as a projection of nature, and of its necessity for this projection. Now, we can focus on the objects of nature that were studied for the most part here: space and time.

> "Space is that in whose smallest division all the time can happen and time is that in whose smallest division all space is contained", Abu al-Ala al-Maarri, Epistle of Forgiveness, 1033

Space and time have, as Dasein, been defined in several ways throughout history. Immanuel Kant, in his famous work Critique of Pure Reason (1781), proposed that these two entities were the a priori conditions for human understanding.

> "Space is not an empirical concept which has been derived from outer experiences. [...] It is the subjective condition of sensibility, under which alone outer intuition is possible for us."

Einstein, after reading Kant's book, immediately pointed out the initial mistake in the Critique: the separation of time and space. However, the fact that the Being of human beings exists in space and time is something one cannot deny. Thus, studying these two topics, which under General Relativity are one, opens the way for many metaphysical questions. What does one study when studying space and time? Why can we not see space bending in the presence of matter (only the effects of this bending)? Why is light the limit speed of the universe?

One thing we take for granted: General Relativity is part of the broader mathematical physics area and thus it is part of humanity's tools to project nature onto its way of understanding the world. When one says the way of understanding the world proper to human beings, we are referring to assumptions like the non-contradiction principle and that everything that happens, it happens for a cause. This latter condition, causality, was one of Kant's arguments against the possibility of answering the ontological question regarding the existence of God. Given that we always understand something as being the cause of another something, the causality chain never ends and, if it were to end, we would not understand why it ended, because that is not the way human understanding was designed to be.

> "Dasein is essentially de-severance - that is, it is spatial. Dasein is spatial in that indeed it constantly comports itself de-severantly towards the entities thus spatially encountered."
>
> "Time is primordial as the temporalizing of temporality, and as such it it makes possible the Constitution of the structure of care. Temporality is essentially ecstatic. Temporality temporalizes itself primordially out of the future. Primordial time is finite.", Martin Heidegger, Being and Time

In his magnum opus (Being and Time), Heidegger concludes that space is essentially temporal, given that we experience space as the Being of Dasein, in the way it comports to what is within-the-world. And this experience must be felt along some given time.

We are born in spacetime. We never lived outside of spacetime, there was never a single moment we felt that time was not going forward nor that space ceased to exist. We can never be somewhere that is not space. We can never be if time stops. Thus, after space and time are united in spacetime, as Einstein proposed and as it has been confirmed by several experimental observations, this entity still continues to be the a priori condition for what we experience to happen. We live within-a-world and our understanding is limited to this being, much like the language we use to communicate.

As was done in the Critique of Pure Reason, one could propose that, given that our understanding is limited by spacetime, one cannot understand outside of it and thus we cannot give a precise definition of it. If we could define spacetime, we could define also what is not spacetime, but this would be beyond our understanding, similar to the definition of God.

What does General Relativity describe then?

Given that it cannot define spacetime, the only thing it provides is a description of how space and time relate to one another. It is just a phenomenological theory, like physics in general, in the sense that it provides an interpretation of how space and time relate in a mathematical construction, but does not explain why it happens.

> "The original theory has to reinvent itself every time it is exposed to a new context.", Slavoj Žižek, in the introduction to On Practice and Contradiction, Mao Tse Tung, 1937

The work done in this thesis is a mere experimentation of General Relativity, it is a pushing forward the limits of the understanding that we can retrieve of the theory. One can further ask: why is this important? Why do we need to test theories?

As was mentioned before, physics is a phenomenological description of nature, given that it is based on the mathematical projection of the latter. Thus, we shall never understand the why of things, only the how. With this limitation, the only way out is to delve deep into the existing theories and test them, to check whether they produce results that are compatible with the expectations of human understanding. We are the only tool we have to check whether what we propose is true.

> "Once entities have been uncovered, they show themselves precisely as entities which beforehand already were. Such uncovering is the kind of Being which belongs to 'truth'", Martin Heidegger, Being and Time, 1927

Although truth belongs to each Dasein, it is not necessarily subjective. But this is also why we are limited in our understanding. I hope this brief Critique of Spacetime provides the reader with some insight into the metaphysical questions related to this work.

Afterword

Some months after having written the above considerations, I came to notice the existence of a still ongoing debate in the philosophy of science regarding something related to what I wrote, due to a fruitful conversation with Jordan Grujić (Munich Center of Mathematical Philosophy). The debate is about the nature of spacetime and the question is whether spacetime is a substance or a structure (p. e. [85, 86]).

This comes from the "hole" argument, which was immediately pointed out by Einstein in 1913 [87], forgotten for some years and later the discussion was revived by John Earman and John Norton back in 1987. The main idea is that General Relativity is invariant under diffeomorphisms, i.e., the equations that we can derive from Einstein's field equations are invariant under smooth changes of coordinates. Now, suppose we are looking at some region of spacetime, and in the middle of it, there is a hole.

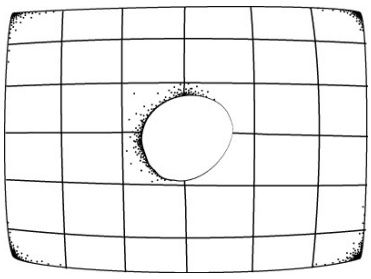

Figure D.1: Region of spacetime with a hole in it. Source: [88].

If we apply a diffeomorphism to the metric inside this hole but leave its boundary and the rest of that region as it was before, this new metric will continue to be a solution to the EFEs. Thus, the question that one can ask is: are the points of spacetime inherently meaningful without reference to the fields or objects defined on them, or is the meaning in the relationships between the fields or objects in spacetime? The people who believe in the first option are called substantivalists and the latter ones are relationalists. The main argument in favor of relationalism is the following: if spacetime points have meaning, we will get two solutions to the same region of spacetime, which means we will have a superposition of futures that are

equally possible according to the EFEs. Ontologically, this presents many challenges, but until now there has not been a proof or a refutation of this argument.

Given our natural limitation of living in our present which has its own future and of living this in spacetime, it should be impossible to actually see spacetime from the outside and say whether spacetime points do or do not have meaning by themselves. The absence of this possibility, of going out of spacetime, could be an indication of the absence of meaningfulness of spacetime points itself, but this argument would need some follow-up investigation work, which is out of the scope of this thesis.

D.2 On Scalar Fields

Although many discussions have already occurred about scalar field theories [89, 90], this work will benefit of a brief debate on scalar fields. What are we seeing when we are simulating a scalar field?

Quite a few proposals of scalar fields have been around for some decades, but until now only one of them has been confirmed (2012): the Higgs boson [91]. It is by the spontaneous symmetry breaking of an internal Lie symmetry that a scalar field gives mass to vectors and leptons and quarks [89], which indeed is what the Higgs boson does: it gives mass to the fundamental particles of the universe.

How do we connect this with our work? As it stands, the Higgs boson, through the eyes of General Relativity, is but a particle with mass and as such it is a minimally coupled massive scalar field with gravity. To incorporate a uncharged boson-type field in our work, we would have to replace the mass in (2.12) with the given boson mass (assuming only the real part of the scalar field).

Going back to Higgs, there has been some work in extending how the Higgs boson couples to gravity: by having a non minimal coupling, this would mean that the Higgs boson could have had an impact in early-universe cosmology [92]. However, when it comes to the inflation period of early universe, cosmologists have for a long while already given their go at another scalar field: the inflaton, which serves as an explanation for the inflation period [93] and also for the Cosmic Microwave Background observations. This latter is the only indirect indication that the inflaton might exist. There has been also some work with a two-scalar-field-proposal that could better explain inflation [94], but again this still lacks proof. There is a significant difference from the Higgs boson in the inflaton theories, for they presuppose a coupling to gravity, typically described as

$$S = \int d^4x\sqrt{-g}\left[\frac{1}{2}m_P^2 R - \frac{1}{2}\partial^\mu\partial_\mu\phi - V(\phi) - \frac{1}{2}\xi R\phi^2\right],$$

where ϕ here is the magnitude of the inflaton field and ξ is the strength of the interaction between R and ϕ. This non minimal coupling includes more dynamics that would need to be redone if to be included in this work, for example. We would recover the real scalar field by setting ξ to 0.

There have been some other proposals of scalar fields: the dilaton, the axion, moduli fields and quintessence. From these, only quintessence has an indirect proof, the observation of cosmic acceleration, but still no direct detection. The axion has ongoing experiments [95] to detect it, but until now still no direct observation as well. However, the question still remains, what is exactly a scalar field?

Mathematically, it is just a function of space and time that gives a specific value for each point in space and time. Examples of this could be the potential energy or the temperature in a room. However, scalar fields can behave in different ways. For example, for the case of temperature we know that it usually follows the heat equation [96],

$$\frac{\partial T}{\partial t} = \alpha \nabla^2 T \,,$$

which is fundamentally different from the Klein-Gordon equation. Thus, we are faced with the fact that we cannot give physical meaning to a scalar field without having its governing equation attached to it. In the case that was presented in this work, we focused on the Klein-Gordon equation, which is indeed the one that describes the Higgs-Boson, for example. However, we used the massless version, which is the four dimensional version of the wave equation, so this could not possibly describe the Higgs boson. We could then propose that when we are simulating a massless scalar field, we are actually seeing how waves would propagate in that world, in a generic way. Furthermore, a wave can be thought of as a packet of energy which moves around (in waves).

There is still another possibility, Goldstone bosons, that are created when there is a spontaneous symmetry breaking. This is derived from the Goldstone theorem [97], which we will not go to deep into here.

For the case of a massless complex scalar field, which is exactly what we had here, this is equivalent to having two real scalar fields, one corresponding to the real and another to the imaginary part. Given that it is minimally coupled to electromagnetism through A_μ, this will also have further dynamics if any symmetry is broken. Physically, a complex scalar field, given that it has charge, can represent a charged particle.

Even though we lacked more precise examples, I hope this brief debate has helped to demistify what is a scalar field.

TÉCNICO LISBOA

Electrically Charged Hyperboloidal Evolution

João Dinis Ribeiro Machado de Carvalho Álvares